Role of the Alpha-1 Subunit of the Na^+, K^+-ATPase (ATP1A1) in the Macropinocytic Entry of Respiratory Syncytial Virus, and Development of a Live-Attenuated Vaccine against Ebola Virus

Von der Fakultät für Lebenswissenschaften

der Technischen Universität Carolo-Wilhelmina zu Braunschweig

zur Erlangung des Grades eines

Doktors der Naturwissenschaften

(Dr. rer. nat.)

genehmigte

D i s s e r t a t i o n

von Matthias Lingemann

aus Sonthofen

1. Referent: Professor Dr. Michael Steinert
2. Referent: Dr. Peter L. Collins
eingereicht am: 04.02.2019
mündliche Prüfung (Disputation) am: 30.04.2019

Druckjahr 2019

Vorveröffentlichungen der Dissertation

Teilergebnisse aus dieser Arbeit wurden mit Genehmigung der Fakultät für Lebenswissenschaften, vertreten durch den Mentor der Arbeit,
in folgenden Beiträgen vorab veröffentlicht:

Publikation

Lingemann, M, Liu X, Surman S, Liang B, Herbert R, Hackenberg AD, Buchholz UJ, Collins PL and Munir S. (2017) "Attenuated Human Parainfluenza Virus Type 1 Expressing Ebola Virus Glycoprotein GP Administered Intranasally Is Immunogenic in African Green Monkeys." J Virol **91**(10).

Tagungsbeiträge

Lingemann M, McCarty T, Liu X, Surman S, Martin SE, Collins PL and Munir S. "New Insights into RSV Entry: ATPase Sodium/Potassium-Transporting Subunit Alpha-1 (ATP1A1) is Important for Macropinocytic Entry of RSV." 11th International Respiratory Syncytial Virus Symposium, Asheville, NC (2018)

Lingemann M, Liu X, Surman S, Liang B, Herbert R, Hackenberg AD, Buchholz UJ, Collins PL and Munir, S. "Development and Preclinical Evaluation of a Live-Attenuated Parainfluenza Virus Type 1 Vector Expressing Ebola Virus Glycoprotein GP as an Intranasal Ebola Vaccine Candidate." 36th Annual Meeting of the American Society for Virology, Madison, WI (2017)

Posterbeitrag

Lingemann M, Liu X, Surman S, Liang B, Buchholz UJ, Collins PL and Munir S. "Development and Preclinical Evaluation of Live Attenuated Parainfluenza Virus Vectors expressing Ebola Virus Glycoprotein GP as Intranasal Ebola Vaccine Candidates." 13th Annual NIH Graduate Student Research Symposium, National Institutes of Health, Bethesda, MD (2017)

Patentantrag

Collins PL, **Lingemann M** and Munir S. "Use of ouabain antagonists to inhibit viral infection." U.S. Patent application No. 62/737,899, filed Sept 27, 2018

Acknowledgements

This dissertation would not have been possible without the great support from many people. I am very thankful for all the support, guidance, and mentoring I have received during the time of my dissertation research. Special mention goes to the following people:

First and foremost, I am deeply appreciative to my supervisor **Dr. Peter L. Collins** for providing me the opportunity to work on these projects and to perform my dissertation research in his lab. I appreciated the freedom and trust he has given me to pursue any direction of these projects, wherever science led me. His guidance and mentorship made this “endeavor” a very positive experience.

I am also hugely thankful to **Dr. Shirin Munir** for her great support and guidance to steer through the “scientific clouds” without losing the hope to find a glimpse of light! Thank you, Shirin, for your collegial and very supportive attitude, and the many stimulating discussions! Without your warm encouragement and contribution, this dissertation would not have materialized.
I have always enjoyed working with you!

I am deeply grateful to **Prof. Dr. Michael Steinert** for his longstanding mentorship, support, and guidance. Michael, thank you for making this collaboration between the TU Braunschweig and NIH for my dissertation possible.

I would like to thank **Prof. Dr. Melanie Brinkmann** for accepting the chair of my dissertation committee.

I am grateful to **all former and current members of the RNA Viruses Section who supported me**. Special thanks go to **Emérito Amaro-Carambot, Dr. Xueqiao Liu and Sonja Surman** for their help and support whenever it was needed.

I would like to express my gratitude to the following **members of the NIAID RTB core facilities** for their technical support and expertise: **Dr. Sundar Ganesan, Dr. Juraj Kabat** and **Dr. Margery Smelkinson** from the Biological Imaging Facility for their help with all the microscopy-based experiments. **David Stephany** from the Flow Cytometry Facility for his support with the flow cytometer. **Ryan Kissinger** from the Medical Arts Unit for designing the illustration for this dissertation thesis.

I thank **Dr. Jaspal S. Khillan** from the NIAID Mouse Genetics and Gene Modification Section for the resuscitation of the ATP1A1$^{+/-}$ mutant mice and **Dr. Crystal Thomas and all technicians of the animal facilities** from the NIAID Comparative Medicine Branch for their expertise and technical support with all the animal studies.

I also would like to express my appreciation to **Dr. Philip Wang** and **Dr. Philip Ryan** from the NIH Graduate Partnerships Program at the Office of Intramural Training & Education (OITE) for providing invaluable support and providing a training rich environment. I felt very fortunate to be able to participate in the numerous training opportunities offered by OITE.

I would like to thank the administrative office of the Laboratory of Infectious Diseases for their help, especially with all the visa regulations and for making sure to keep me in the country. Thank you to **Elizabeth Bivins-Smith**, **Alicia Brockington** and **Nicole German** for your invaluable help with all the paper work. Sorry, if I gave you once in a while some headache with my visa situation!

Thank you to **Dr. Christine Krempl** for her longstanding mentorship and for connecting me to the NIH, which turned out to be the foundation of the possibility to perform my dissertation research there.

A special shout-out and BIG Thank you to **all my friends in the U.S., back home in Germany, and around the world**! I am deeply appreciative to ALL of them for being there for me; even if we haven't seen us sometimes for a long time. I am also feeling very fortunate to have found many new friends in the U.S. during this time, especially within the NIH Sailing Association, that allowed me to find some balance to the lab work and to recharge for upcoming scientific challenges during some great sails on the Chesapeake Bay.

A very special "Thank you" goes to **my wife Judy**! Thank you for your love and graceful understanding if science had occupied the majority of my time again.
Thank you for being there! 谢谢!

Last, but by no means least, a big "Thank you" and "DANKE" goes to my amazing family!
To **my parents** and **my sister** for their never-ending support; even across the Atlantic.
Without your support, this would have never been possible. "Vielen lieben Dank!"

Looking for the answer:
You hunt it,
you catch it,
you fool yourself;
the answer,
is always,
a step ahead.

J.C.S. (Skou 2004)

Table of Contents

Abstract

Human respiratory syncytial virus (RSV) is the leading viral cause of severe bronchiolitis and pneumonia in infants and young children worldwide. It is estimated that RSV-associated acute lower respiratory tract infections cause up to 118,000 deaths of children under five years of age annually. It also causes substantial morbidity and mortality in the elderly and individuals with immunosuppression or cardiopulmonary disease. No vaccine or effective antiviral drug for general use is available. The mechanism of RSV entry into the host cell, and the host factors involved in this process, are not well understood. To gain insight into virus-host interactions, a genome-wide siRNA screen was performed. The expression of over 20,000 cellular genes was individually knocked down in human airway epithelial A549 cells, followed by infection with RSV expressing enhanced green fluorescent protein (GFP), which was used as a surrogate for infection. Knockdown of expression of the cellular ATP1A1 protein, the major subunit of the Na^+, K^+-ATPase, had the strongest inhibitory effect on GFP expression and viral titer, with minimal effects on cell viability. The inhibitory effect due to the ATP1A1 knockdown was not observed for vesicular stomatitis virus (VSV), indicating that it was RSV-specific rather than a general effect. This study identified and characterized the pro-viral role of ATP1A1 during RSV infection. It was found that RSV induced the formation of ATP1A1 clusters in the plasma membrane of the host cell very early during infection. This phenomenon was independent of viral replication, but dependent on the viral attachment glycoprotein G. RSV infection also triggered ATP1A1-mediated signaling, involving c-Src activation that resulted in the transactivation of epidermal growth factor receptor (EGFR) by Tyrosine 845 phosphorylation. Further signaling events downstream of EGFR culminated in the formation of macropinosomes. There was extensive uptake of RSV virions into macropinosomes, suggesting that this is a major route of RSV uptake, with fusion presumably occurring at the membrane of the macropinosomes rather than at the plasma membrane. In addition, this study identified chemical compounds with anti-RSV activity: Ouabain, a cardiotonic steroid, and PST2238, a synthetic digitoxigenin derivative, that bind specifically to the extracellular domain of ATP1A1, inhibited RSV-induced signaling and resulted in the inhibition of RSV entry. Taken together, this study describes a novel ATP1A1-enabled mechanism used by RSV to enter the host cell, and identified candidate antiviral drugs that block this entry pathway.

The second part of this dissertation thesis describes the development and preclinical evaluation of a live-attenuated human parainfluenza virus type 1 (HPIV1)-vectored intranasal vaccine against Ebola virus (EBOV). This project was prompted by the 2014 - 2016 EBOV outbreak in West Africa; the largest in history. Recombinant HPIV1 viruses expressing the membrane-anchored form of EBOV glycoprotein GP were developed and preclinically evaluated. GP is the major immunogen providing protective immunity against an EBOV infection. GP was codon-optimized and expressed either as a full-length protein or an engineered chimeric form in which its transmembrane and cytoplasmic tail (TMCT) domains were substituted with those of the HPIV1 F protein, in an effort to enhance packaging into the vector particle and improve

immunogenicity. GP was inserted either preceding the N gene (pre-N) or between the N and P genes (N-P) of the HPIV1 genome bearing a stabilized attenuating mutation in the P/C gene ($C^{\Delta 170}$). The viral constructs grew to high titers and efficiently and stably expressed GP *in vitro*. All viruses showed the expected attenuation in the respiratory tract of African green monkeys (AGMs), replicating at low titers over several days. Two doses of candidates expressing GP from the pre-N position elicited higher GP neutralizing serum antibody titers than the N-P viruses, and expression of unmodified GP resulted in higher levels than its chimeric TMCT counterpart. Unmodified GP was packaged into the HPIV1 particle, and the TMCT modification did not increase packaging or immunogenicity but rather reduced the stability of GP expression during *in vivo* replication. In conclusion, this study developed an attenuated and immunogenic intranasal vaccine candidate expressing GP from the pre-N position of an attenuated HPIV1 vector. It is expected to be well-tolerated in humans and is available for clinical evaluation.

Zusammenfassung

Das Respiratorische Synzytial-Virus (RSV) ist der bedeutendste virale Erreger von Bronchiolitiden und Pneumonien bei Säuglingen und Kleinkindern. Schwere RSV-Infektionen der unteren Atemwege verursachen jährlich weltweit bis zu 180.000 Todesfälle von Kleinkindern unter 5 Jahren. Bisher ist kein Impfstoff oder eine effektive antivirale Therapie gegen RSV-Infektionen verfügbar. Die mechanistischen Details des Eintritts von RSV in die Zelle und die Wirtsfaktoren, die dabei notwendig sind, sind nur unzureichend charakterisiert. Um ein besseres Verständnis dieser Virus-Wirts-Interaktionen zu erlangen, wurde eine genomweite Untersuchung mittels siRNA-Knockdown durchgeführt. In der humanen Lungenepithelzelllinie A549 wurde die Expression von mehr als 20.000 zellulären Genen einzeln mittels siRNA-Transfektion herunterreguliert (knockdown), wonach eine Infektion der Zellen mit RSV, welches das grün fluoreszierende Protein (GFP) exprimierte, erfolgte. Die virale GFP-Expression wurde als Indikator für die Infektionseffizienz verwendet. Die Verringerung der zellulären Expression von ATP1A1 hatte den stärksten Effekt auf die virale GFP-Expression und den Virustiter, ohne die Zellviabilität signifikant zu beeinflussen. ATP1A1 ist die Hauptuntereinheit der in der Plasmamembran lokalisierten Na^+, K^+-ATPase. Die inhibitorische Wirkung aufgrund des ATP1A1-Knockdowns wurde nicht für das vesikuläre Stomatitis-Virus (VSV) beobachtet, was darauf hinweist, dass es sich eher um einen RSV-spezifischen als einen allgemeinen Effekt handelte. In der vorliegenden Arbeit wurde damit ATP1A1 als pro-viraler Faktor identifiziert. Dabei kam es sehr früh während der Infektion zur Bildung von ATP1A1-Aggregaten in der Plasmamembran der Wirtszelle. Dieses Phänomen war unabhängig von der viralen Replikation, aber abhängig vom viralen Glykoprotein G. Mechanistisch induzierte RSV eine ATP1A1-abhängige Signaltransduktion, welche zur Aktivierung der zellulären Src-Kinase und infolge dessen der Transaktivierung des epidermalen Wachstumsfaktorrezeptors (EGFR) durch die Phosphorylierung von Tyrosin 845 führte. Die Aktivierung der EGFR-abhängigen Signalkaskade induzierte die Bildung von Makropinosomen, die behüllte RSV-Virionen extensiv enthielten. Dies deutet darauf hin, dass dies ein Hauptmechanismus der RSV-Aufnahme in die Wirtszelle darstellt, wobei die Fusion von Virus- und Zellmembran vermutlich erst in Makropinosomen stattfindet, anstatt bereits an der Plasmamembran. Darüber hinaus identifizierte diese Studie zwei antiviral wirkende Verbindungen, Ouabain, ein Herzglykosid, und PST2238, ein synthetisches Digitoxigeninderivat, die spezifisch an die extrazelluläre Domäne von ATP1A1 binden. Dies führte zur Inhibierung der RSV-induzierten ATP1A1-Signalkaskade und folglich der Hemmung des RSV-Eintritts in die Zelle. Zusammenfassend beschreibt diese Arbeit einen neuen ATP1A1-abhängigen Signalweg, der von RSV aktiviert wird, um in die Wirtszelle einzudringen. Zusätzlich wurden potentielle antivirale Medikamente, die diesen Eintrittsweg blockieren, identifiziert.

Der zweite Teil dieser Doktorarbeit beschreibt die Entwicklung und präklinische Evaluation eines attenuierten humanen Parainfluenzavirus Typ 1 (HPIV1) basierenden Lebendimpfstoff gegen das Ebolavirus (EBOV). Dieses Projekt wurde infolge des EBOV-Ausbruches (2014 - 2016) in Westafrika initiiert, welcher der größte EBOV-Ausbruch in der Geschichte darstellt. Die membranverankerte Form des EBOV-Glykoproteins GP, das das Hauptantigen für die Induktion einer schützenden Immunität gegen EBOV-Infektionen darstellt, wurde in einen rekombinanten HPIV1-Vektor eingefügt. Dabei wurde die Sequenz von GP codon-optimiert und entweder als vollständiges GP-Protein oder als chimäre Form, in der die Transmembran- und zytoplasmatische- (TMCT-) Domäne des EBOV-GP durch die des HPIV1 F-Proteins ersetzt war, exprimiert. Letztere, chimäre Variante sollte die Verpackung in das Viruspartikel erhöhen und dadurch die Immunogenität verbessern. Das GP-Gen wurde in zwei verschiedene Positionen, vor dem N-Gen (pre-N) oder zwischen dem N- und P-Gen, eines rekombinanten HPIV1-Genoms eingefügt, welches außerdem eine stabilisierte attenuierende Mutation im P/C-Gen ($C^{\Delta 170}$) enthielt. In Zelllinien replizierten alle Vektoren effizient zu hohen Titern und wiesen eine effiziente und stabile Expression von GP auf. Die *In-Vivo*-Vermehrung aller Viren in den Atemwegen von Grünen Meerkatzen war, wie erwartet, attenuiert. Durch zweimalige Immunisierung mit den Impfstoffkandidaten, bei denen das GP-Gen proximal der N-Position eingefügt war, wurden höhere GP-neutralisierende Serumantikörpertiter induziert als durch die Viren mit dem GP-Gen in der N-P Position. Die Expression des vollständigen, unveränderten EBOV GP-Proteins, das effizient in HPIV1-Viruspartikel integriert wurde, induzierte höhere Antikörpertiter als die des chimären TMCT-Konstrukts. Dahingegen beeinflusste die TMCT-Modifikation weder die Verpackung noch die Immunogenität positiv, sondern reduzierte sogar eher die Stabilität der GP-Expression während der Vermehrung *in vivo*. Zusammenfassend wurde in dieser Studie ein attenuierter und immunogener intranasaler Impfstoffkandidat identifiziert, von dem erwartet wird, dass dieser für Menschen gut verträglich ist. Dieser Impfstoffkandidat steht nach der hier vorgelegten präklinischen Evaluierung für weiterführende klinische Studien zur Verfügung.

1. Introduction

1.1. Role of the alpha-1 subunit of the Na^+, K^+-ATPase (ATP1A1) in the macropinocytic entry of respiratory syncytial virus

1.1.1. Respiratory syncytial virus (RSV)

1.1.1.1. Phylogeny of *Mononegavirales*

RSV belongs to the genus *Orthopneumovirus* of the family *Pneumoviridae* within the order *Mononegavirales* (Afonso et al. 2016). In addition to human RSV, the genus *Orthopneumovirus* contains two additional viruses: the bovine RSV (BRSV) and the murine pneumonia virus (MPV). The family *Pneumoviridae* is closely related to *Paramyxoviridae*. In fact, viruses of the family *Pneumoviridae* were previously included in the family *Paramyxoviridae* as the subfamily *Pneumovirinae* (International Committee on Taxonomy of Viruses. 2012). The re-classification of the subfamily *Pneumovirinae* as a new family took place in the 2016 Taxonomy update of the order *Mononegavirales* [International Committee on the Taxonomy of Viruses (ICTV) (Afonso et al. 2016)]. This change was made because of the recognition that the members of *Pneumovirinae* were as closely related to the family *Filoviridae* as they were to the members of the subfamily *Paramyxovirinae* of *Paramyxoviridae* (Afonso et al. 2016). Different conclusions on the phylogenetic relationships can be made depending on the viral proteins utilized for the phylogenetic comparison (Russell et al. 2018). For instance, the *Pneumoviridae* large (L) polymerase protein has a similar extent of relatedness to that of *Filoviridae* and *Paramyxoviridae* (Figure 1A). However, the *Pneumoviridae* fusion (F) glycoprotein is more closely related to the F protein of *Paramyxoviridae* than to single glycoprotein GP of *Filoviridae*, e.g. Ebola virus, which serves the same role as F (Figure 1B).

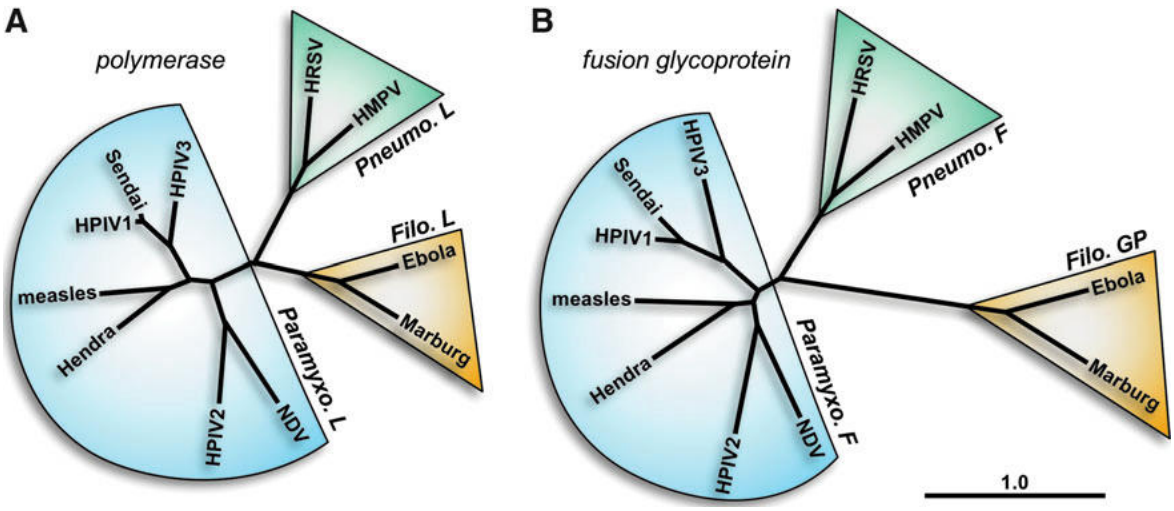

Figure 1: **Phylogenetic comparison of members of the family *Paramyxoviridae*, *Pneumoviridae* and *Filoviridae* of the order *Mononegavirales*.** The amino acid sequences of the large (L) polymerase (A) or fusion (F) glycoprotein (B) were used for comparing phylogenetic relationships. Human respiratory syncytial virus (HRSV), human metapneumovirus (HMPV), Newcastle disease virus (NDV), Human parainfluenza virus type 1 (HPIV1), type 2 (HPIV2), and type 3 (HPIV3). Virus families are shown in accordance with the 2016 Taxonomy update of the order *Mononegavirales* of the International Committee on the Taxonomy of Viruses (ICTV) (Afonso et al. 2016). Adapted from (Russell et al. 2018).

In addition, *Pneumoviridae* and *Paramyxoviridae* contain an attachment protein (G or HN) beside the F protein, whereas GP of *Filoviridae* mediates both attachment and fusion. Moreover, the genomes of the members of family *Pneumoviridae* contain an additional gene called M2, which encodes for two unique proteins (M2-1 and M2-2) by two overlapping open reading frames (ORFs), and which is absent in *Paramyxoviridae* and *Filoviridae*.

The family *Pneumoviridae* also contains, in addition to the genus *Orthopneumovirus,* a second genus, *Metapneumovirus,* to which the avian and human metapneumoviruses (AMPV and HMPV) belong. The other families within the order *Mononegavirales* are *Bornaviridae*, *Filoviridae*, *Mymonaviridae*, *Nyamiviridae*, *Paramyxoviridae*, *Rhabdoviridae* and *Sunviridae* (Amarasinghe et al. 2018).

The order *Mononegavirales* is defined primarily by the characteristics of the viral genome (Lamb 2013). All members are enveloped virus particles that contain a linear, single-stranded, non-segmented, negative-sense RNA genome that is tightly encapsidated by a viral nucleoprotein. Transcription initiation occurs at a single promoter situated at the 3' leader sequence, which is the genomic 3' untranslated region (UTR). Viral genes are separated by non-transcribed intergenic (IG) regions with variability in length and sequence among viruses and can be conserved or differ within a viral genome between different gene junctions. Each viral gene is flanked by a gene start (GS) and gene end (GE) sequence.

The gene junctions, containing the GE, IG and GS sequences, guide the viral RNA-dependent RNA polymerase (RdRp), of which the major protein, which bears the catalytic domains, is the L polymerase protein. At the GE and GS sequence, transcription of the upstream gene is terminated and that of the downstream gene is initiated, respectively. Due to the occasional failure of the RdRp to re-initiate transcription at the adjacent gene, the number of RdRp molecules that are available to transcribe mRNA continues to decrease towards the 5' end of the viral genome. This results in a 3' to 5' polar transcription gradient of the viral genes, which is typical for the order *Mononegavirales* (Lamb 2013). The polar gradient is influenced by the efficiency of the GE and IG sequences to terminate transcription. Inefficient GE sequence causes read-through transcription and a bicistronic mRNA. Since the second ORF of a bicistronic mRNA is in general not efficiently translated in eukaryotes (Kozak 2005), the expression of the gene downstream of an inefficient GE would be reduced, as shown for example for the aberrant M GE in human parainfluenza virus type 3 (HPIV3) (Lingemann et al. 2015). Similar observations have been made for other members [reviewed in (Karron and Collins 2013)], for example the M GE of PIV5 has a single nucleotide substitution with effect similar to that of HPIV3 M GE (Rassa and Parks 1998); simian virus 41 lacks an M GE signal entirely (Kato et al. 1999); and clinical isolates of RSV showed variations in the G GE that resulted in a reduced F protein expression (Moudy et al. 2003).

The families *Filoviridae*, *Paramyxoviridae*, *Pneumoviridae*, and *Rhabdoviridae* have genome arrangements that have a number of similar genes (Lamb 2013) and include, in 3' to 5' order, a 3' leader region followed by the viral nucleocapsid protein (N or NP) gene, phosphoprotein

(P) gene, internal matrix or membrane (M) gene, one or more envelope protein genes (including HN, H, F, G, and SH, depending on the virus), and the L polymerase gene. The viral genome ends with the 5' trailer (Lamb 2013).

Depending on the virus family, the genome encodes a different number of envelope proteins. In *Filoviridae* and prototypical members of *Rhabdoviridae*, there is a single envelope glycoprotein GP or G, respectively, that mediates both attachment and fusion. *Paramyxoviridae* and *Pneumoviridae* have separate attachment (H, HN, or G) and fusion (F) proteins. Some members of *Paramyxoviridae* and all members of *Pneumoviridae* contain a third envelope protein called the small hydrophobic (SH) protein. Additional genes or open reading frames (ORFs) encoding other proteins may be present in certain viruses, such as an interferon antagonist C protein encoded by certain members of *Paramyxoviridae* and the RNA synthesis factor proteins M2-1 and M2-2 encoded by all members of *Pneumoviridae* (and described below). Thus, members of these families (and most members of *Mononegavirales*) have the general genome arrangement of leader-N-P-M-(glycoproteins)-L-trailer, with possible additional intervening genes present depending on the virus (Karron and Collins 2013, Lamb 2013).

The encapsidated viral RNA with the nucleocapsid proteins N, P, and L is called the ribonucleoprotein (RNP) complex and, for most of these viruses, is considered infectious since it contains the viral proteins required for transcription/replication initiation and the *de novo* synthesis of viral proteins essential for viral replication. Members of *Pneumoviridae* may require in addition the M2-1 protein. Naked viral RNA is not infectious since it is negative-sense and thus does not directly encode protein, and is not associated with the viral RdRp and nucleocapsid that is necessary for direct transcription and thereby initiate viral replication. *Filoviridae*, *Paramyxoviridae*, *Pneumoviridae*, and *Rhabdoviridae* replicate in the cytoplasm of the host cell, with the exception of plant viruses in the genus *Nucleorhabdovirus* (Lamb 2013). *Bornaviridae* is different compared to the other families of *Mononegavirales*, since their replication and transcription occur in the nucleus (Lamb 2013).

Maturation of the virions occurs by budding from a cellular membrane that provides the viral envelope with the incorporated viral surface glycoproteins. Most members of the order *Mononegavirales* bud from the host plasma membrane, with a few exceptions of some plant rhabdoviruses, which bud from the inner nuclear membrane (Lamb 2013).

1.1.1.2. Genome organization and replication

RSV has a single-stranded, non-segmented, negative-sense RNA genome that is 15.2 kilo base (kb) long and contains 10 genes that encode 11 proteins (Figure 2), namely (in 3' to 5' genomic order) two nonstructural proteins NS1 and NS2, nucleocapsid (N), phosphoprotein (P), matrix protein (M), the three envelope glycoproteins including the small hydrophobic (SH), attachment (G) and fusion (F) glycoproteins, followed by the M2-1 and M2-2 proteins, which are encoded by the two overlapping ORFs in the M2 gene, and the large polymerase L (Collins and Karron 2013).

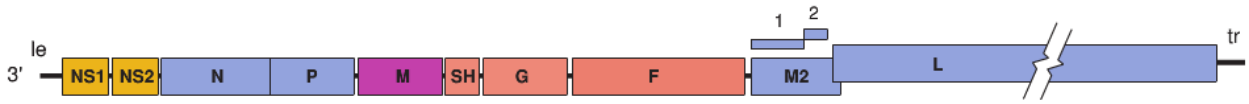

Figure 2: **Genome structure of RSV.** Genes are color-coded for their general location in the virion. The nonstructural proteins (NS1, NS2) are yellow, proteins involved in the viral transcription and replication are blue, the matrix protein is magenta and the envelope glycoproteins are red. The M2 gene has two partially-overlapping open reading frames (ORFs) that are depicted on the top of the M2 gene and encode two distinct proteins M2-1 and M2-2. le: leader; tr: trailer. Adapted from (Collins and Karron 2013).

The RSV envelope glycoproteins G and F mediate viral attachment and fusion for entry into the host cell, while the role of SH in infection remains unclear. The glycoprotein G is a highly glycosylated type II transmembrane glycoprotein and is considered to be the attachment protein for RSV. The small hydrophobic protein SH is a small transmembrane protein that forms pentamers and may have properties of a viroporin (Collins and Karron 2013). SH and G are thought to be non-essential for virus replication as their deletion mutants can grow in cell culture (Bukreyev et al. 1997, Karron et al. 1997, Techaarpornkul et al. 2001). However, RSV lacking the G protein is impaired for HEp-2 cell entry and is highly attenuated in mice, indicating an important role of G in virus replication *in vivo*, presumably due to its role in cell attachment (Teng et al. 2001). The G protein contains a highly basic heparin binding domain and a CX3C motif [characteristic of a CX3C chemokine called fractalkine (Zlotnik and Yoshie 2000)] that mediate cell attachment by binding to the cell surface glycosaminoglycans (GAGs) (Hallak et al. 2000, Shields et al. 2003) and the CX3CR1 chemokine receptor (Tripp et al. 2001, Johnson et al. 2015), respectively. GAGs are commonly expressed on immortalized cell lines *in vitro* but do not appear to be significantly expressed on the apical surface of epithelial cells lining the respiratory tract, which is the site of RSV infection *in vivo*. Therefore, GAGs may be important for RSV attachment in immortalized cell lines but likely are not important for infection of differentiated primary humane airway epithelial cultures or *in vivo*, situations in which CX3CR1 appears to be the more important receptor for G (Tripp et al. 2001, Johnson et al. 2015).

The RSV F protein mediates fusion of the viral envelope with the plasma membrane and is essential for virus infectivity. It is a type I transmembrane surface protein that assembles into a homotrimer. F is expressed as an inactive F_0 precursor which is activated via cleavage at two sites by cellular furin endoprotease into a smaller, N-terminal F_2 subunit and a larger, C-terminal F_1 subunit that are linked by two disulfide bonds. The N-terminus of the F_1 subunit, generated as a result of F_0 cleavage, contains a hydrophobic domain that acts as a fusion peptide and is inserted into the host cell plasma membrane to mediate fusion (Collins and Karron 2013). RSV F is produced in a metastable pre-fusion F (pre-F) conformation. Upon contact with a host cell, pre-F undergoes structural rearrangement that brings the viral envelope and plasma membrane in close proximity resulting in lipid bilayer fusion and the release of the viral nucleocapsid into the cytoplasm to initiate infection (Colman and Lawrence 2003). Limited evidence suggests that RSV may not fuse at the plasma membrane and is taken up in an enveloped form by macropinocytosis followed by fusion occurring in the macropinosomes (Krzyzaniak et al. 2013).

Beside the fusion activity, RSV F also has been described to interact with surface proteins of the host cell. For example, it has been reported that the F protein binds to a host cell protein called nucleolin, which may serve as an alternate attachment protein (Tayyari et al. 2011). A recent study also described a strain-specific (RSV A2-2-20F) interaction of the F protein with the epidermal growth factor receptor (EGFR) that results in EGFR activation and mucin expression (Currier et al. 2016). Knockdown of EGFR resulted in a strain-specific reduction of infectivity that was not observed with the prototypic RSV strain A2. The underlying mechanisms of these observed effects were not further elucidated.

Additional host proteins and pathways with suggested roles in RSV entry have been reported. For instance, it was shown that RSV utilizes lipid rafts in cholesterol-rich microdomains on the cell surface, known as caveolae, as a docking platform essential for entry (San-Juan-Vergara et al. 2012). Similarly, EGFR signaling was postulated to play an important role in triggering macropinocytic uptake of RSV (Krzyzaniak et al. 2013). So far, it is not known how these previously described host factors for RSV entry might be linked to each other or function cooperatively to facilitate RSV entry. It remained unknown if EGFR alone is sufficient, or requires other factors, to initiate signaling or if EGFR and its associated signaling are somehow physically linked with caveolae. Limited evidence supports the existence of two incongruous RSV uptake mechanisms including the exclusive involvement of either the EGFR-triggered macropinocytosis (Krzyzaniak et al. 2013) or the clathrin-mediated endocytosis (Kolokoltsov et al. 2007) as the primary mode of uptake. It is unclear if one or both are involved.

After viral entry, transcription of the viral genes is initiated by the viral RdRp complex, that is delivered by the virus particle and contains the L, N, P, and M2-1 proteins in association with the viral genome (Collins and Karron 2013). The large polymerase L contains the major catalytic domains for transcription. The phosphoprotein P is the major viral phosphoprotein and is an essential co-factor for the polymerase complex. M2-1 is an essential transcription processivity factor and its absence causes a premature and nonspecific termination of transcription (Fearns and Collins 1999). Viral mRNA contains a methylated 5’ cap structure and is polyadenylated by the viral polymerase copying reiteratively at the poly-U tract at the end of the GE signal. The viral mRNA is translated by the host translation machinery.

The accumulation of the M2-2 protein in the RSV-infected cell switches the viral nucleocapsid/polymerase complex from mRNA transcription to RNA replication (Bermingham and Collins 1999) so that the polymerase ignores the gene junction signals and transcribes the entire viral genome into a continuous full-length anti-genome. The complementary sequence (anti-genome) of the 5’ trailer contains a strong promoter that initiates RNA synthesis of the nascent negative-sense genome using the anti-genome as the template. As they are being synthesized, the nascent positive-sense (anti-genome) and negative-sense (genome) viral RNAs are encapsidated by the nucleoprotein N that protects the viral genome from degradation (Collins and Karron 2013). It has been shown that proteins involved in the transcription and replication process are concentrated in cytoplasmic inclusion bodies (Garcia et al. 1993) where viral transcription and

RNA replication are thought to occur. This isolation might be a strategy to avoid innate immune recognition but the mechanism of how the inclusion bodies function is not well understood.

The nonstructural proteins NS1 and NS2, encoded by the most 3' proximal genes of the genome, are unique to the genus *Orthopneumovirus*. They are known to interfere with the induction and signaling of type I interferon and have anti-apoptotic activity (Collins and Karron 2013).

The matrix protein M is a non-glycosylated internal virion component that organizes the virion components at the plasma membrane. The surface proteins F, G and SH are expressed and transported through the secretory pathway to, and inserted into, the plasma membrane. The budding of new pleomorphic viral particles occurs from the plasma membrane and is orchestrated by the M protein (Collins and Karron 2013).

1.1.1.3. Epidemiology and pathogenesis

RSV was discovered in the mid 1950s (Blount et al. 1956, Chanock et al. 1957) and is considered the leading viral cause of severe lower respiratory tract infection (LRI), primarily bronchiolitis and pneumonia, resulting in hospitalization of newborns and infants worldwide (Lozano et al. 2012). Infants are more susceptible to RSV earlier in life than to other common viruses such as HPIV1-3, influenza, HMPV, and measles virus (Figure 3).

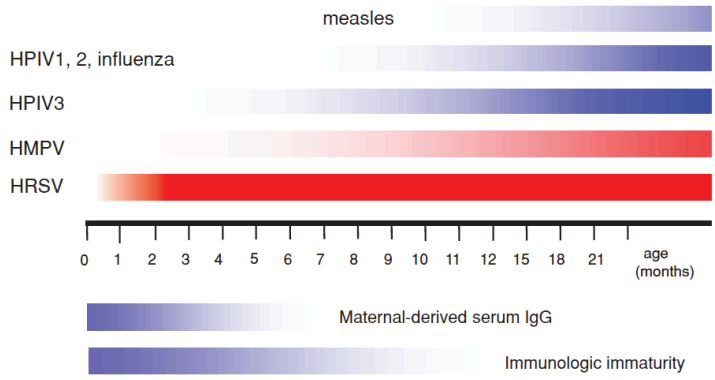

Figure 3: **Susceptibility to the indicated viruses during early infancy (top) and host factors that influence the immune response to vaccines (bottom).** Adapted from (Karron and Collins 2013).

It was estimated that, in 2015, RSV infections of children younger than 5 years of age caused 33.1 million (uncertainty range [UR] 21.6 - 50.3 million) cases of RSV-associated acute lower respiratory infections (RSV-ALRI) that resulted in 3.2 million (UR 2.7 - 3.8 million) hospital admissions and 59,600 (UR 48,000 - 74,500) in-hospital deaths (Shi et al. 2017). Of these, 1.4 million (UR 1.2 - 1.7 million) hospital admissions and 27,300 (UR 20,700 - 36,200) in-hospital deaths were estimated for children younger than 6 months (Shi et al. 2017). The estimated overall RSV-ALRI mortality for 2015 could be as high as 118,200 (UR 94,600 - 149,400) (Shi et al. 2017) and is slightly decreased compared to the estimations for 2005 (Nair et al. 2010). It also has been shown that infants two months of age or younger constitute 44% of all RSV-related hospitalizations. One-month old infants were at the greatest risk for RSV hospitalization and most (80%) of the hospitalized children had no prior conditions and were considered healthy (Hall et al. 2013).

RSV infections also have a major impact on the health of elderly adults. It has been estimated that RSV causes 178,000 hospitalizations and 14,000 deaths (8% of those hospitalized) in the U.S. alone in people older than 65 years (Falsey et al. 2005).

RSV occurs in yearly seasonal epidemics that typically occur in the winter or rainy season, but can vary depending on the climate and regional factors. For 2014 – 2017 the median onset in the U.S. occurred mid-October and lasted until early May, and the median national peak occurred in early February (Rose et al. 2018).

The clinical manifestations of RSV infection vary and depend on age, general immune status, RSV serum antibody titer and other pre-existing conditions of the infected individuals [reviewed in (Collins and Karron 2013)]. Newborns mostly develop upper respiratory tract infections (URI) only, since they are protected by the maternal antibodies against LRI. With decreasing maternal antibody protection due to antibody decay (Figure 3), infants 6 weeks to 9 months of age develop URI with up to 40% developing LRI with bronchiolitis and pneumonia that are the primary manifestations of RSV-associated LRI. Less frequently RSV also causes croup. In most instances, the URI are uneventful and recovery occurs after an illness of 7 to 12 days. A major problem that can cause additional complications is that infants infected with RSV often feed poorly, since the nasal obstruction prevents adequate respiration during feeding. The reasons for hospitalization due to RSV-associated LRI can range from bronchiolitis to severe pneumonia. LRI are associated with cough, sneezing, low-grade fever, wheezing, profuse rhinorrhea, and frequently otitis media. With increasing age and number of re-infections the disease severity usually decreases. Symptomatic infections in normal adults are common and usually are mild, but patients may develop rhinorrhea, pharyngitis, cough and bronchitis. The disease usually lasts about 5 days. Underlying pulmonary or cardiac diseases as well as immunocompromised individuals are at greater risk for RSV-ALRI.

1.1.1.4. Vaccine and antiviral therapies

Extensive research on various vaccine strategies and antiviral therapies has not thus far yielded a licensed vaccine or effective antiviral drug against RSV. The first attempt to create a vaccine against RSV infection was made in the 1960s. Formalin-inactivated RSV (FI-RSV) was evaluated as a vaccine in infants and children. The immune response to FI-RSV did not protect from infection but rather caused RSV disease enhancement upon infection in the following RSV season that resulted in the deaths of two vaccinees (Kapikian et al. 1969, Kim et al. 1969). FI-RSV induced antibodies with poor neutralization activity and primed for a $CD4^+$ T helper cell response more biased towards T helper type 2 (Th2) than type 1 (Th1), which is believed to be a major cause of vaccine-induced enhanced disease (Acosta et al. 2015, Knudson et al. 2015). FI-RSV or subunit vaccines are associated with disease enhancement in RSV-naïve but not RSV-experienced individuals.

Immunization of RSV-naïve individuals, such as infants, with live-attenuated vaccine candidates does not cause enhanced disease upon subsequent natural RSV infection (Wright et al. 2007). Hence, the pediatric vaccines (for RSV-naïve individuals) under development focus on live-attenuated RSV and live-attenuated vectored vaccines. In addition, subunit vaccines are being developed for RSV-experienced individuals, particularly for maternal vaccination and for the elderly.

Various live-attenuated RSV vaccine approaches are being evaluated in Dr. Peter Collins' laboratory at the Laboratory of Infectious Diseases (LID) of the National Institute of Allergy and Infectious Diseases (NIAID) within the National Institutes of Health (NIH). The two main strategies being pursued are (i) live-attenuated RSV vaccine candidates and (ii) live-attenuated vectored vaccines:

For live-attenuated RSV vaccine candidates, various attenuating mutations are being evaluated, such as temperature-sensitive mutations and/or the deletion of genes [e.g. SH and M2-2 (Bermingham and Collins 1999)] that impart an attenuating phenotype but maintain its immunogenicity. The optimal balance between attenuation and sufficient immunogenicity has been difficult to achieve and various vaccine candidates have been evaluated in phase I clinical trials (Karron et al. 2015).

Live-attenuated vectored vaccines that express RSV F protein from an added gene also are being developed as candidate pediatric RSV vaccines. Different vector backbones [human parainfluenza virus type 1 (HPIV1) (Mackow et al. 2015), bovine/human parainfluenza virus type 3 (B/HPIV3) (Liang et al. 2014), and MPV (Brock et al. 2018)] have been evaluated, and the immunogenicity of RSV F could be improved by a variety of modifications. Recently it has been found that the F protein can be locked by structural modifications in the pre-F conformation to stabilize the highly neutralizing antigenic site Ø that is lost in the post-fusion conformation (McLellan et al. 2013, Krarup et al. 2015). Codon-optimization of the RSV F ORF and replacing the transmembrane and cytoplasmic tail (TMCT) domain of RSV F with the TMCT domain of the vector F protein, making it compatible to the vector proteins, increased expression and incorporation into vector particles, respectively (Liang et al. 2014, Liang et al. 2016). All current vaccine candidates were made by reverse genetics (Collins et al. 1995, Durbin et al. 1997) that provided the benefit of short passage history, rational vaccine design and the possibility of deletion and introduction of entire genes.

In addition to the live-attenuated vaccine approach, different research groups and companies are also continuing to develop subunit vaccines for elderly and pregnant women [reviewed in (Mazur et al. 2018)]. The objective of these subunit vaccines are to boost the antibody titer to provide protection for the elderly and increase the maternally-derived antibody titer for newborn. Subunit vaccines should be a feasible approach for these groups as disease enhancement does not develop in individuals with previous RSV exposure. A live-attenuated vaccine approach might be difficult for this population due to the presence of serum antibodies against RSV and/or the viral vector. Pre-F-based and other RSV F- and G-based subunit vaccines

as well as various virus like particle- (VLP) and nanoparticle-based approaches are under development, and some of them are tested in clinical trials (Mazur et al. 2018).

Ribavirin, a nucleoside analog inhibitor, is licensed as an antiviral treatment for RSV, but it is not recommended for routine use in pediatric patients (American Academy of Pediatrics Subcommittee on Diagnosis Management of Bronchiolitis 2006). The only licensed and effective prophylaxis for RSV infection is a monoclonal antibody-based passive immunoprophylaxis specific for RSV F protein. It was licensed under the name Synagis (palivizumab) by MedImmune in 1998 and is a humanized murine monoclonal antibody (MEDI-493) in which the complementarity-determining regions (CDRs) of the murine monoclonal antibody 1129 (Beeler and van Wyke Coelingh 1989) were recombinantly transferred onto a human immunoglobulin G (IgG) subclass 1 backbone (Johnson et al. 1997). Due to its high cost, its use is limited to infants at high risk for developing a severe RSV disease, such as premature infants, those with pulmonary abnormalities, or congenital heart disease (American Academy of Pediatrics Committee on Infectious Diseases Guidelines Committee 2014). Therefore, there is no prophylaxis or antiviral treatment available for general use in infants and the elderly that are at the highest risk of severe RSV infections.

1.1.2. Genome-wide siRNA high-throughput screen

Suppression of cellular protein expression using small interfering RNA (siRNA) emerged as a powerful tool to examine the functions of individual proteins. During virus infection, certain host proteins are utilized by the virus for efficient replication, while some host factors inhibit replication as part of the host antiviral defense. Knockdown of host protein expression offers a great tool to identify both types of proteins and can be performed on a large scale. Genome-wide siRNA libraries are readily available and allow the screen for potential pro- and anti-viral host-factors in a high throughput manner. A number of siRNA screens have been performed for viruses such as human immunodeficiency virus, Influenza, Flaviviruses, and other pathogens (Hirsch 2010). Novel host proteins involved in the viral replication cycle, as well as antiviral factors, have been identified that have contributed significantly to the understanding of host-virus interactions during infection.

1.1.2.1. RNA interference (RNAi)

RNAi is a process of post-transcriptional gene silencing resulting in reduced protein expression. RNAi is a naturally occurring phenomenon that is conserved in most eukaryotes to regulate gene expression and provide a rudimentary immune response (Hannon 2002, Ambros 2004). RNAi can be divided into two different groups of effectors that mediate different silencing mechanisms [reviewed in (Meister and Tuschl 2004)]: siRNA and micro RNA (miRNA) (Figure 4). miRNAs, encoded by the cellular genome, naturally regulate messenger RNA (mRNA) translation and are transcribed by RNA polymerase II. The primary miRNA (pri-miRNA) transcripts are 5’

capped, 3' polyadenylated RNAs and contain a stem-loop structure. The pri-miRNA is cleaved by the Drosha enzyme complex in the nucleus and forms the pre-miRNA hairpin that is exported to the cytoplasm by Exportin 5. miRNAs possess partial complementarity to the target mRNA, which is their characteristic for inhibiting mRNA translation.

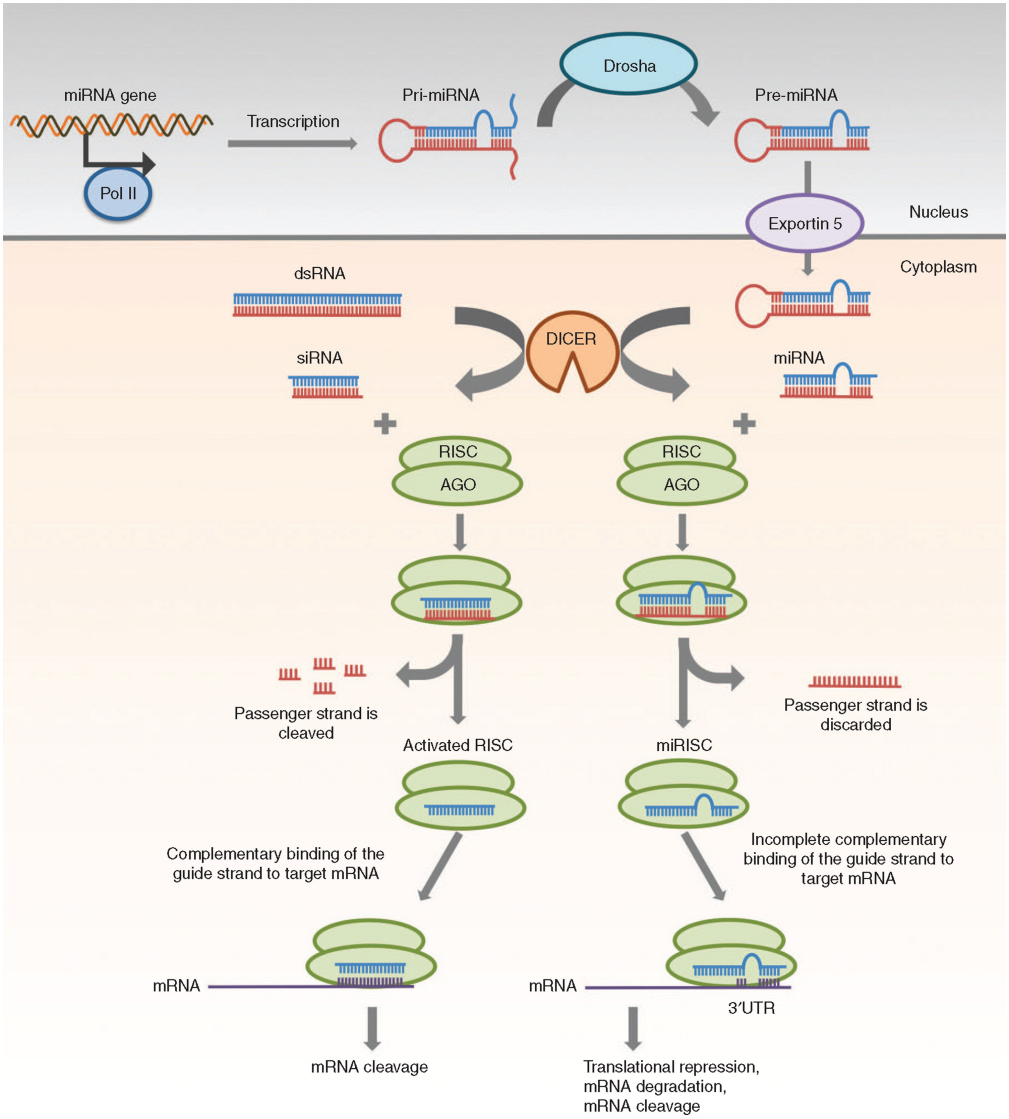

Figure 4: **Mechanism of RNA interference (RNAi) by siRNA (left) and miRNA (top and right).** The schematics shows the differences between siRNA and miRNA processing and gene silencing. miRNA precursor is transcribed by RNA polymerase II (Pol II) and processed by Drosha prior to the export via Exportin 5 from the nucleus. Double stranded RNA (dsRNA) and pre-miRNA are processed by Dicer to siRNA or miRNA, respectively, and loaded into the RNA-induced silencing (RISC) complex. Synthetic siRNA also can be directly transfected into the cell. The passenger strand is cleaved (siRNA) or discarded (miRNA). The RISC is led by the guide strand to the target mRNA. siRNA requires full complementarity that results in the target mRNA cleavage. miRNA binds to partially complementary target sequences and causes translational inhibition and mRNA degradation. Schematic obtained from (Lam et al. 2015).

On the other hand, siRNAs are derived from long double-stranded RNAs (dsRNAs) present in the cytoplasm and are processed similarly as the exported pre-miRNAs. Both are processed by the ribonuclease III-like enzyme (Dicer) into RNA duplexes of 21 to 23 nucleotides (nt) in length with a 3' 2 nt overhang. These processed short dsRNAs are incorporated into the RNA-induced silencing complex (RISC) (Agrawal et al. 2003). The endonuclease argonaute 2

(AGO) of the RISC complex cleaves or discards the passenger strand of the siRNA and miRNA, respectively. The remaining siRNA guide strand (antisense) of the activated RISC binds to its complementary target sequence on mRNAs and initiates the cleavage by AGO. siRNAs only bind to fully complementary target sequences. Hence, it causes specific mRNA cleavage and expression silencing. In principal, siRNAs target one specific mRNA, however off-target effects can occur that cause siRNA-nonspecific effects and are discussed later. miRNAs, on the other hand, bind to the target mRNAs with partial complementarity and therefore, can bind to different mRNA sequences, resulting in the translation inhibition, mRNA degradation and/or mRNA cleavage of various mRNAs. miRNAs typically bind to the 3'UTR of the mRNA and cause the translational repression, whereas siRNAs always mediate cleavage of its target mRNA (Figure 4).

1.1.2.2. Knockdown of gene expression in mammalian cells using siRNA

RNAi induced by artificially introduced dsRNA was first described in *Caenorhabditis elegans* by the Nobel prize-awarded work of Andrew Fire and Craig C. Mello in 1998 (Fire et al. 1998). *C. elegans* allowed the introduction of long dsRNA that was processed to siRNAs by Dicer and induced gene silencing. However, the transfection of long dsRNA into mammalian cells induces the innate immune response pathways, such as the activation of the dsRNA-dependent protein kinase (PKR) that results in the sequence-unspecific degradation of RNAs. To avoid the induction of the innate immune response, synthetic pre-processed siRNAs can be introduced into mammalian cells. The first siRNA knockdown in mammalian cells was successfully performed in 2001 (Elbashir et al. 2001). Since then, many approaches to deliver siRNAs into mammalian cells have been developed. Target-specific synthetic siRNAs are commercially available and can be transfected into many different mammalian cells, without inducing the innate immune response. Another way of introducing siRNAs for the knockdown of a cellular protein is the introduction of short hairpin RNA (shRNA) -expressing DNA vectors, either by transient transfection or via retroviral vectors (Lam et al. 2015). shRNAs are processed by the cell in a miRNA-like manner (as described in section 1.1.2.1 and Figure 4) but its product has siRNA characteristics and only targets fully complementary mRNA sequences and therefore leads to specific mRNA degradation (Hannon 2002).

With the rise of high-throughput siRNA screens and the vast availability of synthetic siRNAs, it was discovered that siRNAs also can target mRNAs nonspecifically. So-called "off-target effects" can be induced by partial complementarity of the siRNA similar to miRNAs. The seed region of the siRNA sequence, nucleotide positions 2 to 8, has been shown to have the dominant effect in regards to off-target effects and might bias the siRNA screen results (Franceschini et al. 2014).

1.1.2.3. Identification of pro-viral host factors for RSV

Previously, a genome-wide siRNA screen had been performed in collaboration with Dr. Scott E. Martin at the National Center for Advancing Translational Sciences (NCATS) to identify pro-viral host factors for RSV. Human lung epithelial A549 cells were used and individual host proteins were knocked down by transfection with individual siRNAs. The siRNA library "Ambion Silencer Select" contained three siRNAs per gene targeting over 22,000 genes. The effect on RSV replication was evaluated by viral GFP expression from a recombinant RSV-GFP virus that expressed enhanced GFP from an added gene inserted between the P and M genes in the viral genome (Munir et al. 2008). At 48 h post siRNA transfection, the cells were infected with RSV-GFP and the GFP intensity, as a reporter for viral infection and replication, was quantified 48 h post infection. The results were compared with non-targeting negative siRNA and a common seed analysis was performed to identify off-target effects within the siRNA screen (Marine et al. 2012). The median seed-corrected Z-score was calculated for each gene target that factors out the influence of possible off-target effects. The corrected Z-score is calculated by subtracting the median Z-score for all siRNAs which have the same seed sequence as the siRNA. The calculated median corrected Z-score is used to rank genes in order of likelihood of confirmation. The strongest median seed adjusted Z-score of - 2.83 was obtained for the host gene ATP1A1 (ATPase Na^+/K^+ transporting subunit alpha 1; GenBank[1] Gene ID: 476), which was selected for further characterization in this study.

Other hits of the same high-throughput screen have been independently characterized. It has been postulated that the actin-related protein 2 (ARP2), identified as another pro-viral factor in the same siRNA screen, plays a role in viral spread during RSV infection (Mehedi et al. 2016).

1.1.3. Na^+, K^+-ATPase

1.1.3.1. Physiological role

The sodium, potassium ATPase (Na^+, K^+-ATPase) is a plasma membrane protein essential for all animal cells. In 1957 it was discovered by Jens Christian Skou, who received the Nobel prize for this work in 1997 (Skou 2004). Na^+, K^+-ATPase actively transports Na^+ and K^+ across the plasma membrane against their concentration gradient in an adenosine triphosphate (ATP)-dependent manner. The hydrolysis of the terminal phosphate of ATP provides the energy for the pump to transport three Na^+ ions out of the cell in exchange for two K^+ ions into the cell per ATP hydrolysis (Kaplan 2002). Na^+, K^+-ATPase maintains the electrochemical gradient and resting potential of the cell that is essential for many physiological processes. For example, the Na^+, K^+-electrochemical gradient is needed as a driving force for secondary active membrane protein transport of ions (e.g. H^+, Ca^{2+}, Cl^-, PO_4^{3-}, SO_4^{2-}) and substrates (e.g. glucose and amino acids). It also provides the neuronal signaling potential and is involved in controlling the cell volume by maintaining the osmotic balance. Na^+, K^+-ATPase plays a primary role in the

[1] https://www.ncbi.nlm.nih.gov/genbank

reabsorption of sodium and water in the kidney and is essential in the maintenance of body fluid and electrolyte homeostasis (Blanco and Mercer 1998).

Beside its pumping function of Na^+ and K^+ ions, it also has been described as signal transducer induced by the binding of cardiotonic steroids (CTS) at the ectodomain, which will be described in more detail in the following sections.

1.1.3.2. Structure and function

The Na^+, K^+-ATPase belongs to the family of the P-type ATPases, a family that contains more than 300 members. P-Type ATPases form an acyl phosphate intermediate during the ATP hydrolysis where the terminal (gamma-) phosphate of ATP is transferred to an aspartate residue within a conserved seven amino acid motif of the phosphorylation (P) domain of the Na^+, K^+-ATPase. The most common amino acid motif of P-type ATPases, beginning with the aspartate, is DKTGTLT (Kaplan 2002).

For the transport of Na^+ and K^+ ions across the plasma membrane the Na^+, K^+-ATPase cycles between the conformational E1 and E2 state [reviewed in (Jorgensen et al. 2003, Morth et al. 2011)]: Its conformational change is facilitated by ATP hydrolysis. Three Na^+ ions bind intracellularly to the membrane transport domain in the E1-ATP state of the ATPase. ATP hydrolysis causes the transfer of the phosphate to the P-domain resulting in a conformational change of the actuator (A) domain to the E2P state, allowing the Na^+ ions to be released to the extracellular side in exchange for two K^+ ions. The E2P state closes that leads to the E2P dephosphorylation and the occluded E2 state. Upon binding of ATP to the nucleotide binding- (N) domain, the conformation changes to the initial E1-ATP state that results in the release of the bound K^+ ions into the cell, binding of Na^+ ions, and the restart of the cycle.

The Na^+, K^+-ATPase complex contains an α-, ß-, and most often also a γ- (FXYD protein) subunit (Figure 5) (Morth et al. 2011, Reinhard et al. 2013). The ß- and γ-subunits are important for the transport properties of the Na^+, K^+-ATPase and also stabilize the complex (Geering 2008). The α-subunit is the major subunit of the Na^+, K^+-ATPase complex and contains ten transmembrane helices that embed the protein complex in the plasma membrane and forms the ion channel (Figure 5). It also provides its major cytoplasmic domains for the ATPase function (Figure 5): actuator- (A, yellow), nucleotide binding- (N, red) and phosphorylation- (P, blue) domain.

Humans express four different α-subunit isoforms (α1 - α4) whose expression profile is cell type-specific (Blanco and Mercer 1998, Reinhard et al. 2013). The α1-isoform ATP1A1 is the most common isoform, is expressed ubiquitously on the plasma membrane of all cells, and is the predominant isoform in human airway epithelial A549 cells (Liu et al. 2016). Minor amounts of the α3-isoform (ATP1A3) have been found in A549 cells, but are 50-fold reduced compared to ATP1A1 (Liu et al. 2016). In the ciliated epithelial cells lining the nasopharynx and the bronchi of both mice and humans, Na^+, K^+-ATPase bearing ATP1A1 is present in greater abundance on the

basolateral surfaces and in lower abundance on the apical surface; it also is readily detected in human alveolar cells including on the luminal surface (Nieto-Torres et al. 2014, Uhlen et al. 2015, Human Protein Atlas 2018).

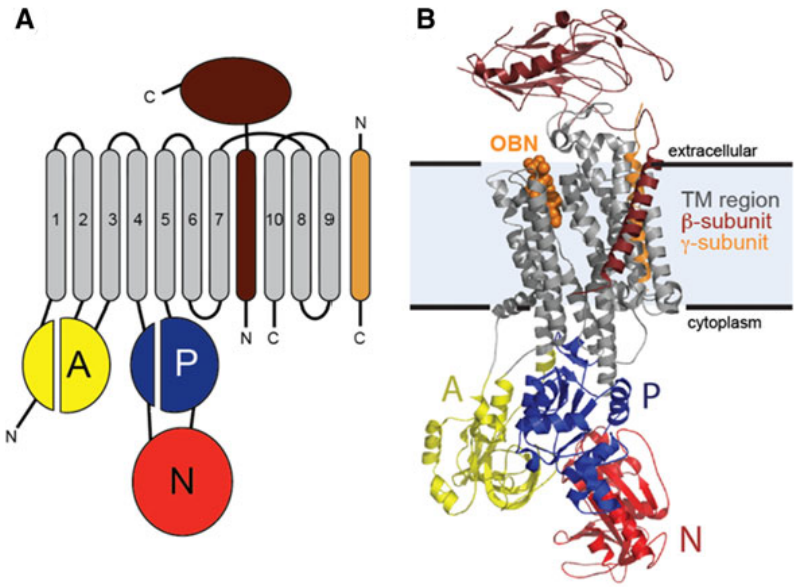

Figure 5: **Structure of the Na^+, K^+-ATPase. (A)** Schematic presentation of the transmembrane orientation of the α- (gray), ß- (brown) and γ- (orange) subunits of the Na^+, K^+-ATPase. The cytoplasmic ATPase domains are color-coded and show the actuator- (A, yellow) nucleotide binding- (N, red) and phosphorylation- (P, blue) domains. **(B)** Crystal structure of the Na^+, K^+-ATPase complex with bound ouabain (OBN, shown as orange molecule). Adapted from (Reinhard et al. 2013).

A proportion of Na^+, K^+-ATPase is localized in caveolae due to the interaction of two caveolin-binding motifs of ATP1A1 with caveolin-1 (Xie and Cai 2003, Reinhard et al. 2013). Caveolae are membrane invaginations on the plasma membrane that are assembled by caveolin-1 at microdomains that are rich in cholesterol and sphingolipid. In addition, caveolae are considered specialized “signaling organelles” since they contain many signal transduction molecules (e.g. Src, EGFR, Raf, MEK, ERK, PI3-kinase and others that also are involved in ATP1A1-mediated signaling, described in more detail in 1.1.3.4) and can facilitate the crosstalk of signaling pathways (Razani et al. 2002). Caveolae also are involved in the caveolin-mediated endocytosis [reviewed in (Conner and Schmid 2003)].

ATP1A1 also contains an extracellular binding site for CTS, such as ouabain (Figure 5B) which in effective doses (≥µM concentrations) inhibit the Na^+, K^+-ATPase ion pump activity. CTS bind selectively to the E2P state and lock it in this state, resulting in the inhibition of the ion pump function (Kaplan 2002). On the other hand, if CTS are present in sub-nanomolar concentrations, it does not inhibit the pumping activity, but has a hormone-like effect and induces ATP1A1-mediated signaling (described in section 1.1.3.4. Na^+, K^+-ATPase signalosome). The sensitivity of ATP1A1 to CTS varies among isoforms and is different between species. For example, human ATP1A1 is relatively more sensitive to ouabain compared to the rodent ATP1A1 counterpart, which lacks the ouabain binding motif that results in a low affinity to ouabain and is therefore insensitive to it (Xie and Cai 2003).

1.1.3.3. Cardiotonic steroids (CTS)

The family of CTS are naturally derived compounds that can bind to the Na^+, K^+-ATPase and affect the performance of the heart. The compounds of this family are natural toxins and have been found as secondary metabolites in plants and several toad species (Melero et al. 2000). They all share common structural motifs [reviewed in (Prassas and Diamandis 2008)]: CTS contain a steroid core, which is considered to be responsible for the activity and binding of these compounds to ATP1A1. The steroid core contains a sugar moiety and an unsaturated lactone. The lactone moiety defines the subgroup of the CTS. Bufadienolides (derived from toads) possess a six-membered pyrone ring (Figure 6A), whereas cardenolides (derived from plants, e.g. digitalis from the foxglove plant) have a five-membered butyrolactone ring (Figure 6A). Bufalin and ouabain are examples of each of these subgroups, respectively (Figure 6).

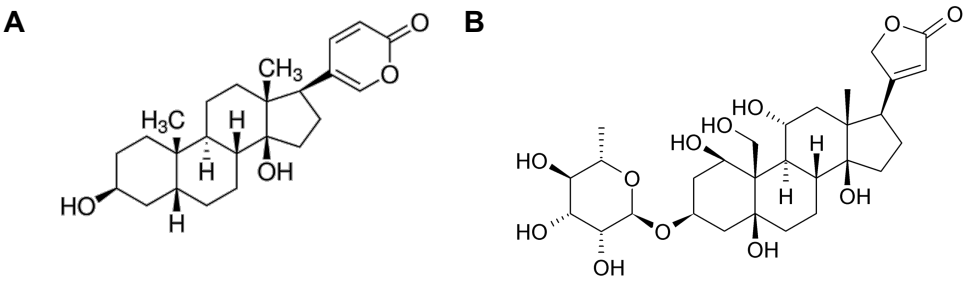

Figure 6: **Chemical structure of the CTS Bufalin (A) and Ouabain (B),** as example structures for the CTS subgroups of bufadienolides and cardenolides, respectively.

These compounds show positive effects on the performance of the heart and have been used traditionally (over 200 years) to treat congestive heart failure and cardiac arrhythmia. The FDA approved drug for it is Digoxin (Drug Name Lanoxin, FDA Application Number: 40-282). Due to the inhibition of the Na^+, K^+ pump activity of the Na^+, K^+-ATPase, the cytoplasmic Na^+ concentration is increased which inhibits the cellular Na^+, Ca^{2+} exchange that leads to higher level of intracellular Ca^{2+} in cardiac myocytes. The increase of Ca^{2+} results in a positive inotropic effect which increases the cardiac contractile force (Prassas and Diamandis 2008).

The best characterized CTS is ouabain (PubChem CID[2]: 439501), which could be considered the prototype of CTS. Ouabain is the most hydrophilic CTS and has been extensively studied in cardiovascular research. Ouabain has been found endogenously in humans and is associated with hormone-like effects (Schoner and Scheiner-Bobis 2007). It has been shown that continuous administration of ouabain causes hypertension in rats (Manunta et al. 1994) and elevated levels of endogenous ouabain also are associated with hypertension in humans (Schoner and Scheiner-Bobis 2007). It also had been reported that ouabain has antiviral effects for various viruses, such as coronavirus (Burkard et al. 2015), herpes simplex virus (Dodson et al. 2007, Su et al. 2008), chikungunya virus (Ashbrook et al. 2016), human immunodeficiency virus (Wong et al. 2013), adenovirus (Grosso et al. 2017), and porcine reproductive and respiratory syndrome virus 1 (Karuppannan et al. 2012). However, in none of these studies was the antiviral mechanism further elucidated.

[2] Compound ID (CID) number of the PubChem database (https://pubchem.ncbi.nlm.nih.gov)

1.1.3.4. Na^+, K^+-ATPase signalosome

Besides its ATPase and ion channel function, ATP1A1 of the Na^+, K^+-ATPase can form protein-protein complexes and can engage in signal transduction (Figure 7) [reviewed in (Reinhard et al. 2013)]. ATP1A1 does not possess a known cytoplasmic signaling domain, but it has been shown that ATP1A1 localized in the caveolae is associated with the cellular non-receptor tyrosine kinase c-Src and is thought to be involved in signal transduction via c-Src activation and most often EGFR transactivation (Liu et al. 2003, Wang et al. 2004). CTS can have hormone-like effects if present in nanomolar concentrations that are not inhibiting the ion channel function of ATP1A1 (Reinhard et al. 2013). ATP1A1 has been well-characterized as a sole receptor for CTS, such as ouabain. CTS-induced ATP1A1 signaling can regulate blood pressure and influences cellular processes (e.g. proliferation, differentiation and metabolism) (Schoner and Scheiner-Bobis 2007).

C-Src is part of the Src kinase family and consists of an SH3, SH2, and kinase domain (Boggon and Eck 2004). The SH2 and kinase domains of c-Src interact with the cytoplasmic domain 2 and 3 of ATP1A1 (Tian et al. 2006). Upon ouabain binding, the ATP1A1 cytoplasmic domain undergoes conformational changes and activates the c-Src kinase by releasing the catalytic core of the Src kinase domain and autophosphorylation of Src Tyr418 (Tian et al. 2006). c-Src is the only known signaling kinase associated with ATP1A1 and is the immediate effector of ouabain-induced ATP1A1 signaling.

Multiple downstream signaling pathways can be triggered by ouabain-induced ATP1A1 signaling [Figure 7, reviewed in (Xie and Cai 2003, Reinhard et al. 2013)] including the induction of the following:

(i) Phospholipase C-gamma (PLC-γ) pathway. Activation occurs by the phosphorylation of the PLC-γ protein via c-Src kinase. PLC-γ hydrolysis phosphatidylinositol 4,5-biphosphate (PIP2) that results in the increase of 1,2-diacylglyerol (DAG) and inositol 1,4,5 triphosphate (IP3). Latter is recognized by the IP3-receptor that can result in the release of calcium from the endoplasmic reticulum.

(ii) Classical mitogen activated protein kinase (MAPK) pathway. The classical MAPK cascade includes Src-EGFR-Shc-Grb2 (growth factor receptor-bound protein 2) -SOS (Son of Sevenless) and involves Raf (MAP3K), MEK (mitogen-activated protein kinase kinase, MAP2K) and MAPK (ERK1/2). The MAPK signaling cascade can influence cellular processes, such as proliferation, differentiation, migration and metabolism.

(iii) Phosphoinositide 3-kinase (PI3K) pathway. PI3K can be activated by c-Src (Wages et al. 1992, Pleiman et al. 1994) but the N-terminus of ATP1A1 also is able to interact directly with PI3K. This complex together with EGFR is able to attract AP2 (adaptor protein-2) and clathrin that result in the formation of clathrin-coated pits and endocytosis of Na^+, K^+-ATPase; a mechanism to downregulate the level of Na^+, K^+-ATPase on the plasma membrane (Liu et al. 2004).

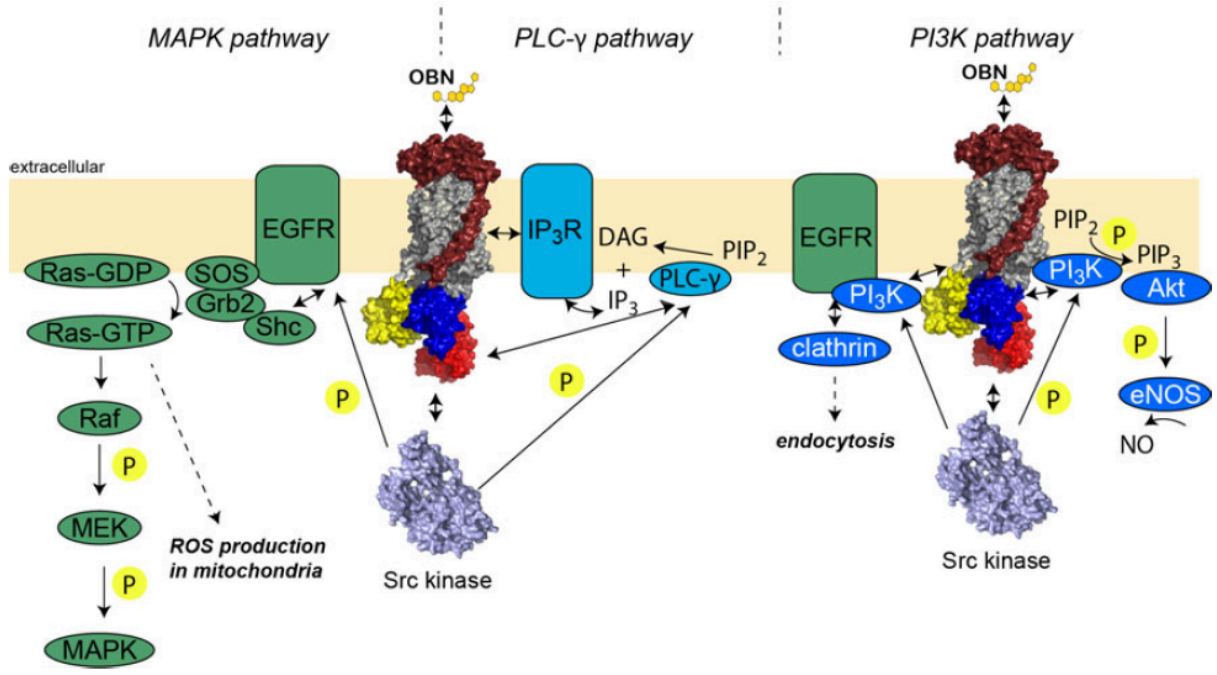

Figure 7: **Overview of ATP1A1-mediated signaling pathways that are induced by Ouabain (OBN).** MAPK, mitogen activated protein kinase; EGFR, epidermal growth factor receptor; Shc, Src homology and collagen; Grb2, growth factor receptor-bound protein 2; SOS, son of sevenless; GDP, guanin triphosphate; GTP, guanin diphosphate; Raf, rapidly accelerated fibrosarcoma kinase; MEK, mitogen-activated protein kinase kinase; PLC-γ, phospholipase C-gamma; IP_3R, inositol 1,4,5-triphosphate receptor; PIP2, phosphatidylinositol 4,5-biphosphate; DAG, 1,2-diacylglycerol; IP3, inositol 1,4,5-triphosphate; PI3K, phosphoinositide 3-kinase; Akt, protein kinase B; eNOS, endothelial nitric oxide synthase (Ahmed and Prigent 2017). Obtained from (Reinhard et al. 2013)

Most of the ATP1A1-mediated pathways involve c-Src as an immediate downstream signaling partner that transactivates EGFR or other effectors. Thus, c-Src and EGFR play a central role in ATP1A1-initiated signaling.

EGFR is a receptor tyrosine kinase. Upon EGF binding at the EGFR ectodomain, the receptor dimerizes and the cytoplasmic domain is autophosphorylated, resulting in the induction of downstream signaling [reviewed in (Wee and Wang 2017)]. EGFR can also be phosphorylated by c-Src, in an EGF-independent manner, at otherwise atypical Tyrosine residues (i.e. Tyr845 or Tyr1101) (Biscardi et al. 1999, Donepudi and Resh 2008). The c-Src-mediated phosphorylation of EGFR triggers macropinocytosis (Donepudi and Resh 2008), similar to the well characterized EGF-induced macropinocytosis (Hewlett et al. 1994, Swanson and Watts 1995).

1.1.3.5. PST2238 (rostafuroxin) – an anti-hypertensive drug

PST2238, also named rostafuroxin, (PubChem CID: 153976) is a synthetic digitoxigenin derivative with the chemical name 17β-(3-Furyl)-5β-androstane-3β,14β,17α-triol (Figure 8). PST2238 was identified in a chemical compound screen to selectively bind Na^+, K^+-ATPase and to possess anti-hypertensive activity (Quadri et al. 1997).

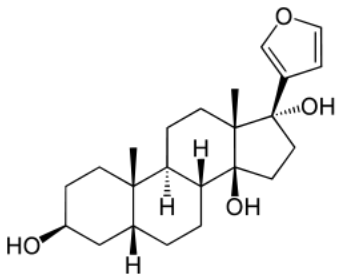

Figure 8: **Chemical structure of PST2238** (17β-(3-Furyl)-5β-androstane-3β,14β,17α-triol).

PST2238 has been shown to bind to the ouabain-binding site of ATP1A1 and is able to competitively displace ouabain (Ferrari et al. 1998). Binding of PST2238 does not affect the ion pump activity of the Na^+, K^+-ATPase and antagonizes the ouabain-induced hypertension in rats, due to the competitive displacement of ouabain from its binding site at the ATP1A1 ectodomain (Ferrari et al. 1998, Ferrandi et al. 2002).

PST2238 has also been tested in clinical trials as an anti-hypertensive drug for hypertension induced by elevated levels of endogenous ouabain. It lowered the blood pressure in hypertensive patients, but had no effect on the normal blood pressure of healthy individuals (Ferrari et al. 2006).

1.1.3.6. Aim of this study

The host-virus interactions are not well understood for RSV. A previously performed genome-wide siRNA screen was an attempt to gain a better understanding of the cellular factors playing a role in infection. This screen identified ATP1A1 as a potentially important pro-viral factor for RSV. The objective of this research project was to validate the screen results and characterize the role of ATP1A1, its pro-viral mechanism, and the associated pathways during RSV infection. Besides investigating the mechanistic role of ATP1A1 in facilitating RSV infection, chemical compounds that specifically act on ATP1A1 were evaluated for their antiviral activity to establish a foundation for developing an antiviral drug for RSV disease.

1.2. Development and pre-clinical evaluation of a human parainfluenza virus type 1 (HPIV1)-vectored Ebola virus vaccine.

The 2014 Ebola virus (EBOV) outbreak in West Africa and the resulting WHO declaration of an international health emergency prompted our laboratory to pursue the development of live-attenuated HPIV-vectored EBOV vaccines. Peter Collins' laboratory at the LID, NIAID, NIH had previously developed HPIV3-expressing EBOV envelope glycoprotein GP as an intranasal vaccine candidate that was evaluated in non-human primates (NHPs) (Bukreyev et al. 2006, Bukreyev et al. 2007, Bukreyev et al. 2009). In addition, HPIV1 and HPIV3 had been extensively characterized as live-attenuated vaccine vectors for RSV (Liang et al. 2014, Mackow et al. 2015, Liang et al. 2016, Liang et al. 2017, Liu et al. 2017) and provided a promising foundation for a rapid development of HPIV-vectored EBOV vaccine candidates.

1.2.1. Ebola virus (EBOV)

1.2.1.1. Phylogeny of *Filoviridae*

EBOV is an enveloped, non-segmented, negative-sense RNA virus that belongs to the order *Mononegavirales* and family *Filoviridae* (Figure 1), which consists of three genera: *Marburgvirus*, *Ebolavirus*, and *Cuevavirus* (Misasi and Sullivan 2014). The genus *Ebolavirus* has five known species: Zaire, Sudan, Bundibugyo, Tai Forest, and Reston (Amarasinghe et al. 2018); and a recently characterized new proposed species, named Bombali (Goldstein et al. 2018). Zaire EBOV (ZEBOV) is the most pathogenic species and caused the 2014 - 2016 outbreak in West Africa. The ZEBOV variant Mayinga, the prototype strain, was isolated from the first outbreak in 1976 (WHO 1978). The Makona variant of ZEBOV was responsible for the 2014 - 2016 outbreak in West Africa.

1.2.1.2. Genome organization and replication

The EBOV genome is a negative-sense single-stranded RNA of approximately 19 kb and encodes for seven viral proteins, namely (in 3' to 5' gene order) the nucleoprotein (NP), virion protein (VP) 35 (comparable to a P protein), VP40 (comparable to an M protein), glycoprotein GP, VP30 (a novel nucleocapsid protein), VP24 (a novel, minor matrix protein) and the viral polymerase L (Figure 9) (Feldmann et al. 2013). The genome structure is typical for the order *Mononegavirales*: the genome is flanked by 3' leader and 5' trailer sequences that contain the promoter sequences for transcription and replication initiation. Each gene is flanked by GS and GE sequences. Several genes overlap with each other (Figure 9). The adjacent genes that do not overlap are separated by an IG sequence that is variable between different junctions (Feldmann et al. 2013).

The viral genome is encapsidated by NP and associated with the transcriptional activator VP30 that supports primary transcription and RNA editing (Baseler et al. 2017). The transcription and replication of the viral genome is performed by the viral polymerase L that is associated with

the cofactor VP35, which is the equivalent of the P protein of other mononegaviruses (Baseler et al. 2017). VP40 and VP24 are the major and minor matrix proteins, respectively, and have a role in the assembly and budding of the filamentous virions (Feldmann et al. 2013).

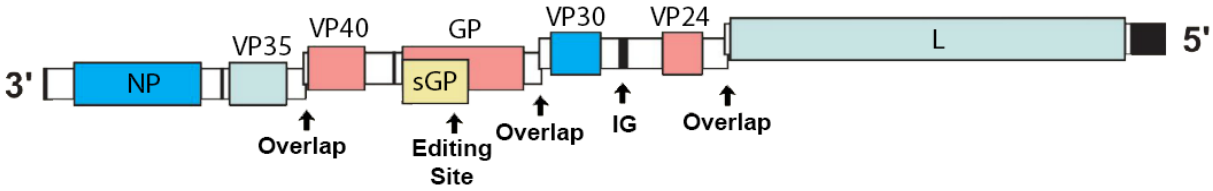

Figure 9: **Genome structure of EBOV.** Genes are color-coded for their general location in the virion. The nucleoproteins are blue, membrane-associated proteins are red, the polymerase complex is light blue and the nonstructural soluble GP (sGP) is yellow. The gene non-coding regions are white and extragenic sequences are black. IG; intergenic region. Adapted from (Feldmann et al. 2013).

All viral genes contain a single monocistronic ORF, except for GP that expresses, in addition to the transmembrane GP form, two soluble forms: soluble GP (sGP) and small soluble GP (ssGP) (Baseler et al. 2017). The sGP is a 50 - 70 kDa protein encoded by the unmodified GP mRNA. The full-length, transmembrane form of GP (which is sometimes called GP_0) is a 110-160 kDa glycoprotein [676 amino acids [aa], MW varies based on the glycosylation (Volchkov et al. 1998)] encoded by an edited form of the EBOV GP mRNA. A single non-template A residue (mRNA-sense) is added at a specific editing site by transcriptional editing of the viral RdRp that results in a frame shift and encodes for the full-length transmembrane form of GP. It is cleaved by a furin-like protease into two subunits, GP_1 and GP_2 [representing the N-terminal (469 aa) and C-terminal (175 aa) ends of GP_0, respectively; MW approximately 140 and 26 kDa, respectively (Volchkov et al. 1998)] that remain linked by a single disulfide bond (Feldmann et al. 2013). The EBOV GP is a highly glycosylated type I transmembrane protein (i.e., the membrane anchor is near the C-terminus). GP is the sole viral surface glycoprotein and mediates viral attachment and entry (Sanchez et al. 1996) and is the major EBOV neutralization antigen. Vectored vaccines expressing EBOV GP can elicit protective immunity against lethal EBOV challenge in NHPs (Bukreyev et al. 2007, Stanley et al. 2014, Meyer et al. 2015, Mire et al. 2015, Ewer et al. 2016). The vectored vaccine candidates developed in the present study (described in 1.2.4) involved expression of the transmembrane form of EBOV GP from a live-attenuated HPIV1 vector.

1.2.1.3. Epidemiology and pathogenesis

The first EBOV outbreak was documented in northern Zaire (now Democratic Republic of Congo) in 1976 (WHO 1978). The outbreak occurred at a mission hospital in Yambuku, close to the Ebola river that gave the virus its name. Almost simultaneously, another outbreak occurred near Maridi in Sudan. Retrospectively, it was recognized that these two outbreaks of EBOV were independent from each other and were caused by different EBOV species that were named after the countries of origin: Zaire and Sudan (Feldmann et al. 2013).

EBOV is considered to be a zoonotic infection and is initiated by contact with body fluids of EBOV-infected animals. The animal reservoir is uncertain but substantial evidence suggests

that bat species might be the natural reservoir. It has not yet been possible to isolate infectious virus from bats, but indirect evidence, such as viral RNA and EBOV-specific serum antibodies in endemic regions, suggests that bats could be the natural reservoir for EBOV. In addition, experimental inoculation of bats showed viral replication without fatalities, which make them a suitable natural reservoir (Coltart et al. 2017).

Since the discovery of EBOV and prior to the large 2014 outbreak in West Africa, many small outbreaks occurred, but were limited to remote and rural areas in Sudan, Democratic Republic of Congo, Republic of Congo, Gabon and Uganda (Coltart et al. 2017). Due to the geographical isolation, it was easy to contain the outbreaks and they lasted from several weeks to approximately 3 months (Bell et al. 2016).

EBOV can be transmitted from human to human by puncture wounds or contact of a patient's body fluids with skin or mucosal surfaces. Nosocomial transmissions, ceremonial washings, and touching of deceased EBOV-infected persons during burial practices are important routes of transmission. More recently, aerosol transmission via airborne droplets of body fluids has received increased recognition as an important mode of transmission (Osterholm et al. 2015). For example, aerosolized EBOV can cause lethal infection in NHPs and guinea pigs (Johnson et al. 1995) and can be transmitted from infected to naïve animals by aerosols (Jaax et al. 1995, Wong et al. 2015). Guinea pigs infected with aerosolized EBOV are more infectious for naïve animals than those infected intraperitoneally (Wong et al. 2015). This stresses the need to develop an EBOV vaccine capable of inducing both systemic and mucosal immunity, particularly in the respiratory tract.

The incubation period of EBOV infections can last from several days to 21 days, but usually it takes between 7 and 14 days from exposure to the onset of first disease symptoms (Kaner and Schaack 2016). Infected individuals first develop general flu-like symptoms and rapidly progress to advanced disease. EBOV causes severe hemorrhagic fever in humans, multiple organ failure and a shock-like syndrome with case fatality rates ranging from 25 - 90% (Kuhn et al. 2011, Coltart et al. 2017).

1.2.1.4. EBOV outbreak in West Africa (2014 - 2016)

Zaire EBOV caused the 2014 - 2016 EBOV outbreak in West Africa that is the largest outbreak in history with over 28,000 cases and more than 11,000 deaths (Centers for Disease Control and Prevention (CDC) 2016). The affected area is one of the poorest in the world and was not equipped for dealing with an outbreak of this magnitude. The index case of this outbreak was retrospectively identified as a two-year old child in Meliandou in southeastern Guinea (Figure 10) who died in December 2013. It is assumed that family members and the midwife of the child transmitted the virus further. The high mobility of the people in the Kissi tribal area, which includes areas in Guinea, Sierra Leone and Liberia (Figure 10), accelerated the spread into larger, densely populated cities and neighboring countries that resulted in the largest EBOV outbreak in history (Coltart et al. 2017).

Figure 10: **Map of the origin of the EBOV outbreak in West Africa (2014 - 2016).** It shows the Kissi tribal area which spans across the border between Sierra Leone, Liberia and Guinea. The index case of the outbreak occurred in Meliandou, Guinea that is located within the Kissi tribal area in December 2013. Obtained from (Coltart et al. 2017)

The first EBOV case in Liberia (Foya) and Sierra Leone (Kenema) were confirmed on March 30th and May 25th 2014, respectively. On August 8th 2014, the WHO declared the outbreak as an international public health emergency. Many factors made it challenging to contain the outbreak in a quick and effective manner. Major problems were lack of infrastructure in these resource-limited countries as well as cultural and behavioral factors. Traditional burial ceremonies, that include washing and touching of the deceased, were responsible for a large number of transmissions in Guinea during the outbreak (Coltart et al. 2017). In addition, the population did not trust the foreign support and also mistrusted their own government. With international support and public education, it was eventually possible to reduce the number of transmissions by classic epidemiological methods (quarantine and contact tracing). Besides Guinea, Sierra Leone and Liberia, which had the majority of EBOV cases, seven other countries, including the United States and European countries, had EBOV cases that were linked to the West African outbreak due to international travel or health care personnel that were infected during their work in the outbreak area [reviewed in (Coltart et al. 2017)]. It was eventually possible to contain and end the outbreak in 2016. After 42 days (twice the maximum incubation period for EBOV) past the last confirmed EBOV case, which is the WHO criteria to declare the end of an EBOV outbreak, the countries Sierra Leone (March 17th), Guinea (June 1st) and Liberia (June 9th) were finally declared EBOV-free (Coltart et al. 2017).

1.2.2. EBOV vaccine strategies

No vaccine or post-exposure treatment is currently licensed, and the unprecedented scale of the recent outbreak raised concerns of larger outbreaks and spread. This outbreak prompted multiple initiatives with enhanced efforts to develop an EBOV vaccine, and multiple experimental vaccines moved forward into clinical trials during the outbreak. It has been shown that neutralizing

antibodies directed against GP, the viral attachment and fusion glycoprotein, can provide protection against an EBOV infection. Therefore, vaccination to induce an immune response against EBOV GP should be a promising strategy to protect against EBOV infection and to limit further spread. It also has been demonstrated that treatment of rhesus macaques post-EBOV-exposure with a combination of monoclonal antibodies (ZMapp) directed against EBOV GP resulted in the rescue of infected animals from a lethal outcome (Qiu et al. 2014). ZMapp was also used as an experimental treatment during the outbreak (Group et al. 2016).

Most efforts were made to develop vaccine strategies that induce a sufficient serum titer of neutralizing antibodies against the EBOV GP to provide protection. Currently the most advanced vaccine candidate is a recombinant vesicular stomatitis virus (VSV) that expresses Zaire EBOV GP (rVSV-ZEBOV) instead of the VSV glycoprotein G (Garbutt et al. 2004). It protects NHPs against EBOV infection and was administered in ring vaccinations in Guinea during the recent outbreak (Henao-Restrepo et al. 2015). This candidate showed promising immunogenicity in humans. Due to the replication competence of the VSV vector, adverse side effects, such as fatigue, myalgia, headache, fever (subjective), and frequent viremia were observed (Regules et al. 2017).

Another vaccine strategy, which has advanced into clinical trials, is based on the recombinant replication-deficient chimpanzee adenovirus serotype 3 vector that encodes the Zaire EBOV GP and is called ChAd3 ZEBOV (De Santis et al. 2016). It has been previously shown to provide immune protection against EBOV infection in NHPs (Sullivan et al. 2006).

HPIV3 vectors expressing EBOV GP also were developed prior to the outbreak in West Africa. HPIV3 (JS strain) expressing EBOV GP from an added gene (rHPIV3/EboGP) was evaluated as an intranasal mucosal vaccine candidate (Bukreyev et al. 2006, Bukreyev et al. 2007, Bukreyev et al. 2009). In NHPs, one intranasal dose was moderately immunogenic, with 88% protection, but two doses provided complete protection against an intra-peritoneal EBOV challenge. When delivered by aerosol, a single dose of this vaccine conferred 100% protection in NHPs, and was more immunogenic than an alphavirus replicon vaccine (Meyer et al. 2015). In addition, an HPIV3 vector with the deletion of its surface glycoproteins F and HN, and EBOV GP as the sole surface glycoprotein was evaluated. The goal of this construct (PIV3/ΔHNF/EbovZ GP) was to avoid the restriction of vector replication in human population due to pre-existing immunity to HPIV3 F and/or HN (Bukreyev et al. 2009). Initial clinical studies to evaluate safety and immunogenicity of these HPIV3-based vaccine candidates are in progress in the U.S (ClinicalTrials.gov identifiers for HPIV3-EbovZ GP: NCT02564575; and PIV3/ΔHNF/EbovZ GP: NCT03462004).

1.2.3. Human parainfluenza virus (HPIV)

1.2.3.1. Phylogeny of *Paramyxoviridae*

HPIV1 is an enveloped, non-segmented, single-stranded, negative-sense RNA virus that belongs to the genus *Respirovirus* of the family *Paramyxoviridae* within the order *Mononegavirales* (Figure 1). Four serotypes of HPIV are known: HPIV3 belongs to the same genus as HPIV1, whereas HPIV2 and HPIV4 belong to the genus *Rubulavirus* within the family *Paramyxoviridae*. HPIV3 has a bovine counterpart (BPIV3), and a recombinant chimeric form of bovine and human PIV3 (B/HPIV3) has been evaluated as a vaccine for seronegative children in a clinical trial (Karron et al. 2011). B/HPIV3 has the BPIV3 genome backbone with only the surface glycoproteins F and HN substituted with the HPIV3 counterparts (Haller et al. 2000, Schmidt et al. 2000). The B/HPIV3 vector has been developed as an attenuated vaccine vector that induces a protective immune response against HPIV3 and can be used as a bivalent vaccine by expressing an additional foreign protein, such as RSV F (Liang et al. 2014) or the severe acute respiratory syndrome coronavirus (SARS-CoV) spike protein (Bukreyev et al. 2004).

1.2.3.2. Genome organization and viral replication

The HPIV1 genome consists of 6 genes (Figure 11) encoding (in 3' to 5' order) the nucleoprotein (N), phosphoprotein (P/C), matrix protein (M), fusion glycoprotein (F), hemagglutinin-neuraminidase glycoprotein (HN), and the large polymerase protein (L) (Karron et al. 2013). The P gene carries an additional overlapping ORF, with an alternative start codon, expressing the C protein that antagonizes the host interferon and apoptosis responses (Bartlett et al. 2008). HPIV3 shares considerable sequence relatedness and similarities in genome organization with HPIV1. In addition to the C ORF, HPIV3 P gene also carries one additional ORF coding for a D protein that is expressed by RNA editing (Galinski et al. 1992).

Figure 11: **Genome structure of HPIV1.** Gray boxes indicate the gene start (GS, light gray) and gene end (GE, dark gray) sequences flanking each gene. Intergenic (IG) sequences are indicated by lines between the genes.

As it is common for the order *Mononegavirales,* the genome of HPIVs contain a linear array of genes (Figure 11), that each are flanked by GS and GE transcription signals and are separated by IG sequences. HPIVs undergo cytoplasmic gene expression and replication typical for the members of the family *Paramyxoviridae*, as described in 1.1.1.1.

The RNP complex of HPIVs is comprised of the viral RNA that is associated with the viral proteins N, P and L. The nucleoprotein N encapsidates the viral genomic (negative-sense) and anti-genomic (positive-sense) RNAs. It is predicted that each N protein molecule can bind to exactly 6 nt of RNA and this is thought to be the basis for the observation that the paramyxovirus genomes can replicate efficiently only when they are a multiple of 6 nt in length. This phenomenon is called "rule of six" (Calain and Roux 1993, Kolakofsky et al. 1998) and is important to be followed

for generating recombinant viruses and vaccine vector designs to ensure a stable genome that could efficiently replicate.

HPIVs have two surface glycoproteins incorporated into the virion envelope (Karron and Collins 2013); namely, the fusion protein F and the hemagglutinin-neuraminidase glycoprotein HN. HN binds to sialic acid on the host cell and mediates attachment. It also binds to red blood cells and causes hemagglutination or hemadsorption, a property that can be used to detect and quantify virus. In the later phase of infection, the neuraminidase activity of the membrane-incorporated HN protein cleaves nearby sialic acids to facilitate the release of progeny virions. The fusion protein F mediates fusion with the host cell plasma membrane to allow nucleocapsid entry into the cytoplasm. F is expressed as an F_0 precursor that is cleaved by host proteases into the F_1 (the larger, C-terminal fragment) and F_2 (the smaller, N-terminal fragment) subunits that, for the HPIVs, are connected by a single disulfide bond (Karron and Collins 2013). Cleavage is required to expose the fusion peptide at the N-terminus of F_1 which makes PIVs infectious, since it mediates the insertion of the F protein into the plasma membrane for fusion to occur. Many PIVs (HPIV2, HPIV3, BPIV3) have a furin cleavage site (R-X-R/K-R) that allows the ubiquitously available cellular furin protease to cleave and "activate" F_0 in cell culture. HPIV1 (and also Sendai virus and HPIV4) lacks the furin cleavage motif and depends on trypsin-like proteases for cleavage, which *in vivo* are present in mucosal secretions and *in vitro* can be added exogenously to the cell culture medium (Karron and Collins 2013).

1.2.3.3. Epidemiology and pathogenesis

HPIV3 is second only to RSV as a cause of hospitalization in children younger than 5 years of age. Infection with HPIV1 and HPIV2 occurs later in early childhood compared to HPIV3 and RSV (Figure 3), and typically 75% of children have been infected with HPIV1 by 5 years of age (Karron and Collins 2013). The later onset of HPIV1 infections in infants make it suitable for a live-attenuated vector for use in slightly older infants that typically have not yet been exposed to HPIV1 (Figure 3). Due to the possible later time point of vaccination, the maternally-derived antibodies and immature immune system (Figure 3) would interfere less with the efficacy of the vaccination as compared to the vaccination of younger infants.

HPIV infection mostly causes mild URI but can develop clinical manifestations of croup, (most common for HPIV1) or bronchiolitis and pneumonia (typical for HPIV3). The seasonality of HPIVs vary between serotypes. HPIV1 outbreaks occur every other year in odd numbered years, whereas HPIV2 and HPIV3 circulate annually (Abedi et al. 2016).

1.2.4. The development of an HPIV1-vectored EBOV GP vaccine

In a recent study, our laboratory demonstrated that incorporation of RSV F protein in a PIV3 vector particle was substantially enhanced by substituting its TMCT domain with those of the vector F protein (Liang et al. 2016). The TMCT modification also resulted in a significant increase in both the quantity and quality of the RSV-neutralizing serum antibodies. This may

reflect increased immunogenicity of an antigen presented to the immune system in a particle, and also may reflect increased immunogenicity of antigen presented in a native, ordered array (Bachmann et al. 1993). Similar results have been observed for HPIV1 vectors expressing the RSV F protein (Liu et al. 2017). This indicates that, for HPIV3 and HPIV1 vectors, incorporation of a heterologous glycoprotein into the vector particle increases its immunogenicity. It is noteworthy that the incorporation of EBOV GP into the previously developed rHPIV3/EboGP virus particles (described in 1.2.2) was only 13% as efficient as the HPIV3 HN protein, suggestive of inefficient packaging of EBOV GP into an HPIV vector (Bukreyev et al. 2006). Moreover, the HPIV3 JS strain backbone used for developing the rHPIV3/EboGP had not been specifically attenuated and has a potential risk of vector-related respiratory illness (Kapikian et al. 1961), especially in children and the elderly, and thus an attenuated vector would be preferable. Also, the comparative properties of the different types of HPIVs as vectors have not been examined, and it is unclear which type would be the most effective as a human vaccine vector.

Previously, a non-temperature-sensitive attenuating mutation consisting of a 6 nt deletion in the overlapping P and C ORFs called $C^{\Delta 170}$ was introduced in the HPIV1 genome (Bartlett et al. 2007, Mackow et al. 2015). This mutation reduces the ability of the C protein to inhibit the host type I interferon response and apoptosis (Newman et al. 2004, Bartlett et al. 2006, Bartlett et al. 2008), resulting in viral attenuation. Previous evaluation of HPIV1-$C^{\Delta 170}$ as a live-attenuated vaccine backbone for expressing the RSV F glycoprotein showed that it was suitably attenuated for vaccine development (Mackow et al. 2015). In the present study, efforts were made to enhance GP immunogenicity by increasing its packaging in the vector virions and an attenuated HPIV1-$C^{\Delta 170}$ backbone was evaluated to provide an attenuated vaccine expected to be safe for all age groups, including children and the elderly.

1.2.5. Aim of this study

The study was initiated in response to the 2014 EBOV outbreak in West Africa. The aim was to develop live-attenuated rHPIV1-$C^{\Delta 170}$ vectors expressing EBOV GP from two different positions (pre-N or between N-P) of the HPIV1 genome. Two different sites were chosen to determine the effect of GP insert position on HPIV1 attenuation, GP expression, and immunogenicity. To enhance immunogenicity, the EBOV GP ORF was codon-optimized for human expression and the TMCT domains were substituted with those of the HPIV1 F protein in an effort to obtain efficient incorporation into the vector particle. At each site, membrane-anchored EBOV GP was expressed either as a full-length unmodified GP protein, or as a derivative of GP with an HPIV1 F TMCT domain.

The pre-clinical evaluation of these vaccine candidates was performed. All constructs were analyzed *in vitro* for replication and expression of EBOV GP and in NHPs for replication, stability of EBOV GP expression, and immunogenicity. The objective of this EBOV vaccine project was to identify a suitable vaccine candidate for further clinical development as a live-attenuated mucosal vaccine that could elicit protection against a lethal EBOV exposure.

2. Materials and Methods

2.1. Materials

In the following section, the materials are listed that were specifically used for the described studies. General laboratory supplies were purchased from various vendors, including NIH Supply Center (Bethesda, MD), Fisher Scientific (Hampton, NH), Thermo Fisher Scientific (Waltham, MA), Life Technologies (Carlsbad, CA) and Sigma-Aldrich (St. Louis, MO).

2.1.1. Chemicals and Solutions

The following table (Table 1) lists all chemicals and solutions used in this study along with their source companies.

Table 1: List of chemicals and solutions

Name	Company
4′,6-diamidino-2-phenylindole (DAPI)	Life Technologies
5-(N-Ethyl-N-isopropyl)amiloride (EIPA)	Sigma-Aldrich
Agarose gel, 1% (w/v), containing ethidium bromide	BioRad
Amphotericin, 250 µg/ml	Quality Biological
Ampicillin	Sigma-Aldrich
Big Dye Terminator v1.1	Applied Biosystems
Bis-Tris SDS gels, 4-12% (w/v)	Thermo Fisher Scientific
Bovine serum albumin (BSA)	Sigma-Aldrich
Chlorpromazine	Sigma-Aldrich
Cleocin, 150 mg/ml	Pfizer
Dextran (MW 10,000), Alexa Fluor 568-conjugated	Life Technologies
Dimethyl sulfoxide (DMSO)	Sigma-Aldrich
Dipotassium phosphate (K_2HPO_4)	Fluka
Dithiobis(succinimidyl propionate) [DSP]	Sigma-Aldrich
DNA gel loading solution, 5x	Quality Biological
Ethanol, 200 proof	Pharmco Products
Ethylenediaminetetraacetic acid (EDTA) solution, 0.5 M	Quality Biological
F12-K medium	ATCC
Fetal bovine serum (FBS)	Thermo Fisher Scientific
Geneticin, 50 mg/ml	Life Technologies
Gentamycin, 50 mg/ml	Life Technologies
Glasgow's MEM (GMEM)	Life Technologies
Guinea pig complement	Lonza
HEPES buffer, 1 M	Sigma-Aldrich
Hydrochloric acid (HCl), 1 M	Sigma-Aldrich
Isopropyl alcohol	Avantor Performance Materials
Kanamycin	Sigma-Aldrich
L-Glutamine, 200 mM (100x)	Life Technologies

Name	Company
LB-Medium	Mediatech
Leibovitz's L15 medium	Life Technologies
MEM Amino Acids, 50x	Life Technologies
Methanol	Fisher Scientific
Methyl-beta-cyclodextrin (MBCD)	Sigma-Aldrich
Methylcellulose	Sigma-Aldrich
Mevinolin (Lovastatin)	Sigma-Aldrich
Monopotassium phosphate (KH_2PO_4)	Fluka
NP-40 (Igepal CA-630)	Sigma-Aldrich
NuPAGE Antioxidant, 10x	Life Technologies
NuPAGE Loading Dye Solution (LDS) sample buffer, 4x	Life Technologies
NuPAGE MOPS SDS running buffer, 20x	Life Technologies
NuPAGE Sample Reducing Reagent, 10x	Life Technologies
Opti-MEM I GlutaMax-I medium	Life Technologies
Ouabain	Sigma-Aldrich
Paraformaldehyde, 16% (w/v)	Electron Microscopy Science
PBS, 1x	Life Technologies
Penicillin/Streptomycin, 10x	Quality Biological
Phosphate buffered saline (PBS), 10x	Life Technologies
PP2	Sigma-Aldrich
ProLong Diamond Antifade mountant	Life Technologies
PST2238 (Rostafuroxin)	Sigma-Aldrich
RPMI 1640 medium	Life Technologies
siLentFect transfection reagent	Bio-Rad
Sodium chloride (NaCl)	Sigma-Aldrich
Sodium deoxycholate	KD Medical
Sodium dodecyl sulfate (SDS), 10% (w/v)	Sigma-Aldrich
Src-Inhibitor-I (SrcI-I)	Sigma-Aldrich
Sucrose	Sigma-Aldrich
TAE solution, 10x	Quality Biological
TaqMan reaction mastermix	Life Technologies
TBE solution, 10x	Quality Biological
Timentin	Glaxo Smith Kline
Tris-HCl solution, 1M	KD Medical
Triton X-100	Sigma-Aldrich
TrypeLE Select (Trypsin)	Life Technologies
Tween 20	Sigma-Aldrich
Ultra Complete Mini protease inhibitor	Roche
Ultrapure water (dH_2O)	Fisher Scientific
Western blot blocking buffer	Li-Cor

Table 2 shows the composition for each of the solutions that were prepared for these studies.

Table 2: Composition of solutions

Solution	Composition
30% (w/v) Sucrose solution	300 g Sucrose 15 ml 5 M NaCl 25 ml 1 M HEPES add dH_2O to 500 ml total
60% (w/v) Sucrose solution	150 g Sucrose 15 ml 5M NaCl 25 ml 1M HEPES add dH_2O to 500 ml total
Plaque assay overlay medium	500 ml Opti-MEM I GlutaMax-I 0.8% (w/v) Methylcellulose 2.0% (v/v) FBS 1x L-Glutamine 50 µg/ml Gentamicin For HPIV1 only: 4% (v/v) trypsin (no FBS) For animal derived samples: 200 µg/ml Ampicillin 30 µg /ml Cleocin 400 µg /ml Timentin 100 µg /ml Gentamycin 5 µg/ml Amphotericin
RIPA lysis buffer	20 mM Tris-HCl, pH 8.0 200 mM NaCl 1.0 mM EDTA 1.0% (v/v) NP-40 (Igepal CA-630) 1.0% (w/v) Sodium deoxycholate 0.1% (w/v) SDS 1x Ultra Complete Mini protease inhibitor
10x SP solution	2.18 M Sucrose, 38.0 mM KH_2PO_4 72.0 mM K_2HPO_4 pH 7.1

2.1.2. Instruments

The following instruments (Table 3) were used for performing the experiments described in this study.

Table 3: Instruments

Instrument	Company
-20 ˚C freezer	VWR
-80 ˚C freezer	Thermo Fisher Scientific
3730 DNA Analyzer	Applied Biosystems
4˚C fridge	VWR
7900HT Fast Real-Time PCR system	Applied Biosystems
Agarose gel electrophoresis chamber, Sub-Cell Model	BioRad
Analytical balance, Adventure Pro	Ohaus
Bacterial incubator, 10-140E	Quincy Lab
Bacterial shaker incubator, I-10002	Infors USA
Benchtop centrifuge, Alegra 25R	Beckman Coulter
Biosafety cabinet, Class II Type A/B3	Nuaire
Cell culture incubator, Forma Steri-Cult CO_2 Incubator	Thermo Fisher Scientific
Confocal fluorescence microscope, SP5 and SP8	Leica
ELISA reader Synergy 2	BioTek
Epi fluorescence microscope	Leica
Flow cytometer Canto II	BD
Hemocytometer, Neubauer improved	Fisher Scientific
iBlot2 transfer system	Life Technologies
Infrared imaging system Odyssey	Li-Cor
Inverse bright field microscope, DMIL	Leica
Liquid nitrogen storage tank, MVE 1520HE-190	Chart Industries
Magnetic stirrer	Corning
Microcentrifuge 5417R	Eppendorf
Mid speed centrifuge, Avanti J-20 XP	Beckman Coulter
Mini centrifuge, myFUGE	Benchmark Scientific
Nanodrop 1000	Thermo Fisher Scientific
Orbital shaker	VWR
PCR thermal cycler, C1000	BioRad
pH meter, SevenMulti	Mettler Toledo
Power supply, EC 300 XL	Thermo Fisher Scientific
QIAcube	Qiagen
Rocking platform	VWR
SDS gel electrophoresis chamber, XCell4 SureLock	Life Technologies
Stratalinker UV Crosslinker 1800	Agilent
Thermomixer, Modell R	Eppendorf
Tissue homogenizer	OMNI International

Instrument	Company
Typhoon imaging system	GE Healthcare
Ultracentrifuge, Optima L-100XP	Beckman Coulter
UV-Gel imaging system, Gel Logic 200	Kodak
Vortexer	Scientific Industries
Water bath	Thermo Fisher Scientific
X-ray film developer, X-Omat 2000A processor	Kodak

2.1.3. Software programs

The software programs listed in Table 4 were used for acquiring and analyzing the data.

Table 4: Software programs

Name	Version	Company
Lasergene suite	14.0	DNASTAR
Sequencher	5.4	Gene Codes Corporation
ImageJ	1.46r	NIH
ImageStudio	5.2.5	Li-Cor
Imaris	9.0.0	Bitplane AG
UCSF Chimera	1.10.2	University of California
FlowJo	10.1r1	FlowJo, LLC
Image acquisition software	LAS-X	Leica
FACSDiva	8.0.1	BD
Prism	7.0	GraphPad Software
ImageQuant TL	Array Version 8.1.	GE Healthcare

2.1.4. Cells and cell culture media

Cell lines used in this study (Table 5) were provided by Peter L. Collins or were purchased from American Type Culture Collection (ATCC; Manassas, VA).

Cell lines were cultured in the cell line-specific medium listed in Table 5. Cells were maintained in T225 flasks and seeded in various multi-well plate formats (6-well, 12-well, 24-well, 48-well and 96-well) as required for each experiment. All cell culture flasks and plates were obtained from Corning Inc. (Corning, NY).

Table 5: Cells and cell culture media

Cells (Passage Number)	Reference	Medium composition
A549 (P87)	ATCC CCL-185	F12-K medium 10% (v/v) FBS, 1x L-Glutamine
Vero (P149)	ATCC CCL-81	Opti-MEM I GlutaMax-I 5% (v/v) FBS
LLC-MK2 (P27)	ATCC CCL-7	Opti-MEM I GlutaMax-I 5% (v/v) FBS

Cells (Passage Number)	Reference	Medium composition
BHK BSR-T7 (P49)	(Buchholz et al. 1999)	Glasgow's MEM (GMEM) 10% (v/v) FBS, 1x MEM amino acid solution, Every other passage: 1x Geneticin
Primary Small Airway Epithelial Cells (HSAEC); Normal, Human	ATCC PCS-301-010 Lot: 64079184	Airway cell basal medium (ATCC PCS-300-030), supplemented with bronchial epithelial cell growth kit (ATCC PCS-300-040)
H1299-YFP-ATP1A1	(Sigal et al. 2006) Kindly provided by Uri Alon, Weizmann Institute of Science, Rehovot, Israel	RPMI 1640 10% (v/v) FBS

2.1.5. Viruses

Viruses used in this study (Table 6) were provided by Peter L. Collins. Virus working pools were grown and the viral consensus genome sequence was confirmed by Sanger sequencing as described in 2.2.9 of the Methods.

Table 6: Viruses

Virus	Reference
wt RSV A2 (D53)	(Collins et al. 1995); GenBank ID: KT992094
rRSV-GFP (D46/6120)	(Munir et al. 2008)
rgRSV dSH	(Techaarpornkul et al. 2001)
rgRSV dSH/dG	(Techaarpornkul et al. 2001)
rVSV-GFP	(Stojdl et al. 2003)
wt HPIV1	HPIV1/Washington/20993/1964; GenBank ID: AF457102
rHPIV1 $C^{\Delta 170}$	(Bartlett et al. 2007)
rHPIV3/EboGP	(Bukreyev et al. 2006)
rHPIV3/NotI ΔF-HN/EboGP	Virus was recovered for this study. (see Appendix 6.4)

2.1.6. Commercial Reagent Kits

The kits listed in Table 7 were purchased from the indicated companies and were used as described in the manufacturer's protocol, except otherwise mentioned.

Table 7: Commercial Reagent Kits

Name	Company
Advantage-HF PCR kit	Clontech
Antibody Labeling Kit	Thermo Fisher Scientific
BD Cytofix/Cytoperm Fixation/Permeabilization Solution Kit	BD Biosciences
Bicinchoninic acid (BCA) assay	Thermo Fisher Scientific
CellTiter-Glo Luminescent Cell Viability Assay	Promega

Name	Company
DNA Gel extraction kit	Fermentas
DNeasy Blood and Tissue Kit	Qiagen
EGFR phosphorylation antibody array	Ray Biotech, Norcross, GA
EndoFree Plasmid Maxi Kit	Qiagen
LIVE/DEAD fixable dead cell staining kit	Life Technologies
Monkey anti-Zaire EBOV GP IgG ELISA kit	Alpha Diagnostic International
PCR purification kit	Roche
Plasmid Mini Kit	Qiagen
QIAamp Viral RNA Mini Kit	Qiagen
QIAshredder	Qiagen
QuikChange Lightning Site-Directed Mutagenesis Kit	Agilent Technologies
Rapid Ligation Kit	Fermentas
RNeasy Mini Kit	Qiagen
SuperScript TM First-Strand Synthesis System for RT-PCR	Life Technologies
Universal Mycoplasma Detection Kit	ATCC

2.1.7. Oligonucleotide Primers

Sequencing primers used in this study were designed using the online program eprimer3 (Helixweb, NIH). All primers were synthesized by Eurofins Genomics (Louisville, KY) and their sequences are listed in section 6.3 of the Appendix.

2.1.8. Plasmids

The plasmids used in this study are listed in Table 8. *E.coli* XL10-Gold ultracompetent cells (Stratagene, La Jolla, CA) were transformed with the indicated plasmids by the heat shock method, as described by the manufacturer's protocol. Plasmid DNA was purified using the EndoFree Plasmid Maxi Kit (Qiagen, Germantown, MD). DNA concentrations were determined and plasmid stock solutions of 1.0 µg/ml were stored at -20˚C.

Table 8: Plasmids

Name	Reference
HPIV1 support plasmids for virus recovery:	(Newman et al. 2002)
pTM-HPIV1-N	T7-polymerase driven expression plasmids for the
pTM-HPIV1-P/C	HPIV1 N, P and L protein, that are essential for virus
pTM-HPIV1-L	recovery.
HPIV3 support plasmids for virus recovery:	(Durbin et al. 1997)
pTM-HPIV3-N	T7-polymerase driven expression plasmids for the
pTM-HPIV3-P/C	HPIV3 N, P and L protein, that are essential for virus
pTM-HPIV3-L	recovery.

Name	Reference
pFlc HPIV1 $C^{\Delta 170}$ MAN	(Mackow et al. 2015) HPIV1 full-length anti-genome for virus recovery, containing the attenuating $C^{\Delta 170}$ mutation and *Mlu*I (pre-N), *Asc*I (N-P) and *Not*I (P-M) restriction sites.
pFlc HPIV3 (JS)	(Durbin et al. 1997) HPIV3 full-length anti-genome for virus recovery.
EBOV GP inserts in pUC57 plasmid: Ebola GP_GSopt_AscI Ebola GP_TMCT_GSopt_AscI Ebola GP_GSopt_MluI Ebola GP_TMCT_GSopt_MluI	Codon-optimized and synthesized by GenScript. Sequences of the GP and GP-TMCT ORF are shown in Appendix 6.2.

2.1.9. Restriction enzymes

All enzymes used in this study (Table 9) were purchased as Fast Digest enzymes from Thermo Fisher Scientific (Waltham, MA) and used as described in the manufacturer's protocol.

Table 9: Restriction enzymes

Name	Restriction site1) (5'-3')
*Asc*I	GG|CGCGCC
*Mlu*I	A|CGCGT
*BsiW*I	C|GTACG
*Not*I	GC|GGCCGC

1) Vertical line indicates the cleavage site within the palindromic restriction site.

2.1.10. siRNAs

All siRNAs used in this study are listed in Table 10 and were purchased from Qiagen.

Table 10: siRNAs

Target	Name	Target sequence (5'-3')
ATP1A1	siRNA 1	CCC GGA AAG ACT GAA AGA ATA
ATP1A1	siRNA 2	CTT GAT GAA CTT CAT CGT AAA
ATP1A1	siRNA 3	ATC CAT GAA GCT GAT ACG ACA
EGFR	EGFR siRNA	CAG AGG AAA TAT GTA CTA CGA
Negative control siRNA	Neg. siRNA 1	AllStars Neg. control siRNA [Qiagen 1027281], sequence proprietary
Negative control siRNA	Neg. siRNA 2	AAT TCT CCG AAC GTG TCA CGT
Cell death positive control siRNA		AllStars Hs Cell Death siRNA control [Qiagen 1027299], sequence proprietary

2.1.11. Antibodies

The antibodies used for various assays in this study are listed in Table 11, Table 12, and Table 13. Antibodies were either purchased from the indicated companies or were generated by previous members of the laboratory (see listed references) and were provided by Peter L. Collins for this study.

Table 11: Primary antibodies

Reactivity	Host	Clonality	Reference
alpha tubulin	Mouse	monoclonal	T6199, Sigma Aldrich
ATP1A1	Mouse	monoclonal	ab7671, Abcam
ATP1A1	Rabbit	monoclonal	ab76020, Abcam
EBOV GP	Human	monoclonal	KZ52, IBT Bioservices
EBOV GP	Mouse	monoclonal	4F3, IBT Bioservices
EGFR	Rat	monoclonal	ab231, Abcam
EGFR	Mouse	monoclonal	ab181822, Abcam
HPIV1	Goat	polyclonal	ab20791, Abcam
HPIV1 F peptide	Rabbit	polyclonal	SKIA-15, (Bartlett et al. 2010)
HPIV1 HN peptide	Rabbit	polyclonal	SKIA-13, (Mackow et al. 2015)
HPIV1 N peptide	Rabbit	polyclonal	HPIV1-N-485, (Bartlett et al. 2010)
HPIV1 P peptide	Rabbit	polyclonal	SKIA-1, (Bartlett et al. 2010)
HPIV1 F	Mouse	monoclonal	MAb 7.1, (Komada et al. 1992)
RSV F	Mouse	monoclonal	1129, (Beeler and van Wyke Coelingh 1989)
RSV F	Mouse	monoclonal	1243, (Beeler and van Wyke Coelingh 1989)
RSV F	Mouse	monoclonal	1269, (Beeler and van Wyke Coelingh 1989)
RSV G	Mouse	monoclonal	ab94967, Abcam
RSV N	Mouse	monoclonal	ab94806, Abcam
RSV SH peptide	Rabbit	polyclonal	Produced by Noble Life Sciences

Table 12: Primary antibodies (conjugated)

Reactivity	Host	Conjugate[1)]	Source
RSV N	Mouse	APC	NB100-64752APC, Novus Biologicals (Littleton, CO)
RSV F	Mouse	AF488	RSV F 1129, in-house conjugation

[1)] APC: Allophycocyanin; AF: Alexa Fluor

Table 13: Secondary antibodies (conjugated)

Reactivity	Host	Conjugate[1)]	Source
Goat IgG	Donkey	IRDye 680LT	Li-Cor
Human IgG	Goat	AF488	Life Technologies
Mouse IgG	Donkey	AF488	Life Technologies
Mouse IgG	Donkey	AF568	Life Technologies
Mouse IgG	Donkey	AF647	Life Technologies

Reactivity	Host	Conjugate[1)]	Source
Mouse IgG	Donkey	IRDye 680RD	Li-Cor
Mouse IgG	Donkey	IRDye 800CW	Li-Cor
Mouse IgG	Goat	AF647	Life Technologies
Mouse IgG	Goat	IRDye 680RD	Li-Cor
Mouse IgG	Goat	IRDye 680RT	Li-Cor
Mouse IgG	Goat	IRDye 800CW	Li-Cor
Rabbit IgG	Donkey	AF488	Life Technologies
Rabbit IgG	Donkey	AF568	Life Technologies
Rabbit IgG	Goat	AF700	Life Technologies
Rabbit IgG	Goat	IRDye 680RD	Li-Cor
Rabbit IgG	Goat	IRDye 800CW	Li-Cor
Rat IgG	Goat	AF647	Life Technologies

[1)] AF: Alexa Fluor; IRDye: infrared fluorescent dye

2.2. Methods

2.2.1. Cell culture

All cell lines were maintained in T225 cell culture flasks (Corning Inc.) and were split biweekly for maintenance. To maintain cell growth in logarithmic phase, the split ratio for each cell line was adjusted to avoid complete confluency at each split. Cells were grown in the cell line-specific cell culture media, listed in section 2.1.4, and kept at 37˚C and 5% (v/v) CO_2.

For splitting adherent cell cultures to maintain the cell line, cells were once washed with 1x PBS, detached with trypsin, the reaction was stopped by adding cell culture medium and 1/5th to 1/20th of the total cell suspension volume, depending on the cell line, was transferred to a new T225 flask with fresh complete medium. The passage number was tracked and the cell line was discontinued after a certain number of passages: A549 cells were discontinued after 10 passages. All other cell lines used in this study (LLC-MK2, Vero and BHK BSR-T7) were discontinued after 25 passages from the time of thawing. Initial passage number of each cell line used in this study, is listed in Table 5 of section 2.1.4. Primary HSAEC were only passaged for a total of two passages, to ensure the maintenance of the primary cell characteristics. HSAEC were passaged once for expansion and then seeded in the cell culture plates for performing the experiments.

For seeding cells into various cell culture plates, trypsin was removed by centrifugation at 400 x g for 5 min and the cell pellet was resuspended in fresh medium. The cell count was determined with a Neubauer improved hemocytometer and cells were seeded in the appropriate cell culture medium.

For cryo-preservation of all cell lines, confluent cells were detached with trypsin, the reaction was stopped by adding cell culture medium and spun at 400 x g to remove the trypsin. The cell pellet was resuspended in fresh medium and 2x freezing medium (cell line specific medium, containing 20% (v/v) DMSO) was added 1:1 to the cell suspension to obtain a final DMSO concentration of 10% (v/v). Cells were frozen in a Nalgene freezing container (Sigma-

Aldrich) submerged in isopropyl alcohol at -80˚C to obtain a slow cooling rate of 1˚C per min. After 24 h at -80˚C, the frozen cells were transferred to a liquid nitrogen tank, where they were stored in the vapor phase at -190 ˚C until used.

All cell lines were tested for mycoplasma contamination with the Universal Mycoplasma Detection Kit (ATCC) as described by the manufacturer's protocol.

2.2.2. Inoculation of cell cultures

The virus titer of the inoculum for the infection of cell cultures was determined by the multiplicity of infection (MOI). The estimated cell numbers for fully confluent cells (listed in Table 14) of the indicated cell culture vessels were used for the MOI calculation. Depending on the virus and the method of titration (plaque assay or hemadsorption), the MOI was described as plaque forming units (PFU)/cell (for RSV and VSV) or as 50% tissue culture infective dose ($TCID_{50}$)/cell (for HPIV1 and HPIV3).

Table 14: Estimated number[1)] of cells in different cell culture vessels for MOI calculations

Cell culture vessel	Growth area [cm^2]	Inoculum volume	Number of cells
T225 flask	225	10 ml	2×10^7
6-well	9.5	1 ml	1×10^6
12-well	4	200 µl	5×10^5
24-well	2	200 µl	2.5×10^5

[1)] Estimations are based on the manufacturer's information. The estimated number of cells was used for all cell lines.

The virus working pool was diluted based on the MOI calculation in the cell line-specific medium (see 2.1.4) for the indicated inoculum volume, based on the cell culture vessel (Table 14). For infections with HPIV1, 1.2% (v/v) trypsin was added to the cell culture medium, which is required for the production of infectious progeny virus (see introduction section 1.2.3.2). The cell culture medium was removed and the inoculum was added to the cells and incubated for 2-3 h on a rocking platform at 32˚C (for HPIV1 and HPIV3) or 37˚C (for RSV and VSV). For the inoculation of cells in multi-well plates for various experiments, the inoculum was removed, cells were washed three times with fresh cell culture medium and 3 ml (for 6-well), 600 µl (for 12-well) or 500 µl (for 24-well) of fresh medium was added. For the inoculation of T225 flasks for preparing virus working pools, 25 ml cell culture medium was added, without removing the inoculum. The infected cells were incubated at 32˚C (for HPIV1 and HPIV3) or 37˚C (for RSV), with 5% (v/v) CO_2 for the indicated time.

2.2.3. Cell viability assay

The ATP-based cell viability assay CellTiter-Glo (Promega, Madison, WI) was used for the evaluation of cell viability and performed as described by the manufacturer's protocol. In brief, cells that were seeded in white 96-well plates, were lysed after the specified treatment at indicated time points and the ATP concentration was determined by luciferase activity. The light emission

of the luciferase was quantified using the Synergy 2 ELISA reader (BioTek, Winooski, VT). Viability was reported relative to mock-treated cells, based on the reduction of luciferase light emission and hence reduction of ATP, which was used as a parameter for cell viability.

2.2.4. siRNA transfections to knock down the expression of cellular proteins

Synthetic siRNAs (see Table 10 in section 2.1.10) targeting gene specific mRNAs were transfected into cells by a reverse transfection protocol, where the siRNAs were added simultaneously with cells in suspension. The transfection protocol was optimized with the negative control siRNAs (Neg. siRNA 1 and 2) and the cell death positive control siRNA. These control siRNAs were included in every experiment to control for a constant transfection efficiency. The best transfection results with maximal transfection efficiency and no increased cytotoxicity in a 12-well plate format were obtained with 2.0 x 10^5 A549 cells in 500 µl regular F12-K complete cell culture medium (see Table 5 in section 2.1.4), a final siRNA concentration of 40 nM, transfected with 1.0 µl siLentFect transfection reagent (BioRad, Hercules, CA). The transfection mix was prepared in a total of 100 µl per well Opti-MEM I GlutaMax-I medium (without supplements) as described by the manufacturer's protocol. In brief, the siRNA and siLentFect transfection reagent were separately pre-diluted in half of the total volume of Opti-MEM I GlutaMax-I (i.e. 50 µl per well), combined and incubated for 20 min before added to the well with freshly seeded cells. The cells were incubated for 48 h at 37˚C to allow the reduction of the targeted cellular protein, except otherwise stated. At 48 h post transfection (p.t.) the cells were used for further experiments.

2.2.5. Quantitative reverse transcriptase (RT-) PCR TaqMan assay

Cells were harvested and total RNA was isolated with RNeasy Mini Kit (Qiagen) as described by the manufacturer's protocol, including an on-column DNase digestion to avoid any DNA contamination. 1 µg total RNA was used for reverse transcription of mRNA to cDNA with oligo$(dT)_{12\text{-}18}$ primers and the SuperScript TM First-Strand Synthesis System for RT-PCR (Life Technologies, Carlsbad, CA). The synthesized cDNA was pre-diluted 1:10 and used for the TaqMan gene expression analysis of ATP1A1 (Life Technologies, Hs00167556_m1) and 18S rRNA (Life Technologies, Hs99999901_s1) as a normalization control. The TaqMan assay reactions were analyzed on the 7900HT Fast Real-Time PCR system (Applied Biosystems, Foster City, CA). The threshold cycle (Ct) for each reaction was determined by the SDS RQ manager program (Applied Biosystems). The relative changes in transcript level of the targeted transcripts were calculated by the $2^{-\Delta\Delta Ct}$ method (Livak and Schmittgen 2001) and reported relative to cells transfected with Neg. siRNA 1.

2.2.6. Cloning of the EBOV GP ORF into the HPIV1 full-length anti-genome at the first (pre-N) or the second (N-P) gene position

The EBOV GP ORF nucleotide sequence used was that of the EBOV Mayinga strain isolated in 1976 (GenBank ID: AF086833.2) (Volchkov et al. 2001), which is identical to the other candidate vaccines under evaluation (Mire et al. 2015, Ewer et al. 2016). Unedited GP mRNA contains a stretch of 7 A's at the editing site and is translated as secreted GP. Transcriptional editing results in the addition of a non-template A residue at this site causing frame shift and translation of the full-length membrane-anchored GP (Sanchez et al. 1996). For these constructs, an edited GP gene containing 8 U residues (negative sense) at the editing site (nt position 880-887; transcribing to 8 A's in the GP mRNA) was used to synthesize membrane-anchored GP.

The editing site was previously shown to be unstable in HPIV3 and was stabilized by two silent changes to AAGAAGAA (Bukreyev et al. 2006). For the present study, the GP nucleotide sequence was codon-optimized for human expression (GenScript, Piscataway, NJ) with the exception of the editing site sequence (AAGAAGAA), which was left undisturbed. The GenScript-optimized nucleotide sequence of the GP ORF is listed in the Appendix 0. In addition, a derivative of GP was made in which the GP TMCT region was replaced by that of the HPIV1 F protein (Figure 12C), which was presumptively identified based on a hydrophobicity analysis.

The coding sequence for EBOV GP or EBOV GP-TMCT was inserted into the first (pre-N) or second (N-P) gene position of the rHPIV1-$C^{\Delta 170}$ genome (Figure 12). For insertion into the pre-N position, the EBOV GP and GP-TMCT cDNAs were designed to be flanked upstream by an *Mlu*I site and Kozak sequence (Kozak 1987), and downstream by the GE signal of the N gene, followed by an IG trinucleotide CTT, the GS signal of the P gene, and an *Mlu*I site (Figure 12A). For insertion into the N-P gene position, the EBOV GP and GP-TMCT cDNAs were designed to be flanked upstream by an *Asc*I site and Kozak sequence, and downstream by the N GE, IG, and P GS, followed by an *Asc*I site (Figure 12B). All viruses were designed to keep the hexameric genome nucleotide length (rule of six) (Kolakofsky et al. 1998). Each vector gene maintained its wild-type hexamer phasing except the N gene in the pre-N constructs that had the P gene phasing. The GP and GP-TMCT inserts in pre-N and N-P sites had the hexamer phasing of the N and P genes, respectively. All inserts were synthetically derived (GenScript) and cloned into the rHPIV1-$C^{\Delta 170}$ antigenomic plasmid (pFlc HPIV1 $C^{\Delta 170}$ MAN) containing the unique restriction sites *Mlu*I and *Asc*I in the pre-N and N-P positions, respectively, using published methods (Mackow et al. 2015). This resulted in four constructs: the two with inserts in the pre-N position were called GP1 and GP-TMCT1, and the two with inserts in the N-P position were called GP2 and GP-TMCT2.

Figure 12: **Construction of the antigenomic cDNAs of rHPIV1-C$^{\Delta 170}$ expressing full-length EBOV GP or chimeric EBOV GP with HPIV1 F transmembrane (TM) and cytoplasmic tail (CT) domains from the pre-N (A) or N-P (B) position.** The EBOV GP ORF (strain Mayinga; GenBank ID: AF086833.2) was modified by the insertion of a single A residue at the editing site so as to encode full-length GP. The GP ORF was codon-optimized and inserted, as either the full-length GP or as a chimeric form in which the TMCT domain was replaced with that of HPIV1 F, at the pre-N (A) or N-P (B) position of rHPIV1-C$^{\Delta 170}$ bearing an attenuating mutation in the P/C ORF (indicated by an asterisk) using the previously introduced (Mackow et al. 2015) unique *Mlu*I or *Asc*I restriction sites, respectively. The GP insert was engineered with flanking HPIV1 gene transcription signals (GS: gene start; IG: intergenic; GE: gene end) to allow for its expression as a separate mRNA. **(C) The amino acid alignment of EBOV GP, HPIV1 F, and the chimeric EBOV GP-TMCT** containing the GP ectodomain and the TM and CT of HPIV1 F (bold).

2.2.7. Recovery of the rHPIV1-C$^{\Delta 170}$ vectors expressing EBOV GP from cDNA

The recombinant viruses were recovered by co-transfecting BHK BSR T7/5 cells with each of the full-length anti-genome plasmid (described in 2.2.6) and the HPIV1 support plasmids expressing the HPIV1 N, P, and L proteins as described (Newman et al. 2002, Bartlett et al. 2005). Transfected cells were incubated overnight at 37˚C, washed twice with Opti-MEM I GlutaMax-I medium and replaced with fresh Opti-MEM I GlutaMax-I medium containing 1 mM L-glutamine and 1.2 % (v/v) trypsin, followed by incubation at 32˚C. At 48 h post-transfection, cells were harvested by scraping into the medium and the cell suspension was added to 50% confluent monolayers of LLC-MK2 cells in Opti-MEM I GlutaMax-I medium, containing 1 mM L-glutamine, 1.2% (v/v) trypsin. These cells were incubated at 32˚C until cytopathic effects, due to the virus replication, were visible. Recovered virus (seed pool) was amplified by one passage (working pool) in LLC-MK2 cells at 32°C. Virus titers were determined by hemadsorption (HAD) (2.2.11) and titers are reported as $\log_{10}$ $TCID_{50}$/ml.

All HPIV1 viruses were sequenced, as described in section 2.2.9, in their entirety except for the 26 nt at the 5' end and 86, 79, 77, and 77 nt at the 3' end of GP1, GP-TMCT1, GP2, and GP-TMCT2, respectively. All viruses were found to be free of adventitious mutations.

2.2.8. Virus sucrose gradient purification

Partially-purified virus working stocks were generated by centrifugation on a discontinuous sucrose gradient. RSV and HPIV1 were grown in Vero and LLC-MK2 cells, respectively. Confluent cells in T225 cell culture flasks were inoculated, as described in section 2.2.2, with an MOI of 0.1 PFU/cell for RSV and 0.01 $TCID_{50}$/cell for HPIV1 and incubated at 32˚C until the cell monolayer showed high levels of cytopathic effects. For RSV, the cells were scraped into the supernatant and extensively (3 min total, in intervals of 30 sec) vortexed to release bound virus from the cell membrane. For HPIV1, the cell culture supernatant was collected without vortexing.

The supernatant was clarified by centrifugation (478 x g) and loaded onto a discontinuous sucrose gradient containing 60% (w/v) and 30% (w/v) sucrose solution (see 2.1.1) followed by centrifugation for 100 min in a Beckman Coulter SW32 rotor at 26,000 rpm at 4˚C. The cloudy interface, containing the virus particles, was collected with the minimum amount of sucrose solution. The virus containing sucrose solution was diluted with Opti-MEM I GlutaMax-I medium and the virus was spun out of sucrose by centrifugation at 8,000 x g for 2 h at 4˚C. The supernatant was discarded and the virus pellet was resuspended in fresh Opti-MEM I GlutaMax-I medium, aliquoted, flash frozen on dry ice, and stored at -80˚C until further used.

2.2.9. Virus genome sequencing

The consensus genome sequences of all virus working pools used in these studies were confirmed by automated Sanger sequencing of uncloned RT-PCR products copied from RNA from virus preparations. This determined the complete genome sequence except for the 3´end and the 5´end, as indicated, that were obscured by PCR primers. The viral RNA was isolated from 140 µl (for HPIV1 and HPIV3) or 280 µl (for RSV) virus working pool with QIAamp Viral RNA Mini Kit (Qiagen) as described in the manufacturer's protocol, including on-column DNase digestion to eliminate any plasmid DNA used for virus recovery. The RNA was eluted in 50 µl dH_2O and cDNA was generated by reverse transcription of 7 µl viral RNA by SuperScript™ First-Strand Synthesis System for RT-PCR (Life Technologies) with 2 µl random hexamers (50 ng/µl) as described in the manufacturer's protocol. Overlapping fragments of the viral genome were amplified by PCR (Advantage-HF PCR kit) using 2.5 µl of cDNA template and the following sequencing primer pairs, listed in Table 15 to Table 18.

Table 15: Primer sets for the RSV genome fragment amplification for Sanger sequencing

Reaction # (viral amplicon[1])	Size	Forward primer	Reverse primer	T_A[2]
1 (13 – 2189 nt)	2.2 kb	RSV_3UTR_FOR_13	RSV_N_REV_2164	51 ˚C
2 (2051 – 3859 nt)	1.8 kb	RSV_N_FOR_2051	RSV_M_REV_3834	51 ˚C
3 (3254 – 7670 nt)	4.4 kb	RSV_M_FOR_3254	RSV_M2_REV_7645	53 ˚C
4 (7465 – 12406 nt)	4.9 kb	RSV_F_FOR_7465	RSV_L_REV_12382	53 ˚C
5 (12282 – 15216nt)	2.9 kb	RSV_L_FOR_12282	RSV_5UTR_REV_15188	51 ˚C

[1] Referred to the nt position of the unmodified wt RSV A2 genome (GenBank ID: KT992094).
[2] Annealing temperature; optimized for each fragment.

Table 16: Primer sets for the HPIV1 genome fragment amplification for Sanger sequencing (HPIV1 with EBOV GP located in the pre-N position):

Reaction # (viral amplicon[1])	Size	Forward primer	Reverse primer
1 (78 – 244 nt + EBOV GP)	2.2 kb	PIV1_3UTR_FOR_78	PIV1_N_REV_223
2 (153 – 2813 nt)	2.6 kb	PIV1_N_FOR_153	PIV1_P_REV_2792
3 (2353 – 5446 nt)	3.1 kb	PIV1_P_FOR_2353	PIV1_F_REV_5425
4 (4859 – 7858 nt)	3.0 kb	PIV1_F_FOR_4859	PIV1_HN_REV_7837
5 (7291 – 10102 nt)	2.8 kb	PIV1_HN_FOR_7291	PIV1_L_REV_10081
6 (9332 – 12134 nt)	2.8 kb	PIV1_L_FOR_9332	PIV1_L_REV_12113
7 (11396 – 14287 nt)	2.9 kb	PIV1_L_FOR_11396	PIV1_L_REV_14267
8 (13237 – 15600 nt)	2.4 kb	PIV1_L_FOR_13237	PIV1_5UTR_REV_15575

[1)] Referred to the nt position of the unmodified wt HPIV1 genome (GenBank ID: AF457102).

Table 17: Primer sets for the HPIV1 genome fragment amplification for Sanger sequencing (HPIV1 with EBOV GP located in the N-P position):

Reaction # (viral amplicon[1])	Size	Forward primer	Reverse primer
1 (78 – 1125 nt)	1.0 kb	PIV1_3UTR_FOR_78	PIV1_N_REV_1103
2 (910 – 1823 nt + EBOV GP)	3.0 kb	PIV1_N_FOR_910	PIV1_P_REV_1802
3 (GP 1724 nt – 2813 nt)	1.4 kb	optEBOV-GP_For_10	PIV1_P_REV_2792
4 (2353 – 5446 nt)	3.1 kb	PIV1_P_FOR_2353	PIV1_F_REV_5425
5 (4859 – 7858 nt)	3.0 kb	PIV1_F_FOR_4859	PIV1_HN_REV_7837
6 (7291 – 10102 nt)	2.8 kb	PIV1_HN_FOR_7291	PIV1_L_REV_10081
7 (9332 – 12134 nt)	2.8 kb	PIV1_L_FOR_9332	PIV1_L_REV_12113
8 (11396 – 14287 nt)	2.9 kb	PIV1_L_FOR_11396	PIV1_L_REV_14267
9 (13237 – 15600 nt)	2.4 kb	PIV1_L_FOR_13237	PIV1_5UTR_REV_15575

[1)] Referred to the nt position of the unmodified wt HPIV1 genome (GenBank ID: AF457102) or EBOV GP ORF.

Table 18: Primer sets for the HPIV3 genome fragment amplification for Sanger sequencing:

Reaction # (viral amplicon[1])	Size	Forward primer	Reverse primer
1 (1 – 3215 nt)	3.1 kb	PIV3_3UTR_FOR_1	P_REV_3215
2 (3136 – 5768 nt)	2.7 kb	P_FOR_3136	F_REV_5768
3 (5489 – 8649 nt)	3.2 kb	F_FOR_5489	L_REV_8649
4 (8293 – 11294 nt)	3.0 kb	HN_FOR_8293	L_REV_11294
5 (10615 – 14422 nt)	3.8 kb	L_FOR_1061	L_REV_14422
6 (13939 – 15462 nt)	1.5 kb	L_FOR_13939	PIV3_5UTR_REV_15436

[1)] Referred to the nt position of the unmodified wt HPIV3 genome (GenBank ID: Z11575.1).

The PCR program used for the amplification of the fragments is shown below. The annealing temperature (T_A) was optimized for each viral genome amplification. For RSV the T_A for each fragment is listed in Table 15. For HPIV1 and HPIV3 the T_A was 52 ˚C for all fragments.

Initial denaturation:	95˚C	1 min
33x Cycles:	95˚C	30 sec
	T_A	30 sec
	68˚C	4 min
Final elongation step:	68˚C	4 min

The PCR products were purified with the PCR purification kit (Roche, Indianapolis, IN), eluted in 50 µl dH_2O and the purified PCR product was used for the sequencing reaction:

0.5 µl (approx. 40 ng) purified PCR product
8.0 µl BigDye Terminator V1.1
7.5 µl dH_2O
4.0 µl Sequencing primer (1 µM) (see Appendix 6.3 for primer sequence list)

The sequencing reaction was performed on a PCR thermocycler with the following program:

33x Cycles:	95˚C	10 sec
	50˚C	5 sec
	60˚C	4 min

The sequencing reaction was diluted 1:2 by adding 20 µl dH_2O und purified by applying it to a Performa DTR Ultra 96 well plate (EdgeBio, Gaithersburg, MD). The purified sequencing reaction was denatured for 3 min at 95 ˚C before it was loaded onto the 3730 DNA Analyzer to determine the nucleotide sequence. The resulting histograms were analyzed with Sequencher software program and a minimum of three reads were required for each nucleotide to be considered as a confirmed read.

2.2.10. Multi-cycle replication of HPIV1 EBOV GP

To determine the replication characteristics of the recovered HPIV1 vectors expressing EBOV GP, a multi-cycle replication assay was performed over 6 days. Confluent Vero cells in 6-well plates were infected with the recombinant viruses at an MOI of 0.01 $TCID_{50}$/cell in triplicate. At 24 h intervals, starting on day 1 through day 6, 500 µl (one-sixth of the volume) of culture medium supernatant was collected from each well and replaced by fresh medium. The samples were flash frozen on dry ice and stored at -80°C. The virus titer of each sample was determined in duplicate by hemadsorption assay on LLC-MK2 cells as described in section 2.2.11.

2.2.11. $TCID_{50}$ titration of HPIV1 EBOV GP by hemadsorption (HAD)

The hemagglutinin-neuraminidase (HN) is an envelope glycoprotein of human parainfluenza viruses. It is expressed on the surface of infected cells and binds to red blood cells (RBC), a process called hemadsorption that could be visualized with a microscope. Hemadsorption was used to detect infected cells and to determine $TCID_{50}$ titer (Shelokov et al. 1958). For titration, virus-containing samples were 10-fold serially diluted in quadruplicates onto confluent LLC-MK2 cells in 96-well plates. Before performing the serial dilution, the cells were washed twice with 1x PBS to remove any FBS and 180 µl fresh Opti-MEM I GlutaMax-I medium containing 1.2% (v/v) trypsin was added. The inoculated cells were incubated for 6 days at 32˚C. Hemadsorption was performed with 0.1 % (v/v) guinea pig RBC (Lonza, Allendale, NJ) in 1x PBS (1:1000 v/v dilution of packed RBC). The medium supernatant was removed and 100 µl of RBC suspension was added, incubated for 20 min at 4˚C and washed twice with 1x PBS to remove any unbound RBC. Each well was visually screened for bound RBC by bright field microscopy and wells were considered positive if RBC were detected bound to the cells. The $TCID_{50}$ titer was determined by the dilution factor that caused 50% infection of the infected replicates of one sample and was reported as $\log_{10}$ $TCID_{50}$ per ml.

2.2.12. Plaque assay

Plaque assay was performed by inoculating confluent Vero cells in 24-well tissue culture plates with a 10-fold serially diluted inoculum in duplicates and incubated for 6 days at 32˚C (for HPIV1 and HPIV3) or 37˚C (for RSV) under a methylcellulose overlay medium (see 2.1.1). Depending on the virus and the assay readout the plaques were visualized in different ways:

For RSV-GFP, the viral GFP expression was used to visualize the plaques and images were acquired on the Typhoon imaging system (GE Healthcare, Boston, MA) without any further treatment.

For all other plaque assays with viruses that did not express GFP, cells were fixed twice with ice-cold 80% (v/v) methanol and subjected to immunostaining for plaque detection. The fixed cells were blocked with Western blot blocking buffer (Li-Cor, Lincoln, NE) and depending on the virus following antibody dilutions were prepared in the same blocking buffer. Wt RSV plaques were stained with three RSV F-specific mouse monoclonal antibodies (MAbs) (1129, 1243 and 1269, diluted 1:2,000 each). HPIV1 immunostaining was performed with an HPIV1-specific goat polyclonal antibody (ab20791, diluted 1:1600). A double-immunostaining fluorescent plaque assay detecting the co-expression of HPIV1 antigens and EBOV GP was performed to determine the stability of GP expression for all vector working pools and samples derived from AGMs. In addition to the HPIV1 immunostaining, described above, the plaques also were stained for EBOV GP with an EBOV GP-specific mouse MAb (4F3, diluted 1:2,000). The corresponding secondary antibodies were conjugated with infrared fluorescent dye (IRDye) 680LT or 800CW (Li-Cor, for

the list of used antibodies see Table 11 in 2.1.11), each used at a 1:800 dilution. Plaque images were acquired using an Odyssey infrared imaging system (Li-Cor).

For plaque assay titrations, plaques were counted by ImageJ software and an appropriate dilution with counts between 10 - 60 singular plaques were chosen for the titer calculation.

For the HPIV1, EBOV GP double staining, plaques were pseudo colored to appear red and green for HPIV1 and EBOV GP expression, respectively. HPIV1 plaques expressing EBOV GP appeared yellow (HPIV1 and GP staining merged).

2.2.13. RSV infection evaluated by viral GFP expression

Recombinantly generated RSV-GFP contains an additional gene encoding eGFP that is inserted between the P and M genes in the RSV genome (Munir et al. 2008). Viral GFP expression was used as a surrogate for quantifying RSV infection/replication in the infected cells. GFP expression was quantified either by an ELISA reader or flow cytometry. GFP intensity of infected cells in 12-well plates was quantified by an area-scan (excitation 485/20, emission 528/20) with the Synergy2 ELISA reader (BioTek). The area-scan function allowed to obtain 29 individual measurements that covered the entire well and the obtained intensities were averaged to a mean relative light unit (RLU) value for each well. This method allowed to take into account any variations of GFP expression within the infected cell monolayer.

A flow cytometry approach was used for the quantification of viral GFP expression in individual cells. Infected cells were detached with 1 mM EDTA in 1x PBS, stained with a LIVE/DEAD fixable near-infrared amine-reactive dead cell discriminating dye (Life Technologies) and fixed with BD Cytofix/Cytoperm solution (BD, Franklin Lakes, NJ). Data were acquired on BD FACS Canto II flow cytometer and FACSDiva acquisition software. The software program FlowJo (FlowJo, LLC, Ashland, OR) was used for the quantification of the GFP intensity of single, live, GFP^+-gated cells.

2.2.14. Western blot analysis

For the analysis of cellular protein levels of siRNA-transfected cells, A549 or HSAEC cells were seeded in 12-well plates and transfected with the indicated siRNAs, as described in section 2.2.4. Cells were lysed with 75 µl 1x LDS sample buffer (Life Technologies) at indicated time points, homogenized by a QiaShredder (Qiagen) and 22.5 µL lysate of each sample was processed for Western blot analysis.

For the quantification of viral protein expression in infected cells, confluent Vero cells in 6-well plates were infected at an MOI of 3.0 $TCID_{50}$/cell, as described in section 2.2.2, and incubated for 48 h at 32˚C, after which cells were washed with 1x PBS, lysed in 100 µl LDS sample buffer and homogenized by applying the lysate to a QiaShredder. 22.5 µL lysate of each sample was subjected to Western blot analysis.

All samples were reduced with 1x NuPage Sample Reducing Agent (Life Technologies), denatured at 70˚C for 10 min, and electrophoresed (constant 200V for 55 min) on a 4-12% Bis-Tris SDS gel (Life Technologies) with 1x NuPage MOPS (3-(N-morpholino)propanesulfonic acid) SDS running buffer (Life Technologies), containing 1x NuPAGE Antioxidant (Life Technologies) in the upper chamber. Proteins were transferred onto a PVDF membrane using the iBlot2 transfer system (Life Technologies) and analyzed by Western blotting.

ATP1A1 was detected by a ATP1A1-specific rabbit MAb (ab76020, 10,000). EGFR was detected by a EGFR-specific mouse MAb (ab151522, 1:1,000). Tubulin was used as a loading control for all quantifications and was detected by an alpha-tubulin-specific mouse MAb (T6199, 1:10,000). For the detection of HPIV1 proteins, the rabbit polyclonal antibodies raised individually against peptides derived from F, HN, N, or P (see Table 11 in section 2.1.11) were used at a dilution of 1:200 each. EBOV GP was detected by the EBOV GP-specific mouse MAb (4F3, 1:1,000). All primary antibodies were diluted in Western blot blocking buffer (Li-Cor) containing 0.1% (v/v) Tween 20 and incubated on a rocking platform for at least 2 h at room temperature or overnight at 4˚C. The primary antibodies were removed by washing the membrane three times with 1x PBS, containing 0.1% (v/v) Tween 20. The corresponding secondary antibodies were IRDye 680RD- or 800CW-conjugated (for list of used antibodies see Table 13 in section 2.1.11), each diluted 1:10,000 in Western blot blocking buffer, containing 0.1% (v/v) Tween 20 and 0.01% (v/v) SDS. The secondary antibodies were incubated on a rocking platform for 1 h at room temperature. The membranes were washed two times with 1x PBS, containing 0.1% (v/v) Tween 20, followed by a final wash with 1x PBS. Western blot images were acquired on the Odyssey infrared scanner (Li-Cor) and analyzed with Image Studio Software (Version 5.2.5, Li-Cor).

2.2.15. Quantification of protein incorporation into the virus particles

For the evaluation of proteins packaged into the virions, viruses were sucrose purified via a discontinuous sucrose gradient centrifugation (described above in section 2.2.8). 1.5 ml of the harvested virus was spun for at least 2 h at 20,000 x g and 4˚C, to pellet the virus particles. The virus pellet was lysed in 50 µl RIPA lysis buffer (see 2.1.1). The total protein concentration of the lysates was determined by BCA assay (Thermo Fisher Scientific), as described by the manufacturer's protocol. Equal amounts (1 µg) of total protein were loaded onto a 4-12% Bis Tris gel and subjected to Western blot analysis, as described in section 2.2.14.

2.2.16. Flow cytometry assays

For assessing the stability of EBOV GP expression by the HPIV1 vectors, a flow cytometry-based assay was used in addition to the double staining plaque assay described in section 2.2.12. Vero cells infected at an MOI of 5.0 $TCID_{50}$ per cell were harvested at 24 h p.i. with 1 mM EDTA in 1x PBS. Cells were stained with LIVE/DEAD fixable near-infrared amine-reactive dead cell discriminating dye (Life Technologies) followed by HPIV1 F-specific mouse MAb (clone 7.1 at

1:1,000 dilution, pre-titrated to achieve specific F detection with no detectable background staining), and EBOV GP-specific human MAb (KZ52 at 1:300 dilution; IBT Bioservices, Rockville, MD). Cells were washed and stained with the Alexa Fluor (AF)-conjugated secondary antibodies goat anti-mouse AF647 and goat anti-human AF488 (Life Technologies). All antibody dilutions and washes were performed with FACS buffer (1x PBS containing 2.0% (v/v) FBS). Cells were fixed with BD Cytofix/Cytoperm solution. Data were acquired on BD FACS Canto II with FACSDiva acquisition software, followed by analysis using the software program FlowJo. Cells were sequentially gated on single cells, live cells, HPIV1 F^+ cells, and finally GP^+ cells. An average total of 15,000 collected HPIV1 F^+ cells was evaluated to determine the percentage of GP^+ cells.

2.2.17. Immunofluorescence microscopy

Cells were seeded on glass cover slips (Fisher Scientific, Hampton, NH) in 24-well plates and were treated, as indicated, when sub-confluent. For the immunofluorescence microscopy based assays, cells were fixed with 4% (w/v) paraformaldehyde (PFA, Electron Microscopy Science, PA) overnight at 4˚C, permeabilized with 0.1% (v/v) Triton X-100 (Sigma Aldrich) for 15 min, and blocked with 5% (w/v) BSA (Sigma Aldrich) in 1x PBS for 1 h at room temperature. All antibody dilutions were prepared in 1x PBS, containing 5% (w/v) BSA and 0.1% (v/v) Triton X-100. The primary antibody incubation was performed in a humidified chamber for 2 h with the following antibodies, depending on the target of interest for the specific assay: anti-ATP1A1 rabbit MAb (ab76020, 1:100), anti-EGFR rat MAb (ab231, 1:100), anti-RSV N mouse MAb (ab94806, 1:1,500) and anti-RSV F mouse MAb (1129, 1:200). After washing with 1x PBS, the secondary antibody staining was performed with the corresponding AF-conjugated secondary antibodies, diluted 1:1,000: donkey anti-rabbit AF488, goat anti-rabbit AF700, donkey anti-mouse AF647 and goat anti-rat AF647. The primary conjugated mouse MAbs RSV-F (1129)-AF488 and RSV-N-APC were used for the simultaneous detection of RSV F and N. The nuclei were counterstained with DAPI (Life Technologies) at a concentration of 300 nM in 1x PBS for 5 min, mounted on glass-slides (Fisher Scientific) with ProLong Diamond Antifade mountant (Life Technologies) and cured overnight at room temperature.

Images were acquired with the Leica LAS-X software on a Leica TCS-SP8 or SP5 confocal microscope (Leica Microsystems, Mannheim, Germany) using a 63x oil immersion objective (numerical aperture [NA] 1.4) and a zoom between 1.0 to 3.5x. Fluorochromes were excited using an argon laser at 488 nm for AF488, 561 nm for AF568, 633 nm for AF647, and 690 nm for AF700. DAPI was excited using a 450 nm diode laser. Detector slits were configured to minimize any crosstalk between the channels and, if necessary, the channels were collected sequentially and merged afterwards. All images were acquired as z-stacks with 0.3 µm steps. Images were processed with the image processing software Imaris (Version 9.0.0, Bitplane AG, Zurich, Switzerland) and ImageJ.

2.2.18. EGFR phosphorylation antibody array

To analyze the EGFR phosphorylation during RSV infection, an EGFR phosphorylation antibody array (Ray Biotech, Norcross, GA) was used that probed for the phosphorylation of 17 different sites of the EGFR receptor family. Cells were treated as indicated, either transfected with siRNA 48 h prior to inoculation or pre-treated with the indicated chemical compounds for 16 h. Simultaneously to the indicated pre-treatments, all cells were serum-starved for 16 h in FBS-free medium before incubated with wt RSV (MOI = 5 PFU/cell) for 5 h at 37˚C, 5% (v/v) CO_2. Cells were washed twice with cold 1x PBS and lysed in the provided lysis buffer containing the protease and phosphatase inhibitor cocktails (provided in the kit). The protein concentration of the lysate was quantified by BCA assay and lysate containing 150 µg total protein was used for each array. The array was processed as described by the manufacturer's protocol. In brief, the array membrane was incubated with the diluted lysate for 16 h at 4˚C on a rocking platform, washed and incubated with a biotinylated anti-pan EGFR antibody, followed by horse reddish peroxidase-conjugated streptavidin. The light emission from the array spots was detected by exposure to X-ray films. The films were scanned and the intensity of each spot was quantified by ImageQuant TL (Array Version 8.1., GE Healthcare). The EGFR phosphorylation of three independent experiments with two technical replicates were normalized to the signal of the array internal positive controls and pan-EGFR. Signals are reported relative to the signal of mock-treated, RSV-infected samples assigned the value of 1.0.

2.2.19. Macropinosome quantification assay

Macropinosomes have no unique cellular marker and can be best defined by their unspecific fluidic uptake and size. Therefore, a fluorescence confocal microscopy-based dextran assay was used for quantifying the macropinocytic uptake activity of cells (Wang et al. 2014). A549 cells were seeded on cover slips (Fisher Scientific) in 24-well plates two days prior to the assay so that they had reached a sub-confluent density. Cells were inoculated with wt RSV at an MOI of 5 PFU/cell in F12 medium containing 50 mg/ml AF568-conjugated dextran (MW 10,000, Life Technologies). Cells were incubated on a rocking platform at 37˚C, 5% (v/v) CO_2 for 5 h, washed three times with 1x PBS, and fixed overnight with 4% (w/v) PFA at 4˚C. The cells were counterstained with DAPI (300 nM in 1x PBS for 5 min) and mounted on glass-slides with ProLong Diamond Antifade mountant. Multiple, random images, using the mark and find function of the Leica-AF image acquisition software, were acquired as z-stacks (0.15 µm steps) on a Leica TCS-SP8 confocal microscope (Leica) with a 63x Objective (NA 1.4) and a zoom of 1.0x.

For the quantification of dextran-AF568 uptake, the acquired images were analyzed by batch processing using the Imaris image processing software. The DAPI stained nuclei were detected as spots to count the number of cells per field. The uptake of dextran was quantified by creating surfaces that recognize distinct dextran-AF568-positive vesicles and disregards any background staining. The total intensity of dextran-AF568 within the created surfaces, which had

a volume larger than 1.0 μm^3, of each field was normalized to the number of nuclei. The values were reported relative to Neg. siRNA 1-transfected or mock-treated cells that had been infected with RSV. For each experiment at total of at least 600 cells per condition were analyzed.

2.2.20. Animal studies

2.2.20.1. Ethic Statement

All animal studies were approved by the NIH Institutional Animal Care and Use Committee (IACUC) and the mice and African green monkey studies were performed under the animal study protocols #LID 34E and #LID 22, respectively.

The National Research Council's Guide for the care and use of laboratory animals and the Public Health Service Policy on humane care and use of laboratory animals served as the guidelines for the care and use of the animals in this study.

2.2.20.2. Evaluation of replication and immunogenicity of HPIV1 vectors expressing EBOV GP in African green monkeys (AGMs)

2.2.20.2.1. Study design

In vivo replication and immunogenicity of the HPIV1 vectors expressing EBOV GP was assessed in African green monkeys (AGMs, *Cercopithecus aethiops*). Animals were confirmed to be naïve for HPIV1 and HPIV3 by serum hemagglutination inhibition assay (HAI) (van Wyke Coelingh et al. 1988). Groups of four animals were infected with each of the HPIV1 EBOV GP viruses by the combined intranasal (IN) and intratracheal (IT) routes with 10^6 $TCID_{50}$ per site. In parallel two animals were infected with wt HPIV1 for comparison. Two animals infected with the previously described candidate rHPIV3/EboGP (Bukreyev et al. 2006) also were included as a positive reference. Nasopharyngeal swabs (NP) were collected daily for 14 days whereas tracheal lavage (TL) with 3 ml 1x PBS was performed every other day p.i. for 14 days by the technicians of the animal facility. The NP swaps were resuspended in L15 medium containing 1x SP (see Table 2 in section 2.1.1). TL samples were 1:1 diluted in L15 medium containing 2x SP to obtain a final concentration of 1x SP. SP was added stabilize the virus during freezing. All samples were aliquoted, flash frozen on dry ice, and stored at -80˚C.

After 28 days two animals of each group received a second inoculation (boost) with the same virus. Dose, routes, and NP/TL sample collection were the same as for the first dose. Virus titers of NP and TL samples were determined by serial dilution on LLC-MK2 cells and HAD assay (described in section 2.2.11). The viral titers were reported as $log_{10}TCID_{50}$ per ml. Serum was collected from all animals weekly by the technicians of the animal facility, starting on the day of inoculation, to determine GP-specific antibody response following the first and second dose.

2.2.20.2.2. Stability of EBOV GP expression during replication in AGMs

After the titration of all samples to determine the viral shedding in the upper (NP samples) and lower (TL samples) respiratory tract of the inoculated AGMs, the day of peak shedding was defined. For each virus, NP and TL samples from all 4 animals at their peak titer day (P2) following the first inoculation, as well as a day before (P1) and after (P3) the peak day were subjected to double-immunostaining plaque assay, as described in section 2.2.12, to determine the stability of GP expression during *in vivo* replication.

2.2.20.2.3. EBOV GP-specific ELISA

A commercially available monkey anti-Zaire EBOV GP IgG ELISA kit (Alpha Diagnostic International, San Antonio, TX) was used to quantify the GP-specific serum antibody response of the immunized AGMs. The assay was performed as described in the manufacturer's protocol and all incubation steps were performed on an orbital shaker. Briefly, 5-fold serially diluted serum was added to EBOV GP coated wells of a 96-well ELISA plate and incubated for 1 h to capture GP-specific antibodies. The wells were washed and the bound GP-specific antibodies were detected with a secondary horseradish peroxidase conjugated anti-monkey IgG antibody that was incubated for 30 min. After washing the wells, a chromogenic substrate (3,3′,5,5′-Tetramethylbenzidine, TMB) was added and incubated for 10 min. A color was developed by the HRP substrate, the intensity of which is directly proportional to the EBOV GP-specific antibody concentration present in the serum. The reaction was stopped by adding the stop solution (diluted sulfuric acid) and the absorbance at 450 nm (OD_{450}) was measured on the Synergy2 ELISA reader (BioTek). The titer dilution of each sample yielding a value of OD_{450}=1.0 was calculated by linear regression analysis.

2.2.20.2.4. EBOV GP neutralization assay

Serum titers of EBOV GP-specific neutralizing antibodies were determined by 60% plaque reduction neutralization titer ($PRNT_{60}$) on Vero cells, using an HPIV3-based construct (called rHPIV3/NotI ΔF-HN/EboGP) that lacks the HPIV3 F and HN glycoprotein genes and expresses EBOV GP from an added gene as the sole viral surface protein. This virus is very similar to another version reported previously (Bukreyev et al. 2009) and was constructed as described in the Appendix 6.4. Sera from the immunized AGMs were heat inactivated at 56°C for 30 min, and 4-fold serial dilutions in Opti-MEM I GlutaMax-I medium were made. As a positive control the human MAb KZ52 (IBT Bioservices) was included, which is a purified antibody preparation at 1.49 mg/ml. It is an EBOV GP-specific MAb derived from an EBOV survivor, and has been shown to neutralize EBOV to 50% at 0.3 µg/mL (Maruyama et al. 1999). These serum dilutions were combined with a set amount of rHPIV3/NotI ΔF-HN/EboGP and adjusted to contain 10% (v/v) of a commercial preparation of guinea pig complement (Lonza). The virus was incubated with the diluted serum samples for 30 min at 37°C and then transferred to Vero cell monolayers in 24-well plates.

Inoculated cells were rocked for 2 h at 32°C on a rocking platform, overlaid with methylcellulose overlay medium (see 2.1.1) and incubated for 6 days at 32°C. The cells were fixed twice with ice-cold 80% (v/v) methanol, and plaques were detected with anti-GP mouse MAb (4F3, 1:2,000) and a secondary goat anti-mouse IRDye 680LT-conjugated antibody (Li-Cor), as described in section 2.2.12. Images were acquired using an Odyssey infrared imaging system (Li-Cor) and the plaques of each well were counted with ImageJ software. Based on the plaque reduction due to the diluted serum, the $PRNT_{60}$ titer for each serum was calculated by linear regression analysis. To confirm that the HPIV1- or HPIV3-specific antibodies present in the serum samples did not neutralize the rHPIV3/NotI ΔF-HN/EboGP virus, control HPIV1 and HPIV3 hyperimmune rabbit sera, with known high HPIV1- or HPIV3-neutralization titers, were included as controls which showed no detectable neutralizing activity, indicating that neutralization was due to anti-EBOV GP antibodies.

2.2.20.3. ATP1A1 heterozygous knockout ($ATP1A1^{+/-}$) mice

Cryo-preserved embryos of the heterozygous mutant mouse strain B6;129S5-$Atp1a1^{Gt(neo)311Lex/Mmucd}$ (RRID: MMRRC_011687-UCD, referred to as $ATP1A1^{+/-}$ here after) were obtained from the Mutant Mouse Resource & Research Centers (MMRRC) at the University of California, Davis. The ATP1A1 knockout was obtained by targeted retroviral insertion of a trapping cassette that abrogates the protein expression. Insertion of the trapping cassette in this ATP1A1 mutant mouse strain occurred between exon 1 and 2 of the murine ATP1A1 gene on chromosome 3 (Figure 13) (Lexicon Genetics Inc. 2005). The embryos were resuscitated by embryo transfer into 0.5 day pseudopregnant female recipient mice at the Mouse Genetics and Gene Modification Section (NIAID, NIH, Bethesda, MD). The litter was genotyped, as described below in section 2.2.20.3.1, and used to establish breeding colonies.

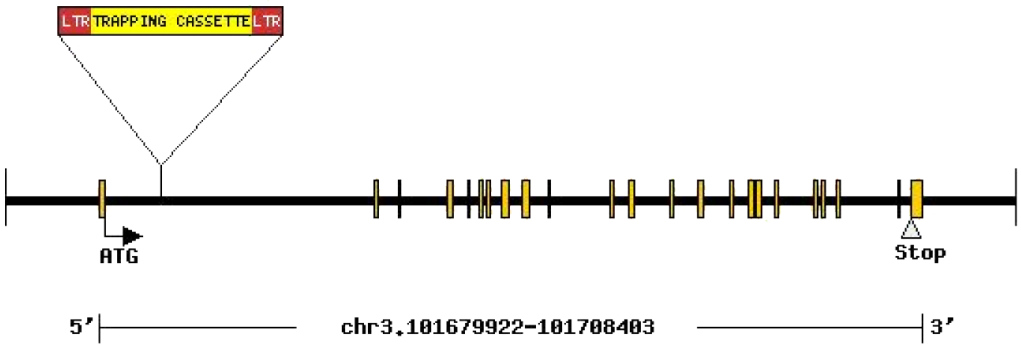

Figure 13: **Insertion site of the trapping cassette in the murine ATP1A1 allele on chromosome 3 (GenBank ID: 11928) by retroviral insertion.** The arrangement of the exons (yellow horizontal bars) and introns (black horizontal lines) of the murine ATP1A1 gene are shown. Obtained from the Mouse Genome Informatics (MGI) (http://www.informatics.jax.org, ID: NIH-0128)

It has been shown that the homozygous mutation causes preweaning lethality and only heterozygous (ATP1A1 +/-) knockout mice were viable. The information available on the Mouse Genome Informatics (MGI) website lists no major defects due to the heterozygous knockout, only behavioral changes of increased anxiety-related response and decreased exploration in new environment were noted (Lexicon Genetics Inc. 2005).

2.2.20.3.1. Genotyping

The resuscitated animals as well as all offspring derived from the breeding colonies were genotyped for the ATP1A1 knockout allele. The genotyping strategy was provided by MMRRC.

New litters were ear tagged and tail samples for genotyping were obtained post-weaning at 21 days of age. The tail tissue was lysed in 180 µl ATL buffer, containing 20 µl Proteinase K and incubated overnight at 56˚C. The genomic DNA (gDNA) was isolated from the lysate with the DNeasy Blood and Tissue Kit (Qiagen) as described in the manufacturer's protocol.

A diagnostic PCR was used to screen for the presence of the trapping cassette in the genome by using the below listed primer set (primer sequences are listed in the Appendix in section 6.3.1). ATP1A1 knockout was detected by an ATP1A1 gene-specific forward primer (128-5'), located upstream of the insertion site of the trapping cassette, and a trapping cassette-specific reverse primer (LTR-rev). Two ATP1A1 gene-specific primers (128-5' and 128-3') were used as a control PCR for the wt genotype:

Knockout ATP1A1 PCR: Primer 128-5' and Primer LTR-rev, Amplicon size: 132 bp

wt ATP1A1 PCR: Primer 128-5' and Primer 128-3', Amplicon size: 131 bp

The PCR reaction was set up with the Advantage-HF PCR kit as followed:

5 µl/rxt 10xHF Buffer
5 µl/rxt dNTPs
1 µl/rxt forward primer, pre-diluted to 10 µM
1 µl/rxt reverse primer, pre-diluted to 10 µM
1 µl/rxt HF polymerase
36 µl/rxt dH2O
-> add 1 µl gDNA (include negative control: 1 µl dH_2O)

The PCR reaction was performed on a thermocycler with the following touch-down PCR program:

10 cycles:	94˚C	15 sec
	65˚C (-1˚C/cycle)	30 sec
	72˚C	40 sec
30 cycles:	94˚ C	15 sec
	55˚C	30 sec
	72˚C	40 sec

The PCR reaction was loaded onto a 1.0% (w/v) agarose gel (BioRad), containing ethidium bromide, separated by electrophoresis (45 min, 100V) and a gel image was acquired at a UV-gel documentation station. The presence of a 132 bp amplicon in the ATP1A1 knockout PCR defined the ATP1A1+/- genotype.

2.2.20.3.2. Evaluation of RSV replication in ATP1A1$^{+/-}$ mice

6-week old mice were genotyped (as described above in section 2.2.20.3.1) and separated into two groups by their genotype as wildtype (ATP1A1 +/+) and heterozygous knockout (ATP1A1 +/-). All mice were inoculated intranasally with 10^6 PFU of rRSV-GFP diluted in 75 µl L15 medium. 4 d p.i. the animals were euthanized with CO_2 and nasal turbinate and lung tissues were collected.

The tissues were homogenized in L15 medium added in a 1:10 weight to volume ratio, clarified by centrifugation and the PFU titer was determined by plaque assay titration on Vero cells (see 2.2.12). The titer of each individual animal was reported as PFU per gram of tissue.

2.2.21. Statistical analysis

All results shown are derived from at least three independent replicates, except otherwise stated. Error bars shown in each graph indicate the standard deviation (SD) for each group. GraphPad Prism was used to create all graphs and to perform the statistical analysis described in the corresponding figure legends. P-values are shown for each comparison and p-values smaller than 0.05 were considered as statistically significant.

3. Results

3.1. Role of ATP1A1 in the macropinocytic entry of RSV

The cellular protein ATP1A1 was identified as a presumptive pro-viral host factor in a high-throughput siRNA screen in human airway epithelial A549 cells infected with RSV-GFP, with GFP expression as reporter for viral infection. Knockdown of the ATP1A1 gene expression reduced RSV infection. Of the top 65 genes identified, ATP1A1 knockdown had the greatest inhibitory effect on viral GFP expression, with minimal effects on cell viability, and was chosen for further characterization.

3.1.1. Knockdown of ATP1A1 expression by siRNA transfection

Three siRNAs with the greatest effect on ATP1A1 expression, without affecting cell viability, were used for further experiments. The efficiency of ATP1A1 knockdown was confirmed both at the mRNA and protein levels. A549 cells were transfected with individual ATP1A1-specific siRNAs or with an individual nonspecific scrambled negative siRNA as a control. Two different negative siRNAs (Neg. siRNA 1 and 2) were used to control for any off-target effects of the negative siRNA itself. At various time points, total cell-associated RNA was isolated, ATP1A1 mRNA was quantified by a TaqMan assay and reported relative to Neg. siRNA 1 (Figure 14A). At 24 h p.t. the level of ATP1A1 mRNA was reduced to below 5% compared to Neg. siRNA 1 and showed only modest further reductions at 48 and 72 h p.t.

To measure the expression of ATP1A1 protein, A549 cell lysates were prepared at 24, 48 and 72 h p.t. and subjected to Western blot analysis. Figure 14B shows a representative blot of ATP1A1 and alpha-tubulin (loading control). The band intensities were quantified and presented relative to Neg. siRNA 1 (Figure 14C). At 24 h p.t. the ATP1A1 protein amount was reduced about 50% for all three ATP1A1-specific siRNAs (siRNA 1 - 3). The protein expression of ATP1A1 was further reduced at 48 h p.t. to 39% (siRNA 1 and 3) and 35% (siRNA 2) and did not show any further reduction at 72 h p.t.

It was critical to evaluate cell viability as this could cause negative effects on virus infection potentially arising from siRNA off-target effects or the reduced ATP1A1 protein expression. The transfected cells showed no visible cytotoxicity or morphological changes over the period of 72 h p.t. For a more sensitive evaluation, an ATP-based viability assay was performed. Cellular ATP, as correlate for cell viability, was measured with a luciferase-based assay in cell lysates at 72 h p.t. The luciferase activity was quantified in relative light units (RLU) by an ELISA reader and were reported relative to mock-transfected cells (treated with transfection reagent only) (Figure 14D). The ATP1A1 siRNA knockdown showed only minimal reductions in cell viability (Figure 14D). The greatest reduction was observed for siRNA 1 at 18%, while siRNA 2 and 3 had reductions of 11% and 5%, respectively (Figure 14D).

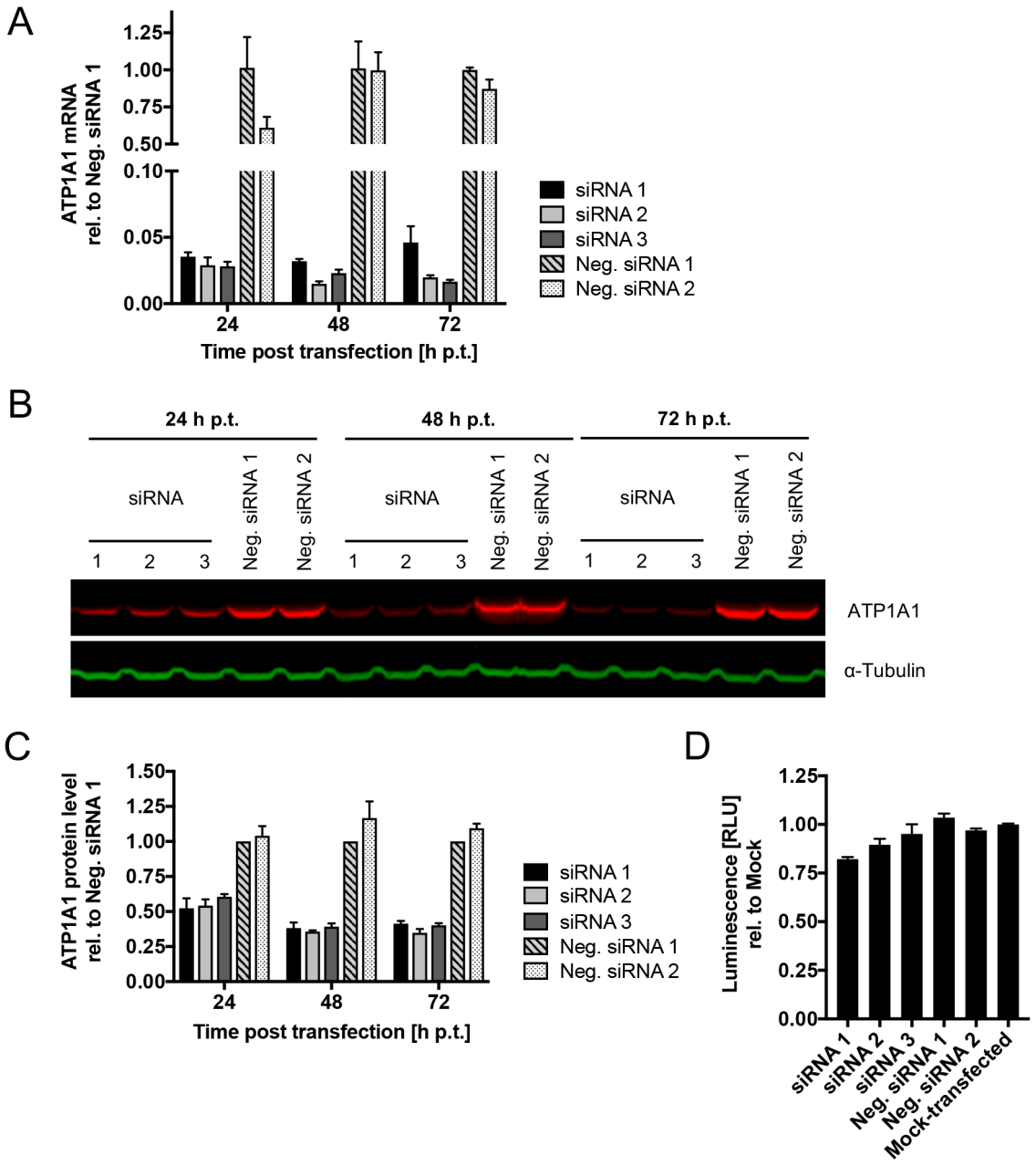

Figure 14: **ATP1A1 knockdown by siRNA transfection.** A549 cells were transfected with three different siRNAs (siRNA 1 - 3) targeting the ATP1A1 mRNA. Cells were harvested 24, 48 and 72 h p.t. and the mRNA and protein levels of ATP1A1 were quantified. As negative control, cells were transfected with two different negative siRNAs (Neg. siRNA 1 and 2) with no known target in human cells. **(A) Relative quantification of ATP1A1 mRNA.** Total cell-associated RNA was isolated and was reverse transcribed. The amount of ATP1A1 mRNA was quantified by an ATP1A1 mRNA-specific TaqMan Assay, values were normalized to 18S rRNA and expressed as mean values relative to Neg. siRNA 1 assigned the value of 1.0, with error bars indicating the standard deviation (SD) of three independent experiments. **(B) Western blot analysis of ATP1A1 expression.** Cells were lysed in 1x LDS buffer and subjected to Western blotting with an anti-ATP1A1 rabbit monoclonal antibody (MAb) and a corresponding infrared fluorescent dye (IRDye) 680RD-conjugated goat anti-rabbit secondary antibody. Alpha-tubulin was used as a loading control and was detected by an anti-alpha-tubulin MAb and an IRDye 800CW-conjugated goat anti-mouse secondary antibody. A representative blot is shown. **(C) Relative quantification of ATP1A1 protein expression**. The protein levels of three independent Western blot analyses, as described in part B, were quantified, normalized to alpha-tubulin, and reported relative to Neg. siRNA 1 assigned the value of 1.0, with error bars indicating the SD. **(D) Cell viability.** An ATP-based cell viability assay [CellTiter-Glo (Promega)] was performed 72 h p.t. to evaluate the viability of the transfected cells. Cells were lysed, the ATP concentration was determined by ATP-dependent luciferase activity, which was detected with an ELISA reader, and the luciferase activity (RLU, relative light units), reflecting the viability, was reported relative to mock-transfected cells assigned the value of 1.0.

3.1.2. Effect of ATP1A1 knockdown on RSV infection

A549 cells were transfected with the three siRNAs targeting ATP1A1 (siRNA 1 - 3), and the two negative control siRNAs (Neg. siRNA 1 and 2), and 48 h later the cells were infected with RSV-GFP at an MOI of 1.0 PFU/cell. The efficiency of virus infection and replication were evaluated at 17 h post inoculation (p.i.) by GFP expression quantified by an ELISA reader, and 24 h p.i. by flow cytometry, shown in Figure 15A and C, respectively. All three ATP1A1-specific siRNAs reduced the intensity of GFP expression by about 45 to 70% compared to Neg. siRNA 1. This level of reduction was substantial given that the residual level of ATP1A1 expression remained 35% or greater, as previously shown in Figure 14C. To determine if this effect was RSV-specific, vesicular stomatitis virus expressing GFP (VSV-GFP) was included for comparison. ATP1A1 knockdown had no effect on GFP expression by VSV-GFP (Figure 15B). This suggested that the reduction in GFP expression observed with RSV-GFP was specific to RSV, did not affect VSV, and was not due to some general effect on cellular functions. The analysis of cells infected with RSV-GFP (MOI = 1.0 PFU/cell) by flow cytometry 24 h p.i. showed that knockdown of ATP1A1 resulted in a broad reduction of GFP expression in the infected cell population rather than a reduction in the number of GFP-expressing cells (Figure 15C).

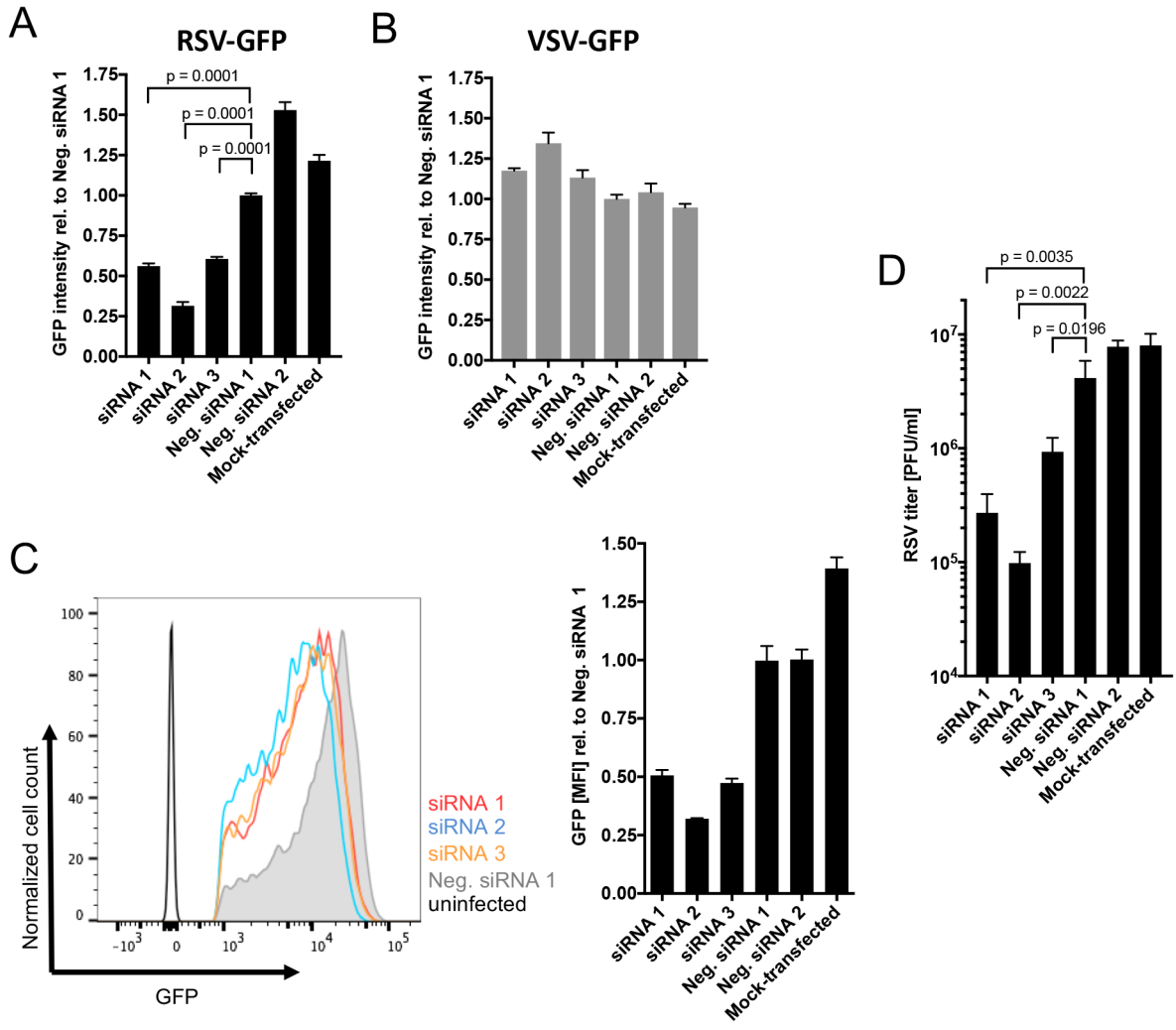

Figure 15: **Effect of ATP1A1 knockdown on infection by RSV-GFP (A, C, D) and VSV-GFP (B).** A549 cells were transfected with the indicated siRNAs and 48 h later were infected with 1.0 PFU/cell RSV-GFP

(A, C, D) or 0.5 PFU/cell VSV-GFP (B). **(A and B) Quantification of viral GFP expression.** The GFP intensity of the total well was quantified by scanning with an ELISA reader at 17 h p.i. (**C) Flow cytometry analysis of RSV-GFP expression.** In addition, RSV-GFP expression also was examined and quantified by flow cytometry at 24 h p.i. **(D) Titer of progeny RSV-GFP.** The production of infectious RSV at 24 h p.i. was quantified by plaque titration on Vero cells. All data in A-D are derived from at least three independent experiments and, in A-C, are shown as mean values relative to Neg. siRNA 1 assigned the value of 1.0, with error bars indicating the SD. The statistical significance of difference was determined by one-way analysis of variance (ANOVA) with Dunnett's multiple comparison post-test and p-values are shown for each comparison.

The effects on the production of progeny RSV were assessed 24 h p.i. The infected cells were scraped off, followed by vortexing of the cell suspension to release bound virions, and virus titers of the clarified supernatants were determined by plaque titration on Vero cells. RSV-GFP plaques were quantified and titers reported as PFU/ml (Figure 15D). The RSV titers were reduced between 5- (siRNA 3) and 42-fold (siRNA 2) compared to Neg. siRNA 1 at 24 h p.i., an effect that was even more dramatic than the reduction in GFP expression described above (Figure 15D versus Figure 15A and C); ATP1A1 siRNA 2 showed the strongest effect in both cases. These data suggest that ATP1A1 has an important role in the RSV replication cycle and that the amount of ATP1A1 expressed by the host cell is a crucial factor for efficient RSV infection.

3.1.3. RSV replication in ATP1A1$^{+/-}$ mice

To evaluate the effect of reduced ATP1A1 protein level on RSV infection and shedding *in vivo*, a heterozygous ATP1A1 knockout mouse strain was obtained and a breeding colony was established. The homozygous knockout is lethal at the preweaning stage and therefore, a heterozygous ATP1A1$^{+/-}$ genotype is the only available mouse strain with a reduced ATP1A1 expression level.

The mutant mice were bred and genotyped post-weaning at 21 days of age. The ATP1A1 protein levels in lung tissue lysates of mutant ATP1A1$^{+/-}$ and wild-type ATP1A1$^{+/+}$ mice were determined by Western blotting (Figure 16A). Due to the heterozygous knockout the ATP1A1 level was reduced only modestly, to 65 - 70% compared to wild-type mice. Thus, following knockdown, the level of residual expression of ATP1A1 *in vivo* (65 - 70%, Figure 16A) was substantially greater than that observed *in vitro* (35 - 39%, Figure 14C).

Nevertheless, the mice that were obtained were used for a pilot study to determine the effects of the modest reduction of ATP1A1 protein expression in these heterozygous knockout mice on RSV infection and shedding. 6-week-old ATP1A1$^{+/-}$ and wild-type litter mates were inoculated intranasally with 10^6 PFU of RSV-GFP. Virus shedding in the lung and nasal turbinate tissues was determined by plaque titration on Vero cells 4 d p.i. (Figure 16B). The mean titers in the lung tissue for ATP1A1$^{+/-}$ and wild-type mice were 8.8 x 10^3 PFU/g and 1.4 x 10^4 PFU/g, respectively. RSV titers in the nasal turbinate tissues were slightly higher as compared to the titers in the lungs and were, for ATP1A1$^{+/-}$ and wild-type mice, 2.4 and 2.5 x10^4 PFU/g, respectively. Thus, RSV shedding was similar for ATP1A1$^{+/-}$ and the control wild-type litter mates, with no significant difference in the infectious virus titers in the lung or nasal turbinate tissues. This was

not surprising, since the heterozygous knockout only showed a modest reduction in ATP1A1 expression, which apparently was sufficient for infectivity and shedding similar to wild-type mice. Due to the modest ATP1A1 reduction, experimentation in this murine model was not continued.

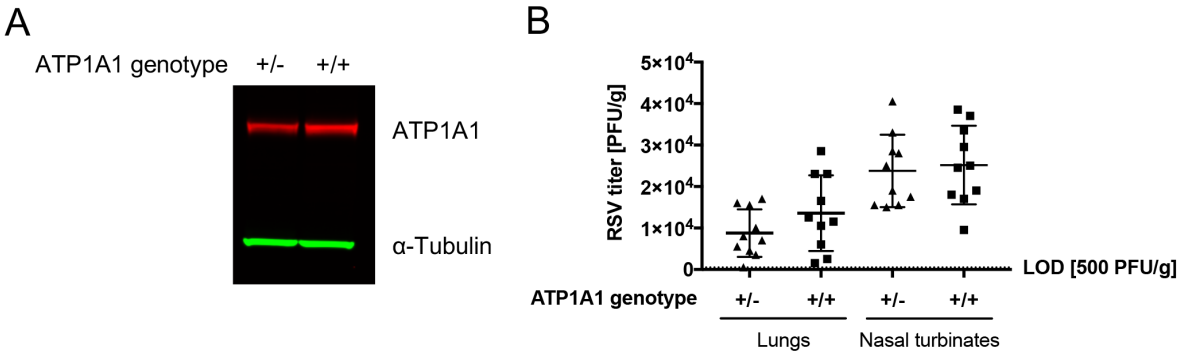

Figure 16: **Heterozygous ATP1A1 knockout mice.** ATP1A1 mutant mice were genotyped by a diagnostic PCR (ATP1A1 genotype: +/-, heterozygous knockout; +/+, wild-type). **(A) ATP1A1 protein expression level in lung tissue of ATP1A1$^{+/-}$ mice.** ATP1A1 protein level in lysates of lung tissues was quantified by Western blotting as described for Figure 14B. A representative blot is shown. **(B) Replication of RSV-GFP in ATP1A1$^{+/-}$ mice 4 d p.i.** Groups of 6-week-old ATP1A1 +/- and +/+ mice were inoculated intranasally with 10^6 PFU of RSV-GFP. Lung and nasal turbinate tissues were collected 4 d p.i. and RSV replication was evaluated by plaque titration of tissue homogenates on Vero cells and was reported as PFU per gram tissue. LOD, limit of detection.

3.1.4. Cellular distribution of ATP1A1 during RSV infection

To gain insight into the role of ATP1A1 in the RSV replication cycle, the ATP1A1 distribution in RSV-infected A549 cells was examined by fluorescence confocal microscopy. A549 cells were infected with wt RSV (MOI = 5 PFU/cell), fixed at 2 h and 5 h p.i., and subjected to immunofluorescence staining for ATP1A1 and RSV F protein. In uninfected cells (Mock), ATP1A1 was homogenously distributed on the plasma membrane (Figure 17A, top row). Upon infection with wt RSV, ATP1A1 clusters were observed that were visible as early as 2 h p.i. (Figure 17A, middle row) and were clearly different, more abundant than anything seen in the uninfected cells. With time, the ATP1A1 clusters became more prominent and numerous, as shown for 5 h compared to 2 h p.i. (Figure 17A, bottom row versus middle row). Some ATP1A1 clusters, but not all, partially co-localized with RSV F protein (Figure 17A, indicated by arrows). The localization of clustered ATP1A1 in close proximity to RSV F became more noticeable at later time points such as 5 h p.i. (Figure 17A, bottom panel). Localization of ATP1A1 clusters close to RSV N protein also could be observed (Figure 18 and Figure 20), suggesting that the RSV-specific staining most likely reflects enveloped virions which had not yet fused. Cross-sections (Figure 17B) of the RSV-infected A549 cells 5 h p.i. indicated that the ATP1A1 clustering occurred at the cell surface and was localized close to the RSV virions. Similar ATP1A1 clustering also was observed for UV-inactivated wt RSV (Figure 18), suggesting that the staining mostly detected virus particles derived from the inoculum and that virus gene expression or replication was not required to trigger clustering. Given the very early appearance of ATP1A1 clusters, independent of viral transcription or replication, it was hypothesized that ATP1A1 might be involved in an early step of infection, such as viral entry.

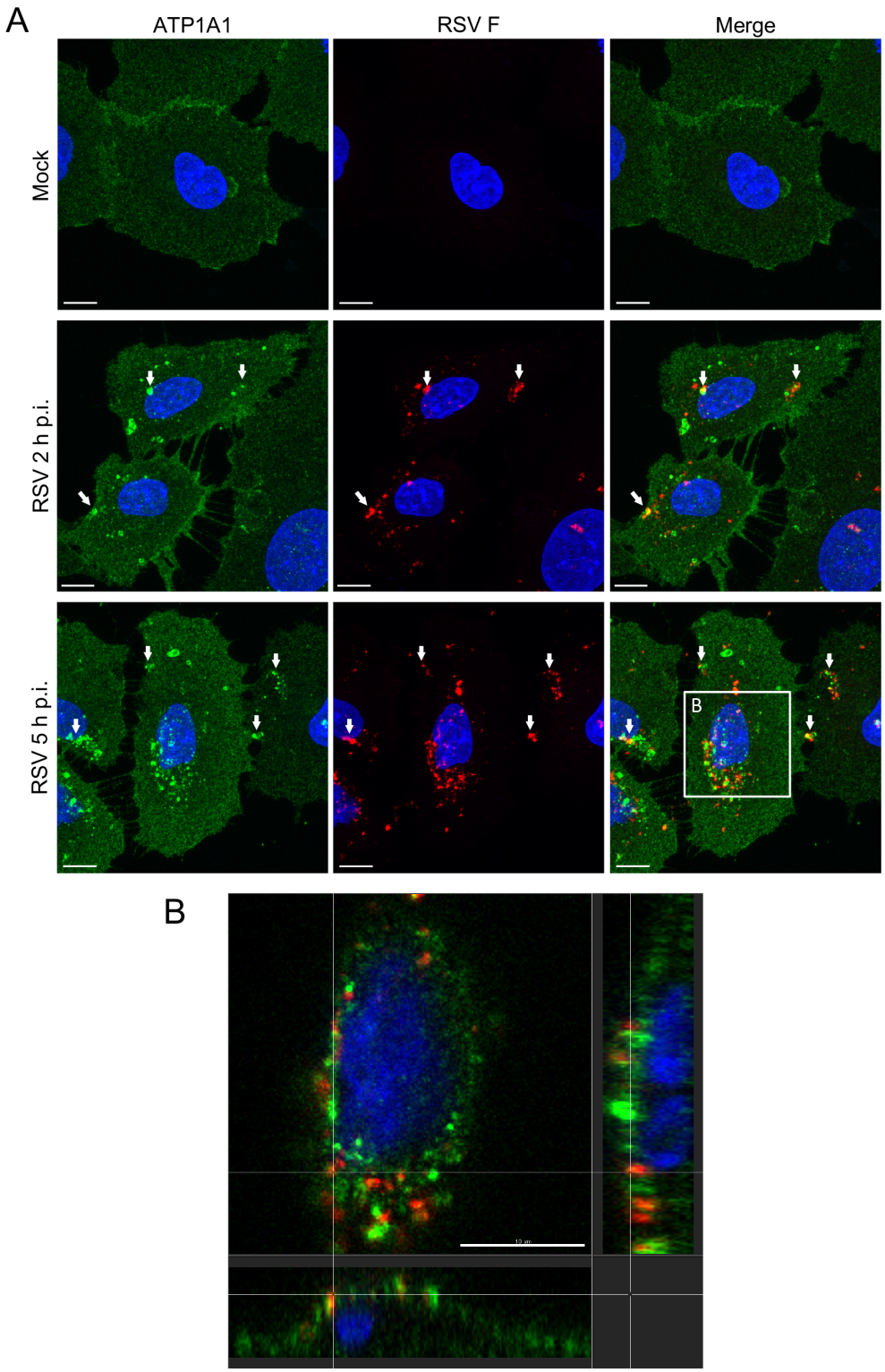

Figure 17: **RSV infection triggers ATP1A1 clustering. (A)** A549 cells were inoculated with wt RSV (MOI = 5 PFU/cell) and incubated for 2 or 5 h. Cells were fixed with 4% (w/v) PFA, permeabilized with 0.1 % (v/v) Triton X-100 and stained for ATP1A1 (green) with an anti-ATP1A1 rabbit MAb (ab76020) and Alexa Fluor (AF) 488-conjugated donkey anti-rabbit secondary antibody. RSV F (red) was detected with anti-RSV F mouse MAb #1129 (Beeler and van Wyke Coelingh 1989) and an AF594-conjugated donkey anti-mouse secondary antibody. The cell nuclei were stained with DAPI (blue). Images (z-stacks) were acquired on a Leica SP5 confocal microscope, with a 63x objective (numerical aperture [NA] 1.4) and a zoom of 3.0. Arrows indicate examples of co-localization of ATP1A1 and RSV F. **(B)** Cross-sectional image of the marked area in A of RSV-infected cell at 5 h p.i. Scale bars, 10 µm.

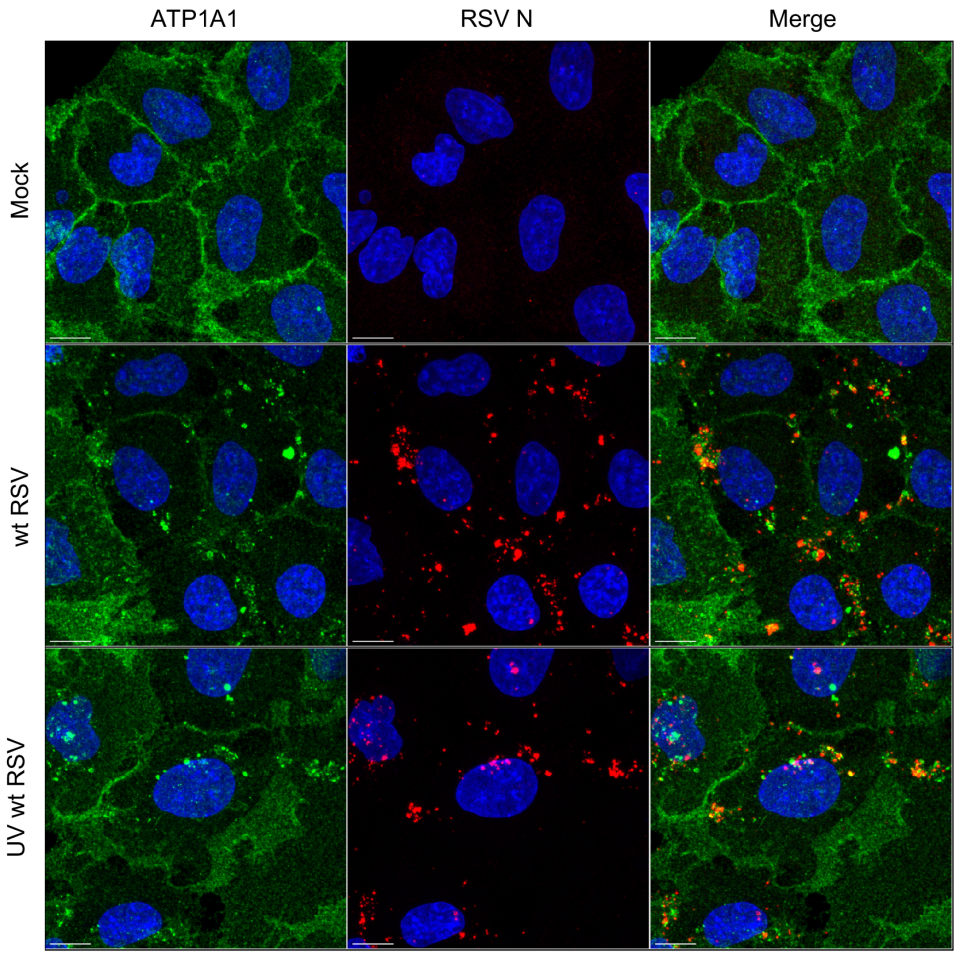

Figure 18: **ATP1A1 clustering induced by UV-inactivated RSV.** A549 cells were inoculated with wt RSV (MOI = 5 PFU/cell) and incubated for 5 h. Additional cultures were inoculated with wt RSV that had been UV-inactivated (0.5 J/cm^2) using a Stratalinker UV Crosslinker 1800 (Agilent, UV wt RSV). Loss of plaque-forming activity in the UV wt RSV inoculum was confirmed by plaque titration on Vero cells. Cells were fixed with 4% (w/v) PFA and subjected to immunofluorescence staining. ATP1A1 (green) was detected with an anti-ATP1A1 rabbit MAb (ab76020) and AF488-conjugated donkey anti-rabbit secondary antibody. RSV N (red) was detected by an anti-RSV N mouse MAb (ab94806) and an AF568-conjugated donkey anti-mouse secondary antibody. The cell nuclei were stained with DAPI (blue). Arrows indicate co-localization of ATP1A1 and RSV N. Scale bars, 10 µm.

3.1.5. Investigation of ATP1A1 interactions with RSV glycoproteins

If ATP1A1 is involved in early steps of infection, it was hypothesized that one or more of the RSV surface glycoproteins F, G, and/or SH, might interact with ATP1A1. Various immunoprecipitation assays were performed to investigate possible interactions. For example, the human lung epithelial cell line H1299 ATP1A1-YFP (Sigal et al. 2006, Frenkel-Morgenstern et al. 2010), that chromosomally expressed ATP1A1 genetically fused to a yellow fluorescent protein (YFP) tag, was used for various co-immunoprecipitation assays. These cells were infected with RSV, lysed, and subjected to co-immunoprecipitation with YFP-specific antibodies, followed by Western blotting with antibodies specific to RSV glycoproteins. Similar co-immunoprecipitation experiments were performed in which, prior to lysis, the cells were treated with the permeable, reversible cross-linker dithiobis(succinimidyl propionate) to covalently link proteins that were close to each other to stabilize and detect any weak or transient interactions [ReCLIP assay, (Smith et

al. 2011)]. In other experiments, RSV virions were incubated with purified ATP1A1 that was immobilized on beads to detect any RSV-ATP1A1 interactions in a cell-independent manner. However, no evidence of binding between ATP1A1 and RSV proteins could be detected in these experiments (data not shown).

A cell-based binding assay also was performed (Figure 19), which had been adapted from an assay described by Martinez and colleagues (Martinez and Melero 2000). In brief, A549 cells were transfected with ATP1A1-specific siRNAs to knock down ATP1A1 protein expression. 48 h post siRNA transfection, cells were detached and incubated with the RSV inoculum (MOI = 10 PFU/cell) on ice for 30 min. Cells were extensively washed and the bound virus was detected with a pool of RSV F-specific mouse MAbs #1129, 1269 and 12443 (Beeler and van Wyke Coelingh 1989) and an AF647-conjugated donkey anti-mouse secondary antibody. The samples were analyzed on Canto II flow cytometer and the median fluorescence intensity (MFI) of AF647 was reported relative to Neg. siRNA 1-transfected cells (Figure 19). ATP1A1 knockdown did not show an appreciable reduction in RSV binding, indicating that ATP1A1 likely did not contribute to RSV attachment. This experiment also was done with the additional step of treating of the cells with heparinase I prior to RSV exposure to remove cell surface GAGs, which was done to eliminate GAG-mediated RSV attachment: this also did not reveal any contribution of ATP1A1 to RSV attachment (data not shown). Therefore, there was no evidence of stable binding of any RSV surface protein to ATP1A1.

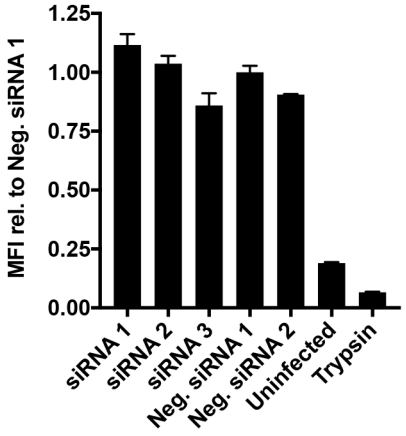

Figure 19: **Effect of ATP1A1 knockdown on RSV binding on the cell surface.** A549 cells were transfected with the indicated siRNAs targeting the ATP1A1 mRNA (siRNA 1 - 3) or unspecific negative siRNA (Neg. siRNA 1 and 2). 48 h p.t. cells were detached with 1 mM EDTA in 1x PBS and the suspended cells were incubated with wt RSV (MOI = 10 PFU/cell) on ice for 30 min. Cells were washed to remove any unbound virus and stained for RSV F with a pool of RSV F-specific mouse MAb [#1129, 1269, and 1243 (Beeler and van Wyke Coelingh 1989)] followed by an AF647-conjugated donkey anti-mouse secondary antibody. Cells treated with trypsin prior to incubation with virus served as a negative control for virus binding. Cells were analyzed by flow cytometry and the MFI of AF647 was reported relative to Neg. siRNA 1-transfected cells assigned the value of 1.0. Protocol was adapted from (Martinez and Melero 2000).

Another way to investigate the involvement of viral surface glycoproteins that might be involved in triggering ATP1A1 clustering was to use recombinant RSV mutants with deletion of the small hydrophobic protein gene (dSH) or the combined deletion of SH and the attachment G glycoprotein genes (dSH/dG). A deletion of RSV F was not feasible since a virus without F protein

would not be infectious. A549 cells were infected with wt RSV, RSV dSH, or RSV dSH/dG (MOI = 10 PFU/cell) and incubated for 5 h. The infected cells were fixed, permeabilized, and immunostained with MAbs specific to ATP1A1 (green) and RSV N (red). The ATP1A1 clustering was examined by fluorescence confocal microscopy (Figure 20).

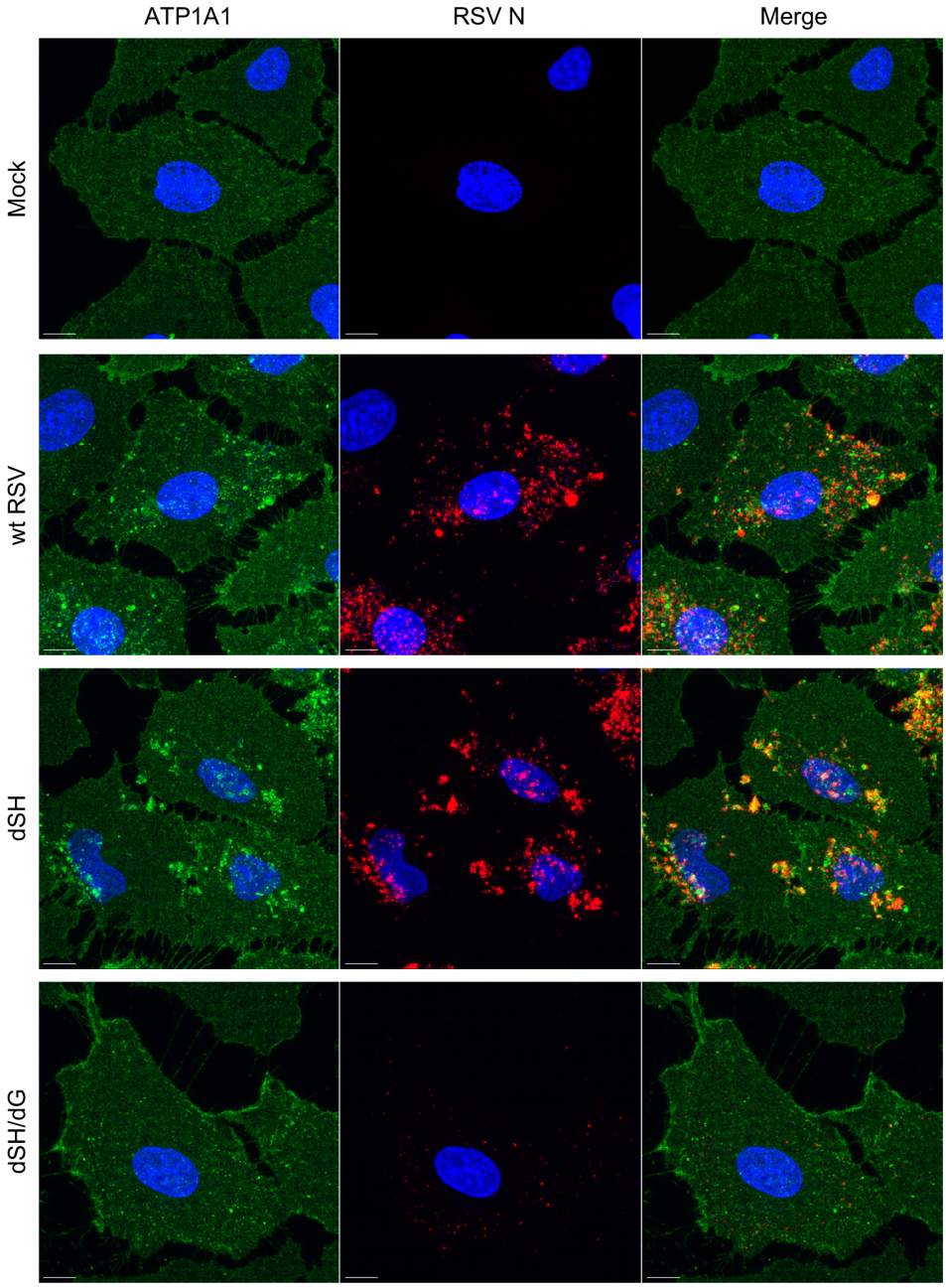

Figure 20: **RSV G is required for ATP1A1 clustering.** A549 cells were inoculated with wt RSV, RSV dSH or RSV dSH/dG (MOI = 10 PFU/cell) and incubated for 5 h. Cells were fixed with 4% (w/v) PFA and subjected to immunofluorescence staining. ATP1A1 (green) was detected with an anti-ATP1A1 rabbit MAb (ab76020) and an AF568-conjugated donkey anti-rabbit secondary antibody. RSV N (red) was detected with an anti-RSV N mouse MAb (ab94806) and an AF647-conjugated donkey anti-mouse secondary antibody. The cell nuclei were stained with DAPI (blue). Images (z-stacks) were acquired on a Leica SP8 confocal microscope, with a 63x objective (NA 1.4) and a zoom of 3.0. Scale bars, 10 µm.

Wt RSV was included as a reference that induced increased cluster formation compared to Figure 17, which may have been due to the increased MOI of 10 PFU/cell compared to 5 PFU/cell used previously. Clustering induced by RSV dSH virus was similar to that observed with wt RSV, suggesting that the deletion of the SH protein had no effect on ATP1A1 clustering. On

the other hand, the dSH/dG virus did not induce any ATP1A1 clusters (Figure 20, bottom panel) and the aggregates of viral protein thought to be virions, stained for RSV N in red, were reduced in amount and much more dispersed compared to wt RSV and the dSH virus. The lack of ATP1A1 cluster formation with the dSH/dG virus suggested that RSV G protein is required for triggering ATP1A1 clustering.

3.1.6. Effects of ouabain and PST2238 on RSV infection

The described clustering of ATP1A1 in response to RSV exposure is reminiscent of the clustering that is generally observed for cell surface receptors known to facilitate intracellular signaling in response to ligand binding (Gopalakrishnan et al. 2005). Formation of ATP1A1 clusters pointed to a possible role for ATP1A1 as a signal transducer. As described in the introduction, the only known signaling function for ATP1A1 is in response to binding of CTS, such as ouabain, with the ATP1A1 extracellular domain. A synthetic digitoxigenin derivative named PST2238 is an ouabain antagonist and competes with its binding site at ATP1A1 (Ferrari et al. 1998). Due to their specific interaction with ATP1A1 and the association with ATP1A1-mediated signaling cascades, ouabain and PST2238 were tested for their effects on RSV infection.

Serial dilutions of ouabain and PST2238 were evaluated for cytotoxicity on A549 cells and primary human small airway epithelial cells (HSAEC), following a 24 h incubation, by an ATP-based viability assay (Figure 21).

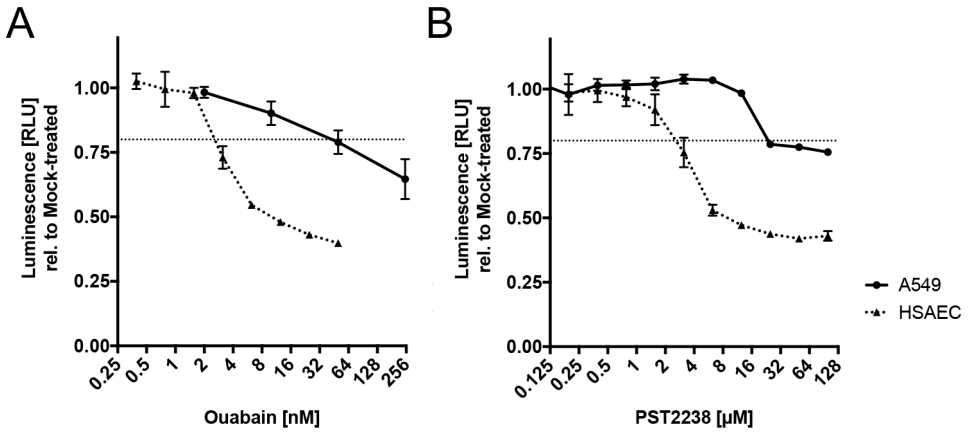

Figure 21: **Cytotoxicity of ouabain and PST2238 on A549 cells and primary human small airway epithelial cells (HSAEC).** A549 cells (solid line) and HSAEC (dotted line) were treated with serial dilutions of ouabain (A) and PST2238 (B) for 24 h. For each cell type, cell viability was determined in triplicates for each concentration by the ATP-based viability assay CellTiter-Glo. The results were reported relative to mock-treated cells assigned the value 1.0, with error bars indicating the SD. The horizontal dotted line indicates 80% viability.

Based on the viability curves in Figure 21 A and B, regression analysis was used to calculate the maximal concentrations of ouabain and PST2238 that could be used for a 24 h treatment without reducing the cell viability below 80% relative to mock-treated cells (Table 19). Surprisingly, the chemical concentrations tolerated by HSAEC were 16.3-fold (ouabain) and 8.4-fold (PST2238) lower than for A549 cells. In order to maintain greater than 80% viability, concentrations of 25 nM ouabain and 20 µM PST2238 were used for subsequent experiments in A549 cells, with maximum treatment periods of 24 h.

Table 19: Calculated[1] maximal concentration for ouabain or PST2238 to maintain 80% viability of A549 cells or HSAEC after a 24 h treatment:

Cells	Ouabain [nM]	PST2238 [µM]
A549	44.0	22.7
HSAEC	2.7	2.7

[1] Concentrations were calculated by regression analysis with GraphPad Prism 7 based on the viability curves shown in Figure 21.

The effects of ouabain and PST2238 on the cellular expression of ATP1A1 and EGFR were analyzed by immunofluorescence microscopy using antibodies specific for each protein (Figure 22). EGFR was evaluated in addition to ATP1A1 because it previously had been shown to be important for RSV entry and it had been reported to be associated with the ATP1A1-signalosome, as described in the Introduction. In mock-treated cells, ATP1A1 and EGFR each had a homogeneous membrane distribution (Figure 22, left column). After a 24 h treatment with ouabain, the ATP1A1 protein level was greatly reduced (Figure 22, middle column, top panel), presumably due to the removal of cell-surface Na^+, K^+-ATPase by clathrin-mediated endocytosis induced by ATP1A1 signaling (Introduction), while EGFR expression and localization appeared unchanged (Figure 22, middle column, bottom panel). On the other hand, PST2238 (Figure 22, right panel) had no discernible effect on the expression and/or localization of ATP1A1 or EGFR. PST2238 did not cause removal of ATP1A1 because it does not induce ATP1A1 signaling and endocytosis (Introduction).

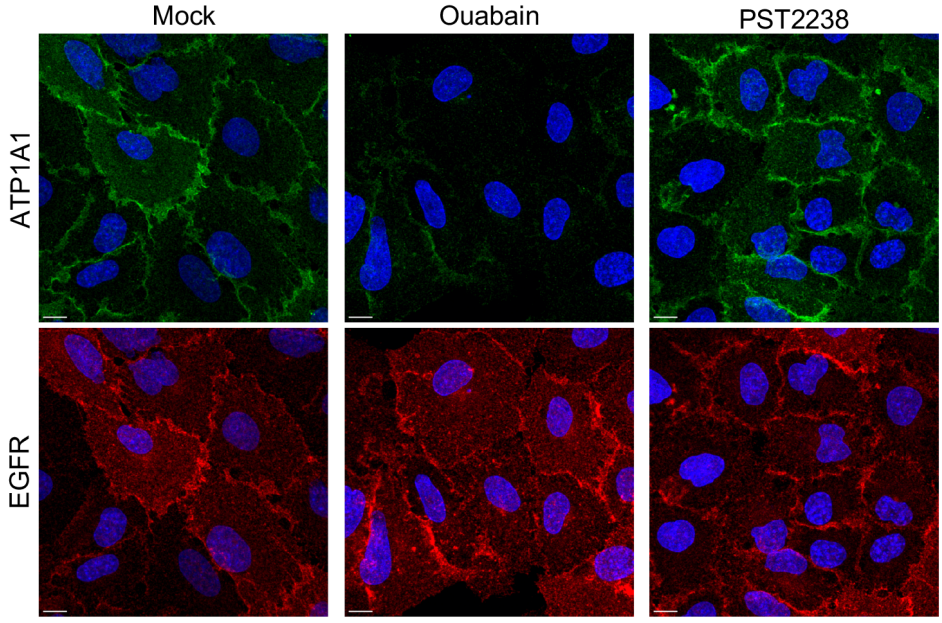

Figure 22: **Effect of ouabain and PST2238 on cellular expression of ATP1A1 and EGFR.** Uninfected A549 cells were treated for 24 h with either 25 nM ouabain or 20 µM PST2238, fixed with 4% (w/v) PFA, and subjected to an immunofluorescence staining. ATP1A1 (green) was detected by an anti-ATP1A1 rabbit MAb (ab76020) and an AF488-conjugated donkey anti-rabbit secondary antibody. EGFR (red) was detected by and an anti-EGFR rat MAb (ab231) and an AF647-conjugated goat anti-rat secondary antibody. The cell nuclei were stained with DAPI (blue). Images (z-stacks) were acquired on a Leica SP8 confocal microscope, with a 63x objective (NA 1.4) and a zoom of 3.0. Scale bars, 10 µm.

To evaluate possible effects of ouabain and PST2238 on RSV infection, A549 cells were pre-treated for 16 h with these ATP1A1-binding compounds, inoculated with RSV-GFP (MOI = 1 PFU/cell) and incubated with the compounds present throughout. RSV infection was evaluated by (i) viral GFP expression 17 h p.i., quantified by an ELISA reader (Figure 23A), and (ii) the yield of progeny RSV harvested 24 h p.i., quantified by plaque titration on Vero cells (Figure 23B). Both methods correlated well, showing a reduction in RSV replication for each compound that was greater than the reduction achieved with the ATP1A1-specific siRNAs (Figure 15). Ouabain had the stronger effect; It reduced the viral GFP expression by 96% and virus yield by almost 3.0 $\log_{10}$ compared to mock-treated cells. PST2238 reduced viral GFP expression by 89% and virus yield by 2.0 $\log_{10}$ compared to cells that were mock-treated. Overall, both compounds showed very strong inhibitory effects on RSV infection.

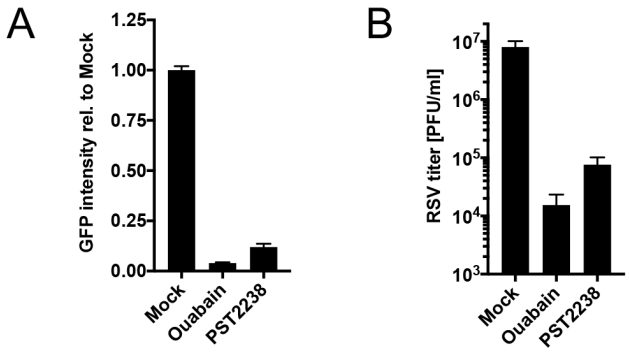

Figure 23: **Effect of ouabain and PST2238 on RSV infection.** A549 cells were pre-treated for 16 h with either 25 nM ouabain or 20 µM PST2238 and subsequently were inoculated with RSV-GFP (MOI = 1 PFU/cell). Infectivity was quantified by: **(A)** GFP intensity of the total well, scanned by an ELISA reader, 17 h p.i. and reported relative to mock-treated infected cells as 1.0; and **(B)** virus titer determined by plaque titration on Vero cells 24 h p.i.

To determine the stage of RSV infection that is inhibited by these compounds, a “time of addition” experiment was performed. A549 cells were infected with RSV-GFP (MOI = 3 PFU/cell) and at different times p.i. ouabain (Figure 24A and B) or PST2238 (Figure 24C and D) was added. Cells were incubated for a total of 24 h p.i. and the GFP intensity of single, live, GFP^+ cells was analyzed by flow cytometry. For both compounds, the strongest inhibitory effect was observed when the inhibitor was added simultaneously with RSV-GFP at 0 h, showing 85% and 66% reduction of GFP expression by ouabain and PST2238, respectively (Figure 24A-D). The inhibition of infection continued to diminish with increasingly later addition of the drugs, and was almost completely lost when the drug was added at 10 h p.i. These results suggested a role for ATP1A1 early in infection, such as in uptake and entry.

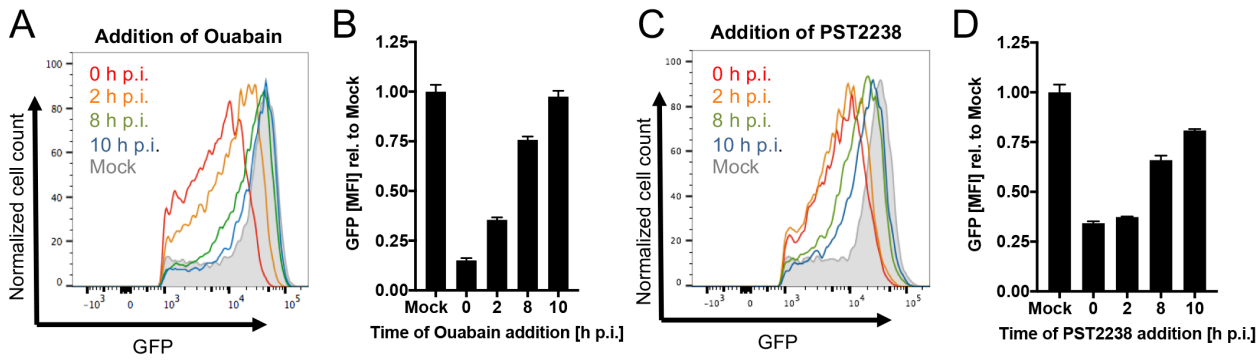

Figure 24: **Time of addition experiment for ouabain and PST2238 during RSV infection.** A549 cells infected with RSV-GFP (MOI = 3 PFU/cell) were incubated in the presence of 25 nM ouabain (A, B) or 20 µM PST2238 (C, D) beginning simultaneously with infection (0 h) or at the indicated times p.i. The GFP intensity of single, live, GFP$^+$ cells was quantified by flow cytometry at 24 h p.i. The GFP-MFI was reported relative to mock-treated RSV-infected cells (shown in gray in the histogram) assigned the value of 1.0, with error bars indicating the SD.

The concentration-dependence of the antiviral efficacy (50% inhibitory concentration; IC_{50}) on RSV-GFP infection was determined for ouabain and PST2238 on A549 cells and HSAEC (Figure 25). A549 cells and HSAEC were inoculated with RSV-GFP (MOI = 1 PFU/cell) in the presence of serially-diluted ouabain (Figure 25A) or PST2238 (Figure 25B), which was added simultaneously with the inoculum. The cytotoxicity of ouabain and PST2238 was previously evaluated and is shown above in Figure 21A and B, respectively. The viral GFP expression was quantified by an ELISA reader 24 h p.i. and reported relative to mock-treated RSV-infected cells.

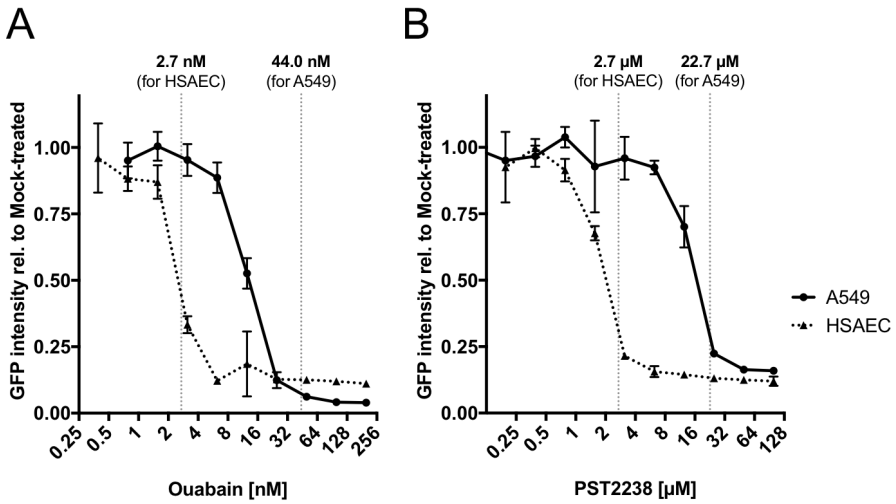

Figure 25: **Concentration-dependence of the antiviral efficacy of ouabain and PST2238 on A549 and HSAEC.** A549 cells (solid line) and HSAEC (dotted line) treated with serial dilutions of ouabain (A) and PST2238 (B) were infected with RSV-GFP (MOI = 1 PFU/cell) and incubated for 24 h. GFP expression, as an indicator of viral infection, was quantified by an ELISA reader and reported relative to mock-treated infected cells assigned the value of 1.0, with error bars indicating the SD. Cytotoxicity of the same serial-dilutions of ouabain and PST2238 on A549 cells and HSAEC were determined in Figure 21 and the maximal concentration for 80% viability (Table 19) for each cell line is indicated by vertical dotted lines.

Ouabain and PST2238 showed an increased inhibition of RSV-GFP with increasing concentration and reached almost maximal inhibition before affecting the cell viability by more than 20%. The inhibition of RSV-GFP in primary HSAEC was more effective compared to A549 cells for both compounds. The efficacy curves for ouabain (Figure 25A) and PST2238 (Figure 25B) were used to calculate the respective IC_{50} values (Table 20) using the software Prism 7 (GraphPad

Software, Inc.). This showed that the IC_{50} values were lower in HSAEC than A549 cells by 4.9-fold for ouabain and 8.2-fold for PST2238.

Table 20: Calculated[1] IC_{50} for RSV-GFP in A549 and HSAEC cells:

Cells	Ouabain [nM]	PST2238 [µM]
A549	12.7	14.8
HSAEC	2.6	1.8

[1] IC_{50} values were calculated with GraphPad Prism 7 based on the efficacy curves shown in Figure 25.

The effect of PST2238 on the phenomenon of ATP1A1 clustering during RSV infection, which was described above (Figure 17), also was investigated. PST2238 was used since it had no visible effect on the expression level of ATP1A1 on the plasma membrane (Figure 22). A549 cells were pre-treated with PST2238 for 16 h and infected with wt RSV (MOI = 5 PFU/cell). 5 h p.i. the cells were fixed, permeabilized, immunostained with antibodies specific to ATP1A1 and RSV F protein, as described above, and analyzed by confocal fluorescence microscopy. PST2238 had no apparent effect on the clustering of ATP1A1 compared to mock-treated infected cells (data not shown). This indicated that clustering of ATP1A1 was not affected by the presence of PST2238, and thus the inhibitory mechanism of PST2238 on RSV infection presumably acts downstream of ATP1A1 clustering.

3.1.7. ATP1A1-mediated signaling during RSV infection

The observed ATP1A1 clustering as well as the inhibitory effects of ouabain and PST2238 pointed towards a role of ATP1A1 in RSV-induced signaling cascades that might be involved in early steps of RSV infection. Therefore, the downstream signaling pathways of ATP1A1 that might be involved in ATP1A1-dependent RSV entry were investigated.

3.1.7.1. Effects of Src-kinase inhibition on RSV infection

As described in the Introduction, ATP1A1 does not contain a known signaling domain, such as kinase activity. However, ATP1A1 located in the caveolae is associated with cellular c-Src – a non-receptor tyrosine kinase - that is activated by the binding of ouabain to ATP1A1. To test the hypothesis that RSV might use an ATP1A1-associated signaling pathway for entry, the requirement of c-Src activity during RSV infection was examined. Two Src-kinase inhibitors, PP2 and Src-Inhibitior-I (SrcI-I), were used to evaluate the effects on RSV. A549 cells were pre-treated with non-cytotoxic concentrations (see Figure 39 for an evaluation of cytotoxicity) of these inhibitors separately or together (SrcI-I +PP2) for 5 h, followed by infection with RSV-GFP (MOI = 1.0 PFU/cell) in the continued presence of the indicated inhibitors. The efficiency of RSV infection was evaluated by (i) GFP expression at 17 h p.i. for all treatments measured by an ELISA reader (Figure 26A), and (ii) production of infectious RSV at 24 h p.i. for cells that had been treated with

both inhibitors (SrcI-I + PP2), assayed by plaque titration (Figure 26B). Each Src inhibitor showed a modest, but significant ($p < 0.0001$) reduction in GFP intensity of 23% (SrcI-I) and 33% (PP2) relative to mock-treated infected cells. When added together (SrcI-I + PP2), the inhibitory effect was additive reaching 45% reduction compared to mock-treated infected cells. The RSV titer for the combined Src-inhibitor treatment showed a 2-fold, significant (two-tailed, unpaired t-test, $p = 0.0014$) reduction compared to mock-treated infected cells (Figure 26B). These data confirmed that Src-kinase activity contributes to RSV infection.

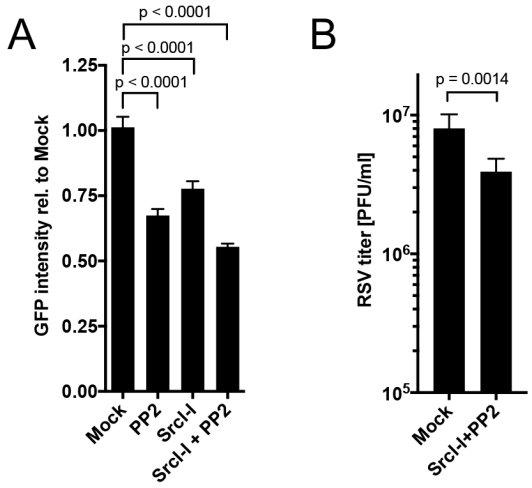

Figure 26: **Src-kinase activity is required for efficient RSV infection.** A549 cells were pre-treated (5 h) with the indicated Src-kinase inhibitors (PP2 [12.5 µM], SrcI-I [6.25 µM] or both) or were mock-treated (DMSO carrier control), and were inoculated with RSV-GFP (MOI = 1 PFU/cell) in medium containing the indicated inhibitors. **(A)** GFP intensity of the total well, scanned by an ELISA reader 17 h p.i. and expressed relative to mock-treated infected cells assigned the value of 1.0. **(B)** The production of infectious RSV at 24 h p.i. was quantified by plaque titration on Vero cells. The statistical significance of differences was determined by one-way ANOVA with Tukey's multiple-comparison post-test, and p-values are shown for each comparison.

3.1.7.2. Effects of EGFR knockdown on RSV infection.

It was investigated whether EGFR, a potential downstream signaling partner of c-Src kinase, was involved in RSV infection. If RSV uses an ATP1A1 signaling pathway, possibly similar to that induced by ouabain, then the downstream presence of EGFR, and transactivation of EGFR by c-Src, might be necessary to facilitate RSV entry.

Commercially available EGFR-specific siRNAs were evaluated for the ability to knock down expression of EGFR, and a siRNA was identified that reduced EGFR protein expression in A549 cells at 48 h p.t. to 15% compared to Neg. siRNA 1 (Figure 27A), with minimal effects on cell viability (Figure 28C). A549 cells were transfected with the indicated siRNAs and the effects on the cellular expression of the non-targeted protein was examined by immunofluorescence staining 48 h p.t. ATP1A1-specific and EGFR-specific siRNAs greatly reduced the expression of their corresponding target proteins (Figure 27B, ATP1A1 top panel; EGFR: bottom panel) without affecting the non-targeted EGFR and ATP1A1, respectively, whose expression remained similar to that of Neg. siRNA 1. This suggested that the ATP1A1 knockdown has no visible effect on the cellular expression of EGFR, or vice versa.

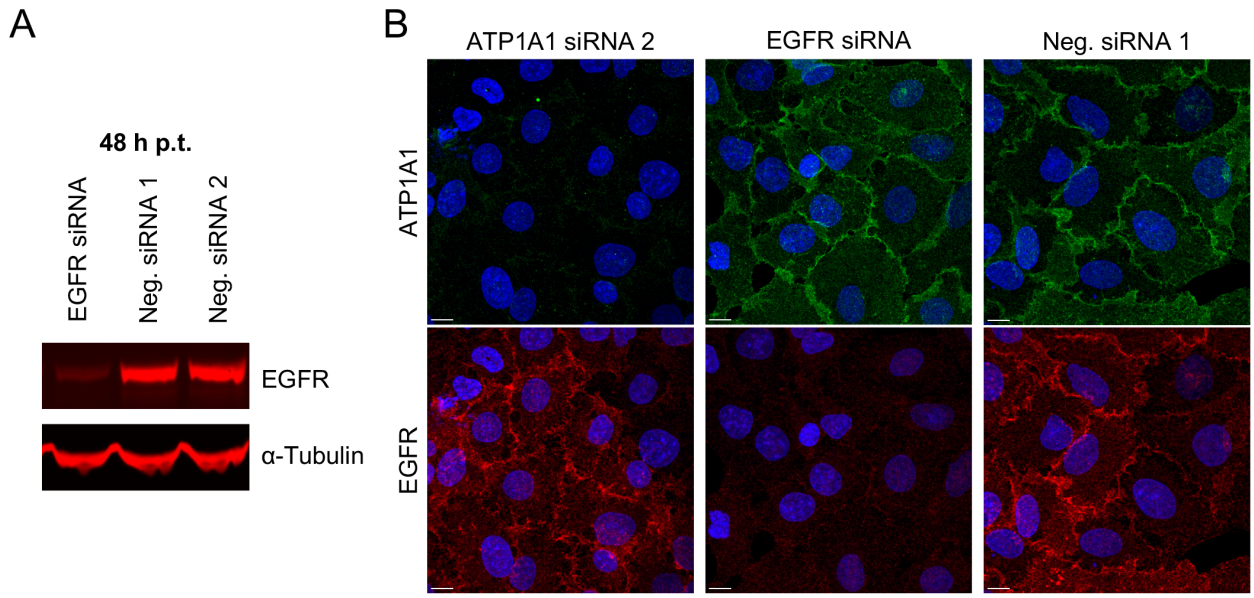

Figure 27: **Expression of ATP1A1 and EGFR proteins in A549 cells following knockdown with EGFR- and ATP1A1-specific siRNAs**. **(A) Western blot analysis of EGFR expression.** A549 cells were transfected with an EGFR-specific siRNA, and at 48 h p.i. the cells were lysed in 1x LDS buffer. The lysates were subjected to Western blot analysis with an EGFR-specific mouse MAb (ab181822) and a corresponding IRDye 680RD-conjugated goat anti-mouse secondary antibody. Alpha-tubulin was used as loading control and was detected by an anti-alpha-tubulin mouse MAb and the same secondary antibody as EGFR. **(B) Immunofluorescence microscopy.** A549 cells transfected with ATP1A1-specific, EGFR-specific, or negative control siRNA (Neg. siRNA 1) were fixed with 4% (w/v) PFA 48 h p.t and subjected to an immunofluorescence staining as described in the Materials and Methods. ATP1A1 (green) and EGFR (red) were detected with MAbs as described for Figure 22. The cell nuclei were stained with DAPI (blue). Images (z-stacks) were acquired on a Leica SP5 confocal microscope with 63x objective (NA 1.4) and 2.0x zoom. Scale bars, 10 µm.

To determine the role of EGFR in a possible ATP1A1-signaling pathway involved in RSV entry, a RSV infection assay was performed following knockdown of EGFR expression. A549 cells were transfected with the EGFR-specific siRNA, or with the negative control Neg. siRNA 1, and incubated for 48 h. In addition, cells transfected with ATP1A1 siRNA 2, which had the strongest inhibitory effect on RSV-GFP infection (as shown in Figure 15), were included as reference. Knockdown cells were infected with RSV-GFP and the infection was evaluated by viral GFP intensity at 17 h p.i., quantified by an ELISA reader (Figure 28A), and by virus titer at 24 h p.i. determined by plaque titration on Vero cells (Figure 28B). EGFR knockdown resulted in a nearly 50% reduction in viral GFP expression (Figure 28A) as compared to Neg. siRNA 1 ($p < 0.0001$). This reduction observed with EGFR knockdown was less than that observed for ATP1A1 siRNA 2-transfected cells. There also was a significant 38% reduction in RSV titer in EGFR siRNA-transfected cells compared to Neg. siRNA 2- ($p = 0.0015$) or mock-transfected ($p = 0.0001$) cells (Figure 28B), but this was substantially less than that observed for the ATP1A1 knockdown. There was a modest but consistent reduction in RSV titer for Neg. siRNA 1 for reasons unknow, and hence the reduction in RSV titer for EGFR siRNA-transfected cells was not significantly reduced as compared to this particular control siRNA (ns, $p = 0.9891$), but as noted above the reduction in GFP expression was highly significant. In summary, these data confirmed that EGFR plays a role during RSV infection.

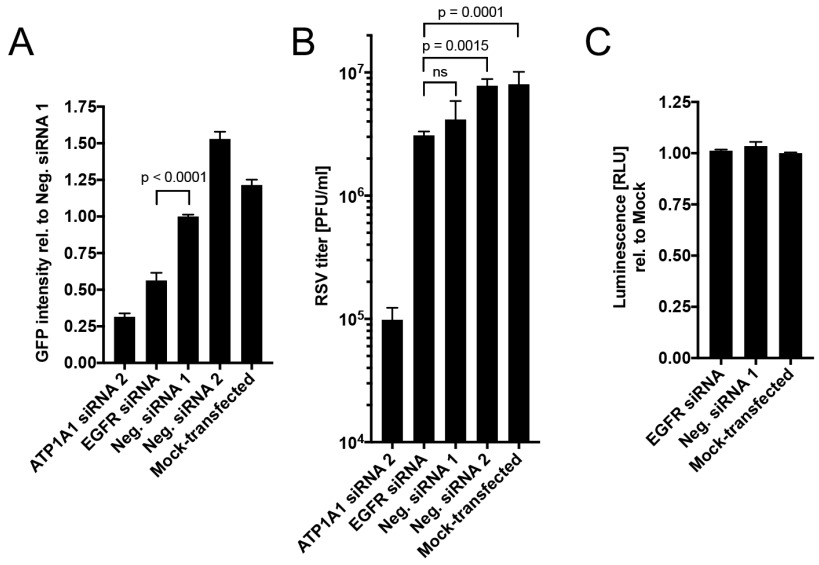

Figure 28: **Effect of EGFR knockdown on RSV infection. (A and B) Efficiency of infection by RSV-GFP.** A549 cells were transfected with an EGFR-specific siRNA or Neg. siRNA 1 or 2, and at 48 h p.i. the cells were infected with RSV-GFP (MOI = 1 PFU/cell). The ATP1A1 siRNA 2 knockdown was included as reference. Infectivity was quantified by: (A) GFP intensity of the total well at 17 h p.i., scanned by an ELISA reader, and reported relative to Neg. siRNA 1-transfected cells assigned the value of 1.0; and (B) virus titer at 24 h p.i., determined by plaque titration on Vero cells. Data were derived from three independent experiments. The statistical significance of differences was determined by one-way ANOVA with Tukey's multiple-comparison post-test, and the p-value for each comparison is indicated. **(C) Cell viability.** An ATP-based cell viability assay (CellTiter-Glo) was performed 72 h p.t. to evaluate the viability of the transfected cells. Cells were lysed, the ATP-concentration was determined by luciferase activity, reflecting the viability, and reported relative to mock-transfected cells assigned the value of 1.0.

3.1.7.3. EGFR phosphorylation in response to RSV infection.

An EGFR phosphorylation antibody array (RayBiotech, Inc.) was used to investigate EGFR phosphorylation during RSV infection. The array contained phospho-specific antibodies against 17 different specific phosphorylation sites of the human EGFR family, plus a positive control antibody that binds EGFR irrespective of phosphorylation, which were spotted in duplicate on a nitrocellulose membrane. Replicate membranes were incubated with the individual cell lysates from independent experimental samples. The bound EGFR was quantified by binding with a second, biotinylated, pan-EGFR antibody, followed by binding with horseradish peroxidase-conjugated streptavidin, and luminescence was detected with an X-ray film.

For the experiments, A549 cells were serum-starved for 16 h and infected with wt RSV (MOI = 5 PFU/cell). 5 h p.i. cell lysates of the infected-cells were prepared and subjected to the EGFR phosphorylation antibody array. Both uninfected and RSV-infected A549 cells had detectable ErbB2 phosphorylation at Thr686 and Ser1113 (Figure 29, blue box), which was not affected by RSV infection (note that ErbB2 is a member of the EGFR family of receptor tyrosine kinases). However, RSV induced the phosphorylation of EGFR Tyr845, which was not observed in mock-treated uninfected cells (Figure 29 and Figure 30). Tyr845 also was the only phosphorylation site, among the 17 screened sites (see Figure 29B), that showed any detectable increase in EGFR phosphorylation induced by RSV infection (Figure 29A, red box).

A

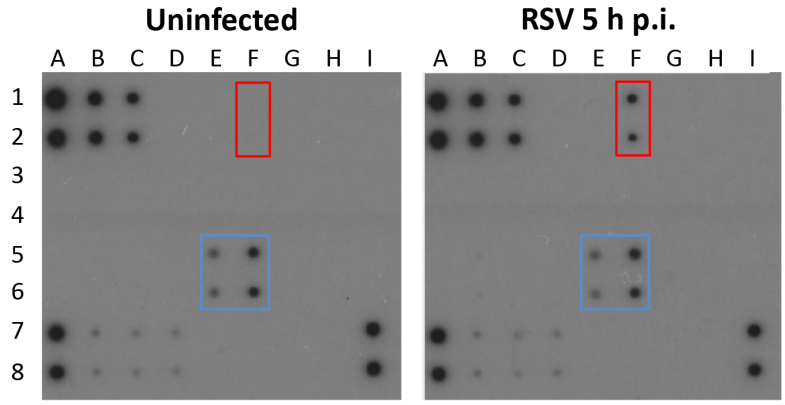

B

	A	B	C	D	E	F	G	H	I
1	P1	P2	P3	Blank	Neg	EGFR (Tyr845)	EGFR (Tyr992)	EGFR (Tyr1045)	EGFR (Tyr1068)
2	P1	P2	P3	Blank	Neg	EGFR (Tyr845)	EGFR (Tyr992)	EGFR (Tyr1045)	EGFR (Tyr1068)
3	Blank	Blank	Blank	Blank	EGFR (Tyr1086)	EGFR (Tyr1148)	EGFR (Tyr1173)	EGFR (Ser1046/1047)	EGFR (Ser1070)
4	Blank	Blank	Blank	Blank	EGFR (Tyr1086)	EGFR (Tyr1148)	EGFR (Tyr1173)	EGFR (Ser1046/1047)	EGFR (Ser1070)
5	ErbB2 (Tyr877)	ErbB2 (Tyr1112)	ErbB2 (Tyr1221/1222)	ErbB2 (Tyr1248)	ErbB2 (Thr686)	ErbB2 (Ser1113)	ErbB3 (Tyr1289)	ErbB4 (Tyr1284)	Blank
6	ErbB2 (Tyr877)	ErbB2 (Tyr1112)	ErbB2 (Tyr1221/1222)	ErbB2 (Tyr1248)	ErbB2 (Thr686)	ErbB2 (Ser1113)	ErbB3 (Tyr1289)	ErbB4 (Tyr1284)	Blank
7	EGFR	ErbB2	ErbB3	ErbB4	Blank	Blank	Neg	Blank	P4
8	EGFR	ErbB2	ErbB3	ErbB4	Blank	Blank	Neg	Blank	P4

Figure 29: **Detection of EGFR phosphorylation using an EGFR phosphorylation antibody array (RayBiotech, Inc.) against 17 potential phosphorylation sites of the EGFR family.**
(A) X-ray film exposures of arrays incubated with uninfected (left) versus RSV-infected (right) A549 cell lysates. Representative image of the EGFR phosphorylation antibody array probed with uninfected or RSV-infected (MOI = 5 PFU/cell, harvested for analysis after 5 h incubation) A549 cell lysates are shown. Arrays were processed as described in the Materials and Methods, and X-ray films are shown that reveal the binding of phosphorylated sites. The red boxes indicate duplicate spots (coordinates F1/2) demonstrating phosphorylation of EGFR Tyr845 in response to RSV infection. The blue boxes indicate duplicate spots at coordinates E5/6 and F5/6 demonstrating phosphorylation of ErbB2 at Thr686 and Ser1113, respectively. **(B) Array layout.** The layout of the EGFR phospho-specific antibodies and the control spots on the array are shown. Each antibody is present in duplicate. In parentheses the phosphorylation site of EGFR, Erb2, ErbB3 and ErbB4 is specified. The specificity of the duplicate spots in coordinates F1/2 are indicated in red (EGFR Tyr845) and E5/6, F5/6 are indicated in blue (ErbB2 Thr686 and Ser1113). P1 - P4 are internal positive controls with decreasing intensity. Neg is the internal negative control.

The phosphorylation of EGFR Tyr845 during RSV infection also was examined under various conditions (ATP1A1 siRNA knockdown, ouabain or PST2238 treatment, and Src-kinase inhibition). Prior to infection, A549 cells were transfected with ATP1A1-specific siRNAs (siRNA 1-3) or Neg. siRNAs and incubated for 48 h. For the chemical compounds, the cells were pretreated with ouabain or PST2238 for 16 h, or with the Src-kinase inhibitors SrcI-I + PP2 for 5 h, as described above. The cells were then infected with wt RSV (MOI = 5 PFU/cell) and lysates were prepared at 5 h p.i. The lysates were analyzed using the EGFR phosphorylation antibody array to quantify the level of EGFR Tyr845 phosphorylation. The arrays were processed as described in the Materials and Methods, and the spots were detected and quantified by X-ray films and densitometry. The spot intensity of pTyr845 for each treatment was normalized to internal array controls and to the total amount of EGFR present in the lysates. Values were reported relative to Neg. siRNA 1 (for siRNA-treated samples, Figure 30B) or to mock-treated infected cells (for

chemical compound-treated samples, Figure 30C). The level of pTyr845 was found to be significantly ($p < 0.0001$) reduced in cells treated with ATP1A1-specific siRNA, to an average of 35% (siRNA 1), 22% (siRNA 2), and 33% (siRNA 3) relative to Neg. siRNA 1-transfected RSV-infected cells (Figure 30B). The phosphorylation of Tyr845 in mock-treated RSV-infected cells was similar to Neg. siRNA 1-infected cells. While phosphorylation of Tyr845 was slightly reduced for Neg. siRNA 2, the difference was not significant ($p = 0.3651$) compared to Neg. siRNA 1. A significant reduction in Tyr845 phosphorylation also was observed when the cells were treated with ouabain, PST2238, or Src-kinase inhibitors (SrcI-I +PP2) prior to infection with RSV (Figure 30C). The phosphorylation level of Tyr845 in cells that were treated with ouabain and PST2238 was reduced to 27% and 26%, respectively, compared to mock-treated RSV-infected cells; the reduction was similar to that observed for ATP1A1 knockdown. Inhibiting the Src-kinase activity (SrcI-I+PP2) reduced the Tyr845 phosphorylation to 12% compared to mock-treated infected cells (Figure 30C).

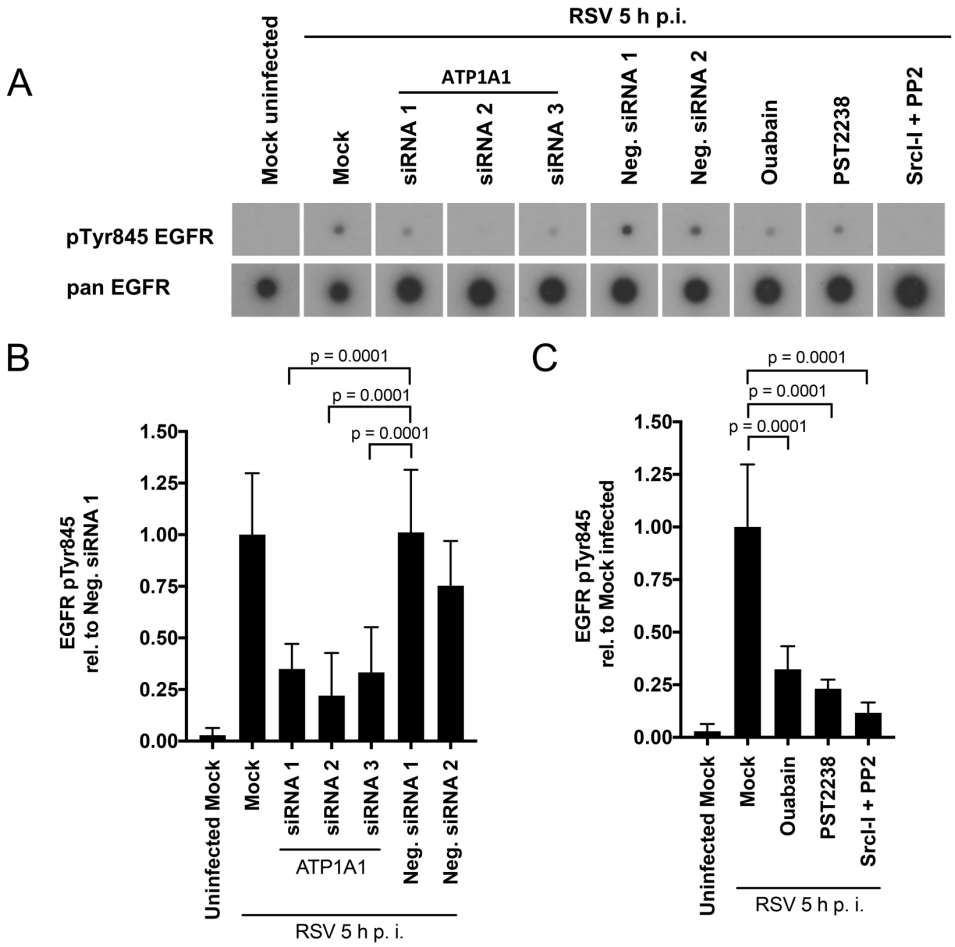

Figure 30: **EGFR phosphorylation at Tyr845 during RSV infection.** A549 cells were treated as indicated (either siRNA knockdown for 48 h, or pre-treatment with the chemical compounds ouabain [25 nM], PST2238 [40 µM] or Src Inhibitor-I (SrcI-I, 6.25 µM) and PP2 (12.5 µM) for 5 h pre-inoculation) and serum-starved for 16 h pre-inoculation, and then the cells were inoculated with wt RSV (MOI = 5 PFU/cell). Cells were lysed 5 h p.i. and subjected to analysis with the EGFR phosphorylation antibody array.
(A) Representative array spots of pTyr845 EGFR and its corresponding pan EGFR for each treatment are shown. **(B and C) Relative quantification of pTyr845 EGFR.** The pTyr845 signals of three independent experiments were normalized to internal positive controls and pan EGFR. pTyr845 phosphorylation was reported relative to Neg. siRNA 1-transfected (B) or mock-treated (C) RSV-infected samples assigned the value of 1.0. The statistical significance of differences was determined by one-way ANOVA with Dunnett multiple-comparison test and the p-values are indicated for each comparison.

In summary, it was shown that RSV-induced phosphorylation of EGFR Tyr845 could be reduced either by decreasing ATP1A1 expression or by ATP1A1- or Src-specific inhibitors. This suggested that EGFR pTyr845 is ATP1A1-dependent and that c-Src kinase serves as a signaling effector to transactivate EGFR by Tyr845 phosphorylation.

3.1.8. Investigation of the RSV uptake mechanism

As described in the Introduction, EGFR activation can induce different endocytic pathways, including clathrin-mediated endocytosis and macropinocytosis [reviewed in (Tomas et al. 2014)]. Macropinocytosis is a non-specific fluidic uptake mechanism and was previously described as a possible mode of RSV entry (Krzyzaniak et al. 2013). On the other hand, clathrin-mediated endocytosis also has been postulated to mediate RSV for entry (Kolokoltsov et al. 2007). Thus, it was not clear whether either or both mechanisms are involved in RSV entry. Therefore, the mode of RSV uptake in response to ATP1A1-mediated signaling was investigated.

3.1.8.1. Evaluation of the mode of uptake using inhibitors

To reproduce previously described findings on the mode of RSV uptake, the effects on RSV infection of the most commonly used inhibitors for each uptake pathway - chlorpromazine for clathrin-mediated endocytosis and EIPA (5-(N-Ethyl-N-isopropyl)amiloride) for macropinocytosis - were tested. A549 cells were pre-treated for 5 h with serially-diluted inhibitor concentrations and inoculated with RSV-GFP (MOI = 1 PFU/cell) in the continuous presence of the inhibitor. RSV infection was evaluated by GFP intensity 17 h p.i., quantified by an ELISA reader and reported relative to mock-treated RSV-infected cells (Figure 31, solid lines). The cytotoxicity for A549 cells of the various inhibitor concentrations after a 24 h treatment was evaluated by the ATP-based viability assay, as described above, and reported relative to mock-treated cells (Figure 31, dotted lines).

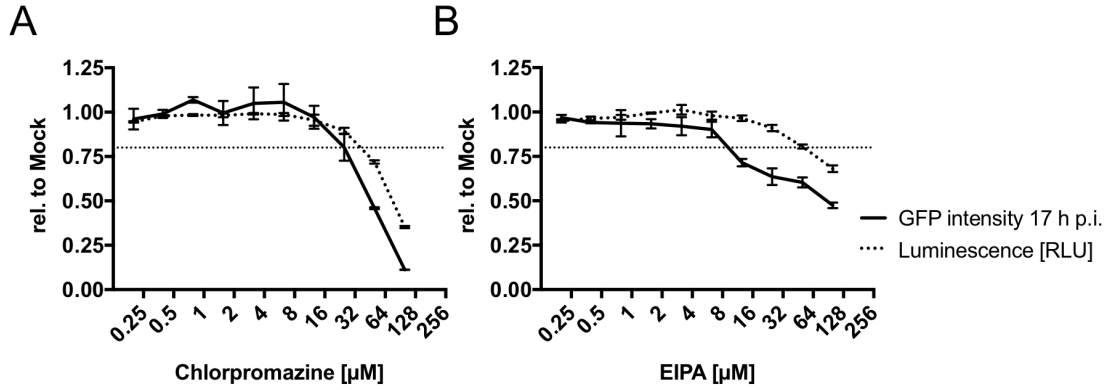

Figure 31: **Effects on RSV-GFP expression and cell viability of inhibitors of clathrin-mediated endocytosis (chlorpromazine) and macropinocytosis (EIPA) on A549 cells.** A549 cells were pre-treated for 5 h with serially-diluted concentrations of chlorpromazine or EIPA [5-(N-Ethyl-N-isopropyl) amiloride] and inoculated with RSV-GFP (MOI = 1 PFU/cell) while the inhibitor was continuously present. GFP was quantified by an ELISA reader 17 h p.i. (solid line) and cell viability was evaluated for each concentration by the ATP-based viability assay CellTiter-Glo (dotted line). GFP-intensity and luciferase activity was reported relative to mock-treated cells assigned the value of 1.0, with error bars indicating the SD. The dashed horizontal line reflects 80% viability.

Chlorpromazine did not significantly affect GFP expression at any non-cytotoxic concentration (Figure 31A). Reduced GFP intensity correlated with reduced viability with increasing concentrations of chlorpromazine, suggesting that the observed effects on viral GFP expression were likely a result of cytotoxicity rather than due to a specific inhibition of clathrin-mediated endocytosis.

The macropinocytosis inhibitor EIPA showed a sigmoid inhibitor response curve (Figure 31B). The GFP intensity was reduced to 63% compared to mock-treated RSV-infected cells at a concentration of 25 µM EIPA that had only minimal effects on the viability (91% viable compared to mock-treated cells). However, the nuclear morphology of EIPA-treated cells observed after DAPI staining by fluorescence microscopy showed a drastic change (Figure 32). The EIPA-treated cells had a diffused DAPI staining across the entire cytoplasm and lacked the distinct nuclear staining compared to mock-treated cells, suggesting that the nucleus had lost its integrity and the nuclear content was distributed in the cytoplasm. This observation indicated that even an apparently non-cytotoxic concentration of EIPA (Figure 31B), based on the ATP-based viability assay, might have generalized effects on cell viability that might reduce RSV infection, regardless of the mode of entry.

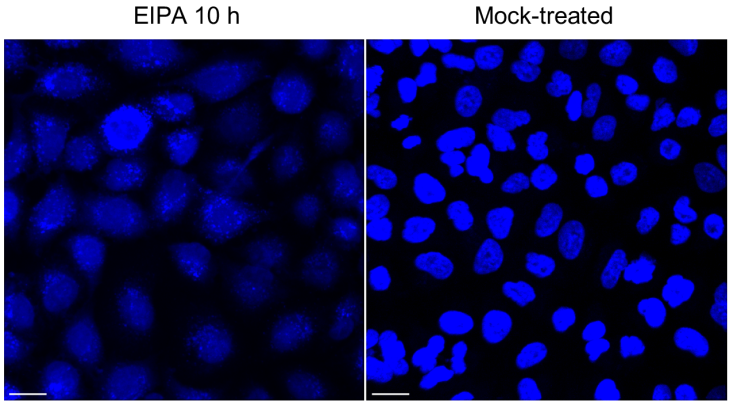

Figure 32: **Effect of EIPA treatment on A549 cells.** A549 cells were treated for 10 h with EIPA (25 µM), fixed with 4% (w/v) PFA and the nuclei were stained with DAPI (blue). The nuclear morphology of EIPA-treated cells was compared to mock-treated cells. Scale bars, 20 µm.

Wortmannin, a PI3K inhibitor, also was tested (data not shown) and also showed high cytotoxicity on A549 cells and did not have any appreciable effect on RSV infection at non-cytotoxic concentrations. Due to the high cytotoxicity and the unspecific side effects of the tested endocytic pathway inhibitors on A549 cells, it was not feasible to make any conclusions, based on these results, on the mode of RSV uptake.

3.1.8.2. Characterization of macropinocytosis as possible mode for RSV uptake

To assess macropinosome formation during RSV infection and the role of ATP1A1 in this process, fluorescent dye-conjugated dextran was used as a fluidic uptake marker for macropinocytosis that was visualized with fluorescence confocal microscopy. A549 cells were infected with wt RSV (MOI = 5 PFU/cell) in the presence of AF568-conjugated dextran (10,000 MW, dextran-AF568). At 5 h p.i., cells were washed and fixed, nuclei were counterstained with DAPI, and the uptake of dextran was analyzed by fluorescence confocal microscopy and quantified with the image processing software Imaris. Cells that had been mock-infected, contained dextran-positive vesicles that were small, round, and homogeneous in size, with an average volume of ~ 0.5 μm^3 (Figure 33, top panel) and reflected the basal level of cellular dextran uptake. This phenotype changed dramatically with wt RSV infection by 5 h p.i (Figure 33, bottom panel). The dextran-positive vesicles were much bigger (average volume of ~5.7 μm^3), irregular in shape, and reflected the typical morphology of macropinosomes. This suggested that RSV infection triggered macropinosome formation in A549 cells.

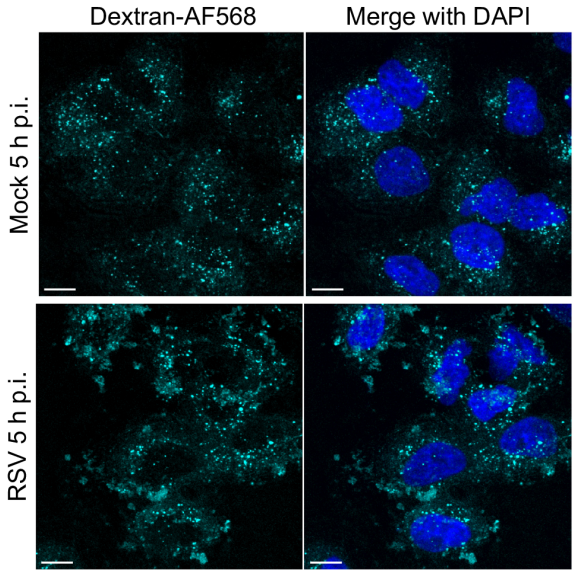

Figure 33: **RSV induces macropinosome formation in respiratory epithelial A549 cells.** A549 cells were serum-starved for 16 h and either mock-infected or infected with wt RSV (MOI = 5 PFU/cell) in medium containing AF568-conjugated dextran (10,000 MW, Dextran-AF568, cyan). Cells were fixed with 4% (w/v) PFA 5 h p.i., nuclei were counterstained with DAPI (blue), and the cells were imaged (z-stacks) on a Leica SP5 confocal microscope with a 40x objective (NA 1.3) and 2.0x zoom. Scale bars, 10 µm.

Additional A549 cells were infected with RSV in the presence of dextran-AF568 and fixed 5 h p.i. The fixed cells were subjected to an immunofluorescence staining for ATP1A1 (green) and RSV N (marker of RSV virions; red), and visualized by fluorescence confocal microscopy (Figure 34A). As noted earlier, 5 h p.i. is very early in RSV infection and the detected RSV N protein would be mostly derived from the inoculum, as was confirmed earlier with UV-inactivated virus (Figure 18). Clusters of ATP1A1 were observed co-localized with RSV N protein in dextran-positive macropinosomes (cyan) (Figure 34A, indicated by arrows), suggesting that RSV was taken up by macropinocytosis. Co-staining for RSV F and N also was performed and showed that both proteins were co-localized in the dextran-positive macropinosomes (Figure 34B, indicated by

arrows). The co-localization of RSV F and N suggested that the RSV-specific staining, detected in the macropinosomes, reflected enveloped RSV virions, suggesting that fusion and release of nucleocapsid presumably occurred subsequently in these internalized vesicles rather than at the plasma membrane.

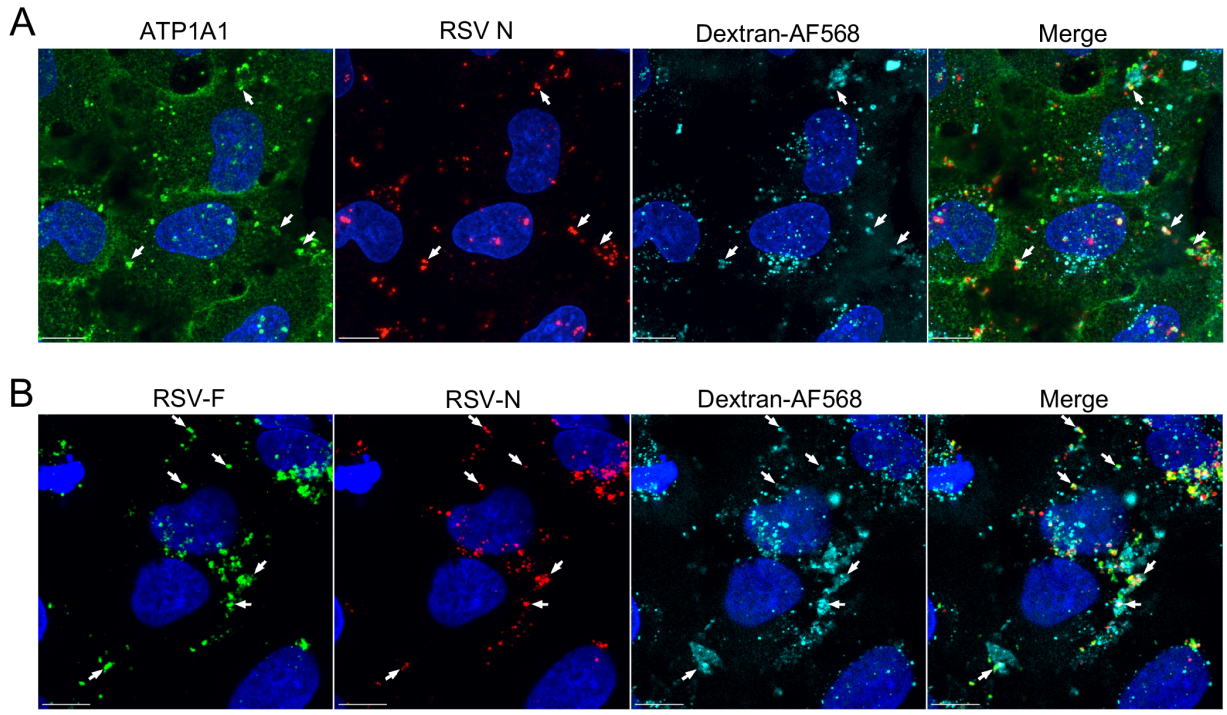

Figure 34: **Co-localization of RSV virions and ATP1A1 in macropinosomes during RSV uptake. (A) Co-localization of ATP1A1 (green) RSV N (red) and dextran-AF568 (cyan) in RSV-infected (MOI = 5 PFU/cell) A549 cells at 5 h p.i**. Cells were infected as described for Figure 33 and fixed with 4% (w/v) PFA 5 h p.i. Fixed cells were permeabilized with 0.1 % (v/v) Triton X-100 and subjected to immunofluorescence staining with an anti-ATP1A1 rabbit MAb (ab76020) and an anti-RSV N mouse MAb (ab94806), followed by AF488-conjugated goat anti-rabbit and AF647-conjugated goat anti-mouse secondary antibodies. Images (z-stacks) were acquired on a Leica SP8 confocal microscope with 63x objective (NA 1.4) and 3.0x zoom. Arrows indicate examples of co-localization of ATP1A1 and RSV N in dextran-AF568-positive vesicles. **(B) Co-localization of RSV F (green) and RSV N (red) with dextran-AF568 (cyan) in RSV-infected (MOI = 5 PFU/cell) A549 cells at 5 h p.i.** Cells were stained as described above for part A. RSV F was detected with an AF488-conjugated anti-RSV F MAb (#1129). RSV N was detected with an allophycocyanin (APC)-conjugated anti-RSV N MAb (Novus Biologicals, LLC). Image acquisition and analysis were performed as described for part A. Arrows indicate examples of co-localization of RSV F and RSV N in dextran-AF568-positive vesicles. All scale bars, 10 µm.

To examine the role of ATP1A1 in this putative uptake mechanism, ATP1A1 protein expression was knocked down by an ATP1A1-specific siRNA (siRNA 2 was used, since it showed the strongest effect in all other assays) or the cells were pre-treated with the ATP1A1-binding compounds ouabain or PST2238. The treated cells were infected with wt RSV in the presence of dextran-AF568, as described above. Macropinosome formation was quantified by fluorescence confocal microscopy. Multiple random z-stack images were acquired and the total amount of dextran uptake was quantified. Dextran-positive vesicles were identified by Imaris imaging software, and the total fluorescence intensity of dextran-AF568-containing vesicles was quantified. Vesicles smaller than 1.0 μm^3 were excluded to omit the basal level of dextran uptake (as shown in Figure 33, top panel) and to focus on the large vesicles that were induced by RSV and are typical for macropinosomes. The total intensity of dextran-AF568 within vesicles larger than 1.0

µm^3 was determined per field, normalized to the number of DAPI-stained nuclei, and expressed relative to Neg. siRNA 1-transfected or mock-treated cells (Figure 35). This showed that dextran uptake was increased 4-fold in RSV-infected cells as compared to uninfected cells, both of which had been both transfected with Neg. siRNA 1 (Figure 35A), confirming the visual observation of an increased dextran-AF568 uptake in response to RSV infection (Figure 33). On the other hand, knockdown of ATP1A1 in RSV-infected cells caused a significant ($p = 0.0003$) reduction of 33% compared to Neg. siRNA 1 (Figure 35A). Ouabain and PST2238 caused an even greater reduction in macropinosomes in RSV-infected cells to less than 50% compared to mock-treated RSV-infected cells (Figure 35B). These results suggested that macropinocytosis is induced by RSV, and that it involves ATP1A1 and is responsible for virion uptake.

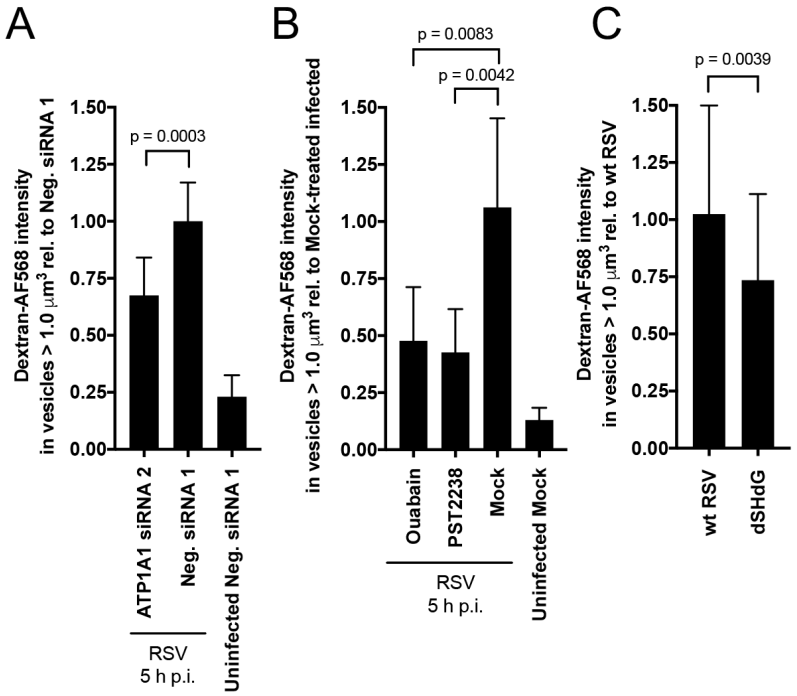

Figure 35: **Relative quantification of dextran-AF568 uptake during RSV infection. (A) ATP1A1 siRNA knock down.** A549 cells were transfected with ATP1A1 siRNA 2 or Neg. siRNA 1 and 48 h p.t. the cells were inoculated with wt RSV (MOI = 5 PFU/cell) in dextran-AF568 containing medium, and 5 h p.i. were analyzed as described below. (**B) ATP1A1-binding compounds.** A549 cells were pre-treated with ouabain or PST2238 for 16 h, inoculated with wt RSV (MOI = 5 PFU/cell) in dextran-AF568 containing medium, and 5 h p.i. were analyzed as described below. **(C) Role of RSV G.** Untreated A549 cells were infected with wt RSV or RSV dSH/dG (MOI = 5 PFU/cell) in dextran-AF568 containing medium, and 5 h p.i. were analyzed as described below.
For all treatments (A-C) cells were fixed 5 h p.i. and counterstained with DAPI, and multiple random z-stacks were acquired on a Leica SP8 confocal microscope with 63x objective (NA 1.4) and 1.0x zoom. For each treatment, the uptake of dextran-AF568 in vesicles greater than 1.0 µm^3 was quantified as described in detail in the Materials and Methods. Mean values were reported relative to RSV-infected cells transfected with Neg. siRNA 1 (A), mock-treated RSV-infected cells (B), or wt RSV-infected cells (C). Error bars indicate the SD of at least three independent experiments. The statistical significance of differences was determined for (A) and (B) by one-way ANOVA with Tukey's multiple comparison post-test and for (C) by two-tailed unpaired t-test. P-values are shown for each comparison.

Since RSV G was found to be important for triggering ATP1A1 activation, as observed by the loss of clustering with the dSH/dG mutant (Figure 20), the role of G in the induction of macropinocytosis also was evaluated. If RSV G protein plays a role in activating the ATP1A1-Src-EGFR pathway culminating in RSV uptake by macropinocytosis, an RSV mutant lacking G should

be inefficient in activating macropinocytosis. To examine this, macropinosome formation was quantified, as described above for Figure 35A and B, in A549 cells infected with wt RSV or the dSH/dG RSV mutant. This showed that macropinosome formation indeed was significantly (p = 0.0039) reduced for the dSH/dG virus as compared to wt RSV (Figure 35C), consistent with a role of the G protein in activating the pathway leading to macropinocytosis.

3.1.9. Effects of cholesterol depletion on RSV infection

As described in the Introduction, ATP1A1-Src-EGFR signaling characteristically is associated with caveolae. The structural integrity of caveolae depends on the presence of cholesterol, and its depletion with a cholesterol-sequestering drug, such as methyl-beta-cyclodextrin (MBCD), disrupts caveolae at the plasma membrane (Rothberg et al. 1992, Hailstones et al. 1998). Therefore, the effects of cholesterol depletion on RSV infection were evaluated. Cholesterol was depleted in A549 cells prior to infection by treatment with MBCD and Mevinolin, individually or in combination, at non-cytotoxic concentrations (Figure 39). MBCD removes cholesterol from the plasma membrane whereas Mevinolin inhibits its biosynthesis. First, cholesterol-depleted A549 cells were infected with RSV-GFP (MOI = 1 PFU/cell) and GFP expression was quantified 17 h p.i. by an ELISA reader (Figure 36A).

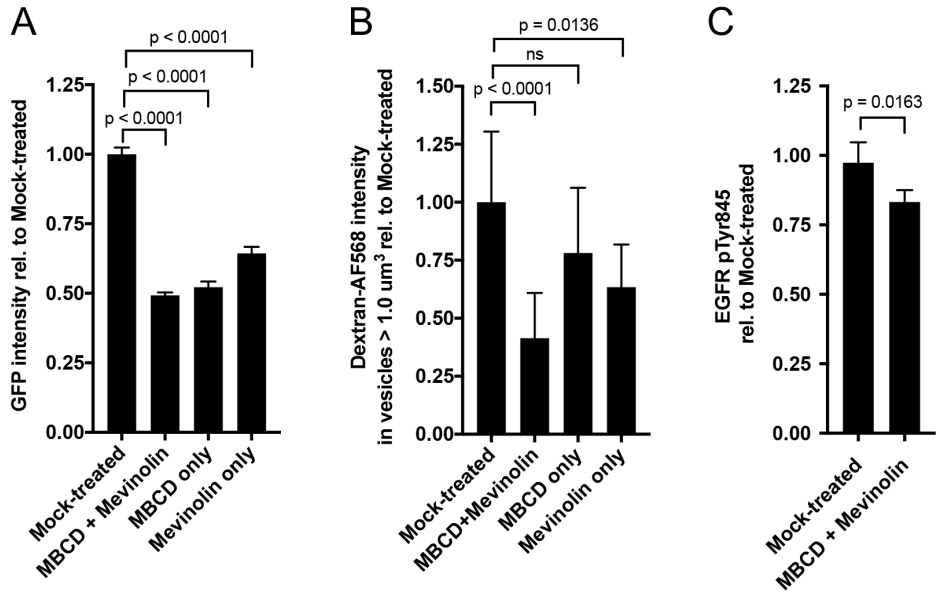

Figure 36: **Effects of cholesterol depletion on RSV infection.** A549 cells were cholesterol depleted by treatment with methyl-beta-cyclodextrin (MBCD) and Mevinolin in combination or separately. **(A) GFP expression by RSV-GFP in cholesterol-depleted A549 cells.** A549 cells were pre-treated for 5 h with the indicated cholesterol-depleting compounds and infected with RSV-GFP (MOI = 1 PFU/cell) while the cholesterol-depleting compounds were present. Viral GFP expression was quantified 17 h p.i. by an ELISA reader and reported relative to mock-treated infected cells assigned the value of 1.0. **(B) Quantification of macropinosome formation in cholesterol-depleted RSV-infected A549 cells.** A549 cells were pre-treated with the indicated cholesterol-depleting compounds for 16 h and infected with RSV (MOI = 5 PFU/cell) in the presence of AF568-conjugated dextran (Dextran-AF568). 5 h p.i the cells were fixed with 4% (w/v) PFA and nuclei were counterstained with DAPI. The total intensity of dextran-AF568 in vesicles larger than 1.0 μm^3 was quantified, as described in detail in Materials and Methods, and reported relative to mock-treated infected cells assigned the value of 1.0. The statistical significance of differences was determined by one-way ANOVA with Tukey's multiple-comparison post-test and p-values are shown for each comparison**. (C) EGFR Tyr845 phosphorylation in cholesterol-depleted cells.** A549 cells were pre-treated with MBCD + Mevinolin for 16 h and infected with wt RSV (MOI = 5 PFU/cell). The phosphorylation

of EGFR Tyr845 was quantified by an EGFR phosphorylation antibody array, as described in the Materials and Methods. The level of pTyr845 was reported relative to mock-treated infected cells. The statistical significance of difference was determined by a two-tailed unpaired t-test.

With each of the cholesterol-depleting compounds, alone or in combination, GFP expression was reduced to approximately 50 - 60% compared to mock-treated RSV-infected cells. Next, the level of RSV-induced macropinocytosis in cholesterol-depleted cells was quantified by dextran-AF568 uptake, as described above. Macropinosome formation was reduced by each of the cholesterol-depletion treatments, with the most significant ($p < 0.0001$) reduction of 59% observed for the combined MBCD-Mevinolin treatment (Figure 36B). The phosphorylation of EGFR Tyr845 also was determined in RSV-infected cells pre-treated with MBCD + Mevinolin. A modest but significant (two tailed t-test, $p = 0.0163$) reduction in pTyr845 was observed (Figure 36C). These results showed that cholesterol depletion results in reduced EGFR transactivation, reduced macropinocytosis, and reduced RSV infection, consistent with caveolae as the site of ATP1A1 signaling.

3.1.10. Confirmation of the role of ATP1A1 in RSV infection using primary human small airway epithelial cells (HSAEC).

All experiments described above were performed with the human airway epithelial A549 cell line, which is generally considered to be the most relevant cell line available for studies involving respiratory viruses. In order to confirm that the described findings derived from A549 cells truly represented a pathway for RSV entry in human airway epithelial cells, some of the major findings were recapitulated using commercially-obtained (ATCC) primary HSAEC from a 16-year old healthy male donor (Figure 37).

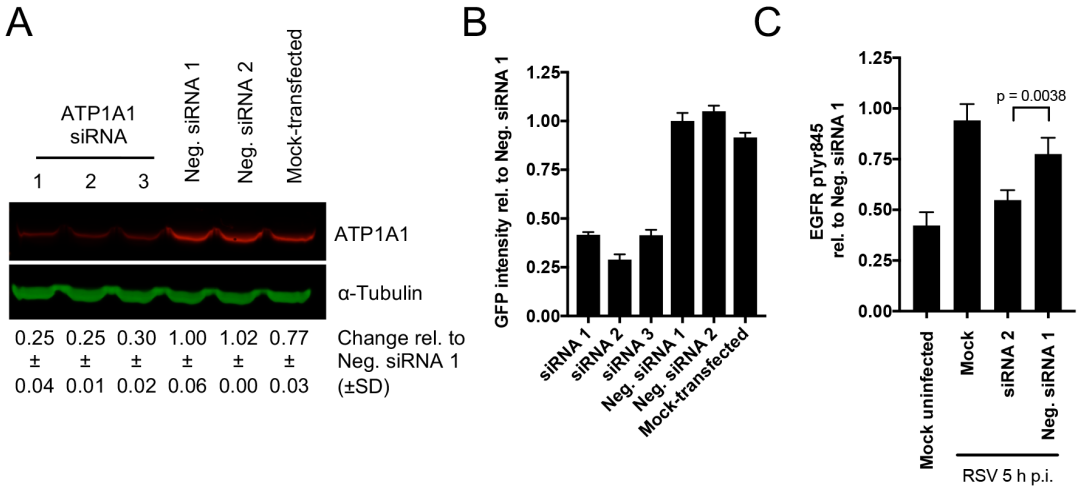

Figure 37: **Confirmation of the results obtained in the A549 cell line by experiments in primary HSAEC.** Experiments were performed as described for A549 cells in the Materials and Methods and preceding figure legends. **(A) ATP1A1 siRNA knockdown.** HSAEC were transfected with ATP1A1-specific siRNAs (siRNA 1 - 3) or Neg. siRNAs, and analyzed 48 h p.t. by Western blot analysis as in Figure 14. **(B) RSV infection assay.** Efficiency of RSV infection in HSAEC cells following knockdown of ATP1A1 expression using the indicated siRNAs. Viral GFP expression was quantified by an ELISA reader, as in Figure 15A. **(C) EGFR Tyr845 phosphorylation.** HSAEC were transfected with ATP1A1-specific siRNA (siRNA 2), and EGFR Tyr845 phosphorylation was quantified as in Figure 30.

It was possible to knock down ATP1A1 protein expression in HSAEC, by transfection with individual ATP1A1 siRNAs, to 25 – 30% compared to Neg. siRNA 1 (Figure 37A), which was slightly more than the reduction obtained in A549 cells (35 - 39%; Figure 14). Following the same assay protocols as used for A549 cells, the results in HSAEC showed that (i) knockdown of ATP1A1 expression reduced RSV-GFP expression to 29 - 42 % relative to the control Neg. siRNA 1 (Figure 37B), similar to what was observed with A549 cells (Figure 15A). (ii) RSV-induced phosphorylation of EGFR Tyr845 was significantly ($p = 0.0038$) reduced in HSAEC that were transfected with ATP1A1-specific siRNA (siRNA 2) prior to RSV infection (Figure 37C), similar to what was seen in A549 cells (Figure 30). (iii) The inhibitory effects of ouabain and PST2238 on the expression of RSV-GFP were even stronger in HSAEC than in A549 cells, as already shown in Figure 25 and Table 20. (iv) The RSV-induced ATP1A1 clustering and colocalization of ATP1A1 and RSV N also was observed in HSAEC (Figure 38), similar to A549 cells (Figure 17). Thus, the experiments performed in primary HSAEC cells confirmed the results obtained in the A549 cell line.

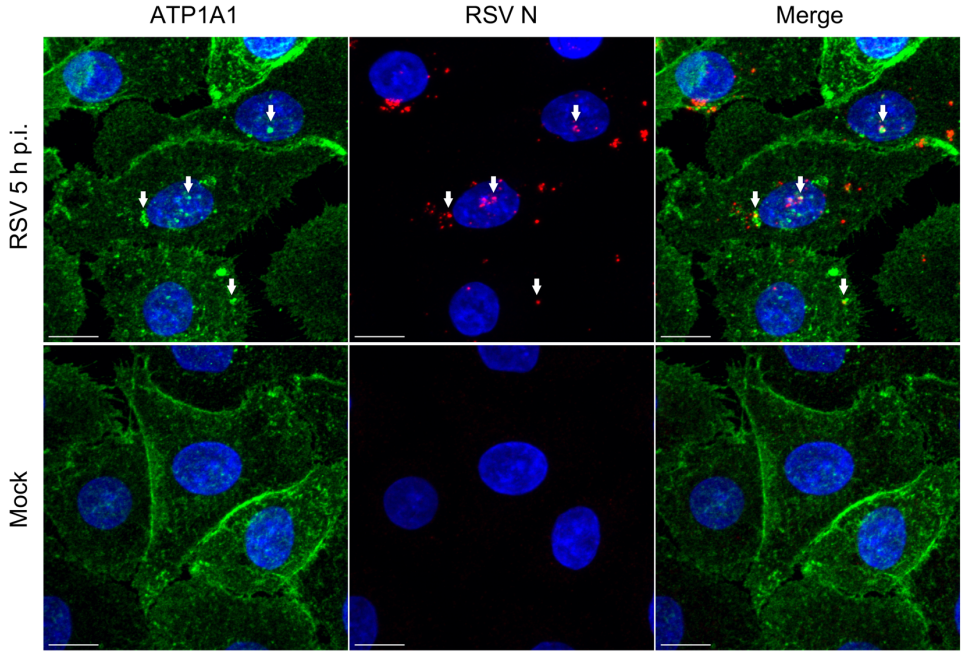

Figure 38: **Confirmation of RSV-induced ATP1A1 clustering in primary HSAEC.** HSAEC were inoculated with wt RSV (MOI = 5 PFU/cell), as described for A549 cells (Figure 17), and incubated for 5 h. Cells were fixed with 4% (w/v) PFA, permeabilized with 0.1 % (v/v) Triton X-100 and stained for ATP1A1 (green) with an anti-ATP1A1 rabbit MAb (ab76020) and AF488-conjugated donkey anti-rabbit secondary antibody. RSV N (red) was detected by an anti-RSV N mouse MAb (ab94806) and an AF594-conjugated anti-mouse secondary antibody. The cell nuclei were stained with DAPI (blue). Images (z-stacks) were acquired on a Leica SP5 confocal microscope, with a 63x objective (NA 1.4) and a zoom of 3.0. Arrows indicate examples of co-localization of ATP1A1 and RSV N. Scale bars, 10 µm.

3.1.11. Cytotoxicity assay of chemical compounds on A549 cells

The chemical compounds used in this study were evaluated in dilution series on A549 cells (data not shown) and non-cytotoxic working concentrations were determined. The working concentration of each compound had to affect the cell viability less than 20% as compared to mock-treated cells in order to be used. A549 cells were treated with the selected working concentrations for 24 h and viability was determined by the ATP-based viability assay CellTiter-Glo (Figure 39).

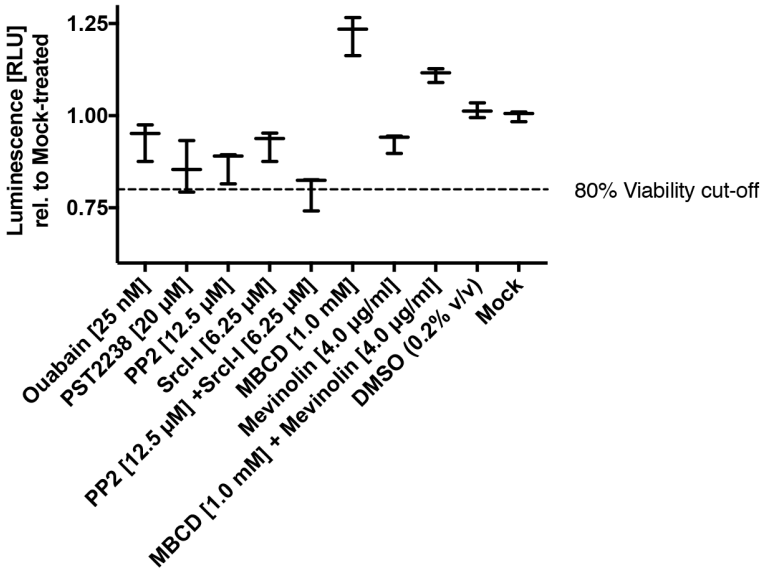

Figure 39: **Cytotoxicity of chemical compounds on A549 cells.** A549 cells were treated for 24 h with each compound at the highest concentrations used in this study. Cell viability was determined in triplicates for each compound by the ATP-based viability assay CellTiter-Glo and was reported relative to mock-treated cells assigned the value of 1.0, with error bars indicating the SD.

3.2. Development and pre-clinical evaluation of a live-attenuated mucosal HPIV1-vectored vaccine against EBOV

Recombinant HPIV1 vectors, bearing the attenuating $C^{\Delta 170}$ mutation, expressing EBOV GP were generated by reverse genetics, as described in section 2.2.6 of the Materials and Methods. The EBOV GP ORF was modified by the insertion of an additional A residue (mRNA-sense) at the gene editing site to obtain translation of full-length membrane-anchored EBOV GP. The ORF also was codon-optimized for human expression by GenScript. With the goal to enhance EBOV GP incorporation into the rHPIV1 vector particle, the TMCT domain of EBOV GP was substituted with that of HPIV1 F protein as shown in Figure 12C. The ORF encoding GP or GP-TMCT was inserted either at the pre-N (Figure 12A) or between the N-P position (Figure 12B) of the HPIV1-$C^{\Delta 170}$ genome as an additional gene under the control of HPIV1 GS and GE transcription signals. All constructs were successfully recovered. After an additional single passage on LLC-MK2 cells to obtain working pools, the viral genome consensus sequences were determined by automated Sanger sequencing of uncloned RT-PCR products, and were found to be free of adventitious mutations.

The viruses were named based on the position and form of EBOV GP that was expressed. The rHPIV1-$C^{\Delta 170}$ vectors expressing full-length EBOV GP from the first (pre-N) or second (N-P) position of their genome were named GP1 and GP2, respectively. The vectors expressing the chimeric form of EBOV GP containing the HPIV1 F TMCT from the first or second position of the HPIV1 genome were called GP-TMCT1 and GP-TMCT2, respectively.

3.2.1. Characterization of the HPIV1-vectored EBOV vaccine candidates *in vitro*

3.2.1.1. Multi-cycle growth kinetics

The ability of vaccine candidates to efficiently replicate *in vitro*, critical for vaccine manufacture, was assessed by determining their multistep growth kinetics on Vero cells (Figure 40). Wt HPIV1 and rHPIV1-$C^{\Delta 170}$ were included as the parental references. The growth kinetics of the viruses were similar with peak titers between 6.5 $\log_{10}TCID_{50}$/ml (GP-TMCT1) and 8.0 $\log_{10}TCID_{50}$/ml (rHPIV1-$C^{\Delta 170}$) and none of the viruses showed a substantial attenuated phenotype in Vero cells. The GP1 virus with full-length EBOV GP in the pre-N position was significantly ($p < 0.0001$) slower on day 2, with more than 1.0 $\log_{10}TCID_{50}$/ml lower titer than the other viruses, but reached peak titer similar to rHPIV1-$C^{\Delta 170}$ on day 3. The lowest peak titer was observed for GP-TMCT1, but this was only slightly lower than the other viruses.

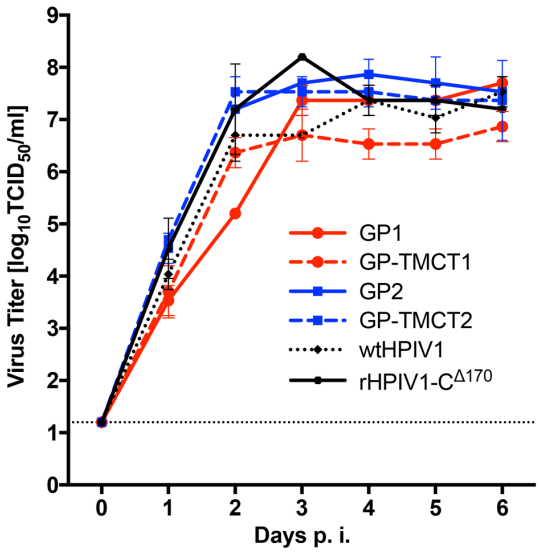

Virus[a]	Days p. i. 1	2	3	4	5	6
GP1	**	****	*	ns	ns	ns
GP-TMCT1	*	*	****	*	*	ns
GP2	ns	ns	ns	ns	ns	ns
GP-TMCT2	ns	ns	ns	ns	ns	ns

[a] Mean titers compared to the rHPIV1-$C^{\Delta 170}$ empty backbone: ns, not significant; *, P < 0.05; **, P < 0.01; ****, P < 0.0001

Figure 40: **Multistep growth kinetics of rHPIV1 expressing EBOV GP in Vero cells**. Vero cells were infected in triplicate with an MOI of 0.01 $TCID_{50}$/cell with each indicated HPIV1-$C^{\Delta 170}$ virus expressing EBOV GP or GP-TMCT. The cells were incubated at 32°C and aliquots of culture supernatant were collected at 24 h intervals over 6 days. Virus titers were determined by limiting dilution on LLC-MK2 cells using an hemadsorption assay. Titers are reported as $log_{10}TCID_{50}$ per ml. Mean titers are shown with the SD as vertical error bars. The statistical significance of differences between EBOV GP viruses (GP1, GP-TMCT1, GP2, GP-TMCT2) and the rHPIV1-$C^{\Delta 170}$ empty backbone was determined by two-way ANOVA with Tukey's multiple-comparisons post-test and is shown in the table beside the graph. The limit of detection (1.2 $log_{10}TCID_{50}$/ml) is marked as a horizontal dotted line in the graph.

3.2.1.2. Stability of EBOV GP expression by the HPIV1 vectors

To examine the plaque phenotype and stability of EBOV GP expression, a double-immunostaining plaque assay was performed. Primary antibodies specific to EBOV GP and HPIV1 proteins, with corresponding secondary antibodies conjugated to different fluorochromes, were used as described in the Methods (2.2.12). The stained plaques were pseudo-colored to appear red and green for HPIV1 and EBOV GP, respectively. HPIV1 plaques expressing EBOV GP appeared yellow and those not expressing EBOV GP would be red. This allowed evaluation of the percentage of infectious HPIV1 particles that expressed GP. For all viruses, no plaques were detected that did not express GP (Figure 41A), suggesting approximately 100% expression. The pre-N viruses (GP1 and GP-TMCT1) had an overall reduced plaque size as compared to N-P viruses (GP2 and GP-TMCT2), suggesting that GP insertion in the promoter-proximal position reduced virus replication and/or spread. The plaque size was further reduced for the GP-TMCT versions as compared to their full-length GP counterparts (Figure 41A), suggesting an attenuating effect of TMCT.

Due to the micro-plaque phenotype of the TMCT viruses, it was difficult to accurately determine the stability of GP expression for these viruses by the dual-stained plaque assay. Therefore, a flow cytometry-based assay was performed. Vero cells were infected with the various vectors at an MOI of 5 $TCID_{50}$/cell and incubated at 32˚C for 24 h. The cells were stained for HPIV1 F and EBOV GP protein and analyzed by flow cytometry. For all constructs, >99% of HPIV1 F+ cells (~15,000 cells analyzed for each construct) also expressed EBOV GP (Figure 41B). Thus,

the plaque assay and flow cytometric analysis showed that essentially all viruses maintained stable expression of EBOV GP or GP-TMCT during *in vitro* replication.

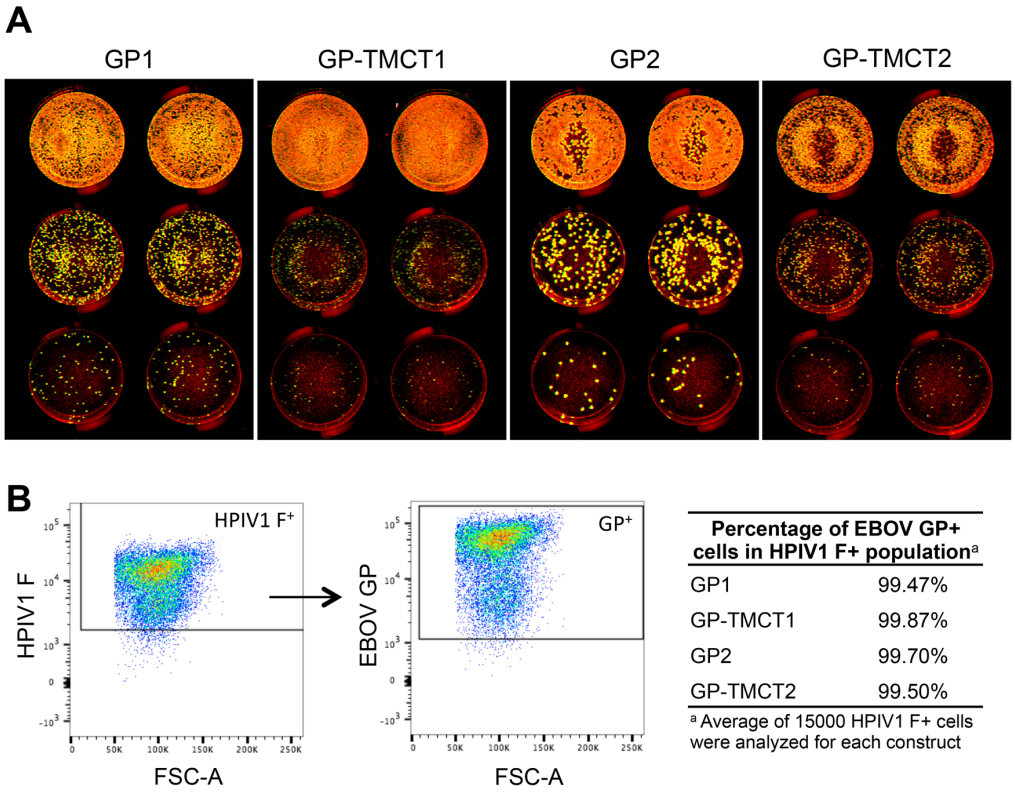

Percentage of EBOV GP+ cells in HPIV1 F+ population[a]	
GP1	99.47%
GP-TMCT1	99.87%
GP2	99.70%
GP-TMCT2	99.50%

[a] Average of 15000 HPIV1 F+ cells were analyzed for each construct

Figure 41: **Stability of EBOV GP expression by HPIV1 vectors**. **(A) Double-immunostaining plaque assay.** Vero cells were inoculated with a 10-fold serial dilution of each virus in duplicate and infected monolayers were incubated for 6 days under 0.8% (w/v) methylcellulose overlay medium. Immunostaining was performed with anti-EBOV GP mouse MAb and goat anti-HPIV1 polyclonal antibodies. Different IRDye-conjugated antibodies (donkey anti-mouse IRDye 800CW and donkey anti-goat IRDye 680LT) were used for detecting and differentiating EBOV GP- and HPIV1- positive plaques. Plaque images were acquired with Odyssey infrared imaging system and the percent of plaques expressing EBOV GP was determined. The IRDyes were pseudo-colored to appear red and green for HPIV1 and EBOV GP, respectively. On merging the colors, the plaques co-expressing GP and HPIV1 antigens would appear yellow and those not expressing GP would be red. Representative monolayers with various dilutions of virus are shown as examples. **(B) Double-immunostaining flow cytometry assay.** Vero cells infected with the indicated vectors were stained with anti-HPIV1 F and anti-EBOV GP (KZ52) MAbs and corresponding AF-conjugated secondary antibodies, as described in the Methods and analyzed on BD FACS Canto II flow cytometer. An example of EBOV GP staining of HPIV1 F+, single, live cells is shown as a pair of scatter plots and the stability of EBOV GP expression (percentage of EBOV GP+ cells in HPIV1 F+ population) for all vectors is shown as a Table.

3.2.1.3. EBOV GP: Expression in infected cell lysates and incorporation into virions

To visualize and quantify the expression of EBOV GP and HPIV1 vector proteins in infected cells, Vero cells were infected with the various vectors at an MOI of 3.0 $TCID_{50}$/cell and subjected to Western blot analysis at 48 h p.i. (Figure 42A). Full-length GP (also called GP_0) and the larger cleaved subunit GP_1 were detected with an MAb specific to both proteins; in the Western blot of cell-associated protein in Figure 42A, these two species appear as an unresolved GP_0 / GP_1 smear (top panel), which is likely due to the glycosylation of the GP protein. GP_2 was not detected by this MAb. All of the constructs, with or without the TMCT modification, expressed a considerable amount of this cell-associated GP_0 / GP_1 protein.

The HPIV1 genome is a single-stranded negative-sense RNA and has a gradient of gene expression, with the greatest expression for 3' proximal genes as compared to the downstream genes. Thus, a gene inserted closer to the 3' end would be expected to express more protein than from a downstream location. However, such a gradient effect was not apparent for the GP and GP-TMCT proteins, which were expressed at similar levels for the pre-N and N-P constructs (Figure 42A, top panel). In contrast, expression of the vector genes exhibited a gradient effect. All viruses bearing a GP or GP-TMCT insert had reduced expression of downstream vector proteins as compared to wt HPIV1 and HPIV1-$C^{\Delta 170}$ empty vector (Figure 42A, 2nd, 3rd, 4th, and 5th panels from the top). This reduction was greater for the pre-N as compared to the N-P viruses and a further reduction in expression was seen with GP-TMCT versions as compared to their respective full-length GP constructs. The reduction due to the TMCT swap was likely not an effect of the transcriptional gradient, since the number of genes was not affected. Thus, the insert position (i.e. pre-N position compared to N-P) appeared to have little or no effect on EBOV GP or GP-TMCT expression, but did reduce vector protein expression.

The goal of making EBOV GP-TMCT versions (expressed by the GP-TMCT1 and GP-TMCT2 vectors) was to increase the packaging of GP into the vector virion by making the TMCT domain of GP HPIV1-specific and therefore compatible with the HPIV1 virion proteins that are involved in virion morphogenesis. To assess packaging of EBOV GP into the vector particles, each virus was propagated in LLC-MK2 cells for 7 days and sucrose gradient-purified as described in section 2.2.8 of the Materials and Methods. The resulting partially-purified virus preparations were lysed, and 1 µg of total virion protein was analyzed by Western blotting.

Full-length GP_0 / GP_1 protein (without the TMCT modification) appeared to be incorporated in substantial amounts into the HPIV1 virions when expressed from the pre-N position (GP1 vector, Figure 42B, top panel, and C), but it was unclear whether this could be increased. Surprisingly, the TMCT modification did not appear to further enhance GP incorporation (vectors GP1 vs. GP-TMCT1). Unexpectedly, the efficiency of GP packaging was substantially reduced when expressed from the N-P position, and surprisingly this was not increased by the TMCT modification. The amount of GP packaged for the pre-N viruses (GP1, GP-TMCT1) was on average 6.3-fold higher than that of N-P viruses (GP2, GP-TMCT2) (Figure 42C). This was calculated relative to the HPIV1 P protein (Figure 42B, 3rd panel from the top), whose efficiency of packaging was expected to remain unchanged among the various GP-expressing constructs.

Expression of the GP and GP-TMCT proteins had effects on the incorporation of vector proteins into the vector virion, as compared to wt HPIV1 and the empty vector rHPIV1- $C^{\Delta 170}$. Viruses expressing GP showed dramatic reductions in the incorporation of vector HN (Figure 42B, 4th panel from the top). In addition, for the N-P viruses (GP2, GP-TMCT2) the level of HPIV1 F incorporation was substantially lower (Figure 42B, 5th panel from the top). Another interesting observation was that, for the N-P viruses (GP2, GP-TMCT2) that had less GP incorporation, most of the HPIV1 F in the virions was in the cleaved form (F_1) with very little F_0. In contrast, the pre-N viruses (GP1, GP-TMCT1), that had considerably higher GP incorporation, had more uncleaved

HPIV1 F_0 protein in the virions. This may suggest that the higher level of EBOV GP processing and incorporation due to its greater abundance may result in reduced cleavage of the vector F protein. Wt HPIV1 and HPIV1- $C^{\Delta 170}$ also had a substantial amount of F_0 in the particles: these vectors expressed an overall higher amount of all vector proteins including F, and thus the higher F_0 could be due the overall higher amount of F.

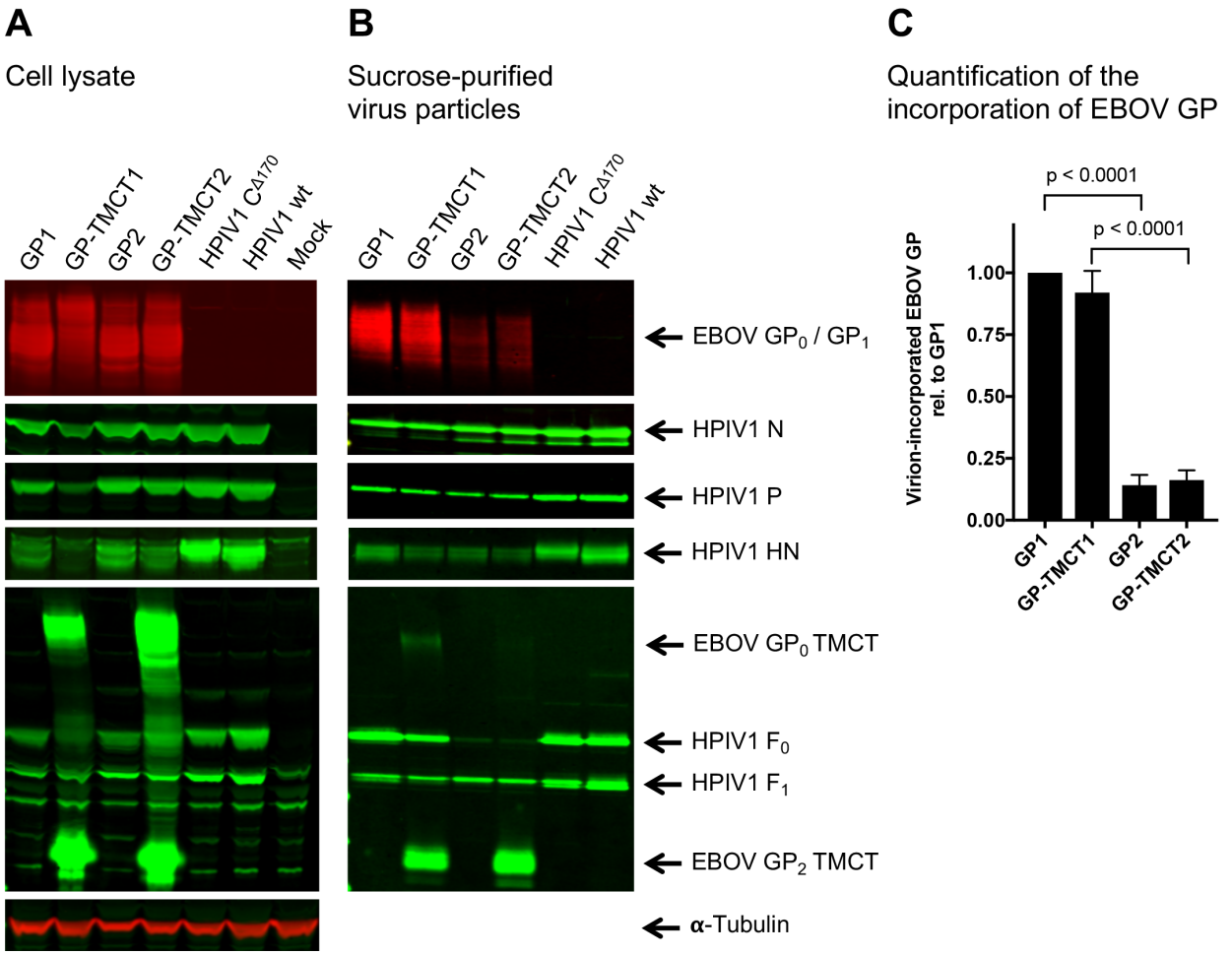

Figure 42: **Western blot analysis of infected cell lysates and sucrose gradient purified virions.** **(A) Cell lysates:** Vero cells were infected with an MOI of 3.0 $TCID_{50}$/cell with the indicated viruses and incubated for 48 h, after which cells were lysed in 1x LDS buffer, denatured and reduced, and analyzed by Western blotting. EBOV GP was detected with an anti-GP mouse MAb (4F3) and IRDye 680RD-conjugated donkey anti-mouse secondary antibody. Individual HPIV1 proteins were detected with rabbit polyclonal hyperimmune sera raised individually against peptides derived from HPIV1 N, P, F, and HN proteins, as previously described (Mackow et al. 2015), and an IRDye 800CW-conjugated donkey anti-rabbit secondary antibody. Tubulin was detected on all blots, as a loading control, using an anti-tubulin mouse MAb and IRDye 680RD-conjugated goat anti-mouse secondary antibody. A representative set of blots is shown: each panel is from a different Western blot with the antibody specificity and identified proteins indicated to the right of Part B (**B**) **Sucrose gradient-purified virus particles:** LLC-MK2 cells were infected at an MOI of 0.1 $TCID_{50}$ per cell with the indicated viruses and incubated for 6 days. Virus particles were purified by sucrose step gradient centrifugation. For each virus, 1.0 µg of total protein, measured by BCA assay, was analyzed by Western blotting using the same antibodies as described for part A. **(C) Relative quantification of EBOV GP incorporation into HPIV1 virions.** EBOV GP signals were quantified (Image Studio) for three independent experiments as in Part B, top panel, and normalized to HPIV1 P, which was detected simultaneously on each blot. Quantification is shown relative to EBOV GP packaged in GP1 particles assigned the value of 1.0. The statistical significance of differences in the amount of virion-packaged GP was determined by one-way ANOVA with Tukey's multiple-comparisons post-test and p-values are shown for each comparison.

The antiserum that was used to detect the HPIV1 F protein (Figure 42A and B, 5th panel from the top) had been raised against a synthetic peptide (YTLESRMRNPYMGNNSN) representing the C-terminus of the HPIV1 F protein. Therefore, in addition to detecting HPIV1 F_0 and F_1, this antiserum also recognized the forms of GP_0 and GP_2 that contained the TMCT modification (Figure 42A and B, 5th panel from the top, EBOV GP_0 TMCT and EBOV GP_2 TMCT). This confirmed that GP containing the HPIV1 F TMCT domain was expressed and incorporated in the virions. In the blot of intracellular protein shown in Figure 42A, this antiserum detected a large amount of GP_0-TMCT protein for the GP-TMCT1 virus, and an even larger amount for the GP-TMCT2 virus, as well as a large amount of the GP_2 band that was similar in abundance for both viruses. In the blot of purified viruses in Figure 42B, a trace of the GP_0-TMCT smear was detected for the GP-TMCT1 virus but not the GP-TMCT2 virus, and a large amount of the GP_2-TMCT band was observed for both viruses. Thus, for the GP-TMCT1 virions, both the GP_0 / GP_1 smear (top panel) and the GP_2-TMCT band (5th panel) were very abundant, whereas for the GP-TMCT2 virions, the GP_0 / GP_1 smear was much less abundant, but the GP_2-TMCT band was similar in abundance (Figure 42B).

The amount of incorporated GP_2-TMCT appeared to be similar for the viruses GP-TMCT1 and GP-TMCT2 (Figure 42B, 5th panel from the top) despite a much higher amount of incorporated GP_0-TMCT/GP_1-TMCT protein for GP-TMCT1 versus GP-TMCT2, as detected with the GP_0 / GP_1-specific MAb (Figure 42, top panel). This suggests that the GP-TMCT1 virus particles contained a higher proportion of uncleaved full-length GP_0-TMCT versus GP_1-TMCT compared to the GP-TMCT2 virus. Therefore, the GP_2-TMCT protein detected by the HPIV1 F antiserum, does not fully reflect the total amount of incorporated GP in the particles. This GP_2-TMCT fragment also was detected in the infected cell lysates for GP-TMCT viruses (Figure 42A, 5th panel from the top).

3.2.2. Evaluation of the HPIV1-vectored EBOV vaccine candidates in AGMs

Replication and immunogenicity of the HPIV1-$C^{\Delta 170}$ vectors expressing EBOV GP or GP-TMCT were evaluated in AGMs (*Cercopithecus aethiops*). Four animals per group were infected intranasally and intratracheally with 10^6 $TCID_{50}$ of virus per site. As a reference, two animals were infected with wt HPIV1 to determine the level of attenuation of the vaccine candidates resulting from $C^{\Delta 170}$ mutation and EBOV GP insertion. Two additional animals were infected with the previously developed rHPIV3/EboGP, consisting of wt rHPIV3 that expresses full-length EBOV GP from the third gene position (P-M) (Bukreyev et al. 2006). Four weeks after the initial inoculation, two animals per group were boosted by reinfection with the same virus, using the same routes and dose as the first inoculation.

3.2.2.1. Virus shedding in the upper and lower respiratory tract

Nasopharyngeal swabs (NP) of the upper respiratory tract (URT) and tracheal lavage (TL) samples of the lower respiratory tract (LRT) were collected daily and every other day, respectively, for 14 d following initial- and boost- inoculation. Virus shedding was quantified by determining the virus titers of the samples by hemadsorption assay (described in section 2.2.11) and were reported as $log_{10}TCID_{50}$/ml (Figure 43).

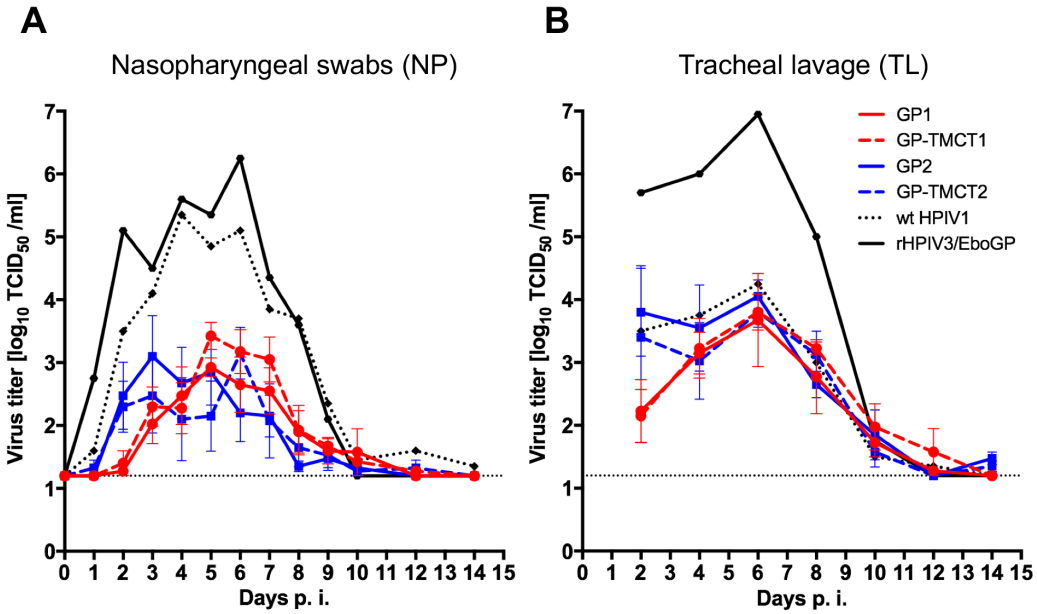

Figure 43: **Replication of rHPIV1 expressing EBOV GP in AGMs.** Groups of four animals were inoculated with the indicated HPIV1-$C^{\Delta 170}$ viruses expressing EBOV GP or GP-TMCT via the intranasal and intratracheal routes with 10^6 $TCID_{50}$ in 1 mL at each site. Two animals were inoculated in the same way with wt HPIV1, and another two with HPIV3/EboGP. Nasopharyngeal swabs (NP) (A) were collected daily and tracheal lavages (TL) (B) were performed every other day over two weeks post inoculation (p.i.). Virus titers were determined by limiting dilution on LLC-MK2 cells and hemadsorption. The average titers are shown as log_{10} $TCID_{50}$/ml with the standard error of mean indicated by error bars. Note: values indicate virus titers after first dose; replication of the booster dose could not be detected and is not shown.

All four HPIV1-$C^{\Delta 170}$ EBOV GP constructs (GP1, GP-TMCT1, GP2 and GP-TMCT2) were attenuated in the URT (NP samples) and grew to a peak titer of approximately 3 $log_{10}TCID_{50}$/ml as compared to wt HPIV1, which grew to a titer of 5 $log_{10}TCID_{50}$/ml (Figure 43A). Virus constructs with GP or GP-TMCT in the N-P position (GP2 and GP-TMCT2) appeared to replicate faster in the URT as compared to those in the pre-N position (GP1 and GP-TMCT1). Specifically, the N-P viruses were recovered at higher titers during days 1 - 3 p.i.; by day 4 p.i. the pre-N and N-P viruses reached similar titers; and thereafter the titers of the pre-N viruses generally were higher. In the LRT (TL samples), there was little evidence of attenuation of the HPIV1-based GP and GP-TMCT constructs compared to wt HPIV1, and all of these constructs reached peak titers of approximately 4 $log_{10}TCID_{50}$/ml on day 6 p.i. (Figure 43B). The replication of the N-P constructs in the LRT was more efficient during the first few days after infection, similar to what was observed in the URT. rHPIV3/EboGP replicated to significantly higher titers than the HPIV1-based vectors, reaching a peak titer of 6.0 and 7.0 $log_{10}TCID_{50}$/ml in URT (NP samples) and LRT (TL samples), respectively. The greater replication of rHPIV3/EboGP presumably reflects its wt HPIV3 backbone

compared to the attenuated HPIV1-$C^{\Delta 170}$ backbone. In addition, it has been previously reported that AGMs are more permissive to HPIV3 than to HPIV1 replication and therefore result in 10- to 30-fold higher wt HPIV3 titers than for wt HPIV1 (Durbin et al. 2000).

NP and TL samples also were collected after inoculation of the booster dose, as described for the first infection. Replication of the booster dose was undetectable by a limiting dilution assay in LLC-MK2 cells with hemadsorption (limit of detection ≤ 1.2 $\log_{10}TCID_{50}$ /ml) of the NP and TL samples of all animals (data not shown), indicating a substantial restriction of replication and shedding due to the pre-existing immune status resulting from the first inoculation.

3.2.2.2. Immunogenicity

3.2.2.2.1. Analysis of EBOV GP-specific serum IgG by ELISA

For the evaluation of the EBOV-specific serum antibody response, serum samples were collected weekly from the immunized AGMs described in the section above. Sera were collected on days 28, 35, and 56 p.i. and were subjected to an EBOV GP-specific IgG ELISA (Figure 44).

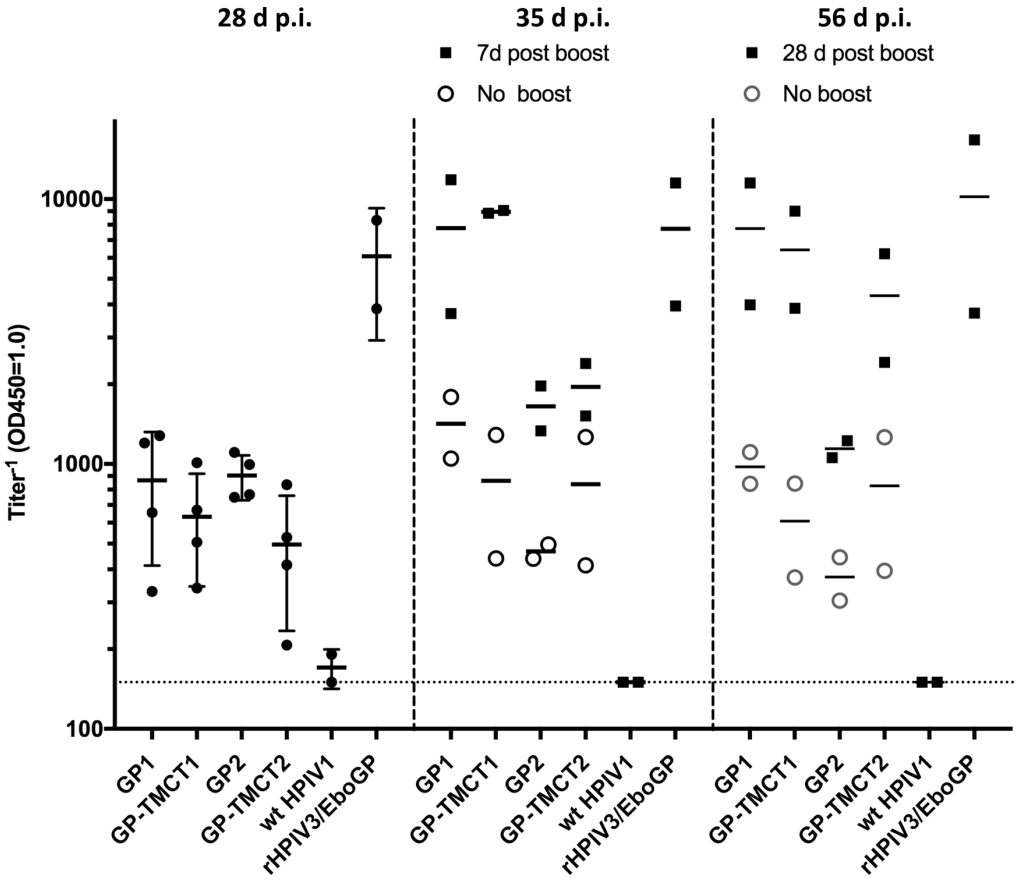

Figure 44: **EBOV GP-specific serum IgG titer.** Sera of the immunized AGMs were collected on days 28 (immediately before a second boosting inoculation), 35 (7 d post-boost) and 56 (28 d post-boost) after the first immunization were analyzed by an EBOV GP capture ELISA specific for IgG (Alpha Diagnostic International, Inc.). Titers for individual animals are shown by symbols. Open circles indicate animals that did not receive the booster dose on day 28. Horizontal bars indicate the mean titer and error bars show the SD for samples on day 28 p.i. Values are reported as reciprocal titer of OD_{450}=1.0.

For sera collected at day 28 (immediately before the booster administration), modest titers of EBOV GP-specific IgG were detected for all the HPIV1-based constructs, compared to high titers with the non-attenuated rHPIV3/EboGP construct. However, animals immunized with HPIV1-based constructs that received a booster dose had a 10-fold increase in antibody titers at day 35 (7 days post boost), reaching levels similar to those of rHPIV3/EboGP. No detectable difference was observed between the GP1 and GP-TMCT1 titers, and the titers did not increase further by the end of the study at day 56. AGMs immunized with GP2 or GP-TMCT2 showed only a modest increase in titer at day 35 and only that of GP-TMCT2 showed a slight increase between day 35 and 56. In contrast, rHPIV3/EboGP induced high IgG titers after the first dose at 28 days, with the booster inducing only a minimal increase at 7 and 28 days post-boost.

Overall, the ELISA results (Figure 44) indicate that two doses of attenuated rHPIV1 vectors expressing GP, particularly GP1 and GP-TMCT1, are able to elicit EBOV GP-specific IgG titers similar to those of an non-attenuated candidate (rHPIV3/EboGP) as early as 7 days post boost.

3.2.2.2.2. Evaluation of the EBOV-neutralizing serum antibody response

A neutralization assay was developed to evaluate the ability of serum antibodies from the AGM study to bind and neutralize viruses bearing EBOV GP. The same sera that had been analyzed by ELISA (Figure 44) were evaluated with this assay. To develop an EBOV neutralization assay that does not require a biosafety level (BSL)-4 facility, an EBOV-pseudotyped HPIV3 virus (called rHPIV3/NotI ΔF-HN/EboGP) was constructed in which the two HPIV3 surface protein genes F and HN were deleted and replaced by a gene encoding full-length wt EBOV GP as the sole virion surface envelope glycoprotein to mediate attachment and entry (construct design is described in Appendix 6.4 and shown in Figure 48). This virus is very similar to another version reported previously (Bukreyev et al. 2009). rHPIV3/NotI ΔF-HN/EboGP was readily recovered from cDNA in cell culture. Although slightly attenuated as compared to wt HPIV3, this virus was capable of efficiently infecting cells and grew to high titers (~7.5 $\log_{10}$ PFU/ml) and formed distinct plaques in a conventional plaque assay, indicating that EBOV GP in the virion particles was functional and likely retained the neutralization epitopes.

Several control antibodies were used to confirm the specificity of this neutralization assay based on rHPIV3/NotI ΔF-HN/EboGP. The EBOV GP-specific antibody KZ52, a human IgG MAb isolated from an EBOV survivor (Maruyama et al. 1999), was used as a positive control to demonstrate that rHPIV3/NotI ΔF-HN/EboGP can be neutralized by EBOV GP-specific antibodies (Figure 45A). It also was important to determine if the HPIV1-specific antibodies, generated in the immunized AGMs due to the HPIV1 vectors, could neutralize rHPIV3/NotI ΔF-HN/EboGP, which lacks the HPIV3 F and HN neutralization antigens but carries all of the HPIV3 internal proteins. Although HPIV1 and HPIV3 are distinct serotypes and do not cross-protect, they belong to the same genus *Respirovirus* and share a low-to-moderate level of amino acid sequence relatedness. In addition, to enable the analysis of sera from rHPIV3/EboGP-immunized animals, it was

necessary to confirm that the HPIV3-specific antibodies induced by rHPIV3/EboGP would not neutralize this EBOV-pseudotyped virus. To address this, the neutralization assay was performed with hyperimmune sera to HPIV1 (titer of 7.3 $\log_2$ $PRNT_{60}$ against HPIV1) and HPIV3 (titer of >13 $\log_2$ $PRNT_{60}$ against HPIV3). Neither antiserum had any detectable neutralizing activity against rHPIV3/NotI ΔF-HN/EboGP (Figure 45A). Therefore, rHPIV3/NotI ΔF-HN/EboGP could be used in a neutralization assay to detect EBOV-specific antibodies without confounding neutralization by HPIV1- or HPIV3-specific antibodies.

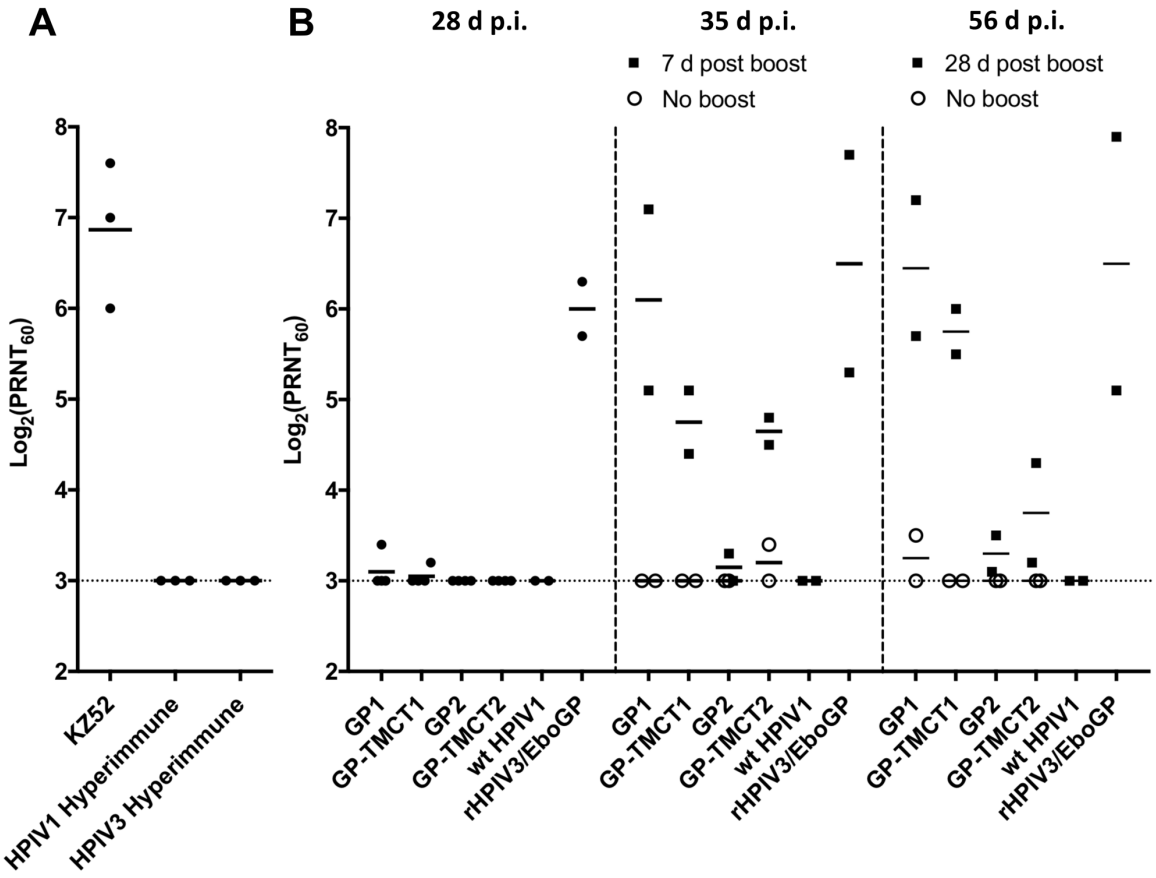

Figure 45: **EBOV GP-specific 60% plaque reduction neutralization ($PRNT_{60}$) assay using rHPIV3/NotI ΔF-HN/EboGP, an HPIV3 virus expressing EBOV GP as the sole surface glycoprotein.** Serum samples were analyzed using rHPIV3/NotI ΔF-HN/EboGP virus. **(A) Validation of the neutralization assay.** KZ52, an anti-EBOV GP human MAb, known to have GP-neutralizing activity, was used as a positive control to confirm neutralization of rHPIV3/NotI ΔF-HN/EboGP. Rabbit hyperimmune sera against HPIV1 and HPIV3 were included as negative controls to confirm a lack of neutralizing activity of HPIV1- and HPIV3-specific antibodies for rHPIV3/NotI ΔF-HN/EboGP. **(B) Sera from the immunized AGMs.** Sera collected 28 d, 35 d (7 d post-boost), and 56 d (28 d post-boost) after the first immunization were analyzed to determine the $PRNT_{60}$ titers for rHPIV3/NotI ΔF-HN/EboGP in the presence of guinea pig complement. Open circles indicate animals that did not receive a booster on day 28 post primary immunization. Average $PRNT_{60}$ values for each group are shown with the horizontal bars.

The sera of the AGMs were analyzed with this neutralization assay (Figure 45B). At 28 d p.i., no significant serum neutralization activity could be detected for any of the rHPIV1 EBOV GP constructs, whereas rHPIV3/EboGP induced a $PRNT_{60}$ of approximately 6.0 $\log_2$. However, the animals that had received a second dose of GP1 virus reached, on average, similar neutralization titer as that of rHPIV3/EboGP-boosted animals as early as 7 days post boost. The boosts with the GP-TMCT1 and GP-TMCT2 viruses did induce an increase in virus neutralization titers but were

lower than those of GP1. Animals that had not received a second dose showed undetectable (limit of detection: 3.0 $\log_2$ $PRNT_{60}$) or very low neutralizing activity. The virus neutralization titers closely reflected the ELISA results and showed that within 7 days post-boost the attenuated GP1 vaccine candidate conferred neutralizing titers comparable to those of the non-attenuated rHPIV3/EboGP virus that had been previously shown to protect NHPs against EBOV challenge (Bukreyev et al. 2006). Although GP-TMCT1 induced ELISA IgG titers similar to those of GP1, its neutralizing titers were slightly lower. Similar to the ELISA results, the virus neutralizing titers also did not substantially increase between 7 and 28 days post boost, suggesting that the maximum attainable titers were achieved by one week after the booster dose.

3.2.2.3. Stability of EBOV GP expression during replication in the respiratory tract

The stability of expression of EBOV GP during replication in AGMs was evaluated by a double-immunostaining plaque assay. The assay was used to analyze NP and TL samples of all animals in each group (GP1, GP-TMCT1, GP2 and GP-TMCT2) collected during the peak of viral shedding, defined by the replication curve of Figure 43. Samples from the day of peak shedding for each particular animal (P2) as well as for the preceding day (P1) and the following day (P3), were analyzed, and the percentage of HPIV1 plaques co-expressing EBOV GP was determined (Table 21). Representative images of double-immunostained plaques are shown for each construct (Figure 46).

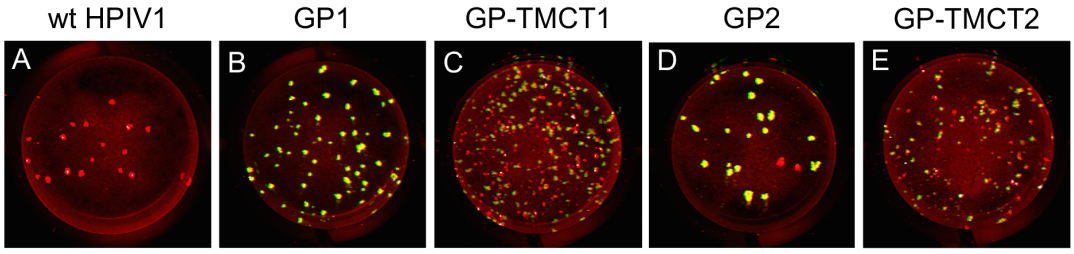

Figure 46: **Representative results of the double-immunostaining plaque assay used to determine the stability of EBOV GP expression during replication in AGMs.** Vero cells were infected with serially diluted NP or TL samples, incubated for 6 days under a methylcellulose overlay medium, fixed, and subjected to immunostaining against EBOV GP (green) and HPIV1 (red) as described in the Methods. Plaques that stained for both HPIV1 and EBOV GP appeared yellow; plaques in which expression of EBOV GP was lost appeared red. The following representative examples of double-immunostained Vero monolayers are shown from the experiment in Table 21: (**A**) **wt HPIV1**, animal #32956, TL, day P2; (**B**) **GP1**, animal #7856, NP, day P1; **(C) GP-TMCT1**, animal #8392, NP, day P3; **(D) GP2**, animal #62403, NP, P2; **(E) GP-TMCT2**, animal #8232, NP, day P2. P2 is the day of peak shedding for that particular animal; P1 is the day before the peak of shedding; P3 is the day following peak shedding. The complete results of the experiment are summarized in Table 21.

Overall, the constructs expressing full-length EBOV GP from either the pre-N or N-P position (GP1 and GP2) had a more stable GP expression than their TMCT counterparts (GP-TMCT1 and GP-TMCT2). In the case of GP1, 3 of 4 animals (#7856, 7867, and 8172) had an average stability of 95% for both the NP and TL samples; the remaining animal (#8054) of this group had a reduced stability of 70% in the NP samples, but was more stable at 92% in the TL samples. GP-TMCT1 was substantially less stable, especially in the NP samples with the stability ranging from 15 - 75% with an average of 45%, whereas TL samples were more stable at 90%.

Similar to GP1, GP2 had relatively stable expression of GP: 3 of 4 animals (#8401, 62403, and 8246) had an average stability of 97% in both the NP and TL samples. The remaining animal (#8555) had only 50% GP expression in the NP sample but 99% stable GP expression in the TL sample. Similar to GP-TMCT1, a tendency of reduced stability also was observed for GP-TMCT2, with an average of 53% and 93% GP expression in the NP and TL samples, respectively. Although the TMCT modification did not increase GP incorporation in the particles and had no evidence of instability during *in vitro* growth, it seemed to encourage *in vivo* selection of virus progeny with silenced GP expression.

Table 21: Percentage of HPIV1-C$^{\Delta 170}$ GP plaques expressing EBOV GP after replication in AGMs, determined by a double-immunostaining plaque assay.

		% plaques positive for EBOV GP[a]					
		Nasopharyngeal swabs			Tracheal lavage		
Virus	Monkey ID #	P1[b]	P2	P3	P1	P2	P3
GP1	7856	98	100	97	90	67 (3)[c]	100 (5)
	8054	65	75	70 (10)	81	94	100
	7867	95	87	92	100	98	98
	8172	99	99	97	100	97	99
GP-TMCT1	8445	56	52	71	100	96	100 (9)
	8195	33	41	47	86	89	79
	8392	75	36	47	92	91	99
	8258	50	19	15	83	67 (6)	93
GP2	8555	67 (3)	50 (8)	33 (3)	97	100	100
	8401	90	100	100 (4)	100	96	94
	62403	98	92	98	100	97	100
	8246	100 (2)	99	100	99	98	95
GP-TMCT2	8577	ND	50 (6)	100	91	84	95
	8573	23	91	14 (7)	100	98	100
	57413	0 (10)	60 (5)	ND	67 (3)	100	100 (4)
	8232	74	56	66	97	96	91

[a] Vero cell monolayers were infected with serially diluted samples of NP and TL specimens from the indicated animals (from the experiment shown in Figure 43), incubated for 6 days under a methylcellulose overlay medium, fixed, and subjected to immunostaining against EBOV GP (green) and HPIV1 (red). Plaques that stained for both appeared yellow; plaques in which expression of GP was lost appeared red. The percentage of plaques positive for expression of EBOV GP was the number of yellow plaques divided by the total number of plaques (red and yellow).

[b] P2, P1, and P3 are the day of peak shedding (P2), the day before the peak shedding (P1), and the day after the peak shedding (P3) for that particular animal.

[c] For samples with ≤ 10 plaques: total number of plaques are shown in parenthesis

ND, not determined because plaque titer was below the limit of detection.

Underlined values represent samples also shown in Figure 46.

4. Discussion

4.1. Role of ATP1A1 in the macropinocytic entry of RSV

4.1.1. ATP1A1 is a pro-viral host factor, involved in RSV entry

Advancing our understanding of the RSV replication cycle and how the virus utilizes host proteins for efficient replication may identify new targets for antiviral drug development. An effort was made to identify, in an unbiased high-throughput fashion, the host proteins utilized by RSV for replication. A genome-wide siRNA screen was performed, where the expression of individual genes was knocked down in human airway epithelial A549 cells, followed by infection with a recombinant RSV that expressed GFP.

Expression knockdown of the gene encoding ATP1A1 provided the greatest reduction in viral GFP expression, with minimal effects on cell viability. ATP1A1 is the major subunit of the Na^+, K^+-ATPase complex, a transmembrane complex that is an ATPase and an ion channel, but is also involved in signal transduction (Reinhard et al. 2013). ATP1A1 also has been implicated in the infection cycle for EBOV (Garcia-Dorival et al. 2014) coronavirus (Burkard et al. 2015), hepatitis C virus (Lussignol et al. 2016), and mammarenaviruses (Iwasaki et al. 2018) but the mechanism of its involvement for these viruses remained largely unknown.

This study provides evidence that ATP1A1 is involved in RSV entry. A reduction of the cellular ATP1A1 level diminished the ability of RSV to infect host cells, an inhibition that was RSV-specific and had no effect on VSV infection. A striking phenomenon of ATP1A1 clustering in the plasma membrane was observed within a few hours following cellular exposure to RSV particles. This also was observed for UV-inactivated RSV, and therefore the induction of ATP1A1 clustering was independent of virus transcription or replication. This phenotype was reminiscent of the behavior of signaling receptors in response to ligand binding and suggested a possible physical interaction between the virions and the cell surface that triggered ATP1A1 clustering.

It was not possible to detect physical interaction between ATP1A1 and any of the RSV surface glycoproteins (G, F or SH) by co-immunoprecipitation techniques (data not shown). However, by using RSV deletion mutants, it was demonstrated that RSV G protein is required to trigger ATP1A1 clustering, implying that an initial virus attachment event, facilitated by G, is needed to initiate ATP1A1 clustering, but the mechanistic details of this process remains unknown. It may be that interaction of RSV and ATP1A1 does occur but is insufficiently stable for detection by the co-immunoprecipitation and Western blotting methods that were used, or that there may be intermediate steps involved between the initial binding of RSV G and clustering of ATP1A1. For signaling receptors in general, clustering is known to increase ligand binding and signal transduction of signaling receptors (Chu et al. 2004) by reducing the effective dissociation rate through enhancing rebinding within the receptor cluster (Gopalakrishnan et al. 2005). This phenomenon would be beneficial for RSV infection as it would enhance ATP1A1-mediated signaling that is required for viral uptake.

Total loss of ATP1A1 expression with homozygous ATP1A1 knockout mice was previously found by others to result in pre-weaning lethality (Lexicon Genetics Inc. 2005), indicating that ATP1A1 is an essential cellular protein. Therefore, complete knockout *in vitro* or in the mouse model was not feasible. However, an ATP1A1 heterozygous knockout mouse had been developed in which one ATP1A1 allele is knocked out and only one functional allele is expected to sustain reduced expression of ATP1A1. This heterozygous knockout mouse strain was used to evaluate the effects on RSV infection. Unfortunately, only a modest reduction in ATP1A1 expression was observed in the lung tissue. Consistent with this inefficient knockdown of ATP1A1 expression, we did not observe any reduction in RSV infection or shedding in the heterozygous mice as compared to wt mice. Therefore, it was not possible to investigate and confirm the role of ATP1A1 in RSV infection *in vivo*.

4.1.2. RSV infection triggers ATP1A1-mediated signaling

Treatment with the cardiotonic steroid ouabain and the synthetic digitoxigenin derivative PST2238, that both specifically act on ATP1A1, also reduced RSV infection. Ouabain has a hormone-like effect on the Na^+, K^+-ATPase when present in sub-nanomolar concentrations (Xie and Cai 2003, Reinhard et al. 2013), that are non-inhibitory for its ion-channel function and do not alter the cytosolic Na^+ and K^+ levels (Liu et al. 2000), but can initiate signaling cascades, as described in the Introduction in greater detail (Haas et al. 2000, Aydemir-Koksoy et al. 2001, Haas et al. 2002). The ouabain-induced ATP1A1 signaling results in the removal of ATP1A1 from the plasma membrane by endocytic uptake and lysosomal degradation (Cherniavsky-Lev et al. 2014). Ouabain and PST2238 inhibited RSV infection efficiently and acted early during infection. PST2238 has been characterized as an anti-hypertension drug and antagonizes ouabain by competitive binding to its ATP1A1 binding site (Quadri et al. 1997, Ferrari et al. 1998). PST2238 shares a common binding site with ouabain on the extracellular domain of ATP1A1 and blocks ATP1A1-mediated signaling in response to ouabain or RSV. Note that reduced ATP1A1 expression in the plasma membrane was observed after 24 h ouabain treatment but its antiviral effect was evident even if added simultaneously with the virus inoculum, suggesting reduced ATP1A1 surface expression is likely not the basis of its anti-RSV activity. The possible mechanism of inhibition by ouabain is discussed later in section 4.1.5. PST2238 treatment inhibited RSV infection to levels similar to ouabain but it did not reduce ATP1A1 on the plasma membrane, consistent with its lack of stimulation of ATP1A1 signaling and downstream effects including increased endocytosis. The robust ATP1A1 clustering observed soon after infection, and the ouabain and PST2238 time-of-addition experiments, both pointed to a role of ATP1A1 as a signaling molecule with a role in an early stage of infection, i.e. entry.

Ouabain binds to ATP1A1 and signals via the ATP1A1-Src-EGFR signaling cascade (described in the Introduction) resulting in endocytosis and degradation of the surface ATP1A1 as a mechanism of regulating blood pressure (Xie and Cai 2003, Reinhard et al. 2013). It was

hypothesized that RSV may utilize this signaling properties of ATP1A1 to induce endocytosis as a mechanism for entry. This potentially could involve any of various pathways including clathrin- or caveolin-mediated endocytosis or macropinocytosis. This study demonstrated that ATP1A1 signaling indeed was induced and was required for RSV infection. Src-kinase activity was found to play an important role in RSV infection, and inhibiting c-Src reduced the efficiency of RSV infection. It also was confirmed that EGFR is essential for RSV infection, as previously shown (Krzyzaniak et al. 2013), but is not sufficient alone and required the upstream activation of ATP1A1 and c-Src for efficient RSV infection. This conclusion was made by examining the activation of EGFR following exposure of cells to RSV. It showed that EGFR Tyr845 was phosphorylated early during RSV infection, detectable at 5 h p.i. This phosphorylation was dependent on ATP1A1 and was significantly reduced in cells whose ATP1A1 expression was knocked down with siRNAs or in which ATP1A1 signaling was reduced by treatment with ouabain or PST2238. EGFR Tyr845 phosphorylation also was dependent on c-Src kinase activity, the downstream signaling effector of ATP1A1. Inhibition of the c-Src kinase abolished the pTyr845 below detectable levels, suggesting that EGFR Tyr845 is phosphorylated by the ATP1A1-activated c-Src kinase.

ATP1A1-mediated signaling cascades have been reported to take place in the cholesterol-rich microdomains called caveolae (Liu et al. 2003, Wang et al. 2004). Due to the spatial sequestration of caveolae, it is believed that it serves as a region to integrate multiple signaling pathways by concentrating signaling proteins and creating temporal and spatial patterns of cell regulation (Ostrom et al. 2001). Many proteins associated with signaling functions are present in the caveolae, including ATP1A1, EGFR and c-Src (Anderson 1998, Razani et al. 2002, Reinhard et al. 2013). It also has been described that cholesterol is needed for the ouabain-induced ATP1A1-Src-EGFR signaling cascade and that depletion of cholesterol reduced the recruitment of c-Src and therefore reduced ATP1A1 signaling (Wang et al. 2004). Interestingly, it also has been reported that the cholesterol-rich lipid rafts are required as a docking platform for RSV entry (Chang et al. 2012, San-Juan-Vergara et al. 2012). It was investigated whether caveolae were the sites of ATP1A1-Src-EGFR signaling required for RSV entry by depleting cholesterol, which is essential to maintain the caveolar structural integrity. Cholesterol depletion indeed reduced the efficiency of RSV infection, which also was associated with decreased EGFR Tyr845 phosphorylation (reflecting reduced ATP1A1 signaling) induced by RSV. This provided evidence that caveolae are the likely sites where ATP1A1 signaling occurs and are thus important for RSV entry. Although significantly reduced, the magnitude of reduction for EGFR pTyr845 was modest as compared to that of RSV-GFP expression. While the reason for this difference is unclear, these data may suggest that, although ATP1A1-mediated EGFR phosphorylation is more efficient in the presence of cholesterol, the complexes might also be signaling in the absence of cholesterol, presumably outside of caveolae.

4.1.3. RSV-induced ATP1A1 signaling results in the macropinocytic uptake of RSV

RSV uptake into the host cell to initiate infection has been controversially suggested to occur by clathrin-mediated endocytosis (Kolokoltsov et al. 2007) or macropinocytosis (Krzyzaniak et al. 2013). Some of the evidence provided in these studies for clathrin-mediated endocytosis and macropinocytosis were based on the use of inhibitors to distinguish between these entry pathways. To confirm these findings, chlorpromazine and EIPA were used in the present study as inhibitors of the clathrin-mediated endocytosis and macropinocytosis, respectively, in A549 cells. Both chemical compounds showed high cytotoxicity at the concentrations used in these previous studies, which used HeLa cells instead of A549 cells. It might be that HeLa cells are more resistant as compared to A549 cells and their viability is less affected by these inhibitors. Chlorpromazine-treated A549 cells showed an inhibition of RSV-GFP expression, but this correlated with the reduction in cellular viability, suggesting an unspecific inhibition of RSV due to cell damage rather than a specific inhibition of clathrin-mediated endocytosis. EIPA, on the other hand, showed a reduction of RSV-GFP at non-cytotoxic concentrations, but fluorescence microscopy showed that even the “non-cytotoxic” concentration caused pathological changes in the cells, indicated by the loss of integrity of the nuclear membrane. Thus, because of these non-specific and generalized effects on the viability of the A549 cells, it could not be inferred if these inhibitors could block one or the other endocytic pathway to affect RSV infection, and therefore this was not further pursued.

Macropinocytosis can be induced through components of the ATP1A1 signaling pathway. For example, it has been described that phosphorylation of EGFR Tyr845 by c-Src, in an EGF-independent manner, can induce macropinocytosis (Biscardi et al. 1999, Donepudi and Resh 2008). Src kinase activity plays an important role during macropinosome formation and trafficking (Kasahara et al. 2007), and can synergistically enhance macropinocytic induction (Mercer and Helenius 2009). Based on the findings of the present study, it was postulated that, upon RSV binding, ATP1A1-induced signaling transactivates EGFR via c-Src resulting in the macropinocytic uptake of RSV. Typical macropinosomes are formed as a result of extensive, unspecific fluidic uptake at the plasma membrane [reviewed in (Swanson and Watts 1995, Conner and Schmid 2003, Mercer and Helenius 2009)] that engulfs fluid and solid cargo from outside of the cell into cytoplasmic vesicles. They are heterogeneous in size and are larger than other endocytic vesicles, with diameters of 0.5 - 5 µm. To assess if the activation of the ATP1A1-Src-EGFR pathway leads to macropinocytosis and uptake of RSV, the fluidic uptake and macropinosome formation were visualized with fluorochrome-conjugated dextran, which is generally used as a marker for macropinosomes (Mercer and Helenius 2009). RSV infection clearly induced extensive macropinocytosis, and a large number of dextran-filled vesicles (macropinosomes) were detectable very early in infection. This finding is in agreement with the previously described mode of RSV uptake reported by Krzyzaniak and colleagues (Krzyzaniak et al. 2013). Co-immunostaining showed that RSV F protein (marker of viral envelope) and RSV N protein (marker of viral nucleocapsid) were present in the dextran-positive macropinosomes, together with ATP1A1. This supports the model that RSV virions are taken up by the macropinosomes, and the

membrane fusion and release of the nucleocapsid presumably takes place at a later step after the macropinocytic uptake. Further analysis showed that macropinosome formation was dependent upon ATP1A1 activation and was significantly reduced if the ATP1A1 expression was decreased by siRNA knockdown or if the cells were treated with the ATP1A1-binding compounds ouabain or PST2238.

Cholesterol depletion was observed to have a greater effect on reducing macropinosome formation and viral entry than it did on reducing EGFR Tyr845 phosphorylation, as mentioned earlier. It is known that macropinosome formation itself also depends on the presence of cholesterol (Grimmer et al. 2002). Therefore, the effects of cholesterol depletion on ATP1A1 signaling combined with direct effects on macropinocytosis may explain the greater inhibition on macropinosome formation and viral entry compared to EGFR Tyr845 phosphorylation.

4.1.4. Model of ATP1A1-mediated entry of RSV

The following model, illustrated in Figure 47, is proposed for RSV entry into the human airway epithelial cells:

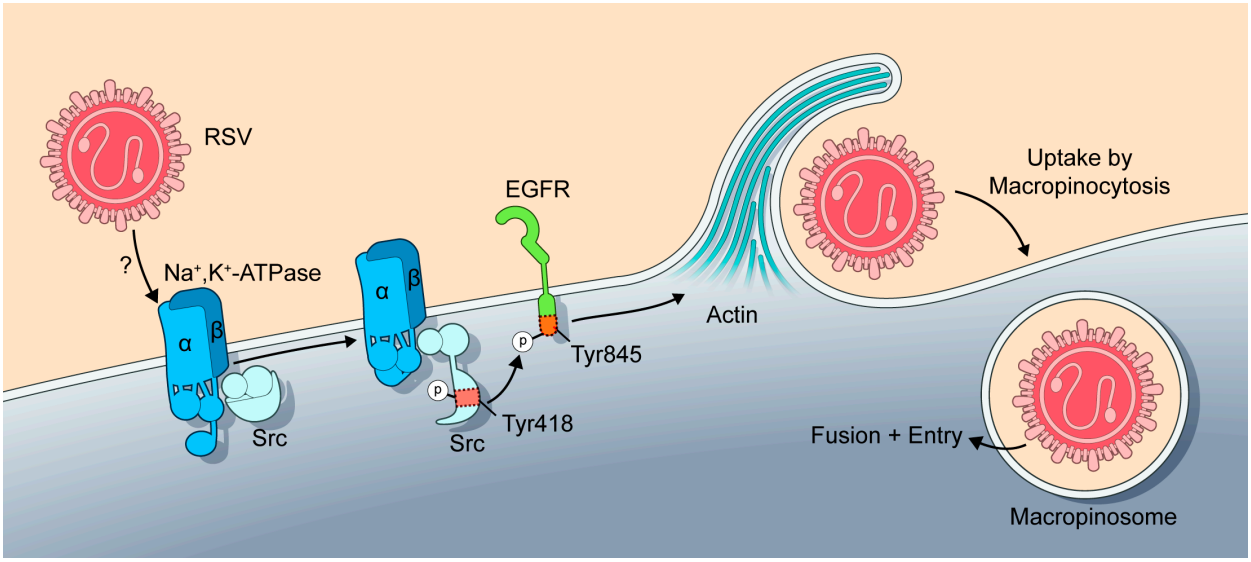

Figure 47: **Proposed model of ATP1A1-dependent macropinocytic entry of RSV.** Exposure to RSV triggers the clustering and activation of ATP1A1 in the plasma membrane through an unknown mechanism. ATP1A1 then signals via Src kinase and transactivates EGFR by phosphorylation at Tyr845. Upon activation, EGFR signaling causes cytoskeletal rearrangement resulting in plasma membrane ruffling and formation of membrane extensions (Hewlett et al. 1994, Swanson and Watts 1995, Donepudi and Resh 2008) that engulf fluid and RSV into macropinosomes. Note that RSV is taken up into the macropinosome in its enveloped state suggesting that it does not fuse at the cell surface; fusion and release of nucleocapsid likely occur within the internalized macropinosome. Illustration for this thesis by Ryan Kissinger (Visual & Medical Arts, RTB, NIAID)

RSV infection triggers ATP1A1 clustering and activates ATP1A1 signaling by an unknown mechanism that involves RSV G protein and does not require viral RNA synthesis or replication. ATP1A1 activation leads to Src-kinase activation, presumably by autophosphorylation of c-Src at Tyr418, as described previously for ouabain-induced signaling (Haas et al. 2000, Haas et al. 2002), followed by transactivation of EGFR by phosphorylation of Tyr845. Signaling events downstream of EGFR cause actin rearrangement and ruffling at the plasma membrane (Hewlett et al. 1994,

Swanson and Watts 1995, Donepudi and Resh 2008) where membrane extensions engulf fluid and RSV into large vesicles, the macropinosomes. RSV is taken up in its enveloped form into the macropinosome followed by fusion and entry into the host cell cytoplasm. EGFR is essential for RSV infection, but not sufficient alone and requires transactivation by ATP1A1-activated c-Src for initiating macropinocytic uptake of RSV. This study also provided evidence that the ATP1A1-Src-EGFR signaling occurs predominantly in the cholesterol-rich domains of the caveolae which are thus important for efficient infection.

4.1.5. PST2238 – an ouabain antagonist as potential antiviral drug

This study provided evidence that RSV induces an ATP1A1-mediated signaling cascade to enter airway epithelial cells (Figure 47). This provides a new target for the development of anti-RSV drugs. Ouabain and PST2238 specifically act on ATP1A1 and decrease the efficiency of infection by reducing the RSV-induced ATP1A1 signaling needed for entry, and thus might be further developed as antiviral drugs for RSV.

It was surprising that both ouabain and PST2238 inhibited RSV infection, since they have opposite effects on ATP1A1 signaling, namely that ouabain induces and PST2238 inhibits. The mechanism by which PST2238 inhibits RSV seems to be straight-forward, specifically, blockade of RSV-induced ATP1A1 signaling. The mechanism by which ouabain inhibits RSV is less clear, since both ouabain and RSV individually induce ATP1A1 signaling. Ouabain binding can induce several signaling pathways (Reinhard et al. 2013) which may be distinct in some aspects as compared to that induced by RSV. This is evident by the different outcomes: ouabain-induced signaling results in clathrin-mediated endocytosis, whereas RSV-induced signaling results in macropinocytosis. In addition, ouabain has been described to cause EGFR phosphorylation (Haas et al. 2000, Haas et al. 2002), but phosphorylation of Tyr845, which occurred in response to RSV-induced ATP1A1 signaling, was not detected with ouabain treatment (data not shown). Therefore, it is proposed that ouabain initiates an ATP1A1-mediated signaling pathway that is distinct from that induced by RSV, and that induction by ouabain competes with and thereby reduces induction by RSV.

Ouabain has been described to have antiviral properties for several viruses, namely herpes simplex virus (Dodson et al. 2007, Su et al. 2008), chikungunya virus (Ashbrook et al. 2016), human immunodeficiency virus (Wong et al. 2013), adenovirus (Grosso et al. 2017) and porcine reproductive and respiratory syndrome virus 1 (Karuppannan et al. 2012), but the mechanism of inhibition was not conclusively identified in any of these studies. Ouabain itself might not be a good candidate drug, since it causes hypertension if present in elevated levels in the blood, as described earlier. Nevertheless, the application intranasally, for example with a nebulizer, has not been evaluated. This route of application might not affect the blood pressure, since most likely the amount absorbed from the lung into the blood stream would be small and might not cause hypertension.

However, PST2238 might be a more promising candidate drug since it is already evaluated as an anti-hypertensive drug in phase II clinical trials for ouabain- and adducin- induced hypertension patients (Lanzani et al. 2010). Hence, the safety of PST2238 as a drug for humans already has been evaluated. It does not have any known adverse effects and does not lower the blood pressure of healthy humans (Ferrari et al. 2006) and therefore could be repurposed as antiviral drug. To the best of our knowledge, PST2238 has not previously been evaluated for antiviral activity against any virus, including RSV, and it may indeed inhibit the replication of other viruses that are ouabain-sensitive and use ATP1A1-mediated signaling for viral entry.

In conclusion, this study identified ATP1A1 as a signaling mediator of RSV entry and a new potential target for the development of an antiviral drug against severe RSV disease. The pharmacological characteristics for a potential antiviral treatment targeting ATP1A1 have not been addressed and need to be characterized in future studies.

4.2. Development and pre-clinical evaluation of a live-attenuated mucosal HPIV1 vaccine against EBOV

This EBOV vaccine project was initiated in response to the devastating EBOV outbreak in West Africa in 2014, with the goal to provide an additional, alternative EBOV vaccine strategy. Respiratory tract immunization with a live-attenuated vector offers several advantages over parenteral vaccines that are currently under development as EBOV vaccines, as described in the Introduction. Replication-competent live virus-based intranasal vaccines induce both systemic and mucosal antibody responses and respiratory tract resident $CD4^+$ and $CD8^+$ T cells (Meyer et al. 2015), which would be expected to protect against EBOV infection via aerosol, skin, or mucosal routes. The availability of an intranasal needle-free vaccine would eliminate the need for trained professionals or the risk of spreading blood-borne pathogens in the EBOV endemic areas.

The goal of this study was to develop an intranasal vaccine against EBOV based on an attenuated HPIV1-$C^{\Delta 170}$ backbone expressing EBOV GP. One aspect of this study was to improve safety by using an attenuated virus instead of a wt virus as was previously used in rHPIV3/EboGP (Bukreyev et al. 2006). Also, it is not possible to predict whether a particular vector backbone (e.g., HPIV1 versus HPIV3) might have better performance in humans. HPIV1-$C^{\Delta 170}$ is well-attenuated in NHPs (Bartlett et al. 2008) and is expected to have increased safety in humans, including elderly and HPIV1-naïve children. Another aspect of this study was to enhance EBOV GP immunogenicity by increasing its packaging in the vector particle by a TMCT modification. As described in the Introduction, it was previously shown that TMCT modification improved the incorporation of RSV F protein into PIV vector particles which enhanced the quantity and quality of the RSV neutralizing antibody response (Liang et al. 2016). In a previous study, EBOV GP was found to be incorporated into HPIV3 particles, but the efficiency of incorporation was only 13% that of the HPIV3 HN protein (Bukreyev et al. 2006). Therefore, increased incorporation would be desirable to increase the immunogenicity. To achieve this, the GP TMCT domain was substituted with that of HPIV1 F protein to enhance GP packaging into HPIV1 virions. A third aspect of this study was to evaluate two different insertion sites for the EBOV GP gene into the HPIV1 genome, namely the pre-N position, which placed the EBOV GP gene in the first, promoter-proximal position, and the N-P position where EBOV GP was inserted between the N and P genes. The EBOV GP ORF was modified to match an “edited” transcript expressing the full-length trans-membrane EBOV GP protein, and the ORF was codon-optimized for efficient human expression.

4.2.1. *In vitro* characterization of the HPIV-$C^{\Delta 170}$ vectors expressing EBOV GP

In this study four different constructs were developed to evaluate two main variables: (i) the position effect (pre-N versus N-P) in the vector genome and (ii) the effect of EBOV GP TMCT modification in comparison with a respective full-length EBOV GP. All four constructs were recovered successfully by reverse genetics. *In vitro* replication in Vero cells did not show a substantial attenuation with regard to final titers, which were similar to wt HPIV1. There was some

evidence of modest attenuating effects in replication kinetics due to the EBOV GP insert. Viruses with EBOV GP at the pre-N position showed a delay in replication kinetics *in vitro*, with the TMCT version being the slower of the two. Both TMCT constructs had smaller plaque size indicating a slight reduction in replication or spread.

EBOV GP has no essential role for vector replication and therefore has the potential to accumulate mutations that might silence its expression. It is important for a vectored vaccine to maintain antigen expression during manufacturing to ensure the highest possible load of antigen. Each of the four constructs maintained stable EBOV GP expression during replication in Vero cells, determined by dual-immunostaining plaque assay and flow cytometry, with no detectable loss of EBOV GP expression.

The level of EBOV GP expression in infected Vero cells was analyzed by Western blotting and was found to be similar for all constructs at 48 h p.i. The similar expression level regardless of the genome position [3' proximal EBOV GP (pre-N) compared to the more-distal EBOV GP (N-P)] suggests that either the expected polar transcription gradient was not observed or that the pre-N viruses were slightly attenuated and thereby the expression of EBOV GP was reduced to a level similar to that of the N-P virus. This also is consistent with the previous findings for RSV F protein expressed by HPIV-$C^{\Delta 170}$ (Mackow et al. 2015). In contrast, Western blot analysis of sucrose-purified virion lysates did show a gradient effect, with 6.3-fold more EBOV GP incorporated in the pre-N as compared to N-P viruses. This contrast between infected cell lysate and purified virus EBOV GP may reflect differences in kinetics and timing of accumulation. Specifically, the Western blot analysis of the cell lysates provided a snapshot of protein accumulation at 48 h p.i., whereas the virus particles were purified after 7 days of propagation. It could be that the overall EBOV GP accumulation over 7 days was higher for the pre-N as compared to N-P viruses, which was reflected by purified virions. This gradient likely was not apparent in the infected cell lysates at 48 h p.i. due to the initial slow growth of pre-N constructs during the first two days. Another important observation was that EBOV GP was readily detected in virions for each of the constructs, as also had been observed in a previous study with HPIV3 (Bukreyev et al. 2006), and that the amount of EBOV GP in virions of GP-TMCT1 and GP-TMCT2 was similar to that in GP1 and GP2, respectively. This indicates that, contrary to expectations, the TMCT modification did not increase the incorporation of EBOV GP into the HPIV1 virions.

4.2.2. HPIV1-$C^{\Delta 170}$ GP1 was the most immunogenic vaccine candidate in AGMs

In vivo replication of the four constructs was evaluated in AGMs. All HPIV1-$C^{\Delta 170}$ viruses expressing EBOV GP replicated over several days to peak titers of approximately 3.0 $\log_{10}TCID_{50}$/ml in the URT (NP swabs) and 4.0 $\log_{10}TCID_{50}$/ml in the LRT (TL sample). Compared to wt HPIV1, all four constructs were attenuated approximately 100-fold in the URT, but did not appear to be attenuated in the LRT. The HPIV1-based constructs replicated to titers that were approximately 1000-fold lower in both URT and LRT as compared to rHPIV3/EboGP. The

difference in replication reflects the presence of an attenuating mutation in the HPIV1 constructs but not the HPIV3 constructs and a greater permissiveness of AGMs for HPIV3 versus HPIV1 (Durbin et al. 2000). The administration of a booster dose with the same respective constructs 28 d after first immunization did not result in any detectable shedding of infectious virus. This indicated that the first dose was sufficiently immunogenic to strongly restrict replication of the booster dose. This restriction was most likely due to the induced immunity against the HPIV1 vector, but also might be partially facilitated by antibodies against the expressed EBOV GP.

The EBOV GP-specific antibody response was evaluated by an ELISA and virus neutralization assay. The ELISA captured any IgG antibodies directed against EBOV GP regardless of their neutralization activity. At 28 d p.i., all HPIV1-C$^{\Delta 170}$ constructs expressing EBOV GP showed only modest levels of EBOV GP-specific IgG titer. In comparison, HPIV3/EboGP induced a higher titer, likely reflecting its much higher (1000-fold) replication in AGMs compared to the attenuated HPIV1-C$^{\Delta 170}$. At 28 days, two animals per group received a booster dose while two remained un-boosted for comparison. Despite the lack of infectious booster virus shedding, evaluation of serum samples taken seven days following the boost revealed increases of 5.5- and 10.4-fold in IgG titers for GP1 and GP-TMCT1, respectively, which reached titers similar to those of rHPIV3/EboGP. These titers did not further increase between 7 and 28 d post-boost indicating that the maximum titers had already been attained by 7 days post boost inoculation. The N-P constructs also showed a slight increase in IgG titers after boost but the magnitude was lower than those of the pre-N viruses, which might possibly be explained by the higher amount of EBOV GP incorporated into the virions at pre-N as compared to N-P position. The rapid increase of IgG titers within 7 days post-boost suggests that, while the first dose did not induce a robust response by day 28, it did prime for an anamnestic response to the booster dose. Thus, two doses of HPIV1 constructs were necessary, but sufficient, to boost the EBOV GP-specific antibodies to titers comparable to those of rHPIV3/EboGP. In addition, since the boost required only 7 additional days to achieve a robust response, this would not be a major impediment to immunization. Furthermore, it likely would be possible to provide the boost earlier than 28 days following the primary immunization.

To determine the EBOV-neutralization activity of these serum antibodies, a neutralization assay was established using the pseudotyped rHPIV3/NotI ΔF-HN/EboGP construct, from which the surface HPIV3 F and HN proteins have been deleted and replaced by EBOV GP as the sole viral surface glycoprotein. This obviated the need to evaluate neutralization using infectious EBOV, which is a BSL-4 agent as well as a Select Agent requiring strict inventory controls (Centers for Disease Control and Prevention (CDC)). In contrast, the expression of the EBOV GP protein previously was shown to have no evident effect on the replication and tissue tropism of HPIV3 *in vivo*, and therefore did not confer increased virulence and did not necessitate increased containment (Bukreyev et al. 2006, Bukreyev et al. 2009). Thus, neutralization assays with the rHPIV3/NotI ΔF-HN/EboGP construct could be performed at BSL-2 laboratory. Antibodies to GP, but not HPIV1 or HPIV3, neutralized this virus, validating this assay for measuring GP-specific

neutralizing serum antibodies in the AGM serum samples without confounding effects from HPIV1- and HPIV3-specific antibodies. The $PRNT_{60}$ titers correlated with the ELISA titers and showed a similar relative profile. At 28 d p.i. only rHPIV3/EboGP had induced detectable neutralization activity. At 7 d post-boost, the $PRNT_{60}$ of GP1-vaccinated animals increased to titers similar to those of rHPIV3/EboGP, which had been shown to protect NHPs against EBOV challenge (Bukreyev et al. 2006). Although GP-TMCT1 had ELISA IgG titers similar to those of GP1 at 7 days post-boost, its neutralizing titers were lower, suggesting a loss of neutralizing epitopes by the TMCT modification. Interestingly, despite the delayed replication of pre-N viruses in AGMs, their antibody titers were higher than those of the N-P viruses, possibly reflecting an overall higher amount of GP incorporated in the virions, which in turn may be taken up efficiently by antigen presenting cells. Although animals in each group showed a similar trend, no statistical analyses were possible due to the limited animal number (two per group).

The observation that the second dose of the HPIV1-based constructs did not result in shedding detectable by an infectivity assay, and yet resulted in substantial antibody boosts, is reminiscent of previous findings with the HPIV3/EboGP vector (Bukreyev et al. 2010). In that previous study, inoculation of HPIV3-experienced rhesus monkeys with two doses of HPIV3/EboGP vector given at an interval of 28 days did not result in any shedding detectable by an infectivity assay, and yet each dose induced an increase in EBOV GP-specific antibodies. In that study, further analysis of the NP and TL specimens by quantitative RT-PCR showed that in fact viral RNA was shed following each dose in HPIV3-experienced animals, probably in the form of virus that was neutralized by antibodies present in the respiratory secretions. The ability of HPIV1 and HPIV3 to reinfect virus-experienced hosts is not unexpected, since reinfection by HPIVs is common in humans. The ability of HPIV1 and HPIV3 to reinfect virus-experienced hosts sufficiently well to be immunogenic suggests that they can be successfully used as vectors in the general population.

4.2.3. TMCT modification did not increase incorporation into virions and immunogenicity of EBOV GP

Modification of EBOV GP to contain the TMCT domains of HPIV1 F protein conferred neither enhancement of particle incorporation nor an increase in the immunogenicity of EBOV GP. This was incongruous to previous findings from this laboratory with RSV F in HPIV1 and HPIV3 vectors, and previous findings of others (Park et al. 2006). It might be that the TMCT modification was successful in the case of RSV F protein because the native RSV F has very inefficient packaging into the HPIV vector particles, making the improvement by swapping TMCT dramatic (Liang et al. 2016). In sharp contrast, native full-length EBOV GP was moderately efficient in packaging into the HPIV3 and HPIV1 vectors, and perhaps this could not be improved by TMCT modification. It is known that the GP of EBOV and other members of the family *Filoviridae* contain a pre-transmembrane region (pre-TM), spanning residues 640-657 (DNDNWWTGWRQWIPAGIG)

and rich in aromatic amino acids, that adopts an α-helical conformation and possesses a strong affinity to partition into membrane interfaces (Saez-Cirion et al. 2003). This unique pre-TM might be driving efficient EBOV GP membrane incorporation and virion packaging that may be independent of the TMCT domain. A very different possibility is that TMCT modification of RSV F not only enhances virion packaging, but also partially stabilizes it in its highly immunogenic pre-F conformation, which together could account for the observed greater immunogenicity. Such an effect may not occur with EBOV GP. In addition, EBOV GP has a uniquely short CT domain containing only four amino acids (KFVF). The TMCT modification replaced this with a 36-residue HPIV1 F CT domain, which may have destabilized or altered EBOV GP structure and antigenicity. This would be consistent with a previous report that changes in the TMCT region of EBOV GP affected its functionality (Medina et al. 2003). This also is supported by the evidence, that, despite several attempts, it was not possible to rescue an HPIV3/ΔF-HN construct, in which the vector F and HN genes were deleted and the sole surface glycoprotein gene expressed a chimeric EBOV GP in which either the CT or the TMCT domains were substituted with those of HPIV3 F protein (data not shown). In contrast, this same backbone expressing full-length EBOV GP was readily rescued, suggesting that the chimeric GP forms with the foreign TMCT domains had structural changes that rendered them non-functional and likely also resulted in the loss of protective epitopes. In line with this, the slightly attenuated replication and smaller plaque sizes of the TMCT versions, compared to full-length EBOV GP, suggest that the TMCT form may be non-functional and even a disadvantage for the vector.

4.2.4. Summary

Overall, the results here showed that two doses of the attenuated HPIV1-based GP1 construct were capable of stimulating high titers of EBOV GP-neutralizing antibodies that were similar in magnitude to those induced by wt rHPIV3/EboGP, previously shown to protect against EBOV challenge (Bukreyev et al. 2006). This was the case despite the relatively attenuated (1000-fold reduced) replication of GP1 in AGMs compared to wt rHPIV3/EboGP. The HPIV1 vector in the present study has the advantage of bearing a $C^{\Delta 170}$ mutation in the P/C gene that confers restricted replication and attenuation needed for safety, although this was evident only in the upper respiratory tract of this particular study. In addition, the fact that HPIV1 naturally is less permissive for replication in AGMs than HPIV3 might suggest that the immunogenicity of the HPIV1-based constructs probably is substantially under-estimated in this animal model. To further enhance immunogenicity that might eliminate the need for two doses, the GP1 vaccine candidate could be administered as an aerosol using a nebulizer, which primes the respiratory tract more robustly, as was recently shown for rHPIV3/EboGP (Meyer et al. 2015).

In conclusion, this study identified GP1 as an immunogenic and promising intranasal EBOV vaccine candidate expected to be well-tolerated in humans, including children and the elderly and is available for clinical evaluation in humans.

5. References

Abedi, G. R., Prill, M. M., Langley, G. E., Wikswo, M. E., Weinberg, G. A., Curns, A. T. and Schneider, E. (2016). "Estimates of Parainfluenza Virus-Associated Hospitalizations and Cost Among Children Aged Less Than 5 Years in the United States, 1998-2010." J Pediatric Infect Dis Soc **5**(1): 7-13.

Acosta, P. L., Caballero, M. T. and Polack, F. P. (2015). "Brief History and Characterization of Enhanced Respiratory Syncytial Virus Disease." Clin Vaccine Immunol **23**(3): 189-195.

Afonso, C. L., Amarasinghe, G. K., Banyai, K., Bao, Y., Basler, C. F., Bavari, S., Bejerman, N., Blasdell, K. R., Briand, F. X., Briese, T., Bukreyev, A., Calisher, C. H., Chandran, K., Cheng, J., Clawson, A. N., Collins, P. L., Dietzgen, R. G., Dolnik, O., Domier, L. L., Durrwald, R., Dye, J. M., Easton, A. J., Ebihara, H., Farkas, S. L., Freitas-Astua, J., Formenty, P., Fouchier, R. A., Fu, Y., Ghedin, E., Goodin, M. M., Hewson, R., Horie, M., Hyndman, T. H., Jiang, D., Kitajima, E. W., Kobinger, G. P., Kondo, H., Kurath, G., Lamb, R. A., Lenardon, S., Leroy, E. M., Li, C. X., Lin, X. D., Liu, L., Longdon, B., Marton, S., Maisner, A., Muhlberger, E., Netesov, S. V., Nowotny, N., Patterson, J. L., Payne, S. L., Paweska, J. T., Randall, R. E., Rima, B. K., Rota, P., Rubbenstroth, D., Schwemmle, M., Shi, M., Smither, S. J., Stenglein, M. D., Stone, D. M., Takada, A., Terregino, C., Tesh, R. B., Tian, J. H., Tomonaga, K., Tordo, N., Towner, J. S., Vasilakis, N., Verbeek, M., Volchkov, V. E., Wahl-Jensen, V., Walsh, J. A., Walker, P. J., Wang, D., Wang, L. F., Wetzel, T., Whitfield, A. E., Xie, J. T., Yuen, K. Y., Zhang, Y. Z. and Kuhn, J. H. (2016). "Taxonomy of the order Mononegavirales: update 2016." Arch Virol **161**(8): 2351-2360.

Agrawal, N., Dasaradhi, P. V., Mohmmed, A., Malhotra, P., Bhatnagar, R. K. and Mukherjee, S. K. (2003). "RNA interference: biology, mechanism, and applications." Microbiol Mol Biol Rev **67**(4): 657-685.

Ahmed, S. B. M. and Prigent, S. A. (2017). "Insights into the Shc Family of Adaptor Proteins." J Mol Signal **12**: 2.

Amarasinghe, G. K., Arechiga Ceballos, N. G., Banyard, A. C., Basler, C. F., Bavari, S., Bennett, A. J., Blasdell, K. R., Briese, T., Bukreyev, A., Cai, Y., Calisher, C. H., Campos Lawson, C., Chandran, K., Chapman, C. A., Chiu, C. Y., Choi, K. S., Collins, P. L., Dietzgen, R. G., Dolja, V. V., Dolnik, O., Domier, L. L., Durrwald, R., Dye, J. M., Easton, A. J., Ebihara, H., Echevarria, J. E., Fooks, A. R., Formenty, P. B. H., Fouchier, R. A. M., Freuling, C. M., Ghedin, E., Goldberg, T. L., Hewson, R., Horie, M., Hyndman, T. H., Jiang, D., Kityo, R., Kobinger, G. P., Kondo, H., Koonin, E. V., Krupovic, M., Kurath, G., Lamb, R. A., Lee, B., Leroy, E. M., Maes, P., Maisner, A., Marston, D. A., Mor, S. K., Muller, T., Muhlberger, E., Ramirez, V. M. N., Netesov, S. V., Ng, T. F. F., Nowotny, N., Palacios, G., Patterson, J. L., Paweska, J. T., Payne, S. L., Prieto, K., Rima, B. K., Rota, P., Rubbenstroth, D., Schwemmle, M., Siddell, S., Smither, S. J., Song, Q., Song, T., Stenglein, M. D., Stone, D. M., Takada, A., Tesh, R. B., Thomazelli, L. M., Tomonaga, K., Tordo, N., Towner, J. S., Vasilakis, N., Vazquez-Moron, S., Verdugo, C., Volchkov, V. E., Wahl, V., Walker, P. J., Wang, D., Wang, L. F., Wellehan, J. F. X., Wiley, M. R., Whitfield, A. E., Wolf, Y. I., Ye, G., Zhang, Y. Z. and Kuhn, J. H. (2018). "Taxonomy of the order Mononegavirales: update 2018." Arch Virol **163**(8): 2283-2294.

Ambros, V. (2004). "The functions of animal microRNAs." Nature **431**(7006): 350-355.

American Academy of Pediatrics Committee on Infectious Diseases Guidelines Committee (2014). "Updated guidance for palivizumab prophylaxis among infants and young children at increased risk of hospitalization for respiratory syncytial virus infection." Pediatrics **134**(2): 415-420.

American Academy of Pediatrics Subcommittee on Diagnosis Management of Bronchiolitis (2006). "Diagnosis and management of bronchiolitis." Pediatrics **118**(4): 1774-1793.

Anderson, R. G. (1998). "The caveolae membrane system." Annu Rev Biochem **67**: 199-225.

Ashbrook, A. W., Lentscher, A. J., Zamora, P. F., Silva, L. A., May, N. A., Bauer, J. A., Morrison, T. E. and Dermody, T. S. (2016). "Antagonism of the Sodium-Potassium ATPase Impairs Chikungunya Virus Infection." MBio **7**(3).

Aydemir-Koksoy, A., Abramowitz, J. and Allen, J. C. (2001). "Ouabain-induced signaling and vascular smooth muscle cell proliferation." J Biol Chem **276**(49): 46605-46611.

Bachmann, M. F., Rohrer, U. H., Kundig, T. M., Burki, K., Hengartner, H. and Zinkernagel, R. M. (1993). "The influence of antigen organization on B cell responsiveness." Science **262**(5138): 1448-1451.

Bartlett, E. J., Amaro-Carambot, E., Surman, S. R., Collins, P. L., Murphy, B. R. and Skiadopoulos, M. H. (2006). "Introducing point and deletion mutations into the P/C gene of human parainfluenza virus type 1 (HPIV1) by reverse genetics generates attenuated and efficacious vaccine candidates." Vaccine **24**(14): 2674-2684.

Bartlett, E. J., Amaro-Carambot, E., Surman, S. R., Newman, J. T., Collins, P. L., Murphy, B. R. and Skiadopoulos, M. H. (2005). "Human parainfluenza virus type I (HPIV1) vaccine candidates designed by reverse genetics are attenuated and efficacious in African green monkeys." Vaccine **23**(38): 4631-4646.

Bartlett, E. J., Castano, A., Surman, S. R., Collins, P. L., Skiadopoulos, M. H. and Murphy, B. R. (2007). "Attenuation and efficacy of human parainfluenza virus type 1 (HPIV1) vaccine candidates containing stabilized mutations in the P/C and L genes." Virol J **4**: 67.

Bartlett, E. J., Cruz, A. M., Boonyaratanakornkit, J., Esker, J., Castano, A., Skiadopoulos, M. H., Collins, P. L., Murphy, B. R. and Schmidt, A. C. (2010). "A novel human parainfluenza virus type 1 (HPIV1) with separated P and C genes is useful for generating C gene mutants for evaluation as live-attenuated virus vaccine candidates." Vaccine **28**(3): 767-779.

Bartlett, E. J., Cruz, A. M., Esker, J., Castano, A., Schomacker, H., Surman, S. R., Hennessey, M., Boonyaratanakornkit, J., Pickles, R. J., Collins, P. L., Murphy, B. R. and Schmidt, A. C. (2008). "Human parainfluenza virus type 1 C proteins are nonessential proteins that inhibit the host interferon and apoptotic responses and are required for efficient replication in nonhuman primates." J Virol **82**(18): 8965-8977.

Baseler, L., Chertow, D. S., Johnson, K. M., Feldmann, H. and Morens, D. M. (2017). "The Pathogenesis of Ebola Virus Disease." Annu Rev Pathol **12**: 387-418.

Beeler, J. A. and van Wyke Coelingh, K. (1989). "Neutralization epitopes of the F glycoprotein of respiratory syncytial virus: effect of mutation upon fusion function." J Virol **63**(7): 2941-2950.

Bell, B. P., Damon, I. K., Jernigan, D. B., Kenyon, T. A., Nichol, S. T., O'Connor, J. P. and Tappero, J. W. (2016). "Overview, Control Strategies, and Lessons Learned in the CDC Response to the 2014-2016 Ebola Epidemic." MMWR Suppl **65**(3): 4-11.

Bermingham, A. and Collins, P. L. (1999). "The M2-2 protein of human respiratory syncytial virus is a regulatory factor involved in the balance between RNA replication and transcription." Proc Natl Acad Sci U S A **96**(20): 11259-11264.

Biscardi, J. S., Maa, M. C., Tice, D. A., Cox, M. E., Leu, T. H. and Parsons, S. J. (1999). "c-Src-mediated phosphorylation of the epidermal growth factor receptor on Tyr845 and Tyr1101 is associated with modulation of receptor function." J Biol Chem **274**(12): 8335-8343.

Blanco, G. and Mercer, R. W. (1998). "Isozymes of the Na-K-ATPase: heterogeneity in structure, diversity in function." Am J Physiol **275**(5 Pt 2): F633-650.

Blount, R. E., Jr., Morris, J. A. and Savage, R. E. (1956). "Recovery of cytopathogenic agent from chimpanzees with coryza." Proc Soc Exp Biol Med **92**(3): 544-549.

Boggon, T. J. and Eck, M. J. (2004). "Structure and regulation of Src family kinases." Oncogene **23**(48): 7918-7927.

Brock, L. G., Liu, X., Liang, B., Lingemann, M., Liu, X., Herbert, R., Hackenberg, A. D., Buchholz, U. J., Collins, P. L. and Munir, S. (2018). "Murine Pneumonia Virus Expressing the Fusion Glycoprotein of Human Respiratory Syncytial Virus from an Added Gene Is Highly Attenuated and Immunogenic in Rhesus Macaques." J Virol **92**(17).

Buchholz, U. J., Finke, S. and Conzelmann, K. K. (1999). "Generation of bovine respiratory syncytial virus (BRSV) from cDNA: BRSV NS2 is not essential for virus replication in tissue culture, and the human RSV leader region acts as a functional BRSV genome promoter." J Virol **73**(1): 251-259.

Bukreyev, A., Lamirande, E. W., Buchholz, U. J., Vogel, L. N., Elkins, W. R., St Claire, M., Murphy, B. R., Subbarao, K. and Collins, P. L. (2004). "Mucosal immunisation of African green monkeys (Cercopithecus aethiops) with an attenuated parainfluenza virus expressing the SARS coronavirus spike protein for the prevention of SARS." Lancet **363**(9427): 2122-2127.

Bukreyev, A., Marzi, A., Feldmann, F., Zhang, L., Yang, L., Ward, J. M., Dorward, D. W., Pickles, R. J., Murphy, B. R., Feldmann, H. and Collins, P. L. (2009). "Chimeric human

parainfluenza virus bearing the Ebola virus glycoprotein as the sole surface protein is immunogenic and highly protective against Ebola virus challenge." Virology **383**(2): 348-361.

Bukreyev, A., Rollin, P. E., Tate, M. K., Yang, L., Zaki, S. R., Shieh, W. J., Murphy, B. R., Collins, P. L. and Sanchez, A. (2007). "Successful topical respiratory tract immunization of primates against Ebola virus." J Virol **81**(12): 6379-6388.

Bukreyev, A., Whitehead, S. S., Murphy, B. R. and Collins, P. L. (1997). "Recombinant respiratory syncytial virus from which the entire SH gene has been deleted grows efficiently in cell culture and exhibits site-specific attenuation in the respiratory tract of the mouse." J Virol **71**(12): 8973-8982.

Bukreyev, A., Yang, L., Zaki, S. R., Shieh, W. J., Rollin, P. E., Murphy, B. R., Collins, P. L. and Sanchez, A. (2006). "A single intranasal inoculation with a paramyxovirus-vectored vaccine protects guinea pigs against a lethal-dose Ebola virus challenge." J Virol **80**(5): 2267-2279.

Bukreyev, A. A., Dinapoli, J. M., Yang, L., Murphy, B. R. and Collins, P. L. (2010). "Mucosal parainfluenza virus-vectored vaccine against Ebola virus replicates in the respiratory tract of vector-immune monkeys and is immunogenic." Virology **399**(2): 290-298.

Burkard, C., Verheije, M. H., Haagmans, B. L., van Kuppeveld, F. J., Rottier, P. J., Bosch, B. J. and de Haan, C. A. (2015). "ATP1A1-mediated Src signaling inhibits coronavirus entry into host cells." J Virol **89**(8): 4434-4448.

Calain, P. and Roux, L. (1993). "The rule of six, a basic feature for efficient replication of Sendai virus defective interfering RNA." J Virol **67**(8): 4822-4830.

Centers for Disease Control and Prevention (CDC) (2009). Biosafety in Microbiological and Biomedical Laboratories. HHS Publication No. (CDC) 21-1112.

Centers for Disease Control and Prevention (CDC). (2016, April 14, 2016). "Ebola Virus Disease. 2014 Ebola Outbreak in West Africa - Case Counts." Retrieved September 12, 2016, from https://www.cdc.gov/vhf/ebola/outbreaks/2014-west-africa/case-counts.html.

Chang, T. H., Segovia, J., Sabbah, A., Mgbemena, V. and Bose, S. (2012). "Cholesterol-rich lipid rafts are required for release of infectious human respiratory syncytial virus particles." Virology **422**(2): 205-213.

Chanock, R., Roizman, B. and Myers, R. (1957). "Recovery from infants with respiratory illness of a virus related to chimpanzee coryza agent (CCA). I. Isolation, properties and characterization." Am J Hyg **66**(3): 281-290.

Cherniavsky-Lev, M., Golani, O., Karlish, S. J. and Garty, H. (2014). "Ouabain-induced internalization and lysosomal degradation of the Na+/K+-ATPase." J Biol Chem **289**(2): 1049-1059.

Chu, C. L., Buczek-Thomas, J. A. and Nugent, M. A. (2004). "Heparan sulphate proteoglycans modulate fibroblast growth factor-2 binding through a lipid raft-mediated mechanism." Biochem J **379**(Pt 2): 331-341.

Collins, P. L., Hill, M. G., Camargo, E., Grosfeld, H., Chanock, R. M. and Murphy, B. R. (1995). "Production of infectious human respiratory syncytial virus from cloned cDNA confirms an essential role for the transcription elongation factor from the 5' proximal open reading frame of the M2 mRNA in gene expression and provides a capability for vaccine development." Proc Natl Acad Sci U S A **92**(25): 11563-11567.

Collins, P. L. and Karron, R. A. (2013). Respiratory Syncytial Virus and Metapneumovirus. Fields virology. D. M. Knipe, P. M. Howley, J. I. Cohen et al. Philadelphia, Lippincott Williams&Wilkins. **1:** 1086-1123.

Colman, P. M. and Lawrence, M. C. (2003). "The structural biology of type I viral membrane fusion." Nat Rev Mol Cell Biol **4**(4): 309-319.

Coltart, C. E., Lindsey, B., Ghinai, I., Johnson, A. M. and Heymann, D. L. (2017). "The Ebola outbreak, 2013-2016: old lessons for new epidemics." Philos Trans R Soc Lond B Biol Sci **372**(1721).

Conner, S. D. and Schmid, S. L. (2003). "Regulated portals of entry into the cell." Nature **422**(6927): 37-44.

Currier, M. G., Lee, S., Stobart, C. C., Hotard, A. L., Villenave, R., Meng, J., Pretto, C. D., Shields, M. D., Nguyen, M. T., Todd, S. O., Chi, M. H., Hammonds, J., Krumm, S. A., Spearman, P., Plemper, R. K., Sakamoto, K., Peebles, R. S., Jr., Power, U. F. and Moore, M. L. (2016).

"EGFR Interacts with the Fusion Protein of Respiratory Syncytial Virus Strain 2-20 and Mediates Infection and Mucin Expression." PLoS Pathog **12**(5): e1005622.

De Santis, O., Audran, R., Pothin, E., Warpelin-Decrausaz, L., Vallotton, L., Wuerzner, G., Cochet, C., Estoppey, D., Steiner-Monard, V., Lonchampt, S., Thierry, A. C., Mayor, C., Bailer, R. T., Mbaya, O. T., Zhou, Y., Ploquin, A., Sullivan, N. J., Graham, B. S., Roman, F., De Ryck, I., Ballou, W. R., Kieny, M. P., Moorthy, V., Spertini, F. and Genton, B. (2016). "Safety and immunogenicity of a chimpanzee adenovirus-vectored Ebola vaccine in healthy adults: a randomised, double-blind, placebo-controlled, dose-finding, phase 1/2a study." Lancet Infect Dis **16**(3): 311-320.

Dodson, A. W., Taylor, T. J., Knipe, D. M. and Coen, D. M. (2007). "Inhibitors of the sodium potassium ATPase that impair herpes simplex virus replication identified via a chemical screening approach." Virology **366**(2): 340-348.

Donepudi, M. and Resh, M. D. (2008). "c-Src trafficking and co-localization with the EGF receptor promotes EGF ligand-independent EGF receptor activation and signaling." Cell Signal **20**(7): 1359-1367.

Durbin, A. P., Elkins, W. R. and Murphy, B. R. (2000). "African green monkeys provide a useful nonhuman primate model for the study of human parainfluenza virus types-1, -2, and -3 infection." Vaccine **18**(22): 2462-2469.

Durbin, A. P., Hall, S. L., Siew, J. W., Whitehead, S. S., Collins, P. L. and Murphy, B. R. (1997). "Recovery of infectious human parainfluenza virus type 3 from cDNA." Virology **235**(2): 323-332.

Elbashir, S. M., Harborth, J., Lendeckel, W., Yalcin, A., Weber, K. and Tuschl, T. (2001). "Duplexes of 21-nucleotide RNAs mediate RNA interference in cultured mammalian cells." Nature **411**(6836): 494-498.

Ewer, K., Rampling, T., Venkatraman, N., Bowyer, G., Wright, D., Lambe, T., Imoukhuede, E. B., Payne, R., Fehling, S. K., Strecker, T., Biedenkopf, N., Krahling, V., Tully, C. M., Edwards, N. J., Bentley, E. M., Samuel, D., Labbe, G., Jin, J., Gibani, M., Minhinnick, A., Wilkie, M., Poulton, I., Lella, N., Roberts, R., Hartnell, F., Bliss, C., Sierra-Davidson, K., Powlson, J., Berrie, E., Tedder, R., Roman, F., De Ryck, I., Nicosia, A., Sullivan, N. J., Stanley, D. A., Mbaya, O. T., Ledgerwood, J. E., Schwartz, R. M., Siani, L., Colloca, S., Folgori, A., Di Marco, S., Cortese, R., Wright, E., Becker, S., Graham, B. S., Koup, R. A., Levine, M. M., Volkmann, A., Chaplin, P., Pollard, A. J., Draper, S. J., Ballou, W. R., Lawrie, A., Gilbert, S. C. and Hill, A. V. (2016). "A Monovalent Chimpanzee Adenovirus Ebola Vaccine Boosted with MVA." N Engl J Med **374**(17): 1635-1646.

Falsey, A. R., Hennessey, P. A., Formica, M. A., Cox, C. and Walsh, E. E. (2005). "Respiratory syncytial virus infection in elderly and high-risk adults." N Engl J Med **352**(17): 1749-1759.

Fearns, R. and Collins, P. L. (1999). "Role of the M2-1 transcription antitermination protein of respiratory syncytial virus in sequential transcription." J Virol **73**(7): 5852-5864.

Feldmann, H., Sanchez, A. and Geisbert, T. W. (2013). Filoviridae: Marburg and Ebola Viruses. Fields Virology. D. M. Knipe, P. M. Howley, J. I. Cohen et al. Philadelphia, Lippincott Williams&Wilkins. **1:** 923-956.

Ferrandi, M., Barassi, P., Minotti, E., Duzzi, L., Molinari, I., Bianchi, G. and Ferrari, P. (2002). "PST 2238: a new antihypertensive compound that modulates renal Na-K pump function without diuretic activity in Milan hypertensive rats." J Cardiovasc Pharmacol **40**(6): 881-889.

Ferrari, P., Ferrandi, M., Valentini, G. and Bianchi, G. (2006). "Rostafuroxin: an ouabain antagonist that corrects renal and vascular Na+-K+- ATPase alterations in ouabain and adducin-dependent hypertension." Am J Physiol Regul Integr Comp Physiol **290**(3): R529-535.

Ferrari, P., Torielli, L., Ferrandi, M., Padoani, G., Duzzi, L., Florio, M., Conti, F., Melloni, P., Vesci, L., Corsico, N. and Bianchi, G. (1998). "PST2238: a new antihypertensive compound that antagonizes the long-term pressor effect of ouabain." J Pharmacol Exp Ther **285**(1): 83-94.

Fire, A., Xu, S., Montgomery, M. K., Kostas, S. A., Driver, S. E. and Mello, C. C. (1998). "Potent and specific genetic interference by double-stranded RNA in Caenorhabditis elegans." Nature **391**(6669): 806-811.

Franceschini, A., Meier, R., Casanova, A., Kreibich, S., Daga, N., Andritschke, D., Dilling, S., Ramo, P., Emmenlauer, M., Kaufmann, A., Conde-Alvarez, R., Low, S. H., Pelkmans, L.,

Helenius, A., Hardt, W. D., Dehio, C. and von Mering, C. (2014). "Specific inhibition of diverse pathogens in human cells by synthetic microRNA-like oligonucleotides inferred from RNAi screens." Proc Natl Acad Sci U S A **111**(12): 4548-4553.

Frenkel-Morgenstern, M., Cohen, A. A., Geva-Zatorsky, N., Eden, E., Prilusky, J., Issaeva, I., Sigal, A., Cohen-Saidon, C., Liron, Y., Cohen, L., Danon, T., Perzov, N. and Alon, U. (2010). "Dynamic Proteomics: a database for dynamics and localizations of endogenous fluorescently-tagged proteins in living human cells." Nucleic Acids Res **38**(Database issue): D508-512.

Galinski, M. S., Troy, R. M. and Banerjee, A. K. (1992). "RNA editing in the phosphoprotein gene of the human parainfluenza virus type 3." Virology **186**(2): 543-550.

Garbutt, M., Liebscher, R., Wahl-Jensen, V., Jones, S., Moller, P., Wagner, R., Volchkov, V., Klenk, H. D., Feldmann, H. and Stroher, U. (2004). "Properties of replication-competent vesicular stomatitis virus vectors expressing glycoproteins of filoviruses and arenaviruses." J Virol **78**(10): 5458-5465.

Garcia, J., Garcia-Barreno, B., Vivo, A. and Melero, J. A. (1993). "Cytoplasmic inclusions of respiratory syncytial virus-infected cells: formation of inclusion bodies in transfected cells that coexpress the nucleoprotein, the phosphoprotein, and the 22K protein." Virology **195**(1): 243-247.

Garcia-Dorival, I., Wu, W., Dowall, S., Armstrong, S., Touzelet, O., Wastling, J., Barr, J. N., Matthews, D., Carroll, M., Hewson, R. and Hiscox, J. A. (2014). "Elucidation of the Ebola virus VP24 cellular interactome and disruption of virus biology through targeted inhibition of host-cell protein function." J Proteome Res **13**(11): 5120-5135.

Geering, K. (2008). "Functional roles of Na,K-ATPase subunits." Curr Opin Nephrol Hypertens **17**(5): 526-532.

Goldstein, T., Anthony, S. J., Gbakima, A., Bird, B. H., Bangura, J., Tremeau-Bravard, A., Belaganahalli, M. N., Wells, H. L., Dhanota, J. K., Liang, E., Grodus, M., Jangra, R. K., DeJesus, V. A., Lasso, G., Smith, B. R., Jambai, A., Kamara, B. O., Kamara, S., Bangura, W., Monagin, C., Shapira, S., Johnson, C. K., Saylors, K., Rubin, E. M., Chandran, K., Lipkin, W. I. and Mazet, J. A. K. (2018). "The discovery of Bombali virus adds further support for bats as hosts of ebolaviruses." Nat Microbiol.

Gopalakrishnan, M., Forsten-Williams, K., Nugent, M. A. and Tauber, U. C. (2005). "Effects of receptor clustering on ligand dissociation kinetics: theory and simulations." Biophys J **89**(6): 3686-3700.

Grimmer, S., van Deurs, B. and Sandvig, K. (2002). "Membrane ruffling and macropinocytosis in A431 cells require cholesterol." J Cell Sci **115**(Pt 14): 2953-2962.

Grosso, F., Stoilov, P., Lingwood, C., Brown, M. and Cochrane, A. (2017). "Suppression of Adenovirus Replication by Cardiotonic Steroids." J Virol **91**(3).

Group, P. I. W., Multi-National, P. I. I. S. T., Davey, R. T., Jr., Dodd, L., Proschan, M. A., Neaton, J., Neuhaus Nordwall, J., Koopmeiners, J. S., Beigel, J., Tierney, J., Lane, H. C., Fauci, A. S., Massaquoi, M. B. F., Sahr, F. and Malvy, D. (2016). "A Randomized, Controlled Trial of ZMapp for Ebola Virus Infection." N Engl J Med **375**(15): 1448-1456.

Haas, M., Askari, A. and Xie, Z. (2000). "Involvement of Src and epidermal growth factor receptor in the signal-transducing function of Na+/K+-ATPase." J Biol Chem **275**(36): 27832-27837.

Haas, M., Wang, H., Tian, J. and Xie, Z. (2002). "Src-mediated inter-receptor cross-talk between the Na+/K+-ATPase and the epidermal growth factor receptor relays the signal from ouabain to mitogen-activated protein kinases." J Biol Chem **277**(21): 18694-18702.

Hailstones, D., Sleer, L. S., Parton, R. G. and Stanley, K. K. (1998). "Regulation of caveolin and caveolae by cholesterol in MDCK cells." J Lipid Res **39**(2): 369-379.

Hall, C. B., Weinberg, G. A., Blumkin, A. K., Edwards, K. M., Staat, M. A., Schultz, A. F., Poehling, K. A., Szilagyi, P. G., Griffin, M. R., Williams, J. V., Zhu, Y., Grijalva, C. G., Prill, M. M. and Iwane, M. K. (2013). "Respiratory syncytial virus-associated hospitalizations among children less than 24 months of age." Pediatrics **132**(2): e341-348.

Hallak, L. K., Spillmann, D., Collins, P. L. and Peeples, M. E. (2000). "Glycosaminoglycan sulfation requirements for respiratory syncytial virus infection." J Virol **74**(22): 10508-10513.

Haller, A. A., Miller, T., Mitiku, M. and Coelingh, K. (2000). "Expression of the surface glycoproteins of human parainfluenza virus type 3 by bovine parainfluenza virus type 3, a novel attenuated virus vaccine vector." J Virol **74**(24): 11626-11635.

Hannon, G. J. (2002). "RNA interference." Nature **418**(6894): 244-251.

Henao-Restrepo, A. M., Longini, I. M., Egger, M., Dean, N. E., Edmunds, W. J., Camacho, A., Carroll, M. W., Doumbia, M., Draguez, B., Duraffour, S., Enwere, G., Grais, R., Gunther, S., Hossmann, S., Konde, M. K., Kone, S., Kuisma, E., Levine, M. M., Mandal, S., Norheim, G., Riveros, X., Soumah, A., Trelle, S., Vicari, A. S., Watson, C. H., Keita, S., Kieny, M. P. and Rottingen, J. A. (2015). "Efficacy and effectiveness of an rVSV-vectored vaccine expressing Ebola surface glycoprotein: interim results from the Guinea ring vaccination cluster-randomised trial." Lancet **386**(9996): 857-866.

Hewlett, L. J., Prescott, A. R. and Watts, C. (1994). "The coated pit and macropinocytic pathways serve distinct endosome populations." J Cell Biol **124**(5): 689-703.

Hirsch, A. J. (2010). "The use of RNAi-based screens to identify host proteins involved in viral replication." Future Microbiol **5**(2): 303-311.

Human Protein Atlas. (2018). "ATP1A1." V18.0. Retrieved 11/30/18, from https://v18.proteinatlas.org/ENSG00000163399-ATP1A1/tissue.

International Committee on Taxonomy of Viruses. (2012). Virus taxonomy : classification and nomenclature of viruses : ninth report of the International Committee on Taxonomy of Viruses. London ; Waltham, MA, Academic Press.

Iwasaki, M., Minder, P., Cai, Y., Kuhn, J. H., Yates, J. R., 3rd, Torbett, B. E. and de la Torre, J. C. (2018). "Interactome analysis of the lymphocytic choriomeningitis virus nucleoprotein in infected cells reveals ATPase Na+/K+ transporting subunit Alpha 1 and prohibitin as host-cell factors involved in the life cycle of mammarenaviruses." PLoS Pathog **14**(2): e1006892.

Jaax, N., Jahrling, P., Geisbert, T., Geisbert, J., Steele, K., McKee, K., Nagley, D., Johnson, E., Jaax, G. and Peters, C. (1995). "Transmission of Ebola virus (Zaire strain) to uninfected control monkeys in a biocontainment laboratory." Lancet **346**(8991-8992): 1669-1671.

Johnson, E., Jaax, N., White, J. and Jahrling, P. (1995). "Lethal experimental infections of rhesus monkeys by aerosolized Ebola virus." Int J Exp Pathol **76**(4): 227-236.

Johnson, S., Oliver, C., Prince, G. A., Hemming, V. G., Pfarr, D. S., Wang, S. C., Dormitzer, M., O'Grady, J., Koenig, S., Tamura, J. K., Woods, R., Bansal, G., Couchenour, D., Tsao, E., Hall, W. C. and Young, J. F. (1997). "Development of a humanized monoclonal antibody (MEDI-493) with potent in vitro and in vivo activity against respiratory syncytial virus." J Infect Dis **176**(5): 1215-1224.

Johnson, S. M., McNally, B. A., Ioannidis, I., Flano, E., Teng, M. N., Oomens, A. G., Walsh, E. E. and Peeples, M. E. (2015). "Respiratory Syncytial Virus Uses CX3CR1 as a Receptor on Primary Human Airway Epithelial Cultures." PLoS Pathog **11**(12): e1005318.

Jorgensen, P. L., Hakansson, K. O. and Karlish, S. J. (2003). "Structure and mechanism of Na,K-ATPase: functional sites and their interactions." Annu Rev Physiol **65**: 817-849.

Kaner, J. and Schaack, S. (2016). "Understanding Ebola: the 2014 epidemic." Global Health **12**(1): 53.

Kapikian, A. Z., Chanock, R. M., Reichelderfer, T. E., Ward, T. G., Huebner, R. J. and Bell, J. A. (1961). "Inoculation of human volunteers with parainfluenza virus type 3." JAMA **178**: 537-541.

Kapikian, A. Z., Mitchell, R. H., Chanock, R. M., Shvedoff, R. A. and Stewart, C. E. (1969). "An epidemiologic study of altered clinical reactivity to respiratory syncytial (RS) virus infection in children previously vaccinated with an inactivated RS virus vaccine." Am J Epidemiol **89**(4): 405-421.

Kaplan, J. H. (2002). "Biochemistry of Na,K-ATPase." Annu Rev Biochem **71**: 511-535.

Karron, R. A., Buchholz, U. J. and Collins, P. L. (2013). "Live-attenuated respiratory syncytial virus vaccines." Curr Top Microbiol Immunol **372**: 259-284.

Karron, R. A., Buonagurio, D. A., Georgiu, A. F., Whitehead, S. S., Adamus, J. E., Clements-Mann, M. L., Harris, D. O., Randolph, V. B., Udem, S. A., Murphy, B. R. and Sidhu, M. S. (1997). "Respiratory syncytial virus (RSV) SH and G proteins are not essential for viral replication in vitro: clinical evaluation and molecular characterization of a cold-passaged, attenuated RSV subgroup B mutant." Proc Natl Acad Sci U S A **94**(25): 13961-13966.

Karron, R. A. and Collins, P. L. (2013). Parainfluenza viruses. Fields virology. D. M. Knipe, P. M. Howley, J. I. Cohen et al. Philadelphia, Lippincott Williams&Wilkins. **1:** 996-1023.

Karron, R. A., Luongo, C., Thumar, B., Loehr, K. M., Englund, J. A., Collins, P. L. and Buchholz, U. J. (2015). "A gene deletion that up-regulates viral gene expression yields an attenuated RSV vaccine with improved antibody responses in children." Sci Transl Med **7**(312): 312ra175.

Karron, R. A., Thumar, B., Schappell, E., Surman, S., Murphy, B. R., Collins, P. L. and Schmidt, A. C. (2011). "Evaluation of two chimeric bovine-human parainfluenza virus type 3 vaccines in infants and young children." Vaccine.

Karuppannan, A. K., Wu, K. X., Qiang, J., Chu, J. J. and Kwang, J. (2012). "Natural compounds inhibiting the replication of Porcine reproductive and respiratory syndrome virus." Antiviral Res **94**(2): 188-194.

Kasahara, K., Nakayama, Y., Sato, I., Ikeda, K., Hoshino, M., Endo, T. and Yamaguchi, N. (2007). "Role of Src-family kinases in formation and trafficking of macropinosomes." J Cell Physiol **211**(1): 220-232.

Kato, A., Kiyotani, K., Hasan, M. K., Shioda, T., Sakai, Y., Yoshida, T. and Nagai, Y. (1999). "Sendai virus gene start signals are not equivalent in reinitiation capacity: moderation at the fusion protein gene." J Virol **73**(11): 9237-9246.

Kim, H. W., Canchola, J. G., Brandt, C. D., Pyles, G., Chanock, R. M., Jensen, K. and Parrott, R. H. (1969). "Respiratory syncytial virus disease in infants despite prior administration of antigenic inactivated vaccine." Am J Epidemiol **89**(4): 422-434.

Knudson, C. J., Hartwig, S. M., Meyerholz, D. K. and Varga, S. M. (2015). "RSV vaccine-enhanced disease is orchestrated by the combined actions of distinct CD4 T cell subsets." PLoS Pathog **11**(3): e1004757.

Kolakofsky, D., Pelet, T., Garcin, D., Hausmann, S., Curran, J. and Roux, L. (1998). "Paramyxovirus RNA synthesis and the requirement for hexamer genome length: the rule of six revisited." J Virol **72**(2): 891-899.

Kolokoltsov, A. A., Deniger, D., Fleming, E. H., Roberts, N. J., Jr., Karpilow, J. M. and Davey, R. A. (2007). "Small interfering RNA profiling reveals key role of clathrin-mediated endocytosis and early endosome formation for infection by respiratory syncytial virus." J Virol **81**(14): 7786-7800.

Komada, H., Kusagawa, S., Orvell, C., Tsurudome, M., Nishio, M., Bando, H., Kawano, M., Matsumura, H., Norrby, E. and Ito, Y. (1992). "Antigenic diversity of human parainfluenza virus type 1 isolates and their immunological relationship with Sendai virus revealed by using monoclonal antibodies." J Gen Virol **73 (Pt 4)**: 875-884.

Kozak, M. (1987). "An analysis of 5'-noncoding sequences from 699 vertebrate messenger RNAs." Nucleic Acids Res **15**(20): 8125-8148.

Kozak, M. (2005). "Regulation of translation via mRNA structure in prokaryotes and eukaryotes." Gene **361**: 13-37.

Krarup, A., Truan, D., Furmanova-Hollenstein, P., Bogaert, L., Bouchier, P., Bisschop, I. J., Widjojoatmodjo, M. N., Zahn, R., Schuitemaker, H., McLellan, J. S. and Langedijk, J. P. (2015). "A highly stable prefusion RSV F vaccine derived from structural analysis of the fusion mechanism." Nat Commun **6**: 8143.

Krzyzaniak, M. A., Zumstein, M. T., Gerez, J. A., Picotti, P. and Helenius, A. (2013). "Host cell entry of respiratory syncytial virus involves macropinocytosis followed by proteolytic activation of the F protein." PLoS Pathog **9**(4): e1003309.

Kuhn, J. H., Dodd, L. E., Wahl-Jensen, V., Radoshitzky, S. R., Bavari, S. and Jahrling, P. B. (2011). "Evaluation of perceived threat differences posed by filovirus variants." Biosecur Bioterror **9**(4): 361-371.

Lam, J. K., Chow, M. Y., Zhang, Y. and Leung, S. W. (2015). "siRNA Versus miRNA as Therapeutics for Gene Silencing." Mol Ther Nucleic Acids **4**: e252.

Lamb, R. A. (2013). Mononegavirales. Fields virology. D. M. Knipe, P. M. Howley, J. I. Cohen et al. Philadelphia, Lippincott Williams&Wilkins. **1:** 880-884.

Lanzani, C., Citterio, L., Glorioso, N., Manunta, P., Tripodi, G., Salvi, E., Carpini, S. D., Ferrandi, M., Messaggio, E., Staessen, J. A., Cusi, D., Macciardi, F., Argiolas, G., Valentini, G., Ferrari, P. and Bianchi, G. (2010). "Adducin- and ouabain-related gene variants predict the antihypertensive activity of rostafuroxin, part 2: clinical studies." Sci Transl Med **2**(59): 59ra87.

Lexicon Genetics Inc. (2005). "Mouse Genome Informatics (MGI) database." Lexicon Knockout Mice Phenotypic Data Summary Retrieved 6/5/17, from http://www.informatics.jax.org/knockout_mice/lexicon/2270.html.

Liang, B., Munir, S., Amaro-Carambot, E., Surman, S., Mackow, N., Yang, L., Buchholz, U. J., Collins, P. L. and Schaap-Nutt, A. (2014). "Chimeric bovine/human parainfluenza virus type 3 expressing respiratory syncytial virus (RSV) F glycoprotein: effect of insert position

on expression, replication, immunogenicity, stability, and protection against RSV infection." J Virol **88**(8): 4237-4250.

Liang, B., Ngwuta, J. O., Herbert, R., Swerczek, J., Dorward, D. W., Amaro-Carambot, E., Mackow, N., Kabatova, B., Lingemann, M., Surman, S., Yang, L., Chen, M., Moin, S. M., Kumar, A., McLellan, J. S., Kwong, P. D., Graham, B. S., Schaap-Nutt, A., Collins, P. L. and Munir, S. (2016). "Packaging and Prefusion Stabilization Separately and Additively Increase the Quantity and Quality of Respiratory Syncytial Virus (RSV)-Neutralizing Antibodies Induced by an RSV Fusion Protein Expressed by a Parainfluenza Virus Vector." J Virol **90**(21): 10022-10038.

Liang, B., Ngwuta, J. O., Surman, S., Kabatova, B., Liu, X., Lingemann, M., Liu, X., Yang, L., Herbert, R., Swerczek, J., Chen, M., Moin, S. M., Kumar, A., McLellan, J. S., Kwong, P. D., Graham, B. S., Collins, P. L. and Munir, S. (2017). "Improved Prefusion Stability, Optimized Codon Usage, and Augmented Virion Packaging Enhance the Immunogenicity of Respiratory Syncytial Virus Fusion Protein in a Vectored-Vaccine Candidate." J Virol **91**(15).

Lingemann, M., Surman, S., Amaro-Carambot, E., Schaap-Nutt, A., Collins, P. L. and Munir, S. (2015). "The aberrant gene-end transcription signal of the matrix M gene of human parainfluenza virus type 3 downregulates fusion F protein expression and the F-specific antibody response in vivo." J Virol **89**(6): 3318-3331.

Liu, J., Kesiry, R., Periyasamy, S. M., Malhotra, D., Xie, Z. and Shapiro, J. I. (2004). "Ouabain induces endocytosis of plasmalemmal Na/K-ATPase in LLC-PK1 cells by a clathrin-dependent mechanism." Kidney Int **66**(1): 227-241.

Liu, J., Tian, J., Haas, M., Shapiro, J. I., Askari, A. and Xie, Z. (2000). "Ouabain interaction with cardiac Na+/K+-ATPase initiates signal cascades independent of changes in intracellular Na+ and Ca2+ concentrations." J Biol Chem **275**(36): 27838-27844.

Liu, L., Mohammadi, K., Aynafshar, B., Wang, H., Li, D., Liu, J., Ivanov, A. V., Xie, Z. and Askari, A. (2003). "Role of caveolae in signal-transducing function of cardiac Na+/K+-ATPase." Am J Physiol Cell Physiol **284**(6): C1550-1560.

Liu, M., Feng, L. X., Sun, P., Liu, W., Wu, W. Y., Jiang, B. H., Yang, M., Hu, L. H., Guo, D. A. and Liu, X. (2016). "A Novel Bufalin Derivative Exhibited Stronger Apoptosis-Inducing Effect than Bufalin in A549 Lung Cancer Cells and Lower Acute Toxicity in Mice." PLoS One **11**(7): e0159789.

Liu, X., Liang, B., Ngwuta, J., Liu, X., Surman, S., Lingemann, M., Kwong, P. D., Graham, B. S., Collins, P. L. and Munir, S. (2017). "Attenuated Human Parainfluenza Virus Type 1 Expressing the Respiratory Syncytial Virus (RSV) Fusion (F) Glycoprotein from an Added Gene: Effects of Prefusion Stabilization and Packaging of RSV F." J Virol **91**(22).

Livak, K. J. and Schmittgen, T. D. (2001). "Analysis of relative gene expression data using real-time quantitative PCR and the 2(-Delta Delta C(T)) Method." Methods **25**(4): 402-408.

Lozano, R., Naghavi, M., Foreman, K., Lim, S., Shibuya, K., Aboyans, V., Abraham, J., Adair, T., Aggarwal, R., Ahn, S. Y., Alvarado, M., Anderson, H. R., Anderson, L. M., Andrews, K. G., Atkinson, C., Baddour, L. M., Barker-Collo, S., Bartels, D. H., Bell, M. L., Benjamin, E. J., Bennett, D., Bhalla, K., Bikbov, B., Bin Abdulhak, A., Birbeck, G., Blyth, F., Bolliger, I., Boufous, S., Bucello, C., Burch, M., Burney, P., Carapetis, J., Chen, H., Chou, D., Chugh, S. S., Coffeng, L. E., Colan, S. D., Colquhoun, S., Colson, K. E., Condon, J., Connor, M. D., Cooper, L. T., Corriere, M., Cortinovis, M., de Vaccaro, K. C., Couser, W., Cowie, B. C., Criqui, M. H., Cross, M., Dabhadkar, K. C., Dahodwala, N., De Leo, D., Degenhardt, L., Delossantos, A., Denenberg, J., Des Jarlais, D. C., Dharmaratne, S. D., Dorsey, E. R., Driscoll, T., Duber, H., Ebel, B., Erwin, P. J., Espindola, P., Ezzati, M., Feigin, V., Flaxman, A. D., Forouzanfar, M. H., Fowkes, F. G., Franklin, R., Fransen, M., Freeman, M. K., Gabriel, S. E., Gakidou, E., Gaspari, F., Gillum, R. F., Gonzalez-Medina, D., Halasa, Y. A., Haring, D., Harrison, J. E., Havmoeller, R., Hay, R. J., Hoen, B., Hotez, P. J., Hoy, D., Jacobsen, K. H., James, S. L., Jasrasaria, R., Jayaraman, S., Johns, N., Karthikeyan, G., Kassebaum, N., Keren, A., Khoo, J. P., Knowlton, L. M., Kobusingye, O., Koranteng, A., Krishnamurthi, R., Lipnick, M., Lipshultz, S. E., Ohno, S. L., Mabweijano, J., MacIntyre, M. F., Mallinger, L., March, L., Marks, G. B., Marks, R., Matsumori, A., Matzopoulos, R., Mayosi, B. M., McAnulty, J. H., McDermott, M. M., McGrath, J., Mensah, G. A., Merriman, T. R., Michaud, C., Miller, M., Miller, T. R., Mock, C., Mocumbi, A. O., Mokdad, A. A., Moran, A., Mulholland, K., Nair, M. N., Naldi, L., Narayan, K. M., Nasseri, K., Norman, P.,

O'Donnell, M., Omer, S. B., Ortblad, K., Osborne, R., Ozgediz, D., Pahari, B., Pandian, J. D., Rivero, A. P., Padilla, R. P., Perez-Ruiz, F., Perico, N., Phillips, D., Pierce, K., Pope, C. A., 3rd, Porrini, E., Pourmalek, F., Raju, M., Ranganathan, D., Rehm, J. T., Rein, D. B., Remuzzi, G., Rivara, F. P., Roberts, T., De Leon, F. R., Rosenfeld, L. C., Rushton, L., Sacco, R. L., Salomon, J. A., Sampson, U., Sanman, E., Schwebel, D. C., Segui-Gomez, M., Shepard, D. S., Singh, D., Singleton, J., Sliwa, K., Smith, E., Steer, A., Taylor, J. A., Thomas, B., Tleyjeh, I. M., Towbin, J. A., Truelsen, T., Undurraga, E. A., Venketasubramanian, N., Vijayakumar, L., Vos, T., Wagner, G. R., Wang, M., Wang, W., Watt, K., Weinstock, M. A., Weintraub, R., Wilkinson, J. D., Woolf, A. D., Wulf, S., Yeh, P. H., Yip, P., Zabetian, A., Zheng, Z. J., Lopez, A. D., Murray, C. J., AlMazroa, M. A. and Memish, Z. A. (2012). "Global and regional mortality from 235 causes of death for 20 age groups in 1990 and 2010: a systematic analysis for the Global Burden of Disease Study 2010." Lancet **380**(9859): 2095-2128.

Lussignol, M., Kopp, M., Molloy, K., Vizcay-Barrena, G., Fleck, R. A., Dorner, M., Bell, K. L., Chait, B. T., Rice, C. M. and Catanese, M. T. (2016). "Proteomics of HCV virions reveals an essential role for the nucleoporin Nup98 in virus morphogenesis." Proc Natl Acad Sci U S A **113**(9): 2484-2489.

Mackow, N., Amaro-Carambot, E., Liang, B., Surman, S., Lingemann, M., Yang, L., Collins, P. L. and Munir, S. (2015). "Attenuated Human Parainfluenza Virus Type 1 (HPIV1) Expressing the Fusion Glycoprotein of Human Respiratory Syncytial Virus (RSV) as a Bivalent HPIV1/RSV Vaccine." J Virol **89**(20): 10319-10332.

Manunta, P., Rogowski, A. C., Hamilton, B. P. and Hamlyn, J. M. (1994). "Ouabain-induced hypertension in the rat: relationships among plasma and tissue ouabain and blood pressure." J Hypertens **12**(5): 549-560.

Marine, S., Bahl, A., Ferrer, M. and Buehler, E. (2012). "Common seed analysis to identify off-target effects in siRNA screens." J Biomol Screen **17**(3): 370-378.

Martinez, I. and Melero, J. A. (2000). "Binding of human respiratory syncytial virus to cells: implication of sulfated cell surface proteoglycans." J Gen Virol **81**(Pt 11): 2715-2722.

Maruyama, T., Rodriguez, L. L., Jahrling, P. B., Sanchez, A., Khan, A. S., Nichol, S. T., Peters, C. J., Parren, P. W. and Burton, D. R. (1999). "Ebola virus can be effectively neutralized by antibody produced in natural human infection." J Virol **73**(7): 6024-6030.

Mazur, N. I., Higgins, D., Nunes, M. C., Melero, J. A., Langedijk, A. C., Horsley, N., Buchholz, U. J., Openshaw, P. J., McLellan, J. S., Englund, J. A., Mejias, A., Karron, R. A., Simoes, E. A., Knezevic, I., Ramilo, O., Piedra, P. A., Chu, H. Y., Falsey, A. R., Nair, H., Kragten-Tabatabaie, L., Greenough, A., Baraldi, E., Papadopoulos, N. G., Vekemans, J., Polack, F. P., Powell, M., Satav, A., Walsh, E. E., Stein, R. T., Graham, B. S., Bont, L. J. and Respiratory Syncytial Virus Network, F. (2018). "The respiratory syncytial virus vaccine landscape: lessons from the graveyard and promising candidates." Lancet Infect Dis.

McLellan, J. S., Chen, M., Joyce, M. G., Sastry, M., Stewart-Jones, G. B., Yang, Y., Zhang, B., Chen, L., Srivatsan, S., Zheng, A., Zhou, T., Graepel, K. W., Kumar, A., Moin, S., Boyington, J. C., Chuang, G. Y., Soto, C., Baxa, U., Bakker, A. Q., Spits, H., Beaumont, T., Zheng, Z., Xia, N., Ko, S. Y., Todd, J. P., Rao, S., Graham, B. S. and Kwong, P. D. (2013). "Structure-based design of a fusion glycoprotein vaccine for respiratory syncytial virus." Science **342**(6158): 592-598.

Medina, M. F., Kobinger, G. P., Rux, J., Gasmi, M., Looney, D. J., Bates, P. and Wilson, J. M. (2003). "Lentiviral vectors pseudotyped with minimal filovirus envelopes increased gene transfer in murine lung." Mol Ther **8**(5): 777-789.

Mehedi, M., McCarty, T., Martin, S. E., Le Nouen, C., Buehler, E., Chen, Y. C., Smelkinson, M., Ganesan, S., Fischer, E. R., Brock, L. G., Liang, B., Munir, S., Collins, P. L. and Buchholz, U. J. (2016). "Actin-Related Protein 2 (ARP2) and Virus-Induced Filopodia Facilitate Human Respiratory Syncytial Virus Spread." PLoS Pathog **12**(12): e1006062.

Meister, G. and Tuschl, T. (2004). "Mechanisms of gene silencing by double-stranded RNA." Nature **431**(7006): 343-349.

Melero, C. P., Medarde, M. and Feliciano, A. S. (2000). "A Short Review on Cardiotonic Steroids and Their Aminoguanidine Analogues." Molecules **5**(1): 51-81.

Mercer, J. and Helenius, A. (2009). "Virus entry by macropinocytosis." Nat Cell Biol **11**(5): 510-520.

Meyer, M., Garron, T., Lubaki, N. M., Mire, C. E., Fenton, K. A., Klages, C., Olinger, G. G., Geisbert, T. W., Collins, P. L. and Bukreyev, A. (2015). "Aerosolized Ebola vaccine protects primates and elicits lung-resident T cell responses." J Clin Invest **125**(8): 3241-3255.

Mire, C. E., Matassov, D., Geisbert, J. B., Latham, T. E., Agans, K. N., Xu, R., Ota-Setlik, A., Egan, M. A., Fenton, K. A., Clarke, D. K., Eldridge, J. H. and Geisbert, T. W. (2015). "Single-dose attenuated Vesiculovax vaccines protect primates against Ebola Makona virus." Nature **520**(7549): 688-691.

Misasi, J. and Sullivan, N. J. (2014). "Camouflage and misdirection: the full-on assault of ebola virus disease." Cell **159**(3): 477-486.

Morth, J. P., Pedersen, B. P., Buch-Pedersen, M. J., Andersen, J. P., Vilsen, B., Palmgren, M. G. and Nissen, P. (2011). "A structural overview of the plasma membrane Na+,K+-ATPase and H+-ATPase ion pumps." Nat Rev Mol Cell Biol **12**(1): 60-70.

Moudy, R. M., Harmon, S. B., Sullender, W. M. and Wertz, G. W. (2003). "Variations in transcription termination signals of human respiratory syncytial virus clinical isolates affect gene expression." Virology **313**(1): 250-260.

Munir, S., Le Nouen, C., Luongo, C., Buchholz, U. J., Collins, P. L. and Bukreyev, A. (2008). "Nonstructural proteins 1 and 2 of respiratory syncytial virus suppress maturation of human dendritic cells." J Virol **82**(17): 8780-8796.

Nair, H., Nokes, D. J., Gessner, B. D., Dherani, M., Madhi, S. A., Singleton, R. J., O'Brien, K. L., Roca, A., Wright, P. F., Bruce, N., Chandran, A., Theodoratou, E., Sutanto, A., Sedyaningsih, E. R., Ngama, M., Munywoki, P. K., Kartasasmita, C., Simoes, E. A., Rudan, I., Weber, M. W. and Campbell, H. (2010). "Global burden of acute lower respiratory infections due to respiratory syncytial virus in young children: a systematic review and meta-analysis." Lancet **375**(9725): 1545-1555.

Newman, J. T., Riggs, J. M., Surman, S. R., McAuliffe, J. M., Mulaikal, T. A., Collins, P. L., Murphy, B. R. and Skiadopoulos, M. H. (2004). "Generation of recombinant human parainfluenza virus type 1 vaccine candidates by importation of temperature-sensitive and attenuating mutations from heterologous paramyxoviruses." J Virol **78**(4): 2017-2028.

Newman, J. T., Surman, S. R., Riggs, J. M., Hansen, C. T., Collins, P. L., Murphy, B. R. and Skiadopoulos, M. H. (2002). "Sequence analysis of the Washington/1964 strain of human parainfluenza virus type 1 (HPIV1) and recovery and characterization of wild-type recombinant HPIV1 produced by reverse genetics." Virus Genes **24**(1): 77-92.

Nieto-Torres, J. L., DeDiego, M. L., Verdia-Baguena, C., Jimenez-Guardeno, J. M., Regla-Nava, J. A., Fernandez-Delgado, R., Castano-Rodriguez, C., Alcaraz, A., Torres, J., Aguilella, V. M. and Enjuanes, L. (2014). "Severe acute respiratory syndrome coronavirus envelope protein ion channel activity promotes virus fitness and pathogenesis." PLoS Pathog **10**(5): e1004077.

Osterholm, M. T., Moore, K. A., Kelley, N. S., Brosseau, L. M., Wong, G., Murphy, F. A., Peters, C. J., LeDuc, J. W., Russell, P. K., Van Herp, M., Kapetshi, J., Muyembe, J. J., Ilunga, B. K., Strong, J. E., Grolla, A., Wolz, A., Kargbo, B., Kargbo, D. K., Sanders, D. A. and Kobinger, G. P. (2015). "Transmission of Ebola viruses: what we know and what we do not know." MBio **6**(2): e00137.

Ostrom, R. S., Gregorian, C., Drenan, R. M., Xiang, Y., Regan, J. W. and Insel, P. A. (2001). "Receptor number and caveolar co-localization determine receptor coupling efficiency to adenylyl cyclase." J Biol Chem **276**(45): 42063-42069.

Park, M. S., Steel, J., Garcia-Sastre, A., Swayne, D. and Palese, P. (2006). "Engineered viral vaccine constructs with dual specificity: avian influenza and Newcastle disease." Proc Natl Acad Sci U S A **103**(21): 8203-8208.

Pleiman, C. M., Hertz, W. M. and Cambier, J. C. (1994). "Activation of phosphatidylinositol-3' kinase by Src-family kinase SH3 binding to the p85 subunit." Science **263**(5153): 1609-1612.

Prassas, I. and Diamandis, E. P. (2008). "Novel therapeutic applications of cardiac glycosides." Nat Rev Drug Discov **7**(11): 926-935.

Qiu, X., Wong, G., Audet, J., Bello, A., Fernando, L., Alimonti, J. B., Fausther-Bovendo, H., Wei, H., Aviles, J., Hiatt, E., Johnson, A., Morton, J., Swope, K., Bohorov, O., Bohorova, N., Goodman, C., Kim, D., Pauly, M. H., Velasco, J., Pettitt, J., Olinger, G. G., Whaley, K., Xu,

B., Strong, J. E., Zeitlin, L. and Kobinger, G. P. (2014). "Reversion of advanced Ebola virus disease in nonhuman primates with ZMapp." Nature **514**(7520): 47-53.

Quadri, L., Bianchi, G., Cerri, A., Fedrizzi, G., Ferrari, P., Gobbini, M., Melloni, P., Sputore, S. and Torri, M. (1997). "17 beta-(3-furyl)-5 beta-androstane-3 beta, 14 beta, 17 alpha-triol (PST 2238). A very potent antihypertensive agent with a novel mechanism of action." J Med Chem **40**(11): 1561-1564.

Rassa, J. C. and Parks, G. D. (1998). "Molecular basis for naturally occurring elevated readthrough transcription across the M-F junction of the paramyxovirus SV5." Virology **247**(2): 274-286.

Razani, B., Woodman, S. E. and Lisanti, M. P. (2002). "Caveolae: from cell biology to animal physiology." Pharmacol Rev **54**(3): 431-467.

Regules, J. A., Beigel, J. H., Paolino, K. M., Voell, J., Castellano, A. R., Hu, Z., Munoz, P., Moon, J. E., Ruck, R. C., Bennett, J. W., Twomey, P. S., Gutierrez, R. L., Remich, S. A., Hack, H. R., Wisniewski, M. L., Josleyn, M. D., Kwilas, S. A., Van Deusen, N., Mbaya, O. T., Zhou, Y., Stanley, D. A., Jing, W., Smith, K. S., Shi, M., Ledgerwood, J. E., Graham, B. S., Sullivan, N. J., Jagodzinski, L. L., Peel, S. A., Alimonti, J. B., Hooper, J. W., Silvera, P. M., Martin, B. K., Monath, T. P., Ramsey, W. J., Link, C. J., Lane, H. C., Michael, N. L., Davey, R. T., Jr., Thomas, S. J. and r, V.-Z.-G. P. S. G. (2017). "A Recombinant Vesicular Stomatitis Virus Ebola Vaccine." N Engl J Med **376**(4): 330-341.

Reinhard, L., Tidow, H., Clausen, M. J. and Nissen, P. (2013). "Na(+),K (+)-ATPase as a docking station: protein-protein complexes of the Na(+),K (+)-ATPase." Cell Mol Life Sci **70**(2): 205-222.

Rose, E. B., Wheatley, A., Langley, G., Gerber, S. and Haynes, A. (2018). "Respiratory Syncytial Virus Seasonality - United States, 2014-2017." MMWR Morb Mortal Wkly Rep **67**(2): 71-76.

Rothberg, K. G., Heuser, J. E., Donzell, W. C., Ying, Y. S., Glenney, J. R. and Anderson, R. G. (1992). "Caveolin, a protein component of caveolae membrane coats." Cell **68**(4): 673-682.

Russell, C. J., Simoes, E. A. F. and Hurwitz, J. L. (2018). "Vaccines for the Paramyxoviruses and Pneumoviruses: Successes, Candidates, and Hurdles." Viral Immunol **31**(2): 133-141.

Saez-Cirion, A., Gomara, M. J., Agirre, A. and Nieva, J. L. (2003). "Pre-transmembrane sequence of Ebola glycoprotein. Interfacial hydrophobicity distribution and interaction with membranes." FEBS Lett **533**(1-3): 47-53.

San-Juan-Vergara, H., Sampayo-Escobar, V., Reyes, N., Cha, B., Pacheco-Lugo, L., Wong, T., Peeples, M. E., Collins, P. L., Castano, M. E. and Mohapatra, S. S. (2012). "Cholesterol-rich microdomains as docking platforms for respiratory syncytial virus in normal human bronchial epithelial cells." J Virol **86**(3): 1832-1843.

Sanchez, A., Trappier, S. G., Mahy, B. W., Peters, C. J. and Nichol, S. T. (1996). "The virion glycoproteins of Ebola viruses are encoded in two reading frames and are expressed through transcriptional editing." Proc Natl Acad Sci U S A **93**(8): 3602-3607.

Schmidt, A. C., McAuliffe, J. M., Huang, A., Surman, S. R., Bailly, J. E., Elkins, W. R., Collins, P. L., Murphy, B. R. and Skiadopoulos, M. H. (2000). "Bovine parainfluenza virus type 3 (BPIV3) fusion and hemagglutinin-neuraminidase glycoproteins make an important contribution to the restricted replication of BPIV3 in primates." J Virol **74**(19): 8922-8929.

Schoner, W. and Scheiner-Bobis, G. (2007). "Endogenous and exogenous cardiac glycosides and their mechanisms of action." Am J Cardiovasc Drugs **7**(3): 173-189.

Shelokov, A., Vogel, J. E. and Chi, L. (1958). "Hemadsorption (adsorption-hemagglutination) test for viral agents in tissue culture with special reference to influenza." Proc Soc Exp Biol Med **97**(4): 802-809.

Shi, T., McAllister, D. A., O'Brien, K. L., Simoes, E. A. F., Madhi, S. A., Gessner, B. D., Polack, F. P., Balsells, E., Acacio, S., Aguayo, C., Alassani, I., Ali, A., Antonio, M., Awasthi, S., Awori, J. O., Azziz-Baumgartner, E., Baggett, H. C., Baillie, V. L., Balmaseda, A., Barahona, A., Basnet, S., Bassat, Q., Basualdo, W., Bigogo, G., Bont, L., Breiman, R. F., Brooks, W. A., Broor, S., Bruce, N., Bruden, D., Buchy, P., Campbell, S., Carosone-Link, P., Chadha, M., Chipeta, J., Chou, M., Clara, W., Cohen, C., de Cuellar, E., Dang, D. A., Dash-Yandag, B., Deloria-Knoll, M., Dherani, M., Eap, T., Ebruke, B. E., Echavarria, M., de Freitas Lazaro Emediato, C. C., Fasce, R. A., Feikin, D. R., Feng, L., Gentile, A., Gordon, A., Goswami, D., Goyet, S., Groome, M., Halasa, N., Hirve, S., Homaira, N., Howie, S. R. C., Jara, J.,

Jroundi, I., Kartasasmita, C. B., Khuri-Bulos, N., Kotloff, K. L., Krishnan, A., Libster, R., Lopez, O., Lucero, M. G., Lucion, F., Lupisan, S. P., Marcone, D. N., McCracken, J. P., Mejia, M., Moisi, J. C., Montgomery, J. M., Moore, D. P., Moraleda, C., Moyes, J., Munywoki, P., Mutyara, K., Nicol, M. P., Nokes, D. J., Nymadawa, P., da Costa Oliveira, M. T., Oshitani, H., Pandey, N., Paranhos-Baccala, G., Phillips, L. N., Picot, V. S., Rahman, M., Rakoto-Andrianarivelo, M., Rasmussen, Z. A., Rath, B. A., Robinson, A., Romero, C., Russomando, G., Salimi, V., Sawatwong, P., Scheltema, N., Schweiger, B., Scott, J. A. G., Seidenberg, P., Shen, K., Singleton, R., Sotomayor, V., Strand, T. A., Sutanto, A., Sylla, M., Tapia, M. D., Thamthitiwat, S., Thomas, E. D., Tokarz, R., Turner, C., Venter, M., Waicharoen, S., Wang, J., Watthanaworawit, W., Yoshida, L. M., Yu, H., Zar, H. J., Campbell, H., Nair, H. and Network, R. S. V. G. E. (2017). "Global, regional, and national disease burden estimates of acute lower respiratory infections due to respiratory syncytial virus in young children in 2015: a systematic review and modelling study." Lancet **390**(10098): 946-958.

Shields, B., Mills, J., Ghildyal, R., Gooley, P. and Meanger, J. (2003). "Multiple heparin binding domains of respiratory syncytial virus G mediate binding to mammalian cells." Arch Virol **148**(10): 1987-2003.

Sigal, A., Milo, R., Cohen, A., Geva-Zatorsky, N., Klein, Y., Alaluf, I., Swerdlin, N., Perzov, N., Danon, T., Liron, Y., Raveh, T., Carpenter, A. E., Lahav, G. and Alon, U. (2006). "Dynamic proteomics in individual human cells uncovers widespread cell-cycle dependence of nuclear proteins." Nat Methods **3**(7): 525-531.

Skou, J. C. (2004). "The identification of the sodium pump." Biosci Rep **24**(4-5): 436-451.

Smith, A. L., Friedman, D. B., Yu, H., Carnahan, R. H. and Reynolds, A. B. (2011). "ReCLIP (reversible cross-link immuno-precipitation): an efficient method for interrogation of labile protein complexes." PLoS One **6**(1): e16206.

Stanley, D. A., Honko, A. N., Asiedu, C., Trefry, J. C., Lau-Kilby, A. W., Johnson, J. C., Hensley, L., Ammendola, V., Abbate, A., Grazioli, F., Foulds, K. E., Cheng, C., Wang, L., Donaldson, M. M., Colloca, S., Folgori, A., Roederer, M., Nabel, G. J., Mascola, J., Nicosia, A., Cortese, R., Koup, R. A. and Sullivan, N. J. (2014). "Chimpanzee adenovirus vaccine generates acute and durable protective immunity against ebolavirus challenge." Nat Med **20**(10): 1126-1129.

Stojdl, D. F., Lichty, B. D., tenOever, B. R., Paterson, J. M., Power, A. T., Knowles, S., Marius, R., Reynard, J., Poliquin, L., Atkins, H., Brown, E. G., Durbin, R. K., Durbin, J. E., Hiscott, J. and Bell, J. C. (2003). "VSV strains with defects in their ability to shutdown innate immunity are potent systemic anti-cancer agents." Cancer Cell **4**(4): 263-275.

Su, C. T., Hsu, J. T., Hsieh, H. P., Lin, P. H., Chen, T. C., Kao, C. L., Lee, C. N. and Chang, S. Y. (2008). "Anti-HSV activity of digitoxin and its possible mechanisms." Antiviral Res **79**(1): 62-70.

Sullivan, N. J., Geisbert, T. W., Geisbert, J. B., Shedlock, D. J., Xu, L., Lamoreaux, L., Custers, J. H., Popernack, P. M., Yang, Z. Y., Pau, M. G., Roederer, M., Koup, R. A., Goudsmit, J., Jahrling, P. B. and Nabel, G. J. (2006). "Immune protection of nonhuman primates against Ebola virus with single low-dose adenovirus vectors encoding modified GPs." PLoS Med **3**(6): e177.

Swanson, J. A. and Watts, C. (1995). "Macropinocytosis." Trends Cell Biol **5**(11): 424-428.

Tayyari, F., Marchant, D., Moraes, T. J., Duan, W., Mastrangelo, P. and Hegele, R. G. (2011). "Identification of nucleolin as a cellular receptor for human respiratory syncytial virus." Nat Med **17**(9): 1132-1135.

Techaarpornkul, S., Barretto, N. and Peeples, M. E. (2001). "Functional analysis of recombinant respiratory syncytial virus deletion mutants lacking the small hydrophobic and/or attachment glycoprotein gene." J Virol **75**(15): 6825-6834.

Teng, M. N., Whitehead, S. S. and Collins, P. L. (2001). "Contribution of the respiratory syncytial virus G glycoprotein and its secreted and membrane-bound forms to virus replication in vitro and in vivo." Virology **289**(2): 283-296.

Tian, J., Cai, T., Yuan, Z., Wang, H., Liu, L., Haas, M., Maksimova, E., Huang, X. Y. and Xie, Z. J. (2006). "Binding of Src to Na+/K+-ATPase forms a functional signaling complex." Mol Biol Cell **17**(1): 317-326.

Tomas, A., Futter, C. E. and Eden, E. R. (2014). "EGF receptor trafficking: consequences for signaling and cancer." Trends Cell Biol **24**(1): 26-34.

Tripp, R. A., Jones, L. P., Haynes, L. M., Zheng, H., Murphy, P. M. and Anderson, L. J. (2001). "CX3C chemokine mimicry by respiratory syncytial virus G glycoprotein." Nat Immunol **2**(8): 732-738.

Uhlen, M., Fagerberg, L., Hallstrom, B. M., Lindskog, C., Oksvold, P., Mardinoglu, A., Sivertsson, A., Kampf, C., Sjostedt, E., Asplund, A., Olsson, I., Edlund, K., Lundberg, E., Navani, S., Szigyarto, C. A., Odeberg, J., Djureinovic, D., Takanen, J. O., Hober, S., Alm, T., Edqvist, P. H., Berling, H., Tegel, H., Mulder, J., Rockberg, J., Nilsson, P., Schwenk, J. M., Hamsten, M., von Feilitzen, K., Forsberg, M., Persson, L., Johansson, F., Zwahlen, M., von Heijne, G., Nielsen, J. and Ponten, F. (2015). "Proteomics. Tissue-based map of the human proteome." Science **347**(6220): 1260419.

van Wyke Coelingh, K. L., Winter, C. C., Tierney, E. L., London, W. T. and Murphy, B. R. (1988). "Attenuation of bovine parainfluenza virus type 3 in nonhuman primates and its ability to confer immunity to human parainfluenza virus type 3 challenge." J Infect Dis **157**(4): 655-662.

Volchkov, V. E., Feldmann, H., Volchkova, V. A. and Klenk, H. D. (1998). "Processing of the Ebola virus glycoprotein by the proprotein convertase furin." Proc Natl Acad Sci U S A **95**(10): 5762-5767.

Volchkov, V. E., Volchkova, V. A., Muhlberger, E., Kolesnikova, L. V., Weik, M., Dolnik, O. and Klenk, H. D. (2001). "Recovery of infectious Ebola virus from complementary DNA: RNA editing of the GP gene and viral cytotoxicity." Science **291**(5510): 1965-1969.

Wages, D. S., Keefer, J., Rall, T. B. and Weber, M. J. (1992). "Mutations in the SH3 domain of the src oncogene which decrease association of phosphatidylinositol 3'-kinase activity with pp60v-src and alter cellular morphology." J Virol **66**(4): 1866-1874.

Wang, H., Haas, M., Liang, M., Cai, T., Tian, J., Li, S. and Xie, Z. (2004). "Ouabain assembles signaling cascades through the caveolar Na+/K+-ATPase." J Biol Chem **279**(17): 17250-17259.

Wang, J. T., Teasdale, R. D. and Liebl, D. (2014). "Macropinosome quantitation assay." MethodsX **1**: 36-41.

Wee, P. and Wang, Z. (2017). "Epidermal Growth Factor Receptor Cell Proliferation Signaling Pathways." Cancers (Basel) **9**(5).

WHO (1978). "Ebola haemorrhagic fever in Zaire, 1976." Bull World Health Organ **56**(2): 271-293.

Wong, G., Qiu, X., Richardson, J. S., Cutts, T., Collignon, B., Gren, J., Aviles, J., Embury-Hyatt, C. and Kobinger, G. P. (2015). "Ebola virus transmission in guinea pigs." J Virol **89**(2): 1314-1323.

Wong, R. W., Balachandran, A., Ostrowski, M. A. and Cochrane, A. (2013). "Digoxin suppresses HIV-1 replication by altering viral RNA processing." PLoS Pathog **9**(3): e1003241.

Wright, P. F., Karron, R. A., Belshe, R. B., Shi, J. R., Randolph, V. B., Collins, P. L., O'Shea, A. F., Gruber, W. C. and Murphy, B. R. (2007). "The absence of enhanced disease with wild type respiratory syncytial virus infection occurring after receipt of live, attenuated, respiratory syncytial virus vaccines." Vaccine **25**(42): 7372-7378.

Xie, Z. and Cai, T. (2003). "Na+-K+--ATPase-mediated signal transduction: from protein interaction to cellular function." Mol Interv **3**(3): 157-168.

Zlotnik, A. and Yoshie, O. (2000). "Chemokines: a new classification system and their role in immunity." Immunity **12**(2): 121-127.

6. Appendix

6.1. Abbreviations

The International System of Units (SI units) was used and chemicals, nucleotides and amino acids were abbreviated based on the International Union of Pure and Applied Chemistry (IUPAC) nomenclature and are not included in the list of abbreviations. Any other abbreviation used in the dissertation thesis is listed in the following table.

Abbreviation	Meaning
AF	Alexa Fluor
AGM	African green monkey
AGO	endonuclease argonaute
ALRI	acute lower respiratory infection
AMPV	avian metapneumovirus
ANOVA	analysis of variance
AP2	adaptor protein-2
APC	Allophycocyanin
ARP2	actin-related protein 2
ATCC	American Type Culture Collection
ATP	adenosine triphosphate
ATP1A1	ATPase Na^+/K^+ transporting subunit alpha 1
BCA	bicinchoninic acid
bp	base pair
BSA	bovine serum albumin
BSL	biosafety level
CDC	Centers for Disease Control and Prevention
cDNA	complementary DNA
CDRs	complementarity-determining regions
CID	Compound ID
CT	cytoplasmic tail
Ct	threshold cycle
CTS	cardiotonic steroids
DAG	1,2-diacylglyerol
DAPI	4′,6-diamidino-2-phenylindole
dH_2O	ultrapure water
Dicer	ribonuclease III-like enzyme
DMSO	dimethyl sulfoxide
DNA	deoxyribonucleic acid
dsRNA	double-stranded RNA
e.g.	for example
EBOV	Ebola virus
EDTA	Ethylenediaminetetraacetic acid

Abbreviation	Meaning
EGFR	Epidermal growth factor receptor
EIPA	5-(N-Ethyl-N-isopropyl)amiloride
ELISA	enzyme linked immunosorbent assay
FBS	fetal bovine serum
FI-RSV	formalin-inactivated RSV
FSC	forward scatter
GAGs	glycosaminoglycans
gDNA	genomic DNA
GE	gene end
GFP	green fluorescent protein
Grb2	growth factor receptor-bound protein 2
GS	gene start
GSopt	GenScript-optimized
HAD	hemadsorption
HAI	hemagglutination inhibition
HMPV	human metapneumovirus
HPIV1	human parainfluenza virus type 1
HPIV2	human parainfluenza virus type 2
HPIV3	human parainfluenza virus type 3
HSAEC	human small airway epithelial cells
i.e.	in other words
IACUC	Institutional Animal Care and Use Committee
IC_{50}	half maximal inhibitory concentration
IG	intergenic region
IgG	immunoglobulin G
IP3	inositol 1,4,5 triphosphate
IRDye	infrared fluorescent dye
kb	kilo base
kDa	kilo Dalton
LDS	loading dye solution
LID	Laboratory of Infectious Diseases
LRI	lower respiratory tract infection
MAb	monoclonal antibody
MAPK	mitogen activated protein kinase
MBCD	Methyl-beta-cyclodextrin
MEK	mitogen-activated protein kinase kinase
MFI	median fluorescence intensity
MGI	Mouse Genome Informatics
miRNA	micro RNA
MMRRC	Mutant Mouse Resource & Research Centers
MOI	multiplicity of infection

Abbreviation	Meaning
mRNA	messenger RNA
MW	molecular weight
NA	numeric aperture
NCATS	National Center for Advancing Translational Sciences
NDV	Newcastle disease virus
NHPs	non-human primates
NIAID	National Institute of Allergy and Infectious Diseases
NIH	National Institutes of Health
NP	nasopharyngeal
nt	nucleotides
OBN	ouabain
OD	absorbance at the indicated wavelength
ORF	open reading frame
p.i.	post inoculation
p.t.	post transfection
PBS	phosphate buffered saline
PCR	polymerase chain reaction
PFU	plaque forming units
PI3K	Phosphoinositide 3-kinase
PIP2	Phosphatidylinositol 4,5-biphosphate
PKR	dsRNA-dependent protein kinase
PLC-γ	Phospholipase C-gamma
Pri-miRNA	primary-miRNA
$PRNT_{60}$	60% plaque reduction neutralization titer
RBC	red blood cells
RdRp	RNA-dependent RNA polymerase
RIPA	radioimmunoprecipitation assay buffer
RISC	RNA-induced silencing complex
RLU	relative light units
RNA	ribonucleic acid
RNAi	RNA interference
RNP	ribonucleoprotein
rpm	revolutions per minute
RSV	respiratory syncytial virus
rxt	reaction
SARS-CoV	severe acute respiratory syndrome coronavirus
SD	standard deviation
SDS	Sodium dodecyl sulfate
shRNA	short hairpin RNA
siRNA	small interfering RNA
SOS	Son of Sevenless

Abbreviation	Meaning
SrcI-I	Src-Inhibitor-I
T_A	annealing temperature
$TCID_{50}$	50% tissue culture infective dose
TL	tracheal lavage
TM	transmembrane
TMCT	transmembrane and cytoplasmic tail
UR	uncertainty range
URI	upper respiratory tract infection
UTR	untranslated region
v/v	volume per volume
VSV	vesicular stomatitis virus
w/v	weight per volume
WHO	World Health Organization
wt	wild-type
YFP	yellow fluorescent protein

6.2. EBOV GP sequences

6.2.1. Wt EBOV GP ORF

The EBOV GP ORF was derived from the EBOV strain Mayinga (GenBank ID: AF086833.2) and was modified by the insertion of a single A residue at the editing site to encode full-length GP. The stabilized editing site (Bukreyev et al. 2006) is bold and underlined.

ATGGGCGTTACAGGAATATTGCAGTTACCTCGTGATCGATTCAAGAGGACATCATTCTTTCTT
TGGGTAATTATCCTTTTCCAAAGAACATTTTCCATCCCACTTGGAGTCATCCACAATAGCACATTACAG
GTTAGTGATGTCGACAAACTAGTTTGTCGTGACAAACTGTCATCCACAAATCAATTGAGATCAGTTGG
ACTGAATCTCGAAGGGAATGGAGTGGCAACTGACGTGCCATCTGCAACTAAAAGATGGGGCTTCAG
GTCCGGTGTCCCACCAAAGGTGGTCAATTATGAAGCTGGTGAATGGGCTGAAAACTGCTACAATCTT
GAAATCAAAAAACCTGACGGGAGTGAGTGTCTACCAGCAGCGCCAGACGGGATTCGGGGCTTCCCC
CGGTGCCGGTATGTGCACAAAGTATCAGGAACGGGACCGTGTGCCGGAGACTTTGCCTTCCATAAA
GAGGGTGCTTTCTTCCTGTATGATCGACTTGCTTCCACAGTTATCTACCGAGGAACGACTTTCGCTGA
AGGTGTCGTTGCATTTCTGATACTGCCCCAAGCTAAGAAGGACTTCTTCAGCTCACACCCCTTGAGA
GAGCCGGTCAATGCAACGGAGGACCCGTCTAGTGGCTACTATTCTACCACAATTAGATATCAGGCTA
CCGGTTTTGGAACCAATGAGACAGAGTACTTGTTCGAGGTTGACAATTTGACCTACGTCCAACTTGAA
TCAAGATTCACACCACAGTTTCTGCTCCAGCTGAATGAGACAATATATACAAGTGGGAAAAGGAGCAA
TACCACGGGAAAACTAATTTGGAAGGTCAACCCCGAAATTGATACAACAATCGGGGAGTGGGCCTTC
TGGGAAACT**<u>AAGAAGAA</u>**CCTCACTAGAAAAATTCGCAGTGAAGAGTTGTCTTTCACAGTTGTATCAAA
CGGAGCCAAAAACATCAGTGGTCAGAGTCCGGCGCGAACTTCTTCCGACCCAGGGACCAACACAAC
AACTGAAGACCACAAAATCATGGCTTCAGAAAATTCCTCTGCAATGGTTCAAGTGCACAGTCAAGGAA
GGGAAGCTGCAGTGTCGCATCTAACAACCCTTGCCACAATCTCCACGAGTCCCCAATCCCTCACAAC
CAAACCAGGTCCGGACAACAGCACCCATAATACACCCGTGTATAAACTTGACATCTCTGAGGCAACT
CAAGTTGAACAACATCACCGCAGAACAGACAACGACAGCACAGCCTCCGACACTCCCTCTGCCACG
ACCGCAGCCGGACCCCCAAAAGCAGAGAACACCAACACGAGCAAGAGCACTGACTTCCTGGACCCC
GCCACCACAACAAGTCCCCAAAACCACAGCGAGACCGCTGGCAACAACAACACTCATCACCAAGATA
CCGGAGAAGAGAGTGCCAGCAGCGGGAAGCTAGGCTTAATTACCAATACTATTGCTGGAGTCGCAG
GACTGATCACAGGCGGGAGAAGAACTCGAAGAGAAGCAATTGTCAATGCTCAACCCAAATGCAACCC
TAATTTACATTACTGGACTACTCAGGATGAAGGTGCTGCAATCGGACTGGCCTGGATACCATATTTCG
GGCCAGCAGCCGAGGGAATTTACATAGAGGGGCTAATGCACAATCAAGATGGTTTAATCTGTGGGTT
GAGACAGCTGGCCAACGAGACGACTCAAGCTCTTCAACTGTTCCTGAGAGCCACAACTGAGCTACG
CACCTTTTCAATCCTCAACCGTAAGGCAATTGATTTCTTGCTGCAGCGATGGGGCGGCACATGCCAC
ATTCTGGGACCGGACTGCTGTATCGAACCACATGATTGGACCAAGAACATAACAGACAAAATTGATC
AGATTATTCATGATTTTGTTGATAAAACCCTTCCGGACCAGGGGGACAATGACAATTGGTGGACAGG
ATGGAGACAATGGATACCGGCAGGTATTGGAGTTACAGGCGTTATAATTGCAGTTATCGCTTTATTCT
GTATATGCAAATTTGTCTTTTAGTGA

6.2.2. GenScript-optimized EBOV GP ORF

The EBOV GP ORF was codon-optimized for human expression by GenScript, with the exception of the stabilized editing site AAGAAGAA sequence (bold and underlined) (Bukreyev et al. 2006), which was left undisturbed. The EBOV GP TMCT domain sequence is bolded and italicized.

ATGGGGGTGACCGGAATCCTGCAGCTGCCTAGAGACAGGTTTAAGAGGACATCATTCTTTCT
GTGGGTCATCATTCTGTTCCAGCGCACTTTTAGCATCCCACTGGGGGTCATTCACAATTCAACACTGC
AGGTGAGCGACGTCGATAAGCTGGTGTGTCGGGACAAACTGAGCTCCACCAACCAGCTGAGAAGCG
TCGGCCTGAATCTGGAGGGGAACGGAGTGGCAACCGATGTCCCAAGCGCCACAAAGAGATGGGGC
TTTCGCTCCGGGGTGCCACCTAAAGTGGTCAATTACGAGGCCGGGGAATGGGCTGAGAATTGCTAT
AACCTGGAAATCAAGAAACCTGACGGATCCGAGTGTCTGCCCGCCGCTCCTGATGGCATTAGGGGG
TTCCCACGCTGCCGATACGTGCACAAGGTCTCTGGCACCGGGCCATGTGCAGGCGACTTCGCATTT
CATAAAGAAGGGGCTTTCTTTCTGTACGATAGACTGGCATCCACCGTGATCTATAGGGGCACCACAT
TCGCAGAGGGAGTGGTCGCTTTTCTGATTCTGCCACAGGCCAAGAAAGACTTCTTTTCTAGTCATCC
ACTGCGGGAACCCGTGAACGCTACCGAGGATCCCTCAAGCGGCTACTATAGCACTACCATCAGATA
CCAGGCCACAGGATTCGGCACCAATGAGACAGAATACCTGTTTGAAGTGGACAACCTGACATATGTC
CAGCTGGAGTCCAGGTTCACTCCCCAGTTTCTGCTGCAGCTGAATGAAACTATCTATACCAGCGGGA
AGCGCTCCAATACAACTGGAAAGCTGATTTGGAAAGTGAACCCTGAGATCGATACCACAATTGGCGA
ATGGGCCTTTTGGGAGACC**AAGAAGAA**CCTGACACGGAAGATCAGATCTGAGGAACTGAGTTTCAC
CGTGGTCTCTAATGGAGCCAAAAACATTTCCGGCCAGTCTCCCGCTCGGACTTCCTCTGACCCTGGC
ACCAATACTACCACAGAAGATCACAAGATCATGGCCAGCGAGAACAGTTCAGCAATGGTGCAGGTCC
ACAGTCAGGGGAGAGAGGCAGCCGTGTCACATCTGACTACCCTGGCCACAATCTCTACTAGTCCTCA
GTCTCTGACAACTAAGCCTGGACCAGACAATAGTACCCATAACACACCAGTGTACAAACTGGATATTA
GTGAAGCCACCCAGGTCGAGCAGCACCATCGGAGAACAGACAATGATAGTACTGCCTCAGACACCC
CAAGCGCTACCACAGCTGCAGGCCCACCCAAGGCTGAGAATACTAACACCTCAAAAAGCACCGACTT
TCTGGATCCAGCAACTACCACATCCCCCCAGAACCACTCTGAGACAGCCGGAAACAATAACACTCAC
CATCAGGATACCGGCGAGGAATCTGCCAGCAGCGGCAAGCTGGGCCTGATCACAAATACTATTGCT
GGGGTGGCAGGACTGATCACAGGCGGGAGGCGCACTCGACGAGAAGCTATTGTGAACGCACAGCC
TAAATGCAATCCAAACCTGCACTATTGGACTACCCAGGACGAGGGAGCAGCTATCGGCCTGGCCTG
GATTCCCTACTTCGGCCCTGCAGCCGAAGGGATCTATATTGAGGGACTGATGCATAATCAGGATGGG
CTGATCTGTGGACTGAGGCAGCTGGCAAACGAAACAACTCAGGCCCTGCAGCTGTTCCTGCGAGCT
ACCACAGAGCTGCGGACCTTTAGCATCCTGAATCGCAAGGCAATTGACTTCCTGCTGCAGCGATGG
GGAGGAACCTGCCACATCCTGGGCCCTGACTGCTGTATTGAGCCACATGATTGGACAAAGAACATCA
CTGACAAAATTGATCAGATCATTCACGACTTCGTGGATAAAACACTGCCCGATCAGGGAGACAATGAT
AACTGGTGGACTGGCTGGCGACAG***TGGATCCCTGCCGGGATTGGCGTCACTGGAGTCATTATTGCT***
GTCATTGCCCTGTTCTGTATTTGTAAGTTCGTCTTCTGATAG

6.2.3. GenScript-optimized EBOV GP HPIV1 F TMCT chimera ORF

The TMCT domain sequence (bold and italic) of the GenScript-optimized EBOV GP ORF (6.2.2) was replaced with the following GS-optimized HPIV1 F TMCT sequence to create the chimeric EBOV GP TMCT ORF:

CAGATCATTATGATCATTATCGTGTGCATTCTGATTATCATTATCTGTGGCATCCTGTACTATC TGTACCGAGTGCGGAGACTGCTGGTCATGATTAACAGCACCCACAATTCCCCCGTCAACGCCTACAC ACTGGAGTCTAGGATGCGCAATCCTTATATGGGGAACAATAGCAACTGATAGTGA

6.3. Primer Sequences

6.3.1. ATP1A1$^{+/-}$ mice genotyping primers

Name	Sequence (5'-3')
128-5'	CCTTTTCTCAAGTGTCATCTAGGG
LTR-rev	ATAAACCCTCTTGCAGTTGCATC
128-3'	TCCAGGAATGATTCAGCAAGCTGG

6.3.2. RSV genome sequencing primers

Name and 5' nt location	Sequence (5'-3')
RSV_3UTR_FOR_13	GCGTACAACAAACTTGCATAAACC
RSV_NS1_REV_94	AATGAATTGCTGCCCATCTCTA
RSV_NS1_FOR_102	GGCAGCAATTCATTGAGTATGA
RSV_NS1_REV_221	GATTGTATGTATCACTGCCTTAGCC
RSV_NS1_FOR_354	GGAGGTTATATATGGGAAATGATGG
RSV_NS1_REV_394	TGTCATCTAGTAGACCATTAGGTTGAG
RSV_NS2_FOR_710	CATCACTAACCAGAGACATCATAACAC
RSV_NS2_REV_710	GTGTTATGATGTCTCTGGTTAGTGATG
RSV_NS2_FOR_990	TCTCAATCCATAAATTTCAACACAA
RSV_N_REV_1128	GCTAAGAGCCATCTTTGTATTTGC
RSV_N_FOR_1343	ATATGCGATGTCTAGGTTAGGAAGA
RSV_N_REV_1432	CCATTAATGTCTTGACGATGTGTTG
RSV_N_FOR_1681	CCGTGATTAGGAGAGCTAATAATGT
RSV_N_REV_1819	CCTCTGGTAGAAGATTGTGCTATAC
RSV_N_FOR_2051	GAACAACCCAAAAGCATCATTATTA
RSV_N_REV_2164	GCTGCATCATATAGATCTTGATTCC
RSV_N_FOR_2266	AGGCTATCAAACATCAGCTTAATCC
RSV_P_REV_2387	TTCTAGGAATTTAGTAGCCCTGTTG
RSV_P_FOR_2609	AGAAGACCCTACACCAAGTGATAAT
RSV_P_REV_2688	TTTCTTCGTATGAATAGCTGGATTC
RSV_P_FOR_3026	GGAAGGGAATGATAGTGACAATG
RSV_P_REV_3111	GGGTTGGTTAGTTTGTTGGTCTT
RSV_M_FOR_3254	GGCAAATATGGAAACATACGTGAAC
RSV_M_REV_3480	CTAGCACTGCACTTCTTGAGTTTAT

Name and 5' nt location	Sequence (5'-3')
RSV_M_FOR_3665	GACACTCAACCCTACACATGATATT
RSV_M_REV_3834	ATCCTGAGTAAGGGATGATTTTTGC
RSV_M_FOR_3904	ACATAAAGCCACAAAGTCAATTCAT
RSV_M_FOR_4138	ACTTATCTGAAGTCCCAGATCATCC
RSV_SH_REV_4231	GTGATTAGTTGGATTTCCTCCAATG
RSV_SH_REV_4459	GAGCTCTTGGTAACTCAAAGGTTTT
RSV_SH_FOR_4551	CCCCTACCTCTTTACAACACCTC
RSV_G_REV_4818	GTTGAGATTATCATTGCCAGAATGG
RSV_G_FOR_4823	CTGGCAATGATAATCTCAACTTCAC
RSV_G_FOR_5028	TACTAGCTTCAACAACACCAGGAG
RSV_G_REV_5237	TGTTTGGTATTCTTTTGCAGATAGC
RSV_G_FOR_5348	AAATCAAAGGAAGTACCCACCAC
RSV_F_REV_5652	GGATTAGCAACTCCATTGTTATTTG
RSV_F_FOR_5798	TGCTCTGAGAACTGGTTGGTAT
RSV_F_REV_5973	GGTAGTTCTCTTCTGGCTCGATT
RSV_F_FOR_6147	GAAGTGAACAAGATCAAAAGTGCTC
RSV_F_REV_6360	CTGCATTAACACTAAATTCCCTGGT
RSV_F_FOR_6507	CAGCAAAGTTACTCTATCATGTCCA
RSV_F_REV_6717	GAACTTTACATGTTTCAGCTTGTGG
RSV_F_FOR_6812	TGACATATTCAACCCCAAATATGAT
RSV_F_REV_6984	CAGTGTCCATCCCTTTATTTGATAC
RSV_F_FOR_7104	GTATTCCCCTCTGATGAATTTGATG
RSV_F_REV_7335	TACCACTCAGTTGATCTTTGCTTAG
RSV_F_FOR_7465	AAAATCTGAACTTCATCGAAACTCT
RSV_M2_REV_7645	GACACCTCTTACCATTTAAGCAATG
RSV_M2_FOR_7828	GGTGTAGTTGGAGTGCTAGAGAGTT
RSV_M2_REV_7960	CTCTTATCTTGGGTGAATTTAGCTC
RSV_M2_FOR_8107	CATAAGAGCATAACCATCAACAACC
RSV_M2_REV_8336	GTCAATCAATTCTTGAGAGGTCCA
RSV_M2_FOR_8482	CAAGTTGTGGGACAAAATGGAT
RSV_L_REV_8568	CCTAAAGCATTACACTCTGAGAAAG
RSV_L_FOR_8888	CTAGGGCTTAAAGAAAAGGACAAGA
RSV_L_REV_8935	GGTCGTAATAACTGAGTTGTCTTCA
RSV_L_FOR_9218	GGATTTCAATTTATTTTGAACCAAT
RSV_L_REV_9291	TTCCATGTCAAGAATTGATTATAGG
RSV_L_FOR_9476	GAGGGGTTCTACATAATAAAAGAGG
RSV_L_REV_9590	TCTGAGCTTTATTAGCAGCATCTGT
RSV_L_FOR_9859	GTTAAGCAGTCTGAGTATGTTAAGAGG
RSV_L_REV_9931	AGCATTTCTTAAAGTAGGCCATCTG
RSV_L_FOR_10211	AAATTTTCCGAGAGTGATAAATCAAG
RSV_L_REV_10300	GGGTTGTTGAGATAACTTTGATTAACT

Name and 5' nt location	Sequence (5'-3')
RSV_L_FOR_10530	GTAACAAATCAAATCGCTACAATGA
RSV_L_REV_10670	ACCAGGAAAATAGAGATTGTACACC
RSV_L_FOR_10847	CTGTGGACCATAGAAGCTATATCAC
RSV_L_REV_11085	TTTTACTCATAAATTGCATATCTCGTG
RSV_L_FOR_11165	GTGGGACCGTGGATAAACACTATAC
RSV_L_REV_11416	GGGTAAATTCATATACAATGTTAATGCT
RSV_L_FOR_11516	GAGGCTATAGTTCACTCTGTGTTCA
RSV_L_REV_11745	GTTTGGAGCTGTACTCAAAACCT
RSV_L_FOR_11853	CTCATGGGCTAAGAGTTGTTTATG
RSV_L_REV_12105	CAAGATCTTTCCCTAACATATTTGC
RSV_L_FOR_12282	GGGTTGGTTCATCTACACAAGAGA
RSV_L_REV_12382	TCTATAGATGCATACACCCAATCC
RSV_L_FOR_12662	ATAAGCTTTGGCCTTAGTTTAATGTC
RSV_L_REV_12766	ATCACCTGTGAATATGGGAGGT
RSV_L_FOR_13049	TGGGGAGAGGGATATATAACTGAT
RSV_L_REV_13154	AAGTGTTCATATCACACTCCAGCTT
RSV_L_FOR_13304	GGATGTCATAGCTTCAAATTATGGT
RSV_L_REV_13362	ATGTTAACAACCCAAGGGCAAA
RSV_L_REV_13613	CTAGGGTTTCTGGTGTAGGATGATA
RSV_L_FOR_13632	CCCTAGAGAATATACTAGCCAATCC
RSV_L_FOR_13901	TTAGTGCACAATAGCACATCACTTT
RSV_L_REV_13921	CCAAGGAAGCATGCAGTAAAGT
RSV_L_REV_14124	GATCATTGCAATCTTTCAGACTTC
RSV_L_FOR_14272	GTTTGCTGAACCTATCAGTCTTTTT
RSV_L_REV_14371	ATTAACTGAGGAACAGTACTTGCAC
RSV_L_FOR_14610	TGCCTAAGAAAGCTGATAAAGAGTC
RSV_L_REV_14765	AGTTTATTGCTGAAAACTTCATTACG
RSV_L_FOR_14833	TGTTTTAAATTTCAGATCAACAGAACTA
RSV_L_REV_14919	AAGTTCATTGGTTGTCAAGCTGT
RSV_5UTR_FOR_15115	AAGTTATCATTTTAATCTTGGAGGAA
RSV_5UTR_REV_15188	AAAAAGTGTCAAAAACTAATATCTCGTA

6.3.3. HPIV1 genome sequencing primers

Name and 5' nt location	Sequence (5'-3')
PIV1_3UTR_FOR_1	ACCAAACAAGAGGAAAAACTTG
PIV1_3UTR_FOR_78	GGGACAAGTCACAGACATTTGA
PIV1_N_FOR_153	AGTTCCAGGAGAAGTGAGAGCA
PIV1_N_REV_223	GGGCCTAATGTGAAGACAGAAA
PIV1_N_REV_342	GCCATTGCAAGGAGTGATACTAA
PIV1_N_FOR_389	CACTACAAACGGTGTCAATGCT

Name and 5' nt location	Sequence (5'-3')
PIV1_N_FOR_534	ATCAACAAGAACCCATTGTTCC
PIV1_N_REV_560	TAGATCCGCATTCTCTCTTTGC
PIV1_N_REV_709	GTTCCATCCTGTCTGAATGCTT
PIV1_N_REV_720	CACTTTTAACGGTTCCATCCTG
PIV1_N_FOR_910	CAGGATTAGCATCTTTCATGAACACC
PIV1_N_FOR_1042	CCCGAGCCCCTTTTATATGT
PIV1_N_REV_1103	CGTAGCTCCACAGTGCTGGATAG
PIV1_N_REV_1240	CAGAGCACTGCTGATTTTGG
PIV1_N_FOR_1316	AAACCTTTCAGGAGGGGATG
PIV1_N_FOR_1337	TGCGTACCACAAGCCTACAG
PIV1_N_FOR_1397	AACATTTGGAGTCGAGGACACT
PIV1_N_FOR_1437	AACTGGACAAATGACAGCAATG
PIV1_N_REV_1502	CAAGTTCTTCTGCACCACGA
PIV1_N_FOR_1594	AGAGACTAAGCCAGGCAAACAA
PIV1_N_REV_1608	TGGTGTCTCGTTTATTGTTTGC
PIV1_P_REV_1802	TGCTGAGGTATCCACTGTGAAG
PIV1_P_FOR_1818	TCAGCATCCAAAACTCTCCTTC
PIV1_P_REV_2006	GCTTGTTTTCTTTTGGGTTGTC
PIV1_P_FOR_2053	CAAAGACAGAGCAATCTCAACG
PIV1_P_REV_2210	TGCCCATATTCTCAGGTAGAGG
PIV1_P_FOR_2251	CGACGAAGATTCTCCAAATGAG
PIV1_P_FOR_2353	TGAGGGATTTCCAGAAGAGGTA
PIV1_P_REV_2425	GCTAGTTTCCATGCTTCTTCCA
PIV1_P_REV_2545	TGATCTTGTTTGGTTACGCTTG
PIV1_P_FOR_2609	AATAGCTCCAACCTCGAAGACC
PIV1_P_FOR_2701	CCACAACCACAGAAAAACAAGA
PIV1_P_REV_2792	ATGTGTTGCTGGTTTCCTCTTC
PIV1_P_FOR_2944	GACATTTAATCTCTGTGGTATGCTTATATC
PIV1_P_REV_3015	TATTTCCTCTTGAATTTGTTTAAGTAATG
PIV1_P_FOR_3045	ATTCATCCAGGGATCTTCACAA
PIV1_P_REV_3219	GGGTCAAACCTTGTCTTTTTGA
PIV1_P_FOR_3333	AAAACAACAATGAGCCTCAAGC
PIV1_P_REV_3509	TGTCTTCCTCGAATAGCTCCAT
PIV1_P_FOR_3510	TGGAGCTATTCGAGGAAGACAT
PIV1_M_FOR_3681	TACAGGTTCCCCAGATTCTCAC
PIV1_M_REV_3695	CCCATTTTCTTCGTGTGAGAAT
PIV1_M_FOR_3787	TAGGAGATCCTCCAAAACATGG
PIV1_M_REV_3904	CCGGATCCACAGATTGAATAAC
PIV1_M_FOR_3933	CCAATTGGCATAGCCAAGTATT

Name and 5' nt location	Sequence (5'-3')
PIV1_M_REV_4126	GGGAGACATTGAGGTGCTAGAG
PIV1_M_FOR_4275	CTGGTTACACTTAGGGCAGGAG
PIV1_M_REV_4451	ACCTACAAGCCCGAGAGAGAAT
PIV1_M_FOR_4487	TGTACATGCAACAGGCACATT
PIV1_M_REV_4668	TTTTGCAACAACATTTGGGTA
PIV1_M_FOR_4685	AAAAAGCATCGGGAAAATCAG
PIV1_F_REV_4854	TGCTTAGGCTGAGCTTTTTGA
PIV1_F_FOR_4859	AAGCTCAGCCTAAGCAGAGAGA
PIV1_F_REV_5014	TTTTGTTCTTGCCTCCGTTT
PIV1_F_FOR_5065	TAAACACCAAGATAGAGACAAAAATGC
PIV1_F_FOR_5267	TGACCTACAAGATGGATGTGGA
PIV1_F_FOR_5277	GATGGATGTGGAACAACTCAAA
PIV1_F_REV_5425	GTACCAATGACAGCACCAAAGA
PIV1_F_FOR_5494	CATTAGCTGAAGCACGAGAAGC
PIV1_F_REV_5669	TTTCAATGCCGTAGTCTCACAC
PIV1_F_FOR_5775	ACCTTGCAGGCATTATCATCTC
PIV1_F_REV_5953	ATCAACACGCCTGGTATTTCTG
PIV1_F_FOR_6058	CATCCTTAGGAGGTGCAGATGT
PIV1_F_FOR_6244	TAGTGGCTAATTGCATTGCATC
PIV1_F_REV_6244	GATGCAATGCAATTAGCCACTA
PIV1_F_FOR_6295	CAGTGAATCAAGATCGCTCAAG
PIV1_F_REV_6404	GATGATTTGATTCCCCCAAGTA
PIV1_F_FOR_6552	GGATGGCACAACACAGAGAGTA
PIV1_F_REV_6729	TGGAGTTGTTACCCATGTAGGG
PIV1_F_FOR_6774	TTGTAGCATACATACAACAATCAAATC
PIV1_HN_FOR_6934	ATTGGTCTACAACCCGAAATGA
PIV1_HN_REV_7114	TCGTTCATGGAGGATACTGTCA
PIV1_HN_FOR_7249	AGCAAAGCAGAGATCTCACACA
PIV1_HN_FOR_7291	ACAGACAGGAATTGGCTCAGAT
PIV1_HN_REV_7408	AATGAGATATTGGGGTTGTTGC
PIV1_HN_REV_7623	AATCAGGATACATATCTGAATTTAAGG
PIV1_HN_FOR_7648	ATGACATCAACGACAACAGGAA
PIV1_HN_FOR_7720	TGCCCACTGTGAATGAGACTAC
PIV1_HN_REV_7837	GCAGAAAAAGGATGGTCAAAAG
PIV1_HN_FOR_7911	CTAGGGTACGGTGGCTTAACAA
PIV1_HN_REV_8082	TTGTCTCGACAACAATCTTTGG
PIV1_HN_FOR_8129	TGCCGAAGGTAGGCTACTTAAA
PIV1_HN_FOR_8197	CCAACCTGCAAATAGGATCATT
PIV1_HN_REV_8303	TATGCATTCTCTCGGACATCTG

Name and 5' nt location	Sequence (5'-3')
PIV1_HN_FOR_8403	TCACGTGTTAATCCCACCATAA
PIV1_HN_FOR_8547	GAAATCAACCAAACCAGCCTTA
PIV1_HN_REV_8547	TAAGGCTGGTTTGGTTGATTTC
PIV1_HN_FOR_8627	TTGAGCAGATCAAGACCCAAC
PIV1_HN_REV_8739	AGGCAGGCATTAACCCTAAGTT
PIV1_L_REV_8823	CAATCGGAGAGTTCAAGTGACA
PIV1_L_FOR_8969	GATCAAAATCAGATCGCTAGGC
PIV1_L_REV_9006	CTTGTTTAAGGATTTTGCCTAGC
PIV1_L_REV_9182	CCCTTCAACACAGCCTAATTGT
PIV1_L_FOR_9332	AAAGAATAAGTCGGGGAACCAT
PIV1_L_REV_9511	CGTCCAGCTGAAGACATATTCC
PIV1_L_FOR_9597	TTATTTCCCAATCTTGGTGAGG
PIV1_L_FOR_9761	CACAGATTCAGAAGCAGACAGC
PIV1_L_REV_9761	GCTGTCTGCTTCTGAATCTGTG
PIV1_L_FOR_9891	GCTGCCGATAAAGTAAGGACAC
PIV1_L_REV_9958	ATTGCACAGAAGATTGCATGAC
PIV1_L_REV_10061	AGAGTTGGATCCTTGTGCATTC
PIV1_L_REV_10081	GCACATTCATACGAAATTGCAG
PIV1_L_FOR_10261	TCCCTGAATCAGAAGAGACTCG
PIV1_L_FOR_10353	GGAGAATGGTTAAATGACGATAGC
PIV1_L_REV_10453	TGCTAATACCTGGACTGCTCTCA
PIV1_L_REV_10523	GGTCAATTTCTCCCTTTACCATC
PIV1_L_FOR_10657	CAAATGGGTATTGGGATGAAAG
PIV1_L_FOR_10801	CGTTGTTCGGTCAAAGATGTAA
PIV1_L_REV_10843	GGGTGCATCCAGTTAAAGAAAG
PIV1_L_REV_10975	TAACCCTCTATTCCCCCTCTTG
PIV1_L_FOR_10978	GAGGGGGAATAGAGGGTTATTG
PIV1_L_REV_11168	GGCACCGAAATATCTTGTGATT
PIV1_L_REV_11363	GTTTTCATCTACAAGAGTCTCTGACC
PIV1_L_FOR_11396	AGCCAAAGCTATTGAGAATGGA
PIV1_L_FOR_11556	TGTGCAATATTGATCCCAGCTA
PIV1_L_REV_11566	CCTCCTATGTTAGCTGGGATCA
PIV1_L_REV_11721	AGCTTGAGTCTCCTGGTTCTTG
PIV1_L_FOR_11742	TTCTTAGATTGGGCATCAGACC
PIV1_L_REV_11927	TACTCTGGGCAATATGGCTTTC
PIV1_L_FOR_11934	ATATTGCCCAGAGTAGCTCACG
PIV1_L_REV_12113	CGGTTTTCTGAGTGTCCTTGTT
PIV1_L_FOR_12233	CCACGGTTTAGAAACTCCAGAC
PIV1_L_REV_12391	TAAGGGATACGTATGGCAGGAC

Name and 5' nt location	Sequence (5'-3')
PIV1_L_FOR_12505	TGGTTTACACTTGGGCTTATGG
PIV1_L_REV_12555	CCCTGGTTTGAGCTATAAGTGC
PIV1_L_REV_12728	TCCTGCCTCTTTTAATGCCATA
PIV1_L_FOR_12732	GCATTAAAAGAGGCAGGAGAGTC
PIV1_L_REV_12931	TCCTGAGTGATCTCTAAGTCCAATG
PIV1_L_FOR_12974	TGATCCTGATCCTCTCAAGGAC
PIV1_L_REV_13228	AATACCCCCGAAAGTGGAAC
PIV1_L_FOR_13237	TCGGGGGTATTCTAATCAATCA
PIV1_L_REV_13408	ACAGGCTCTACAACTCCTGCAT
PIV1_L_REV_13634	TATCTCTGCCAAACTACACAAGTATGC
PIV1_L_FOR_13665	ACATCTCTCGAACGACTCGAA
PIV1_L_REV_13848	CATCAGGATCCCAGTCCTCTAA
PIV1_L_FOR_13860	GATCCTGATGCCGATAGTATGC
PIV1_L_REV_14044	TATCGCCCATCAAAAGGTAGAG
PIV1_L_FOR_14086	TTTTCGGGATTAATAGCACCAG
PIV1_L_FOR_14193	GGTGCAATGCTGTCTTGTTATG
PIV1_L_REV_14267	TCTCTTTGTCCGTTGAGATCG
PIV1_L_FOR_14301	CCTTCAGAAGTGGCACTGGTAG
PIV1_L_FOR_14376	AATGGGAATCCTGGATCAACTT
PIV1_L_REV_14477	ACATTTGTGTTCTCCACCTTCC
PIV1_L_REV_14547	TAACGTCCTTATCCCCAACAAG
PIV1_L_FOR_14598	GGTACAGACTGGACAAAACAATTAAG
PIV1_L_REV_14818	TTCTCAACTAGAATCCATTTTTCTATC
PIV1_L_FOR_14861	GAGTGCATCGTCAGGTATGCTA
PIV1_L_REV_15019	ATCCGAGTCCACTCAAAGATTG
PIV1_L_FOR_15176	AACAGGGTCATTTCCAGACA
PIV1_L_FOR_15325	TCTTGACTAAAGAAATAAAAATATTGATGA
PIV1_L_REV_15376	GCTCTGTCTTGCCCCAAATA
PIV1_5UTR_REV_15575	ACCAGACAAGAGTTTAAGAAATATCG

6.3.4. HPIV3 genome sequencing primers

Name and 5' nt location	Sequence (5’ to 3’)
PIV3_3UTR_FOR_1	ACCAAACAAGAGAAGAAACTTGTCTGGG
PIV3_3UTR_FOR_7	CAAGAGAAGAAACTTGTCTGGGAAT
PIV3_3UTR_REV_53	CCTTCTAGTCAATGTCTTTAATCCTAAG
PIV3_N_FOR_67	CATTGACTAGAAGGTCAAGAAAAGG
PIV3_N_REV_70	TCCCTTTTCTTGACCTTCTAGTCA
PIV3_N_FOR_138	GCACGTAGGCAAGAAAACATAAC
PIV3_N_REV_218	ATCAGTTATTGTCGGTCCAAGG

Name and 5' nt location	Sequence (5’ to 3’)
PIV3_N_FOR_293	TGAGAAACAACATGCACAAAGG
PIV3_N_REV_352	TTGTTAGGTAGAGCTCTGGATTGG
PIV3_N_FOR_513	GACCTGGATTATGATCAGGAAACT
PIV3_N_REV_778	GAGTTACCAAGCTCTGTTGAGACC
PIV3_N_FOR_823	CAATGAATACCAGCAGAAATGACC
PIV3_N_FOR_951	GCAGCTTTGACTCTATCCACTCTC
PIV3_N_REV_1179	TCCTAGCTGGAACATATCAATGTC
PIV3_N_FOR_1310	AAACAGTTCAGAGACATCTTTCCA
PIV3_N_REV_1609	GATCATCTATTTCGTCCTGGTTTG
PIV3_P_FOR_1720	TATCATACCGGAATATAGGGTGGT
PIV3_P_REV_1910	GATTGTGTCGTTTTCCGATAAGTC
PIV3_P_FOR_2083	TGATCAGGAAACTGTACAGAGAGG
PIV3_P_REV_2112	TACTATCTGAGCTGCTTCTTCTCC
PIV3_P_FOR_2466	CTTCAACACATCAAGAAGATGACA
PIV3_P_REV_2466	TGTCATCTTCTTGATGTGTTGAAG
PIV3_P_FOR_2823	ATGGAAAGGAAAGGAAGGATACAG
PIV3_P_REV_2858	AGTAATTGCCCTCTCTGTAAATCG
PIV3_P_FOR_3136	AGAACAACTGTCATTGATCACGTC
PIV3_P_REV_3215	CATGGATACTCTCTCATTGGATTC
PIV3_P_FOR_3450	GATCACTAGTTGCAGTCATCAACA
PIV3_P_REV_3549	TCATTGAACATGTCCATTAATTCAG
PIV3_M_FOR_3826	TACCACTCAAAGTCAATGAACAGAG
PIV3_M_REV_3987	AACTTTGTAACTCGGGTCACTGTC
PIV3_M_FOR_4104	AGAAGAACAGTCAAAGCGAAAGAG
PIV3_M_REV_4371	AACCCCTGTTTTTATGTGTACCTG
PIV3_M_FOR_4515	TGTAAACAGAAAATCGAGAAAATGAG
PIV3_M_REV_4673	GCCCAGATAACTAGATTGAGATGC
PIV3_F_FOR_4879	AGGACAAAAGAGGTCAATACCAAC
PIV3_F_REV_4973	TGTTCTGGTGTTCTGTACCTTTTG
PIV3_F_FOR_5144	CTACAGCACGTAGGTGTATTGGTC
PIV3_F_REV_5386	CTCCAAAGAATCGTTTTGTTCTG
PIV3_F_FOR_5489	GCAAGATCAGACATCGAAAAACTC
PIV3_F_REV_5768	TGTGATATTTGTGCGGTATAATGA
PIV3_F_FOR_5884	GAATGATTACTCAATCACCCTCCA
PIV3_F_REV_6135	ATTGGGATATGTTTCCTGATAAGC
PIV3_F_FOR_6262	TGGTAATAGAATCAATCAACCACCT
PIV3_F_REV_6525	GTAGTGCTAGATTGATGCCAATTTC
PIV3_F_FOR_6630	GAATTCAAAAGAGAAATCGAGTGG
PIV3_HN_REV_6874	TTATTAGTGAGCTTGTTGCCATGA
PIV3_HN_REV_7078	AGCCTTGTATTCACTCCTGACTGT
PIV3_HN_FOR_7080	AGTCAGGAGTGAATACAAGGCTTC

Name and 5' nt location	Sequence (5’ to 3’)
PIV3_HN_REV_7428	TCCTGACAACCTCGAGTAATTAGAT
PIV3_HN_FOR_7562	AGGAAGTCATGTTCTCTAGCACTC
PIV3_HN_REV_7875	TGATTACAGTCTCTCTGTGTTTTCC
PIV3_HN_FOR_7912	TACTTGGTTTTCAGATAGGAGGATG
PIV3_HN_FOR_8293	AGACTCACAAAAATCGAGAGTGAAC
PIV3_HN_REV_8305	GTTATGACTGGGTTCACTCTCGAT
PIV3_L_REV_8649	AGTGCCATTGTTAGATTCAGTGTC
PIV3_L_FOR_8764	AGCCTTATGATATGGATGACGACT
PIV3_L_REV_9126	CCATTTATCTGATTTATAGGTTGTGTG
PIV3_L_FOR_9149	ATGGTATAATCCATTCAAAACATGG
PIV3_L_REV_9430	CCACAGGTTATTACCTTTCTGATACA
PIV3_L_FOR_9472	TGTTTCCAATTATGGGAGAAAAGA
PIV3_L_FOR_9860	TAACGGATATAGAGAGAGGCATGG
PIV3_L_REV_9919	AAGCATTTATGATGAATTCGTGTG
PIV3_L_FOR_10210	TGGATTATGTAGAATCTGGGGACT
PIV3_L_REV_10399	GTAATTCAATCTCTCCCTTCACCA
PIV3_L_REV_10576	CCATCATTGTAGATATCCGTTGACT
PIV3_L_FOR_10615	GCTGTTTCCTAACAACAGATCTCA
PIV3_L_REV_10899	CAGCTGCTAGATGTATTGCACTTAT
PIV3_L_FOR_10984	CCACAAGAGTACCCAACAATTATG
PIV3_L_REV_11294	CATGCATATCCTAGAACAGGTGAA
PIV3_L_FOR_11356	TTGGGATGAATATCAATCCAACTA
PIV3_L_FOR_11705	TGTATTACAAGATTCACCAAATCCA
PIV3_L_REV_11719	ATCCAGATAATAATGGATTTGGTG
PIV3_L_REV_12074	CCTCCTGATAAATGAATCCACATC
PIV3_L_FOR_12193	CAGATGGCACAAACCCATATACT
PIV3_L_REV_12250	ATGACGATATACCTGTTTCTGCTG
PIV3_L_FOR_12480	TTAACACCGGTAGCTACATCAACA
PIV3_L_REV_12546	CTCTGATCAATGATGTACTGGAGAA
PIV3_L_FOR_12845	TTATGATAAAGACCCACTCAAAGATG
PIV3_L_REV_12920	TGTCAGTATCATCCCAATAATTCATA
PIV3_L_FOR_13200	ACACTGAGAGATACTTCCCATTCA
PIV3_L_REV_13262	CAATCCCAGAACCTCTTGAATACT
PIV3_L_FOR_13632	TTAATTAAATCGTTCCCATCAACTG
PIV3_L_REV_13687	GACTAATACCGCGAATCCTTAGAT
PIV3_L_FOR_13939	AAGGAGGGAATTATCTATCGCATC
PIV3_L_REV_14150	TCTCGTTGACCAATTACATCTGTT
PIV3_L_FOR_14220	GGAAATGTGACACAGATTCTTAACAG
PIV3_L_REV_14422	TCATCCCCAATCAAGTATGTAATTC
PIV3_L_REV_14617	TGATAAAACAATTTCACTAGGTTCCA
PIV3_L_FOR_14700	TCAAAGAAGAGGAATAATGAATGG

Name and 5' nt location	Sequence (5' to 3')
PIV3_L_REV_14936	CCGCCTAATTTATGTCTCTTATCA
PIV3_L_FOR_15004	TGCTATCGAGAAGACTAGTATTAAGTTG
PIV3_L_REV_15086	CCAGTCTGTGCTCTATGTTCAAAT
PIV3_L_REV_15293	TTGTAGTTTTCTAATAACTGGTCTTCG
PIV3_L_REV_15377	TGTCTATTCCTAGGCTTAAAGATAAAGG
PIV3_5UTR_REV_15433	AAACAAGAGAAGAACTCTGTTTGGTAT
PIV3_5UTR_REV_15436	ACCAAACAAGAGAAGAACTCTGTTTGG

6.3.5. wt EBOV GP sequencing primers

Name	Sequence (5'-3')
wtEBOV-GP_For_1	AGGAATATTGCAGTTACCTCGTGAT
wtEBOV-GP_For_2	TCCACAATAGCACATTACAGGTTAG
wtEBOV-GP_For_3	GTATGTGCACAAAGTATCAGGAACG
wtEBOV-GP_For_4	ACCCGTCTAGTGGCTACTATTCTAC
wtEBOV-GP_For_5	GGAAAACTAATTTGGAAGGTCAAC
wtEBOV-GP_For_6	TTGTCTTTCACAGTTGTATCAAACG
wtEBOV-GP_For_7	TACACCCGTGTATAAACTTGACATCT
wtEBOV-GP_For_8	AACAACAACACTCATCACCAAGATA
wtEBOV-GP_For_9	GAATTTACATAGAGGGGCTAATGC
wtEBOV-GP_For_10	CACATGATTGGACCAAGAACATAAC
wtEBOV-GP_For_11	CATGATTTTGTTGATAAAACCCTTC
wtEBOV-GP_Rev_1	GGAAAAGGATAATTACCCAAAGAAAG
wtEBOV-GP_Rev_2	CTGAAGCCCCATCTTTTAGTTG
wtEBOV-GP_Rev_3	TACAGGAAGAAAGCACCCTCTTTAT
wtEBOV-GP_Rev_4	TACTCTGTCTCATTGGTTCCAAAAC
wtEBOV-GP_Rev_5	CGAATTTTTCTAGTGAGGTTCTTCTT
wtEBOV-GP_Rev_6	TTTTCTGAAGCCATGATTTTGTG
wtEBOV-GP_Rev_7	GTGTTGGTGTTCTCTGCTTTTG
wtEBOV-GP_Rev_8	AATTGCTTCTCTTCGAGTTCTTCTC
wtEBOV-GP_Rev_9	AGGAACAGTTGAAGAGCTTGAGTC
wtEBOV-GP_Rev_10	GGTTTTATCAACAAAATCATGAATAA

6.3.6. GenScript-optimized EBOV GP sequencing primers

Name	Sequence (5'-3')
optEBOV-GP_For_1	CTTAGGATTAAAGAAGCCGCC
optEBOV-GP_For_2	GACGTCGATAAGCTGGTGTGTC
optEBOV-GP_For_3	GGCTGAGAATTGCTATAACCTGG
optEBOV-GP_For_4	TCTTTCTGTACGATAGACTGGCATC
optEBOV-GP_For_5	TGAGACAGAATACCTGTTTGAAGTG
optEBOV-GP_For_6	GAGTTTCACCGTGGTCTCTAATG

Name	Sequence (5'-3')
optEBOV-GP_For_7	ACTACCCTGGCCACAATCTCTAC
optEBOV-GP_For_8	GCTGAGAATACTAACACCTCAAAAAG
optEBOV-GP_For_9	ACTATTGGACTACCCAGGACGA
optEBOV-GP_For_10	CTACCACAGAGCTGCGGACC
optEBOV-GP_For_11	GATCAGGGAGACAATGATAACTGG
optEBOV-GP_Rev_1	CTGGAACAGAATGATGACCCAC
optEBOV-GP_Rev_2	GCCTCGTAATTGACCACTTTAGGT
optEBOV-GP_Rev_3	CCAGAGACCTTGTGCACGTATC
optEBOV-GP_Rev_4	GCAGTGGATGACTAGAAAAGAAGTC
optEBOV-GP_Rev_5	ATCAGCTTTCCAGTTGTATTGGAG
optEBOV-GP_Rev_6	ATGATCTTGTGATCTTCTGTGGTAGTA
optEBOV-GP_Rev_7	ACTGGTGTGTTATGGGTACTATTGTC
optEBOV-GP_Rev_8	GGTGCTTTTTGAGGTGTTAGTATTC
optEBOV-GP_Rev_9	GTTTGGATTGCATTTAGGCTGTG
optEBOV-GP_Rev_10	AGATCAGCCCATCCTGATTATG
optEBOV-GP_Rev_11	CCAGTTATCATTGTCTCCCTGATC

6.3.7. Mutagenesis primer pairs used to introduce *NotI* restriction sites flanking the F and HN genes in the wt HPIV3 JS full-length anti-genome plasmid

Name	Sequence (5'-3') [underlined: NotI restriction site]
HPIV3_NotI_4818_F	CTA ATA TTA TTG CAA AAG GAG TTG GGA AAA TCA AAC AAT GGA ACT AGT AAG CGG CCG CTT AGT CCG GAC GTA TCT ATT AAG CCG A
HPIV3_NotI_4818_R	TCG GCT TAA TAG ATA CGT CCG GAC TAA GCG GCC GCT TAC TAG TTC CA TTG TTT GAT TTT CCC AAC TCC TTT TGC AAT AAT ATT AG
HPIV3_NotI_8582_F	CAT CAA TCT ATC TAT AAT ACA AGT ATA TGA TAA GTA ATC AGG CGG CCG CCA ATA GAC AAA AGG GAA ATA TAA AAA ACT TAG GAG CAA AGC
HPIV3_NotI_8582_R	GCT TTG CTC CTA AGT TTT TTA TAT TTC CCT TTT GTC TAT TGG CGG CCG CCT GAT TAC TTA TCA TAT ACT TGT ATT ATA GAT AGA TTG ATG

6.4. Design of rHPIV3/NotI ΔF-HN/EboGP

The full-length antigenomic plasmid pFlc HPIV3wt BsiWI (P-M) of wt HPIV3 strain JS (GenBank ID: Z11575.1), containing a unique *BsiWI* restriction site at the P-M position [generated by Matthias Lingemann (2013), Master's thesis: "Regulation of HPIV3 F-protein expression and its consequences for virus fitness and immunogenicity" and published in (Lingemann et al. 2015)] was used for generating the rHPIV3/NotI ΔF-HN/EboGP construct, shown in Figure 48.

Two *NotI* restriction sites, flanking the F and HN genes (Figure 48), were inserted into the pFlc HPIV3wt BsiWI (P-M) plasmid by site directed mutagenesis with the QuikChange Lightning Site-Directed Mutagenesis Kit (Agilent Technologies, Santa Clara, CA), as described by the manufacturer's protocol. Primers used for introducing the *NotI* site at the M-F site were: HPIV3_NotI_4818_F and HPIV3_NotI_4818_R and for the second *NotI* site, downstream of the HN ORF: HPIV3_NotI_8582_F and HPIV3_NotI_8582_R. (for primer sequences see 6.3.7)

After insertion of the EBOV GP gene at the *BsiWI* site (Figure 48), the F-HN genes were removed by a *NotI* restriction digest and re-ligation of the remaining pFlc plasmid, resulting in the pFlc HPIV3/NotI ΔF-HN/EboGP (Figure 48). The virus was recovered by reverse genetics as previously described (Durbin et al. 1997), sequenced and used for the EBOV GP neutralization assay (2.2.20.2.4).

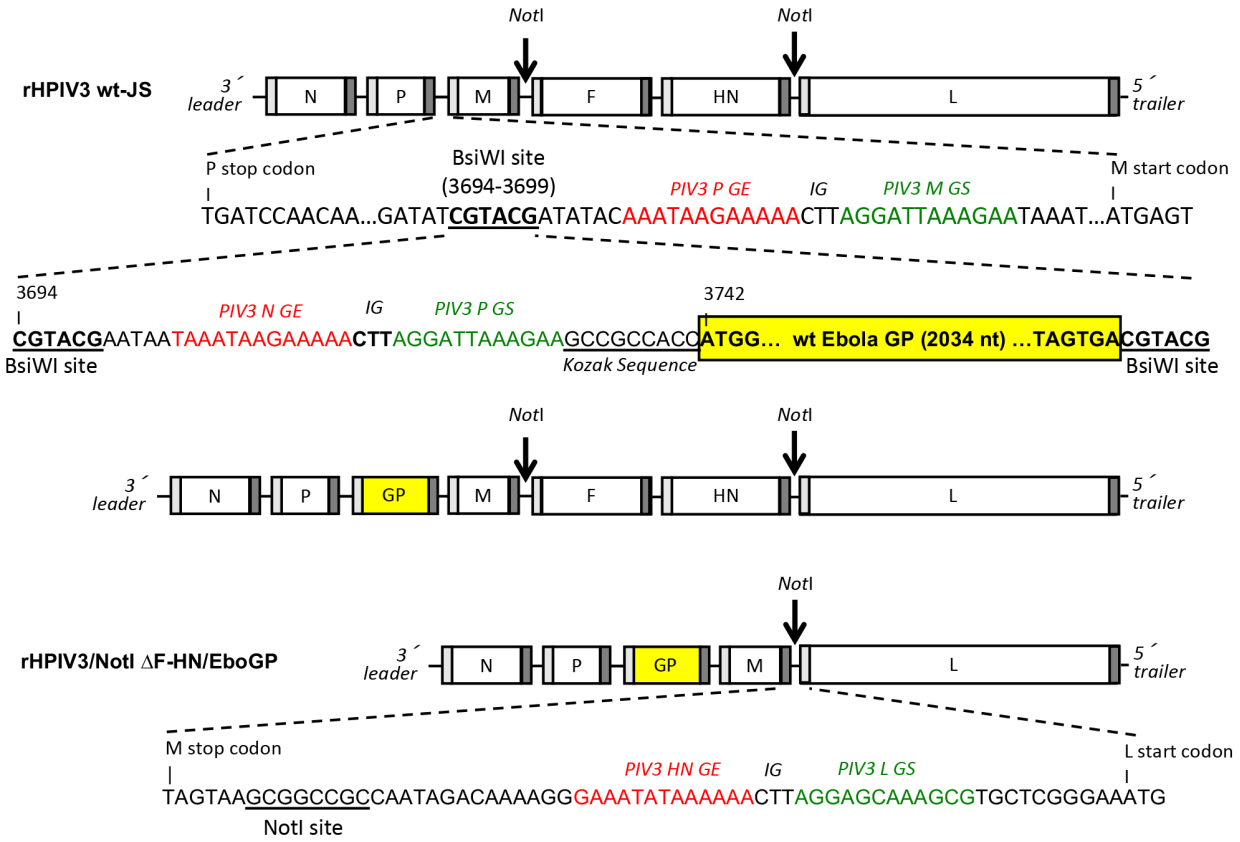

Figure 48: **Design of the rHPIV3/NotI ΔF-HN/EboGP construct used for the EBOV GP neutralization assay.**

6.5. Table of Figures

6.6. Table of Tables